STRINGQFT

String-Theoretic Construction
of Quantum Field Theory

VOLUME IV

Geometry Preliminaries

Xingyang Yu

StringQFT v1.0 / Source build candidate

Drafted with AI assistance under the supervision of the author.
Manuscript free to read. All rights reserved.

Contents

IV.1 Complex and Kähler geometry: working toolkit 1
IV.1.1 A compact curve from two charged coordinates 1
IV.1.2 Complex coordinates as a geometric atlas 1
IV.1.3 Hermitian data and the Kähler condition 4
IV.1.4 The Fubini–Study line from charts to area 6
IV.1.5 Ricci form, first Chern class, and Hodge notation 9
IV.1.6 Moment maps and the two faces of a quotient 10
IV.1.7 Exercises 14
IV.1.8 Take-home message 15
Status and sources 15

IV.2 Calabi–Yau manifolds: holonomy, moduli, Hodge structure 17
IV.2.1 A compact space and a cone 17
IV.2.2 From the Ricci form to a global volume form 17
IV.2.3 Top forms, quotient weights and invariant spinors 19
IV.2.4 Complex and Kähler directions in familiar spaces 21
IV.2.5 Hodge structure and a quintic count 23
IV.2.6 The cone, its link and the Reeb charge 25
IV.2.7 Character poles and link volume 27
IV.2.8 Exercises 28
IV.2.9 Take-home message 30
Status and sources 30

IV.3 ADE singularities, resolutions, and the McKay correspondence 33
IV.3.1 One quotient and two graphs 33
IV.3.2 Characters as a calculation tool 33
IV.3.3 Tensoring and the affine McKay graph 35
IV.3.4 Exceptional curves and finite ADE 36
IV.3.5 The hyperkahler resolution 38
IV.3.6 Beyond SU2 42
IV.3.7 Projective characters 44
IV.3.8 Lie-algebra and theorem interface 45
IV.3.9 Exercises 47
IV.3.10 Take-home message 48
Status and sources 48

IV.4 Toric geometry: fans, polytopes, and GLSM realizations 51
IV.4.1 A conifold in three descriptions . . . 51
IV.4.2 Cones and their dual semigroups . . . 51
IV.4.3 GLSM charges and saturated lattices . . . 53
IV.4.4 FI chambers and triangulations . . . 55
IV.4.5 Graded coordinate rings . . . 57
IV.4.6 From a graph to toric data . . . 59
IV.4.7 Fourfolds and compact quotients . . . 62
IV.4.8 Exercises . . . 64
IV.4.9 Take-home message . . . 65
Status and sources . . . 65

IV.5 The conifold: deformation and small resolutions 67
IV.5.1 One node and three questions . . . 67
IV.5.2 The rank-one matrix cone . . . 68
IV.5.3 Two small resolutions . . . 70
IV.5.4 The deformation and its three-sphere . . . 73
IV.5.5 The link and its normalized volume . . . 75
IV.5.6 Transitions and engine limits . . . 77
IV.5.7 Exercises . . . 78
IV.5.8 Take-home message . . . 79
Status and sources . . . 80

IV.6 Calibrated cycles and wrapped-brane BPS states 81
IV.6.1 A wrapped cycle asks for a volume bound . . . 81
IV.6.2 Volume bounded by a closed form . . . 82
IV.6.3 Kähler calibrations . . . 84
IV.6.4 Special Lagrangians . . . 86
IV.6.5 Wrapped brane central charges . . . 88
IV.6.6 Marginality and limitations . . . 90
IV.6.7 Exercises . . . 93
IV.6.8 Take-home message . . . 94
Status and sources . . . 94

IV.7 K3 surfaces and heterotic/type-II duality 97
IV.7.1 Two spheres at a singularity . . . 97
IV.7.2 The K3 topological data . . . 97
IV.7.3 Roots and collapsing curves . . . 99
IV.7.4 Metric and B-field moduli . . . 101
IV.7.5 Wrapped states . . . 104
IV.7.6 Heterotic/type-II comparison . . . 106
IV.7.7 Exercises . . . 108

IV.8 Elliptic fibrations and the Kodaira classification 111
IV.8.1 The curve and the construction . . . 111
IV.8.2 An elliptic curve varies . . . 112

IV.8.3 Orders and minimal models . . . 115
IV.8.4 Reading a Tate model . . . 118
IV.8.5 Covers over the divisor . . . 121
IV.8.6 From fiber geometry to physics . . . 124
IV.8.7 Exercises . . . 126
IV.8.8 Take-home message . . . 128
Status and sources . . . 128

IV.9 M-theory on special holonomy: G_2 and Spin(7) 131
IV.9.1 Geometry that preserves supersymmetry . . . 131
IV.9.2 The invariant forms and their metrics . . . 132
IV.9.3 Oriented planes and the Gram determinant . . . 134
IV.9.4 Torsion-free structures and exact holonomy . . . 136
IV.9.5 Real spinors and external supercharges . . . 139
IV.9.6 Calibrated cycles and volume minimization . . . 140
IV.9.7 Compact reduction and the zero-flux premise . . . 143
IV.9.8 What a local interacting theory still needs . . . 145
IV.9.9 Exercises . . . 146
IV.9.10 Take-home message . . . 148
Status and sources . . . 148

IV.10 Fluxes and warping 150
IV.10.1 A number on a surface . . . 150
IV.10.2 Flux and free cohomology . . . 151
IV.10.3 Bianchi identities and sources . . . 153
IV.10.4 Warped metrics and boundary data . . . 156
IV.10.5 Shifted magnetic quantization . . . 160
IV.10.6 Flux superpotentials and their limits . . . 162
IV.10.7 Exercises . . . 167
IV.10.8 Take-home message . . . 169
Status and sources . . . 169

IV.11 Mirror symmetry 172
IV.11.1 Which mirror dictionary . . . 172
IV.11.2 Free fields and chiral reflection . . . 173
IV.11.3 Complex structure and dual positions . . . 176
IV.11.4 A special Lagrangian product . . . 179
IV.11.5 Inverting the fibers . . . 182
IV.11.6 From a gauge theory to a Laurent curve . . . 185
IV.11.7 Coefficients and singular points . . . 187
IV.11.8 What a global mirror would require . . . 190
IV.11.9 Exercises . . . 191
IV.11.10 Take-home message . . . 193

Chapter IV.1

Complex and Kähler geometry: working toolkit

IV.1.1 A compact curve from two charged coordinates

Consider two complex numbers (z_0, z_1), neither simultaneously zero, and identify pairs that differ by a common nonzero complex factor. A ratio such as $w = z_1/z_0$ then looks like a coordinate, but it fails where $z_0 = 0$. At that point the other ratio $u = z_0/z_1$ works. The resulting compact curve is $\mathbb{CP}^1$. Its construction asks three questions that recur in string constructions. How do local coordinates describe one global space? Which local metric gives a well-defined area to the curve? When does a gauge quotient produce that same geometry?

This chapter answers those questions for a fixed classical example. The quotient is the positive-level vacuum geometry of a $U(1)$ model with two charge-one fields and vanishing superpotential. The metric and its period are geometric statements. Identifying this quotient with a quantum moduli space, a brane separation, or a physical string-scale parameter requires extra input. In particular, the Kähler form J and the complex structure I have different jobs. We will keep them distinct while deriving the coordinate, area, curvature, and quotient descriptions of the same curve.

The route supplies the geometric language used for exceptional curves in Chapter 3 and for the toric and gauged-linear-sigma-model quotients in Chapter 4. Chapter 2 develops Calabi–Yau holonomy and Hodge theory beyond the small amount needed here. The gauge dynamics of a sigma model belong to Volume 0.

IV.1.2 Complex coordinates as a geometric atlas

The ratio $w = z_1/z_0$ has a domain. Making that domain explicit is the first step toward a global complex curve. On a real $2n$-manifold, an almost-complex structure is a smooth real endomorphism I of the tangent bundle with $I^2 = -1$. In a local chart

with $z^a = x^a + iy^a$, the standard action is

$$I\frac{\partial}{\partial x^a} = \frac{\partial}{\partial y^a}, \qquad I\frac{\partial}{\partial y^a} = -\frac{\partial}{\partial x^a}. \tag{IV.1.1}$$

Thus complex dimension n means real dimension $2n$. This geometric count does not specify a worldvolume spacetime dimension or a number of supercharges. An almost-complex tensor alone does not supply holomorphic coordinates. A complex manifold is given by an atlas whose transition maps are holomorphic, and those charts induce I. The converse for sufficiently smooth almost-complex structures is the Newlander–Nirenberg theorem. Its obstruction is the Nijenhuis tensor; the tensor test and proof are deferred, while the explicit holomorphic overlap below establishes the atlas used here.

Projective coordinates give a complete example. Write $[Z_0 : Z_1]$ for a nonzero pair under $(Z_0, Z_1) \sim (tZ_0, tZ_1)$ with $t \in \mathbb{C}^*$. The two open sets and their coordinates are

$$U_0 = \{Z_0 \neq 0\}, \quad w = \frac{Z_1}{Z_0}, \qquad U_1 = \{Z_1 \neq 0\}, \quad u = \frac{Z_0}{Z_1}. \tag{IV.1.2}$$

Every projective point lies in at least one set. The point $[0 : 1]$ is missing from U_0 but is $u = 0$ in U_1; $[1 : 0]$ is missing from U_1 but is $w = 0$ in U_0. On their overlap, both ratios are nonzero, and

$$u = \frac{1}{w}, \qquad \frac{du}{dw} = -\frac{1}{w^2}, \qquad w \neq 0. \tag{IV.1.3}$$

The transition and its inverse are holomorphic on $\mathbb{C}^*$. Figure IV.1.1 shows why neither affine picture alone contains the entire curve. There is no singularity at $w = \infty$; that notation names $u = 0$ in the second chart.

It is useful to derive the coordinate rule from the equivalence relation rather than memorize the two ratios. On U_0 divide the homogeneous pair by Z_0 to obtain the representative $(1, w)$. On U_1 divide it by Z_1 to obtain $(u, 1)$. When both denominators are nonzero, the two representatives differ by the factor w:

$$(1, w) = w(u, 1), \qquad u = w^{-1}. \tag{IV.1.4}$$

This equality is the complete gluing instruction on the overlap. It also shows why the homogeneous pair $(0, 0)$ cannot be included: neither normalization exists there, and its complex-scaling orbit has a different stabilizer from every nonzero pair. The coordinate singularity of w at $[0 : 1]$ and the singular orbit of the origin are different issues. The first is repaired by a second chart; the second is removed from the projective construction.

The complex structure can be checked directly on the overlap. In the $w = x + iy$ frame, I acts as in (IV.1.1). A holomorphic transition has a real differential commuting with that action. For $u = 1/w$, the Cauchy–Riemann equations hold wherever $w \neq 0$, so

$$du(Iv) = i\,du(v), \qquad d\bar{u}(Iv) = -i\,d\bar{u}(v). \tag{IV.1.5}$$

The same real tensor I is therefore obtained from either chart. The global claim follows from the overlap rule, not from assigning the symbol i to a single coordinate. This

distinction matters in more complicated quotients where a convenient ratio may fail on a divisor or where the proposed transitions are not holomorphic.

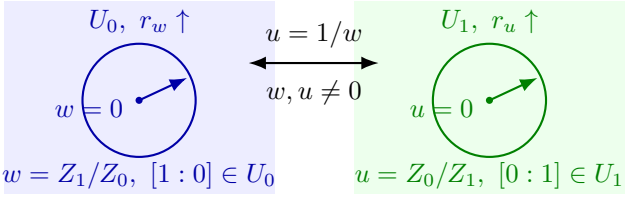


Figure IV.1.1: The two charts of the same projective curve. The left chart uses $w = Z_1/Z_0$ and contains $[1:0]$; the right uses $u = Z_0/Z_1$ and contains $[0:1]$. The arrows identify their nonzero overlap by $u = 1/w$. The arrows mark increasing radial coordinate in each chart, so $r_w \to \infty$ meets $r_u = 0$ rather than a boundary of the curve.

Differential forms inherit a type from this atlas. The complexified cotangent bundle is spanned locally by dz^a and $d\bar{z}^{\bar{a}}$. A form with p holomorphic and q antiholomorphic factors has type (p, q) and belongs to $\Omega^{p,q}$. On a complex manifold the exterior derivative separates as

$$d = \partial + \bar{\partial}, \quad \partial : \Omega^{p,q} \longrightarrow \Omega^{p+1,q}, \quad \bar{\partial} : \Omega^{p,q} \longrightarrow \Omega^{p,q+1}. \tag{IV.1.6}$$

The decomposition is useful because a metric compatible with I has a naturally associated $(1,1)$ form. It also gives a local check on chart changes. For the overlap above, $du = -w^{-2}dw$ and $d\bar{u} = -\bar{w}^{-2}d\bar{w}$, so a $(1,1)$ form transforms with the product of both Jacobians, not with only the holomorphic factor.

For a scalar $f(w, \bar{w})$, the decomposition can be read in ordinary derivatives. The Wirtinger operators are

$$\partial_w = \frac{1}{2}(\partial_x - i\partial_y), \qquad \partial_{\bar{w}} = \frac{1}{2}(\partial_x + i\partial_y), \qquad df = (\partial_w f)dw + (\partial_{\bar{w}} f)d\bar{w}. \tag{IV.1.7}$$

Thus holomorphicity is the local condition $\partial_{\bar{w}} f = 0$. The transition $1/w$ passes this test away from zero, while $1/\bar{w}$ would not. The distinction is visible without invoking a general integrability theorem. Later, the same operators differentiate the Fubini–Study potential, so the chart calculation is already preparing the area calculation rather than adding an independent list of definitions.

As a numerical check, take $w = 2$. Then $u = 1/2$ and $du/dw = -1/4$. The point itself has not changed; only its coordinate and tangent-frame scale have. Exercise 1 asks the reader to use that Jacobian on an actual metric. This is the same local-to-global move needed when an exceptional $\mathbb{CP}^1$ is described by different patches in Chapter 3. A single coordinate formula, even if smooth, cannot establish that a proposed space has a global holomorphic atlas.

One can make the tangent-frame statement quantitative. A vector with w component v^w has u component $v^u = (du/dw)v^w$. At $w = 2$, a unit w component becomes $v^u = -1/4$. Covectors transform in the opposite direction so that a pairing is unchanged. A metric coefficient must therefore absorb two inverse Jacobian factors. This is exactly

the equality we will verify for the Fubini–Study metric. The chart does not change a physical length; it changes the numbers assigned to a tangent vector and to the metric in compensating ways.

An affine singularity beside the smooth atlas

Local algebra can also reveal the shape of a space near a special point, though it does not determine its global metric. Take a trace-zero complex 2×2 matrix

$$N = \begin{pmatrix} a & b \\ c & -a \end{pmatrix}, \qquad N^2 = (a^2 + bc)\mathbf{1}. \tag{IV.1.8}$$

Nilpotent means that some positive power of a matrix vanishes. For a trace-zero 2×2 matrix, the displayed identity makes $N^2 = 0$ equivalent to nilpotence. Thus the nilpotent matrices form the affine hypersurface $F(a, b, c) = a^2 + bc = 0$. Its gradient is

$$\nabla F = (2a, c, b), \qquad F = 0,\ \nabla F = 0 \quad \Longleftrightarrow \quad (a, b, c) = (0, 0, 0). \tag{IV.1.9}$$

For example, $(a, b, c) = (1, 1, -1)$ lies on the hypersurface and has nonzero gradient $(2, -1, 1)$, so it is a smooth point. At a point of a complex hypersurface, a nonzero gradient makes its tangent space the kernel of one nonzero linear equation, of complex dimension two. Here the gradient vanishes only at the origin. Since F is quadratic, every first-order direction at the origin satisfies the linearized equation, giving a three-dimensional Zariski tangent space for this two-dimensional hypersurface; the origin is its unique singular point. A reader of a later Nahm-moduli construction can recognize this equation as a local algebraic model, but the equation supplies neither Nahm boundary conditions nor a complete metric, global orbit classification, or field-theory branch identification. Boundary conditions and global moduli belong to IX.4, on boundary conditions and Nahm poles.

IV.1.3 Hermitian data and the Kähler condition

A complex chart can measure angles only after a metric is chosen. A Hermitian metric is a positive real metric compatible with I, meaning $g(Iv, Iw) = g(v, w)$. We write its local Hermitian components $g_{a\bar{b}}$ in the paired convention

$$ds^2 = 2g_{a\bar{b}}\, dz^a d\bar{z}^{\bar{b}}, \qquad J = i g_{a\bar{b}}\, dz^a \wedge d\bar{z}^{\bar{b}}. \tag{IV.1.10}$$

The product in ds^2 denotes the symmetric real tensor. For $z = x + iy$ and $g_{z\bar{z}} = 1$, it gives $ds^2 = 2(dx^2 + dy^2)$ while $J = 2dx \wedge dy$. The normalization keeps metric lengths and form areas paired. A different normalization can be used, but it must change both statements together.

This pairing is easiest to see on one real tangent plane. Let $v = \partial_x$ and $Iv = \partial_y$ in the flat one-coordinate example. The real metric gives $g_{\mathbb{R}}(v, v) = 2$, and the form evaluates to $J(v, Iv) = 2$. Consequently a positive Hermitian metric determines a positive $(1, 1)$ form, with the complex orientation fixed by (v, Iv). Hermitian symmetry

reads $g_{a\bar{b}} = \overline{g_{b\bar{a}}}$; positivity says $g_{a\bar{b}} v^a \bar{v}^{\bar{b}} > 0$ for nonzero complex v. These are pointwise conditions. Closure compares the coefficients at neighboring points.

The extra Kähler requirement is $dJ = 0$. On an integrable complex manifold, a Kähler form has a local real potential K, with

$$g_{a\bar{b}} = \partial_a \partial_{\bar{b}} K, \qquad J = i\partial\bar{\partial} K. \tag{IV.1.11}$$

The potential is local. If K changes by $f(z) + \overline{f(z)}$ for holomorphic f, then $\partial\bar{\partial}K$ does not change. This is the gluing mechanism we will use on $\mathbb{CP}^1$. Conversely, the local-potential statement for closed positive $(1,1)$ forms is a standard local result in Kähler geometry; a potential on every chart need not be one global function.

The difference between local and global potentials can be anticipated from Stokes' theorem. If a closed compact curve C admitted one smooth global function K with $J = i\partial\bar{\partial}K$, then $J = d(i\bar{\partial}K)$ on C and

$$\int_C J = \int_C d(i\bar{\partial}K) = 0. \tag{IV.1.12}$$

A positive Kähler form has positive area on a nonempty compact curve. Its local potentials therefore cannot combine into one global potential. Their differences carry information about a nonzero cohomology class. The next section makes this obstruction concrete through a logarithmic shift on the $\mathbb{CP}^1$ overlap.

Closure follows directly from the local expression. On an integrable chart, $\partial^2 = \bar{\partial}^2 = 0$ and $\partial\bar{\partial} = -\bar{\partial}\partial$, hence

$$dJ = i(\partial + \bar{\partial})\partial\bar{\partial}K = 0. \tag{IV.1.13}$$

Flat $\mathbb{C}^n$ is the immediate example. With $K = \sum_a |z^a|^2$, one obtains $g_{a\bar{b}} = \delta_{a\bar{b}}$ and $J = i\sum_a dz^a \wedge d\bar{z}^a = 2\sum_a dx^a \wedge dy^a$. Its coefficients are constant, so $dJ = 0$. Its noncompactness, however, makes a compact-cycle period a separate question.

The flat potential is an explicit global function on $\mathbb{C}^n$. This does not mean every Kähler metric on a noncompact space has a global potential, but it gives a simple control case for signs. For $n = 2$, the real four-form $J \wedge J$ has the positive orientation fixed by the ordered planes (x^1, y^1) and (x^2, y^2):

$$\frac{J^2}{2} = 4\, dx^1 \wedge dy^1 \wedge dx^2 \wedge dy^2. \tag{IV.1.14}$$

This is the volume form of the paired real metric in our units. It provides a control when a quotient removes one real level direction and one circle direction.

Positivity alone is insufficient. On $\mathbb{C}^2$, use the diagonal Hermitian matrix

$$(g_{a\bar{b}}) = \begin{pmatrix} 1 & 0 \\ 0 & 1 + |z^1|^2 \end{pmatrix}, \qquad J = i\, dz^1 \wedge d\bar{z}^1 + i(1 + |z^1|^2) dz^2 \wedge d\bar{z}^2. \tag{IV.1.15}$$

Both eigenvalues are positive everywhere. Yet the second coefficient varies in the first complex direction, and direct differentiation gives

$$dJ = i\big(\bar{z}^1 dz^1 + z^1 d\bar{z}^1\big) \wedge dz^2 \wedge d\bar{z}^2. \tag{IV.1.16}$$

At $z^1 = 1 + i$, the coefficient of $dz^1 \wedge dz^2 \wedge d\bar{z}^2$ is $i(1 - i) = 1 + i$, so closure fails. More generally it fails wherever $z^1 \neq 0$. The issue is not a loss of positive lengths; it is the absence of a closed form suitable for deformation-invariant cycle periods and symplectic reduction.

The derivative in that component is a Wirtinger derivative, not an ordinary derivative in the two real coordinates at once. Explicitly,

$$\partial_{z^1}(1 + |z^1|^2) = \bar{z}^1, \qquad \partial_{\bar{z}^1}(1 + |z^1|^2) = z^1. \tag{IV.1.17}$$

At the numerical point the first coefficient is $1 - i$. With a factor of two in the metric perturbation, as in Exercise 2, it becomes $2 - 2i$. These checks distinguish genuine nonclosure from a mismatch of complex-derivative conventions. Both metrics remain positive at the point.

One can see why no local Kähler potential produces this specific metric by inspecting mixed derivatives. A potential would require $\partial_1 g_{2\bar{2}} = \partial_2 g_{1\bar{2}}$, because the third derivatives of K commute. Here the left side is $\bar{z}^1$ and the right side is zero:

$$\partial_1 g_{2\bar{2}} = \bar{z}^1 \neq 0 = \partial_2 g_{1\bar{2}} \quad (z^1 \neq 0). \tag{IV.1.18}$$

This local obstruction is a practical test before trying to call a Hermitian metric Kähler. In Chapter 2 a closed Kähler form also becomes part of the setting for Hodge and holonomy statements. Neither positivity nor a convenient choice of complex coordinates supplies that closure automatically.

The factor-two variant in Exercise 2 makes the point numerical. Put $g_{2\bar{2}} = 1 + 2|z^1|^2$. At $z^1 = 1 + i$ the matrix has diagonal entries 1 and 5, both positive, but

$$\partial_{z^1} g_{2\bar{2}} = 2\bar{z}^1 = 2 - 2i, \qquad (dJ)_{z^1 z^2 \bar{z}^2} = i(2 - 2i) = 2 + 2i. \tag{IV.1.19}$$

Changing the coefficient rescales the obstruction without changing its cause. The statement that the form is nonclosed rests on the nonzero three-form component; the statement that the metric is positive rests on its eigenvalues. Keeping both computations visible prevents the common misconception that one property entails the other.

IV.1.4 The Fubini–Study line from charts to area

The two affine charts become a compact metric curve when their local forms agree on the overlap. Let $\lambda > 0$ and use the potentials

$$K_0 = \lambda \log(1 + |w|^2), \qquad K_1 = \lambda \log(1 + |u|^2). \tag{IV.1.20}$$

These potentials are regular at $w = 0$ and $u = 0$, respectively. On $u = 1/w$, we have $1 + |u|^2 = (1 + |w|^2)/|w|^2$, and therefore

$$K_1 = K_0 - \lambda \log |w|^2. \tag{IV.1.21}$$

On any simply connected piece of the overlap, $\log |w|^2 = \log w + \overline{\log w}$. The difference is a local Kähler transformation, so $i\partial\bar{\partial}K_0 = i\partial\bar{\partial}K_1$ there. The logarithm is only local; a single global potential on compact $\mathbb{CP}^1$ would contradict its positive period.

The real function $\log|w|^2$ exists on the punctured overlap even though $\log w$ has no single-valued branch around zero. It is locally holomorphic plus antiholomorphic, so $\partial\bar\partial\log|w|^2 = 0$ there.

Differentiation gives a concrete tensor in either chart:

$$g_{w\bar w} = \partial_w\partial_{\bar w}K_0 = \frac{\lambda}{(1+|w|^2)^2}, \qquad g_{u\bar u} = \frac{\lambda}{(1+|u|^2)^2}. \tag{IV.1.22}$$

For example, the first derivative is $\partial_w K_0 = \lambda\bar w/(1+w\bar w)$ and the second reduces to $\lambda/(1+w\bar w)^2$. On the overlap, the tensor transformation explicitly reproduces the same metric:

$$g_{u\bar u}\left|\frac{du}{dw}\right|^2 = \frac{\lambda}{(1+|w|^{-2})^2}|w|^{-4} = \frac{\lambda}{(1+|w|^2)^2}. \tag{IV.1.23}$$

At $w = 2$ and $\lambda = 3/2$, one obtains $g_{w\bar w} = 3/50$, while $u = 1/2$ gives $g_{u\bar u} = 24/25$. Multiplying the latter by $|du/dw|^2 = 1/16$ returns $3/50$. The unequal coefficients are precisely what one expects from unequal coordinate scales.

The same check can be made directly at the level of the two-form. Using $du = -w^{-2}dw$ and its conjugate, one finds

$$i\frac{\lambda\,du\wedge d\bar u}{(1+|u|^2)^2} = i\frac{\lambda|w|^{-4}\,dw\wedge d\bar w}{(1+|w|^{-2})^2} = i\frac{\lambda\,dw\wedge d\bar w}{(1+|w|^2)^2}. \tag{IV.1.24}$$

This confirms the overlap equality without appealing only to the potential shift. It also makes positivity manifest in each chart: the coefficient is positive for $\lambda > 0$, and the holomorphic coordinate change preserves the chosen complex orientation. The scalar λ multiplies the entire form; it does not change the complex atlas.

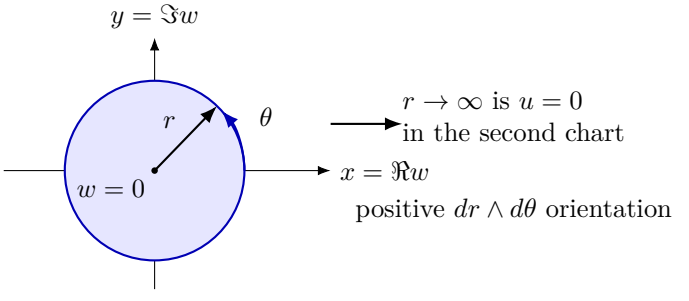


Figure IV.1.2: The positive complex orientation in the $w = x + iy$ plane is $dx\wedge dy = r\,dr\wedge d\theta$. The circle at radius r approaches $[0:1]$ as $r\to\infty$, where the u chart is regular. The radial weight $2\lambda r/(1+r^2)^2$ makes that omitted point carry zero area, while the two local forms agree across the annular overlap.

The global form is $J = i\lambda\,dw\wedge d\bar w/(1+|w|^2)^2$ on U_0. To integrate it, write $w = re^{i\theta}$, with the complex orientation $dx\wedge dy = r\,dr\wedge d\theta$. Since $i\,dw\wedge d\bar w = 2r\,dr\wedge d\theta$, the entire curve is covered by $0 \le r < \infty$ except one point of zero area. Thus

$$J = \frac{2\lambda r}{(1+r^2)^2}\,dr\wedge d\theta, \qquad 0 \le \theta < 2\pi. \tag{IV.1.25}$$

$$\int_{\mathbb{CP}^1} J = 2\pi\lambda \int_0^\infty \frac{2r\,dr}{(1+r^2)^2} = 2\pi\lambda \left[-\frac{1}{1+r^2}\right]_0^\infty = 2\pi\lambda. \tag{IV.1.26}$$

The integral can be checked with a finite disk before taking the limit. On $|w| \le R$, the same antiderivative gives

$$\int_{|w|\le R} J = 2\pi\lambda \frac{R^2}{1+R^2}. \tag{IV.1.27}$$

At $R = 1$ the disk has area $\pi\lambda$, exactly half the full area. Under $u = 1/w$, the region $|w| \ge 1$ is the disk $|u| \le 1$ in the other chart. The halves meet along $|w| = |u| = 1$. This finite-radius calculation checks that the point at infinity has no hidden area contribution and that the two chart descriptions cover the same compact surface. For $\lambda = 3/2$, each half has area $3\pi/2$. Figure IV.1.2 keeps the orientation and the second chart visible while using this single-chart integral. For $\lambda = 3/2$, the area is 3π. Missing the factor two in $i\,dw \wedge d\bar{w}$ would produce the wrong area even though the potential differentiation was correct. Cannas da Silva's native Fubini–Study form has one half of our $\lambda = 1$ form and hence area π. The discrepancy is a normalization translation, not a disagreement about the geometry.

This period is a geometric size in the declared normalization. The class $[J/(2\pi)]$ is integral on $\mathbb{CP}^1$ precisely when λ is an integer; positive noninteger λ still defines a Kähler metric. The string-theoretic complexified parameter $t_C = \int (B + iJ)/(4\pi^2\alpha')$ needs a specified B field and α' before the curve's area becomes a physical modulus. Chapter 3 uses such curves in resolution geometry, while Chapter 4 will use an FI chamber to produce them. Neither connection follows from the period alone.

There is a direct regularity check at the point missed by the w chart. Pulling the line element through $w = 1/u$ gives

$$ds^2 = \frac{2\lambda}{(1+|u|^2)^2}\,du\,d\bar{u}. \tag{IV.1.28}$$

Its coefficient approaches 2λ in the real line element as $u \to 0$. The area form has the same finite limit in the u frame. The apparent decay $g_{w\bar{w}} \sim \lambda|w|^{-4}$ as $|w| \to \infty$ is precisely compensated by the divergent coordinate Jacobian $|dw/du|^2 = |u|^{-4}$. A vanishing coefficient in a bad coordinate need not signal a collapsing physical metric. This is why both the chart gluing and the tensor transformation were necessary before integrating across the apparent infinity.

De Rham classes are closed differential forms modulo exact forms. The Kähler class is the class of J in this sense. If J is shifted by an exact two-form $d\eta$, then its period on this compact curve does not change:

$$\int_{\mathbb{CP}^1} (J + d\eta) - \int_{\mathbb{CP}^1} J = \int_{\mathbb{CP}^1} d\eta = 0. \tag{IV.1.29}$$

This is the precise sense in which closure makes a period useful as a geometric label. The metric itself can vary, and pointwise curvature can vary, while the period stays fixed inside a class. Conversely, changing λ changes the class because it changes the period. No such class-based statement follows for the nonclosed Hermitian form of the earlier counterexample.

IV.1.5 Ricci form, first Chern class, and Hodge notation

The same metric also supplies a topological count. In local holomorphic coordinates on a Kähler manifold, define the Ricci form by

$$\rho = -i\partial\bar{\partial}\log\det(g_{a\bar{b}}). \tag{IV.1.30}$$

The determinant depends on the chart, but its change under a holomorphic coordinate transformation is a holomorphic plus antiholomorphic logarithm. The $\partial\bar{\partial}$ operation removes that change. Thus ρ is a global closed real $(1,1)$ form. The Chern–Weil identification $[\rho/(2\pi)] = c_1(TX)$ is a theorem for the smooth complex tangent bundle, with equality understood in real de Rham cohomology. It does not follow merely from a local symbolic derivative; differential forms also cannot see torsion in integral cohomology.

For $\mathbb{CP}^1$, the metric is a single component. Taking its logarithm makes the scale dependence explicit:

$$\log g_{w\bar{w}} = \log\lambda - 2\log(1+|w|^2), \qquad \partial_w\partial_{\bar{w}}\log g_{w\bar{w}} = -\frac{2}{(1+|w|^2)^2}. \tag{IV.1.31}$$

The constant $\log\lambda$ disappears on differentiation. Hence

$$\rho = \frac{2i\,dw\wedge d\bar{w}}{(1+|w|^2)^2} = \frac{2}{\lambda}J. \tag{IV.1.32}$$

The form has the same positive orientation as J in Figure IV.1.2. Combining this result with the already evaluated area yields

$$\int_{\mathbb{CP}^1}\frac{\rho}{2\pi} = \frac{1}{2\pi}\frac{2}{\lambda}(2\pi\lambda) = 2. \tag{IV.1.33}$$

The number is independent of the positive metric scale. At $w=1$ and $\lambda = 5/3$, for example, $g_{w\bar{w}} = 5/12$ and the coefficient of $i\,dw\wedge d\bar{w}$ in ρ is $1/2$; its integrated Chern number is still two. The calculation identifies the tangent bundle's first Chern number only after the global chart gluing and the Chern–Weil theorem have been supplied.

The global gluing of ρ can be seen without treating the local determinant as a scalar. The metric components obey $g_{w\bar{w}} = g_{u\bar{u}}|du/dw|^2$, so their logarithms differ by

$$\log g_{w\bar{w}} - \log g_{u\bar{u}} = \log\left|\frac{du}{dw}\right|^2 = -2\log|w|^2. \tag{IV.1.34}$$

The right side is locally holomorphic plus antiholomorphic. Applying $-i\partial\bar{\partial}$ removes it and gives the same Ricci form from either chart. This explains why a coordinate-dependent determinant yields a global curvature form. It does not replace the Chern–Weil theorem identifying its cohomology class.

If λ doubles, the line element and area double, while the Ricci-form coefficient in the fixed w chart is unchanged. Its contraction with the inverse metric changes; its

integrated first Chern number does not. A geometric size and a topological count can therefore respond differently to a deformation of the same curve. This is useful when a later exceptional curve carries both an area parameter and a characteristic class.

Flat $\mathbb{C}^n$ gives a useful comparison. Its determinant is one in the standard global chart, so $\rho = 0$ there. Yet its noncompactness means the compact-$\mathbb{CP}^1$ integral argument cannot simply be copied. Conversely, knowing $\rho = 0$ in one small chart of another space says nothing by itself about the global first Chern class. Curvature coefficients, cohomology classes, and integrated characteristic numbers are related but distinct statements.

The symbols $H^{p,q}$ will be needed in the next chapter. On any complex manifold one defines Dolbeault cohomology by the $\bar\partial$ complex,

$$H^{p,q}_{\bar\partial}(X) = \frac{\ker(\bar\partial : \Omega^{p,q} \to \Omega^{p,q+1})}{\operatorname{im}(\bar\partial : \Omega^{p,q-1} \to \Omega^{p,q})}. \tag{IV.1.35}$$

For a closed Kähler manifold, meaning compact without boundary, with the usual scalar de Rham complex, Hodge theory supplies the finite-dimensional decomposition

$$H^k_{\mathrm{dR}}(X;\mathbb{C}) \cong \bigoplus_{p+q=k} H^{p,q}_{\bar\partial}(X). \tag{IV.1.36}$$

The compact, boundaryless Kähler hypothesis and trivial flat coefficient bundle are part of this cited statement. Defining $H^{p,q}$ needs a complex structure; identifying it with harmonic representatives and the de Rham decomposition needs the extra theorem and its hypotheses. In particular, this formula is not asserted for an arbitrary noncompact Hermitian space such as the preceding $\mathbb{C}^2$ example. For the compact $\mathbb{CP}^1$, the area form gives a nonzero class in $H^{1,1}$, and the degree-two de Rham class is one-dimensional. Chapter 2 will develop the wider Hodge and holonomy consequences.

IV.1.6 Moment maps and the two faces of a quotient

The chart construction started with complex scaling. A second route starts with a real level condition and removes a circle orbit. This route is useful because such a level appears as a classical zero-energy condition in a charged model. We first do the geometry, then specialize the field-theory potential; they have different premises.

On flat $\mathbb{C}^2$ take $K_{\mathrm{amb}} = |z_0|^2 + |z_1|^2$ and $J_{\mathrm{amb}} = i\sum_{a=0}^{1} dz_a \wedge d\bar z_a$. Simultaneous unit-charge rotation $z_a \mapsto e^{i\theta} z_a$ has real fundamental vector field

$$X = \sum_{a=0}^{1} \left(-y_a \frac{\partial}{\partial x_a} + x_a \frac{\partial}{\partial y_a} \right). \tag{IV.1.37}$$

Since $J_{\mathrm{amb}} = 2\sum_a dx_a \wedge dy_a$, contraction gives

$$-\iota_X J_{\mathrm{amb}} = 2\sum_a (x_a\, dx_a + y_a\, dy_a) = d\sum_a |z_a|^2, \qquad \mu = |z_0|^2 + |z_1|^2. \tag{IV.1.38}$$

This fixes the sign convention $d\mu = -\iota_X J$. It is the opposite sign and twice the flat-form size used in Cannas da Silva's native convention, where $\omega_0 = (i/2)\sum dz_a \wedge d\bar z_a$ and

$\mu_C = (1 - |z|^2)/2$. Explicitly $\mu = -2(\mu_C - 1/2)$. The signs matter when identifying the positive chamber.

Choose $\zeta > 0$. The equation $\mu = \zeta$ is the sphere S^3 of radius $\sqrt{\zeta}$ in $\mathbb{C}^2$. It is a regular level because $d\mu \neq 0$ there, and the circle acts freely because a nonzero pair cannot have a nontrivial common phase stabilizer. The compact-group symplectic reduction theorem then supplies a smooth quotient and a unique reduced form whose pullback is the restricted ambient form. Its real dimension is

$$\dim_{\mathbb{R}}(\mu^{-1}(\zeta)/U(1)) = 4 - 1 - 1 = 2. \tag{IV.1.39}$$

Each circle orbit has the projective ratio $[z_0 : z_1]$. Conversely, every projective point has a representative on the positive sphere, unique up to phase. The quotient is therefore $\mathbb{CP}^1$ as a smooth complex curve. At $\zeta = 0$ the level contains only the origin and the free-level argument fails; a negative level is empty for these charges. Neither is part of this smooth positive-level result.

The chart correspondence can be proved directly. If $z_0 \neq 0$, the ratio $w = z_1/z_0$ is constant under the circle action. At fixed w, the level equation gives $|z_0|^2 = \zeta/(1+|w|^2)$, so all remaining choices of z_0 differ only by a phase. If $z_1 \neq 0$, the same argument uses $u = z_0/z_1$. On the common region $u = 1/w$, exactly as in the atlas construction. There is no residual multiplicity because both charges are one. This also explains why $\zeta > 0$ is needed to represent every projective point on a nonzero sphere.

The dimension count contains two distinct subtractions. The level equation is one independent real constraint at a regular point, taking $\mathbb{C}^2$ from four real dimensions to a three-dimensional sphere. The free circle orbit is another real direction inside that sphere, leaving a two-dimensional real quotient. Complex scaling by $\mathbb{C}^*$ removes two real directions from the stable locus at once. A count alone would not establish smoothness or chart gluing, which is why regularity and freeness were checked first.

The reduced metric is worth deriving because merely restricting the flat potential gives the constant ζ. On U_0, put $q = 1 + |w|^2$ and choose the level section

$$s(w) = \sqrt{\frac{\zeta}{q}}(1, w), \qquad |s_0|^2 = \frac{\zeta}{q}, \quad |s_1|^2 = \frac{\zeta|w|^2}{q}. \tag{IV.1.40}$$

This section fixes a phase locally. Varying it in w has both a horizontal displacement and a vertical component along the circle orbit. The vertical direction has length squared 2ζ in our real-metric convention. Removing it from the induced real metric yields

$$ds^2_{\mathrm{red}} = \frac{2\zeta}{q^2}\, dw\, d\bar{w}, \qquad g^{\mathrm{red}}_{w\bar{w}} = \frac{\zeta}{q^2}. \tag{IV.1.41}$$

There is a compact complex-coordinate way to check the result. Represent the projective line by $v = (1, w)$ and a tangent variation by $dv = (0, dw)$. Projection orthogonal to the complex line spanned by v subtracts its component along v. The squared horizontal variation in the paired real metric is

$$ds^2_{\mathrm{red}} = 2\zeta\left(\frac{dv^\dagger dv}{v^\dagger v} - \frac{|v^\dagger dv|^2}{(v^\dagger v)^2}\right) = 2\zeta\left(\frac{dw\, d\bar{w}}{q} - \frac{|w|^2 dw\, d\bar{w}}{q^2}\right) = \frac{2\zeta}{q^2} dw\, d\bar{w}. \tag{IV.1.42}$$

The first term measures a variation of the representative; the second removes motion along the representative, including the gauge phase after the level is fixed. Their difference is invariant under rescaling the representative. This is the same subtraction performed in real polar variables below. It also explains why replacing the horizontal quotient metric by the metric induced on a chosen slice generally gives an extra angular term.

For clarity, one can see the subtraction directly in polar variables $w = re^{i\theta}$. The level section has real metric

$$ds_s^2 = 2\zeta\left(\frac{dr^2}{q^2} + \frac{r^2}{q}d\theta^2\right), \qquad g_s(\partial_\theta, X) = \frac{2\zeta r^2}{q}. \tag{IV.1.43}$$

Subtracting $g_s(\partial_\theta, X)^2/g(X,X) = 2\zeta r^4/q^2$ from the angular coefficient leaves $2\zeta r^2/q^2$, as required by (IV.1.41). The radial component was already horizontal. Equivalently, pulling back J_{amb} to the level section gives $2\zeta r\, dr \wedge d\theta/q^2$, which is the form paired with the horizontal metric. Figure IV.1.3 distinguishes the sphere, the phase orbit, and the resulting curve.

For a direct reconstruction, write $A(r) = \sqrt{\zeta/(1+r^2)}$ and $s = (A, Are^{i\theta})$. Its radial derivative has squared Hermitian norm

$$|\partial_r s|^2 = (A')^2 + (A + rA')^2 = \frac{\zeta}{(1+r^2)^2}. \tag{IV.1.44}$$

The angular derivative has squared norm $|\partial_\theta s|^2 = \zeta r^2/q$. The common-phase vector has Hermitian norm squared ζ, and its Hermitian angular product is $\zeta r^2/q$. After the factor two in the real line element is included, these give (IV.1.43). Subtracting the phase component leaves $2\zeta(dr^2 + r^2 d\theta^2)/q^2$, the polar form of (IV.1.41). The same factor two appeared in the area calculation; omitting it here would make the metric and reduced form inconsistent.

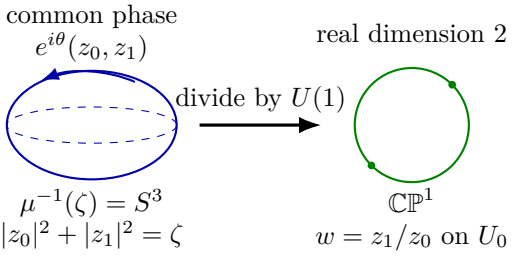


Figure IV.1.3: The same pair (z_0, z_1) is constrained to $|z_0|^2 + |z_1|^2 = \zeta > 0$. The circle arrow is the common unit-charge phase and stays within the level. Removing that orbit leaves $[z_0 : z_1] \in \mathbb{CP}^1$, with the $w = z_1/z_0$ chart shown. The figure encodes the smooth geometric reduction; it does not infer a quantum vacuum branch.

There is also a potential calculation. Along the complexified orbit of a representative $(1, w)$, let its squared scale be e^τ. Subtract the level term and extremize

$$\Phi(\tau, w) = e^\tau q - \zeta\tau, \qquad \frac{\partial\Phi}{\partial\tau} = e^\tau q - \zeta = 0, \qquad \tau = \log\frac{\zeta}{q}. \tag{IV.1.45}$$

At the stationary value, $\Phi = \zeta - \zeta \log \zeta + \zeta \log q$. The first two terms are constant, so the local reduced potential is

$$K_{\mathrm{red}} = \zeta \log(1 + |w|^2) + \text{constant}. \tag{IV.1.46}$$

This reproduces the Fubini–Study result with $\lambda = \zeta$. The level restriction $K_{\mathrm{amb}}|_{\mu=\zeta} = \zeta$ alone would have missed the quotient's metric. On U_1 the potential changes by $-\zeta \log |w|^2$, exactly as before. Holomorphically, the stable locus is $\mathbb{C}^2 \setminus \{0\}$ under common $\mathbb{C}^*$ scaling. Its two chart slices yield the same w, u transition. Including the origin in a naive orbit set $\mathbb{C}^2/\mathbb{C}^*$ adds an exceptional orbit and does not give this positive-level smooth quotient.

The extremization uses one positive real scale because the compact phase has already been divided out. Its second derivative is $e^\tau q > 0$, so the stationary point is unique on every nonzero complex orbit. The remaining w dependence is what restriction to the sphere conceals. The complexified-orbit and moment-level pictures agree here because every nonzero orbit reaches the positive level and its intersection is one circle orbit. The origin fails both properties. General gauged models require their own stable-locus and regularity checks; this example does not show that every complex orbit set is a smooth symplectic quotient.

Now specify the field-theory premise: a two-dimensional $(2, 2)$ supersymmetric classical $U(1)$ gauged linear sigma model with two charge-+1 chiral fields, no other charged fields, $W = 0$, gauge coupling $e > 0$, and positive FI parameter $r = \zeta$. The vector multiplet contains a complex scalar σ and a real auxiliary field D; the chiral multiplets have auxiliary fields F_i. Their on-shell algebraic values appear below. The nonnegative function U is the classical scalar potential, obtained after eliminating the auxiliary fields. Witten's scalar-potential convention specializes to

$$D = -e^2(\mu - \zeta), \qquad F_0 = F_1 = 0, \qquad U = \frac{e^2}{2}(\mu - \zeta)^2 + 2|\sigma|^2 \mu. \tag{IV.1.47}$$

For zero energy each nonnegative term must vanish. The first sets $\mu = \zeta > 0$; then the second forces $\sigma = 0$. Dividing by gauge phase gives precisely the positive-level $\mathbb{CP}^1$ above. At $\zeta = 3$ and $w = 2$, the level section has $q = 5$, $|z_0|^2 = 3/5$ and $|z_1|^2 = 12/5$; the reduced Hermitian coefficient is $g_{w\bar{w}} = 3/25$. This is a classical vacuum geometry of the stated model, with the specified geometric normalization.

The same numerical orbit can be described in the other chart. At $w = 2$ one has $u = 1/2$, and the reduced coefficient there is

$$g^{\mathrm{red}}_{u\bar{u}} = \frac{3}{(1 + 1/4)^2} = \frac{48}{25}, \qquad g^{\mathrm{red}}_{u\bar{u}} \left| \frac{du}{dw} \right|^2 = \frac{48}{25} \frac{1}{16} = \frac{3}{25}. \tag{IV.1.48}$$

This chart check matters because the section $s(w)$ stops being a good phase choice at $z_0 = 0$, while the quotient geometry itself remains smooth. The reduced form is the $\lambda = 3$ Fubini–Study form, so its period is 6π in the declared geometric units. The value follows from the level that fixed the sphere radius, not from an independently specified string-scale area. A physical FI parameter in another convention must be translated with both the moment-map sign and the real-metric normalization.

The distinction from Witten's full pG construction is substantial. That model has n charge-one fields s_i, a charge-$-n$ field p, and $W = pG(s)$ with G homogeneous of degree n. The charges of p and $G(s)$ cancel, so W is gauge invariant and $G = 0$ defines a projective hypersurface. Its positive-level D quotient is the total space of $\mathcal{O}(-n)$ over $\mathbb{CP}^{n-1}$; setting $p = 0$ selects its zero section. The F equations further constrain the vacuum. For instance, at $n = 2$, $G = s_0^2 + s_1^2$, $r = 1$, and $(s_0, s_1, p) = (1, 0, 0)$, the D equation holds but $F_p = G = 1$. Thus D-flatness is not enough to identify a vacuum of that full model. Nor does the equality $\lambda = \zeta$ in our chosen geometric units fix a physical distance or the coefficient in Witten's printed real metric, which uses a different overall real-metric convention. Quantum or infrared equivalence to any string construction requires separate evidence.

The full model illustrates how quickly the answer changes when the field content changes. For charges $(1, \ldots, 1, -n)$, the D equation takes the form

$$\sum_{i=0}^{n-1} |s_i|^2 - n|p|^2 = r. \tag{IV.1.49}$$

At $r > 0$, some s_i must be nonzero. Under complexified scaling, s_i have weight one and p has weight $-n$. After the projective base coordinate $[s_0 : \cdots : s_{n-1}]$ is chosen, the transition law of p is that of a fiber of $\mathcal{O}(-n)$. This is why the positive-level D quotient is larger than its projective zero section. The additional superpotential $W = pG(s)$ gives

$$F_p = G(s), \qquad F_{s_i} = p\,\partial_{s_i} G(s). \tag{IV.1.50}$$

At $p = 0$ the second family vanishes, but the first still imposes $G(s) = 0$. The D quotient, the zero section, and the zero-energy vacuum are therefore three different sets in this model. The numerical $n = 2$ point above makes the distinction visible without relying on a general phase theorem.

The two-field $W = 0$ example has no extra F constraints. Witten's printed real metric omits our factor two, so its kinetic coefficient requires a translation before comparison with ζ.

IV.1.7 Exercises

Use `benchmark/tasks.json` for the public IDs and schemas, and submit through `benchmark/PROTOCOL.md`. The JSON payload is a direct object with the named fields in the chosen schema, without an answer envelope. E5 is written reasoning only. The checker evaluates the declared short-answer fields, not the written explanations.

1. For $\mathbb{CP}^1$ with $\lambda = 3/2$, $w = Z_1/Z_0$ and $u = 1/w$, calculate du/dw at $w = 2$, $g_{w\bar{w}}$ there, and $g_{u\bar{u}}$ at $u = 1/2$. Verify the tensor transformation rather than copying one coefficient. Submit the three exact rational strings in task FI-III-1-E1.

2. On $\mathbb{C}^2$ take $g_{1\bar{1}} = 1$, $g_{2\bar{2}} = 1 + 2|z^1|^2$, and zero off-diagonal entries. At $z^1 = 1 + i$, calculate $g_{2\bar{2}}$ and the real and imaginary parts of $\partial_{z^1} g_{2\bar{2}}$. Decide whether the Hermitian form is Kähler and identify the obstructing component of dJ. Submit task FI-III-1-E2.

3. For $K = (5/3)\log(1+|w|^2)$ on $\mathbb{CP}^1$, find $g_{w\bar{w}}$ and the coefficient $\rho_{w\bar{w}}$ of $i\,dw\wedge d\bar{w}$ at $w=1$. Integrate radially to obtain $\int J/\pi$ and $\int \rho/(2\pi)$. Explain why only the first depends on λ. Submit task FI-III-1-E3.

4. In the separate classical $U(1)$ model with two charge-one fields and $W=0$, use $d\mu = -\iota_X J$ and $J = i\sum_a dz_a\wedge d\bar{z}_a$. At $\mu=3$ and $w=z_1/z_0=2$, find $|z_0|^2$, $|z_1|^2$, $g_{w\bar{w}}$ and the real dimension of the smooth quotient. Derive $\sigma=0$ from the potential, explain the horizontal metric and level-subtracted potential, and distinguish this model from Witten's full pG model and from the orbit set that includes the origin. Submit task FI-III-1-E4.

5. Derive $N^2=(a^2+bc)\mathbf{1}$ for the trace-zero matrix in (IV.1.8). Locate the singular point of $a^2+bc=0$ from its gradient and explain in writing why this local equation does not classify Nahm moduli spaces. This is a written task, FI-III-1-E5.

IV.1.8 Take-home message

Take-home message

A complex curve needs holomorphic transitions, not just one ratio. A positive Hermitian metric becomes Kähler when its associated $(1,1)$ form is closed. For the two-chart Fubini–Study metric on $\mathbb{CP}^1$, $\int J = 2\pi\lambda$ and $\int \rho/(2\pi) = 2$. The separate two-charge-one classical model at $W=0$ and $\zeta>0$ has a smooth circle quotient with $K_{\mathrm{red}} = \zeta\log(1+|w|^2)$, so $\lambda=\zeta$ in the declared geometric units. These operations equip a compact curve with coordinates, area and curvature. They do not identify a quantum branch or a brane-distance parameter.

The reader should now be able to transform tensors across the $\mathbb{CP}^1$ overlap, test Kähler closure, compute a period and first Chern number in fixed units, derive a free regular circle quotient, and distinguish a local singular affine equation from a smooth chart. These are the prerequisites for the Calabi–Yau, ADE-resolution, and toric/GLSM constructions of Chapters 2–4.

Status and sources

Complex coordinates as a geometric atlas. Ballmann's complex-atlas and Newlander–Nirenberg statements are at Ballmann n.d., PDF p. 23, eqs. (2.4)–(2.5); the theorem is cited for sufficiently smooth almost-complex structures, with its tensor test deferred. The two $\mathbb{CP}^1$ charts, their overlap Jacobian, and the rank-two nilpotent cone's gradient and tangent-space test are explicit local calculations [MATH]. The cone equation supplies no Nahm boundary conditions or global moduli statement.
Hermitian data and the Kähler condition. Ballmann's Hermitian pairing and local-potential statement are at Ballmann n.d., PDF pp. 48–55. In the paired convention $ds^2 = 2g_{a\bar{b}}dz^a d\bar{z}^{\bar{b}}$ and $J = ig_{a\bar{b}}dz^a\wedge d\bar{z}^{\bar{b}}$, the displayed nonclosed positive metric and its nonzero dJ component are calculated here [MATH]. The general local-potential result is cited, not established by that example.

The Fubini–Study line from charts to area. Ballmann's projective example appears at Ballmann n.d., PDF pp. 49–50, eqs. (4.12)–(4.13); Cannas da Silva's comparison appears at Cannas da Silva n.d., PDF pp. 104–106. Cannas's native form is half our $\lambda = 1$ form, with area π. The chart gluing and $\int_{\mathbb{CP}^1} J = 2\pi\lambda$ are derived in the displayed convention [MATH]. This geometric period alone does not calibrate a string modulus.
Ricci form, first Chern class, and Hodge notation. The Ricci/Chern–Weil identification is sourced to Ballmann n.d., PDF pp. 62–63, eqs. (4.64)–(4.66); the $\mathbb{CP}^1$ differentiation and integral giving two are explicit [MATH]. The global Chern–Weil theorem remains cited for the smooth complex tangent bundle and equality in real de Rham cohomology; Ballmann n.d., PDF p. 137, Remark A.37 distinguishes real from integral Chern classes. The scalar, trivial-coefficient Hodge decomposition is cited from Ballmann n.d., PDF p. 74, Theorem 5.32 only for compact Kähler manifolds without boundary; no Hodge theorem is proved here.
Moment maps and the two faces of a quotient. The regular-level reduction theorem and projective examples are in Cannas da Silva n.d., PDF pp. 141–142, 149, 176. Her flat form is $i\sum dz_a \wedge d\bar{z}_a/2$ and her moment-map sign is opposite ours; thus $\mu = -2(\mu_C - 1/2)$. The positive regular level, horizontal metric, extremized reduced potential, and numerical overlap are calculated here [MATH]. Witten's two-dimensional $(2,2)$ scalar potential and full pG model are in Witten 1993, PDF pp. 16–18, 44–47, eqs. (3.1)–(3.2). The two-charge-one, $W = 0$ classical model is a separately specified physical premise, not an independently derived equivalence to Witten's full model or to a brane construction. Conditional on that potential, its zero-energy equations give $\mu = \zeta > 0$, $\sigma = 0$, and the regular $\mathbb{CP}^1$ quotient [MATH]. No quantum/infrared equivalence, brane-probe identity, or FI-to-distance calibration is supplied.
Exercises. E1–E4 check the stated chart, closure, curvature, and classical-potential calculations; E5 asks for written reasoning about the rank-two cone. The short-answer checker grades the declared fields only.

References

Ballmann, W. (n.d.). *Lectures on Kähler Manifolds*. Lecture notes, edition consulted 2026-10-15; `https://people.maths.ox.ac.uk/joyce/Nairobi2019/BallmannKahlerManifolds.pdf`.

Cannas da Silva, A. (n.d.). *Lectures on Symplectic Geometry*. Author-hosted lecture notes, edition consulted 2026-10-15; `https://www.math.ist.utl.pt/~acannas/Books/symplectic.pdf`.

Witten, E. (1993). "Phases of $N = 2$ Theories In Two Dimensions". In: *Nuclear Physics B* 403, pp. 159–222. arXiv: `hep-th/9301042`.

Chapter IV.2

Calabi–Yau manifolds: holonomy, moduli, Hodge structure

IV.2.1 A compact space and a cone

Suppose the six internal directions of a ten-dimensional string background form a compact Kähler manifold. Its local metric determines a Ricci form, but a supersymmetry parameter has to return to itself after transport around every loop. A holomorphic volume form must likewise be defined on the whole space, not merely in one chart. Those are three different tests. The contrast becomes visible on a flat torus and on a freely acting quotient of that torus: both are Ricci-flat, while the quotient loses its global holomorphic top form.

Brane constructions also meet noncompact Calabi–Yau cones. A cone has a radial direction, a compact link, and a Reeb flow that grades holomorphic functions; for irrational weights its orbits need not close. Its character can measure link volume under geometric hypotheses. Neither compact Ricci-flat existence nor physical supersymmetry follows from that character. We will develop the compact and cone routes with the same habit: name the condition actually used, calculate it on a simple object, and then identify the additional hypothesis needed for a physical conclusion.

Chapter 1 supplied the Kähler form and Ricci conventions. The present chapter turns them into global holonomy, deformation, Hodge, and cone data. Chapter 3 will revisit quotient singularities; Chapters 4 and 11 will use the grading and periods respectively.

IV.2.2 From the Ricci form to a global volume form

When does a compact Kähler space support the geometric data sought in a supersymmetric compactification? Let X be a connected complex n-fold with complex structure I.

Its canonical bundle $K_X = \Lambda^n T^{*(1,0)}X$ has local frame $dz^1 \wedge \cdots \wedge dz^n$. A holomorphic trivialization means a nowhere-vanishing holomorphic section Ω of this bundle. It is stronger than a vanishing first Chern class in real cohomology. We retain the Chapter 1 convention

$$ds^2 = 2g_{a\bar{b}}dz^a d\bar{z}^{\bar{b}}, \qquad J = ig_{a\bar{b}}dz^a \wedge d\bar{z}^{\bar{b}}, \qquad dJ = 0. \tag{IV.2.1}$$

The Ricci form of this Kähler metric is

$$\rho = -i\partial\bar{\partial}\log\det(g_{a\bar{b}}), \qquad [\rho/(2\pi)] = c_1(TX)_{\mathbb{R}} = -c_1(K_X)_{\mathbb{R}}. \tag{IV.2.2}$$

The last equality concerns real de Rham classes. It cannot detect a flat bundle with a finite nontrivial holomorphic transition character. In a holomorphic coordinate change $z \mapsto w$, a top-form frame changes by $\det(\partial w/\partial z)$. Equation (IV.2.2) measures the curvature of the induced canonical connection, while that transition determinant also records its global gluing.

The compact existence theorem has precise input. On a closed connected Kähler manifold, choose a Kähler class $[J]$ and a real closed $(1,1)$ form representing $2\pi c_1(TX)$. The Calabi–Yau theorem gives a unique Kähler metric in that class whose Ricci form is the chosen form. In particular, when $c_1(TX)_{\mathbb{R}} = 0$, we may choose the target form to be zero and obtain

$$c_1(TX)_{\mathbb{R}} = 0, \quad [J] \text{ fixed} \quad \Longrightarrow \quad \rho(J_{\mathrm{RF}}) = 0, \quad [J_{\mathrm{RF}}] = [J]. \tag{IV.2.3}$$

This is a cited compact theorem, not a solution of its nonlinear Monge–Ampère equation here. Its uniqueness is within the selected complex structure and Kähler class. The theorem does not apply directly to an affine singularity or an incomplete noncompact metric.

Parallel transport along contractible loops generates the restricted holonomy $\mathrm{Hol}^0(g)$; transport along all loops generates the full group $\mathrm{Hol}(g)$. For a Kähler metric, holonomy starts inside $U(n)$. Its determinant acts on K_X, and the determinant connection has curvature proportional to ρ. Consequently

$$\rho = 0 \quad \Longleftrightarrow \quad \mathrm{Hol}^0(g) \subseteq SU(n). \tag{IV.2.4}$$

Flat curvature removes infinitesimal determinant rotation. It need not remove a finite determinant acquired around a noncontractible loop. If K_X has a nowhere-vanishing holomorphic Ω on compact Ricci-flat Kähler X, the Bochner argument makes Ω parallel, and then $\mathrm{Hol}(g) \subseteq SU(n)$. Conversely, full holonomy contained in $SU(n)$ fixes a nonzero top tensor; parallel transport carries it to a global parallel complex top form. Even this inclusion need not be equality: a flat complex torus has trivial holonomy, and $K3 \times T^2$ has smaller product holonomy than $SU(3)$. Exact $SU(n)$ holonomy needs further irreducibility and exclusion of smaller special holonomy.

An explicit free quotient tests the global step. Take a square product torus

$$T = \mathbb{C}^2/(\mathbb{Z} + i\mathbb{Z})^2, \qquad g(z_1, z_2) = (-z_1, z_2 + \tfrac{1}{2}), \qquad g^2 = 1 \text{ on } T. \tag{IV.2.5}$$

The translation in z_2 makes g free: a fixed point would require $1/2$ to be a lattice element. Thus $X = T/\langle g\rangle$ is a smooth compact flat Kähler manifold. On the cover, $\Omega_T = dz_1 \wedge dz_2$, but

$$g^*\Omega_T = (-dz_1) \wedge dz_2 = -\Omega_T. \tag{IV.2.6}$$

Any holomorphic top form on T has constant coefficient, so no nonzero one is invariant and descends. The quotient has $\rho = 0$ and $\mathrm{Hol}^0 = \{1\}$, yet its full holonomy includes a determinant -1 element and its holomorphic canonical bundle has order two. It is useful to check the topological claim more carefully. In real coordinates $z_2 = x_2 + iy_2$, the smooth nowhere-zero form

$$\widetilde{\Omega} = e^{2\pi i x_2}\, dz_1 \wedge dz_2, \qquad g^*\widetilde{\Omega} = (-1)(-1)\widetilde{\Omega} = \widetilde{\Omega} \tag{IV.2.7}$$

descends as a smooth canonical section. It is not holomorphic. Hence $c_1(K_X) = 0$ even integrally in this example, despite the nontrivial holomorphic bundle. The example distinguishes holomorphic triviality from both real and integral Chern-class vanishing; it is not an example of nonzero integral torsion.

Figure IV.2.1 keeps these implications distinct. The flat torus has Ω and trivial holonomy; K3 has a global holomorphic two-form and, for its Ricci-flat metric, $SU(2)$ holonomy; the free quotient blocks the descent of Ω. The next section asks which of these geometric distinctions a spinor can see. Chapter 3 will revisit finite actions with fixed points, where even smoothness of the quotient must be checked separately.

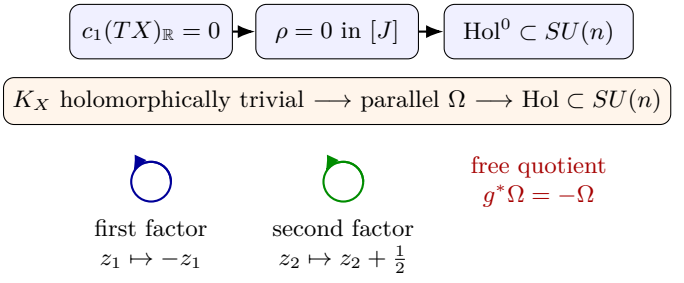


Figure IV.2.1: Curvature and global transport test different data. The horizontal implication uses the compact Kähler theorem in a fixed class; the vertical branch needs a globally defined holomorphic top form. The free affine quotient of the flat torus has zero Ricci form but a sign around its quotient loop. The arrows show the involution on both torus factors; the half shift makes the quotient action free.

IV.2.3 Top forms, quotient weights and invariant spinors

Which part of a diagonal quotient can be calculated before solving a compactification? Let $\omega_k = e^{2\pi i/k}$ and let the generator act on $\mathbb{C}^n$ by $z_a \mapsto \omega_k^{a_a} z_a$, where the integers a_a are understood modulo k. Differentiating each coordinate gives

$$g^*(dz_1\wedge\cdots\wedge dz_n) = \omega_k^{\sum_a a_a}(dz_1\wedge\cdots\wedge dz_n), \qquad g \in SU(n) \iff \sum_a a_a \equiv 0 \pmod{k}. \tag{IV.2.8}$$

The second statement concerns this unitary diagonal representation. It says a local top form is invariant on the smooth quotient locus. It does not make the affine quotient smooth: a scalar action fixes the origin. Nor does it choose a spin structure on a later compact global space.

For a specified subgroup $\Gamma \subset SU(n)$ and its canonical $SU(n)$ spin lift, the complex spin module has the exterior-algebra realization

$$S \simeq \bigoplus_{p=0}^{n} \Lambda^p \mathbb{C}^n, \qquad S^+ = \bigoplus_{p \text{ even}} \Lambda^p \mathbb{C}^n, \quad S^- = \bigoplus_{p \text{ odd}} \Lambda^p \mathbb{C}^n. \tag{IV.2.9}$$

Its basis vector $e_A = e_{a_1} \wedge \cdots \wedge e_{a_p}$ is indexed by a subset $A \subset \{1, \ldots, n\}$. Under the diagonal action it acquires phase $\omega_k^{\sum_{a \in A} a_a}$. Therefore the count of invariant complex components in each chirality is the finite enumeration

$$N_\pm = \#\{A \subset \{1, \ldots, n\} : \sum_{a \in A} a_a \equiv 0 \pmod{k}, \quad |A| \text{ even/odd}\}. \tag{IV.2.10}$$

This counts components in the chosen lift. A different allowed lift can multiply a generator by -1, when compatible with the group relation, changing which subsets are invariant. A global parallel spinor must also survive the full lifted holonomy of a genuine spin bundle.

For the scalar $\mathbb{Z}_3$ action with weights $(1, 1, 1)$, the invariant subsets are $\varnothing$ and $\{1, 2, 3\}$, since subset sums of sizes one and two are one and two modulo three. Thus

$$(a_1, a_2, a_3) = (1, 1, 1) \pmod 3, \qquad \sum a_a = 3 \equiv 0, \qquad (N_+, N_-) = (1, 1). \tag{IV.2.11}$$

The action is effective and has an isolated fixed point at the affine origin. For the $SU(2)$ subgroup embedded in $SU(3)$ with $\mathbb{Z}_4$ weights $(1, 3, 0)$, the invariant subsets are $\varnothing, \{3\}, \{1, 2\}, \{1, 2, 3\}$. Their parities split evenly:

$$(1, 3, 0) \pmod 4, \qquad \sum a_a = 4 \equiv 0, \qquad (N_+, N_-) = (2, 2). \tag{IV.2.12}$$

The zero-weight coordinate is a fixed complex line, so the quotient singular locus differs from the isolated scalar case. The action $(1, 1, 2)$ modulo four illustrates a separate failure: $\sum a_a = 4$ actually preserves the top form, whereas $(1, 1, 1)$ modulo four has determinant phase ω_4^3 and fails it. One must compute the determinant with the actual modulus rather than infer it from a familiar-looking list of weights.

To connect the geometric count with a physical question, specify a ten-dimensional $N = 1$ heterotic product background: unwarped four-dimensional Minkowski space times a smooth compact internal six-manifold, zero flux in the stated specialization, and constant dilaton. A candidate supersymmetry parameter is an external spinor tensored with an internal parallel spinor. Under the standard real ten-dimensional Majorana–Weyl reduction, the $SU(3)$, $SU(2)$-embedded, and trivial-holonomy cases above supply respectively one, two, and four candidate four-dimensional Weyl parameters, or

$$N_{\text{internal}} = 1, 2, 4 \quad \longmapsto \quad Q_{\text{geom}} = 4, 8, 16 \text{ real four-dimensional charges.} \tag{IV.2.13}$$

The first two affine quotients provide the representation count, not themselves smooth compact solutions. To saturate these numbers physically, a smooth global spin lift and the full background are needed. In particular every counted η must satisfy the gaugino condition

$$\nabla_m \eta = 0, \qquad F_{mn}\Gamma^{mn}\eta = 0, \tag{IV.2.14}$$

and the chosen gauge field and background must obey the appropriate anomaly and Bianchi consistency conditions. A gauge bundle can remove candidates. Equation (IV.2.13) is therefore a geometric upper bound in this physical specialization, not an unconditional vacuum count. Type-II and eleven-dimensional charge counts require their own premises. The same warning applies to the affine torus quotient in the preceding section: its determinant character already prevents the naive inference of a global top-form spinor from $\rho = 0$.

Figure IV.2.2 makes the two subset enumerations visible. Chapter 3 will use the same quotient weights to describe fixed loci, while Chapter II.4 supplies a fuller spinor toolkit.

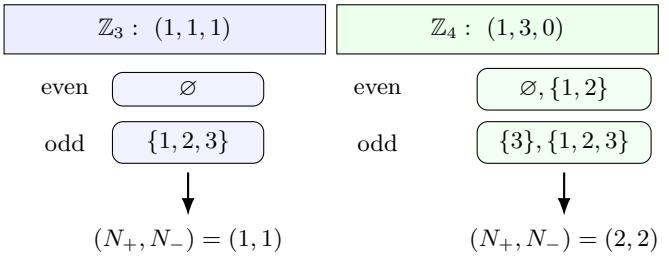


Figure IV.2.2: The canonical $SU(3)$ lift grades exterior basis states by subset size. For the scalar $\mathbb{Z}_3$, only the empty and full subsets survive. For weights $(1,3,0)$ modulo four, the unchanged third direction doubles the invariant pair. The boxes show a local representation calculation; the physical background and global spin lift remain separate.

IV.2.4 Complex and Kähler directions in familiar spaces

What can change while the manifold remains Kähler with a trivial holomorphic canonical bundle? Two elementary changes already appear on a marked two-torus: its complex shape changes, and its area changes. Write $z = x + \tau y$ with x, y periodic modulo one and $\operatorname{Im}\tau > 0$. A flat metric of area $A > 0$ is

$$ds^2 = \frac{A}{\operatorname{Im}\tau}|dx + \tau dy|^2, \qquad J = A\, dx \wedge dy. \tag{IV.2.15}$$

The Hermitian coefficient in the convention of (IV.2.1) is $g_{z\bar{z}} = A/(2\operatorname{Im}\tau)$. The associated form is $ig_{z\bar{z}}dz \wedge d\bar{z} = A\, dx \wedge dy$, since $i\, dz \wedge d\bar{z} = 2\operatorname{Im}\tau\, dx \wedge dy$. Thus the

two formulas carry the same area normalization. Expanding the real line element gives

$$(g_{\mathbb{R}}) = \frac{A}{\operatorname{Im}\tau}\begin{pmatrix} 1 & \operatorname{Re}\tau \\ \operatorname{Re}\tau & |\tau|^2 \end{pmatrix}, \quad \det g_{\mathbb{R}} = A^2, \quad \int_{T^2} J = A. \tag{IV.2.16}$$

At $A = 7/3$ and $\tau = 1/2 + 2i$, the prefactor is $7/6$, so

$$(g_{xx}, g_{xy}, g_{yy}) = (7/6, 7/12, 119/24), \qquad \det g_{\mathbb{R}} = \frac{7}{6}\frac{119}{24} - \left(\frac{7}{12}\right)^2 = \frac{49}{9}. \tag{IV.2.17}$$

The determinant gives $\sqrt{\det g} = A$ on the unit coordinate square in (x, y). Its image under $z = x + \tau y$ is the parallelogram spanned by 1 and τ in the complex z-plane. That drawing has Euclidean area $\operatorname{Im}\tau$, while the metric factor $A/\operatorname{Im}\tau$ converts it to metric area A. Changing A scales the metric at fixed complex chart; changing τ shears the marked parallelogram and changes complex shape at fixed area. Modular changes of the marked lattice can describe the same unmarked torus. A string compactification also has a B field and other data; this metric example isolates the two geometric directions.

The general infinitesimal complex-structure question uses the holomorphic tangent bundle TX. A first-order deformation is represented by a class $[\mu] \in H^1(X, TX)$, locally a $(0,1)$ form valued in $(1,0)$ vectors. If K_X is holomorphically trivial and Ω is its nowhere-zero section, contraction lowers one holomorphic degree:

$$\mu = \mu^a{}_{\bar{b}}\, d\bar{z}^{\bar{b}} \otimes \partial_a \quad \longmapsto \quad \mu \lrcorner \Omega \in \Omega^{n-1,1}(X), \qquad H^1(X, TX) \simeq H^{n-1,1}(X). \tag{IV.2.18}$$

The final isomorphism is the compact Kähler cohomological identification under the stated trivialization. In a local frame $\Omega = f\, dz^1 \wedge \cdots \wedge dz^n$, the contraction removes dz^a with sign $(-1)^{a-1}$ and inserts $d\bar{z}^{\bar{b}}$. Because f never vanishes, the operation is invertible on bundles. This linear algebra explains the tangent-space count. It does not solve the nonlinear deformation equation.

For smooth compact Kähler X with holomorphically trivial K_X, the local Bogomolov–Tian–Todorov statement says the Kuranishi base is unobstructed near the given complex structure: sufficiently small infinitesimal complex deformations occur in actual local families. We cite Popovici's published Theorem 1.2 at precisely this compact Kähler specialization. Its theorem is stated for compact Calabi–Yau $\partial\bar{\partial}$ manifolds; compact Kähler manifolds satisfy the required $\partial\bar{\partial}$ condition. The theorem includes the nonlinear existence and local convergence missing from (IV.2.18). It says nothing by itself about continuation to arbitrary finite distance, singular quotients, or a smooth global coarse moduli space.

At fixed complex structure, Kähler forms move differently. Their cohomology classes lie in the open Kähler cone

$$\mathcal{K}_X = \{[J] \in H^{1,1}(X, \mathbb{R}) : [J] \text{ contains a positive closed } (1,1) \text{ form}\}. \tag{IV.2.19}$$

Its tangent dimension is $h^{1,1}$, but the entire vector space is not positive: on a compact curve C, a Kähler class obeys $\int_C J > 0$. The class $-[J]$ gives a direct counterexample. The compact Ricci-flat theorem assigns a metric to each class in this cone when its real Chern hypothesis holds; varying the class is not the fixed-class uniqueness statement.

K3 exposes another common conflation. For a marked smooth K3 surface, $H^2(K3,\mathbb{R})$ has intersection signature $(3,19)$. The real and imaginary parts of its holomorphic two-form span an oriented positive two-plane P; the period line obeys

$$[\Omega]^2 = 0, \qquad [\Omega]\cdot[\bar{\Omega}] > 0, \qquad P = \mathrm{span}_{\mathbb{R}}\{\mathrm{Re}\,\Omega, \mathrm{Im}\,\Omega\}. \tag{IV.2.20}$$

For a Ricci-flat hyperkähler metric, the Kähler class supplies a positive direction orthogonal to that chosen complex period plane. The self-dual three-plane $\Pi = \mathrm{span}_{\mathbb{R}}\{\mathrm{Re}\,\Omega, \mathrm{Im}\,\Omega, J\}$, together with a separate positive scale, describes metric data in this marked setting. Rotating the complex structure within a fixed hyperkähler metric changes which two-plane is called the complex period plane; it need not change the metric three-plane. These are different moduli questions, and neither treats all of $H^{1,1}(K3,\mathbb{R})$ as positive. Figure IV.2.3 contrasts this geometry with the torus area and shape. Mirror geometry in Chapter 11 will compare complex and Kähler directions after additional string data are included.

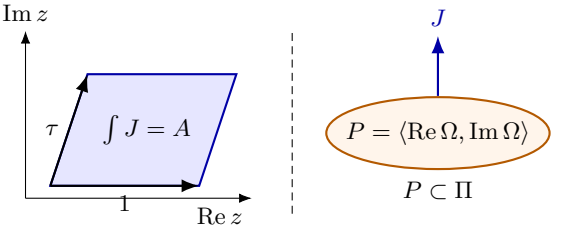


Figure IV.2.3: Left: the unit-period (x,y) square maps under $z = x + \tau y$ to the $1,\tau$ parallelogram in the complex plane. Its Euclidean area is $\mathrm{Im}\,\tau$ and its metric area is A. Right: on a marked K3, $\mathrm{Re}\,\Omega$ and $\mathrm{Im}\,\Omega$ span a positive two-plane; adjoining a compatible Kähler direction gives a metric positive three-plane, with scale recorded separately. The diagram indicates types of data, not a globally fixed coordinate chart on either moduli space.

IV.2.5 Hodge structure and a quintic count

Can one count geometric deformation directions without writing an explicit Ricci-flat metric? On a compact Kähler manifold, complex cohomology decomposes by type, $H^k(X,\mathbb{C}) = \bigoplus_{p+q=k} H^{p,q}(X)$, with $h^{p,q} = \dim H^{p,q}$. For a smooth compact threefold with holomorphically trivial K_X, the top form occupies $H^{3,0}$ and its conjugate occupies $H^{0,3}$. The Hodge symmetries give

$$h^{3,0} = h^{0,3} = 1, \qquad h^{p,q} = h^{q,p} = h^{3-p,3-q}, \qquad \chi(X) = 2\big(h^{1,1} - h^{2,1}\big) \tag{IV.2.21}$$

for the usual connected Calabi–Yau threefold setting with $h^{1,0} = h^{2,0} = 0$. The vanishing conditions matter: a complex three-torus also has trivial canonical bundle but a different Hodge diamond.

Let $Q \subset \mathbb{P}^4$ be a smooth degree-five hypersurface and let H be the hyperplane class restricted to Q. Adjunction uses $K_{\mathbb{P}^4} = \mathcal{O}(-5)$ and the normal bundle $N_{Q/\mathbb{P}^4} = \mathcal{O}(5)|_Q$:

$$K_Q = (K_{\mathbb{P}^4} \otimes \mathcal{O}(5))|_Q \simeq \mathcal{O}_Q, \qquad c(TQ) = \frac{(1+H)^5}{1+5H}. \tag{IV.2.22}$$

The first equality gives a holomorphically trivial canonical bundle, not an explicit metric. To see the Euler number, expand the total Chern class through degree three. The inverse denominator is $1 - 5H + 25H^2 - 125H^3 + \cdots$, so

$$c(TQ) = (1+5H+10H^2+10H^3)(1-5H+25H^2-125H^3)+\cdots = 1+10H^2-40H^3+\cdots . \tag{IV.2.23}$$

Because $[Q] = 5H$ in $\mathbb{P}^4$, $\int_Q H^3 = \int_{\mathbb{P}^4} 5H^4 = 5$. The top Chern number is therefore

$$\chi(Q) = \int_Q c_3(TQ) = -40 \int_Q H^3 = -200. \tag{IV.2.24}$$

This is a topological calculation; it neither constructs nor approximates the Ricci-flat metric guaranteed for each Kähler class by the compact theorem.

The complex-deformation count starts with polynomial coefficients. Degree-five homogeneous monomials in five variables number $\binom{9}{4} = 126$. Multiplying the defining equation by a nonzero scalar changes no hypersurface, and a generic projective coordinate transformation contributes $\dim PGL(5) = 25 - 1 = 24$ redundant directions. Hence the polynomial family has

$$126 - 1 - 24 = 101 \quad \text{independent polynomial directions.} \tag{IV.2.25}$$

Why identify this count with $h^{2,1}$? Restricting the ambient tangent bundle to Q, the normal sequence and its cohomology sequence contain

$$\begin{gathered} 0 \longrightarrow TQ \longrightarrow T\mathbb{P}^4|_Q \longrightarrow \mathcal{O}_Q(5) \longrightarrow 0, \\ H^0(Q,TQ) \longrightarrow H^0(Q,T\mathbb{P}^4|_Q) \longrightarrow H^0(Q,\mathcal{O}_Q(5)) \longrightarrow H^1(Q,TQ) \longrightarrow H^1(Q,T\mathbb{P}^4|_Q). \end{gathered} \tag{IV.2.26}$$

For a smooth generic quintic, the cited cohomological inputs are $H^0(Q,TQ) = 0$ and $H^1(Q,T\mathbb{P}^4|_Q) = 0$, together with $h^0(Q,\mathcal{O}_Q(5)) = 125$ and $h^0(Q,T\mathbb{P}^4|_Q) = 24$. Exactness therefore gives $H^1(Q,TQ) \simeq H^0(Q,\mathcal{O}_Q(5))/H^0(Q,T\mathbb{P}^4|_Q)$ and dimension $125 - 24 = 101$. The first vanishing excludes infinitesimal automorphisms; it does not exclude all finite automorphisms. Contraction with Ω identifies this space with $H^{2,1}(Q)$. The cited cohomology bridge, rather than subtraction alone, shows that these polynomial directions exhaust the abstract first-order deformations. Independently, the Lefschetz hyperplane theorem gives $h^{1,1}(Q) = 1$. We obtain

$$h^{2,1}(Q) = 101, \qquad h^{1,1}(Q) = 1, \qquad 2(1-101) = -200 = \chi(Q). \tag{IV.2.27}$$

The last equality checks the two routes against each other. It is not used as a substitute for the normal-sequence bridge or Lefschetz input. The resulting middle cohomology has $b_3 = 2 + 2h^{2,1} = 204$, giving a sizeable period space even though $h^{1,1} = 1$.

Figure IV.2.4 separates the coefficient arithmetic from the cited cohomological step. Periods refine the numerical Hodge data. In a smooth proper holomorphic family X_t of compact Kähler threefolds, choose a local marking and a nowhere-zero relative holomorphic top form $\Omega(t)$. The groups $H^3(X_t, \mathbb{Z})$ form a Gauss–Manin local system; quotienting torsion gives the lattice embedded in complex cohomology. Choose a local parallel basis $\{\gamma_I\}$ of the free part of integral three-cycle homology and integrate the varying form (torsion cycles have zero periods):

$$\Pi_I(t) = \int_{\gamma_I} \Omega(t), \qquad \nabla_{\partial_t}\Omega \in H^{3,0}(X_t) \oplus H^{2,1}(X_t). \tag{IV.2.28}$$

The second inclusion is a statement in complex cohomology using the Gauss–Manin connection: the first-order variation of Hodge structure. It can also be seen locally: differentiating the changing complex structure inserts one antiholomorphic index into a three-form, precisely the contraction in (IV.2.18), while rescaling Ω contributes the $(3,0)$ part. A cycle basis is locally fixed by the Gauss–Manin connection, but transport around a loop in parameter space may return a different integral basis. Thus periods vary and can have monodromy even where the Hodge numbers stay constant. This bounded framework is the starting point for Chapter 11 and later topological sectors; an explicit mirror map or worldsheet vacuum statement does not follow from the Hodge diamond alone.

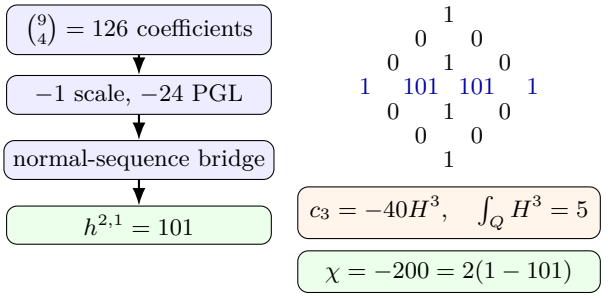


Figure IV.2.4: The smooth quintic's two counts meet at $h^{2,1} = 101$: homogeneous coefficients are divided by equation rescaling and projective automorphisms, with a separate normal-sequence cohomology step; adjunction and $\int_Q H^3 = 5$ give $\chi = -200$. The diagram labels the logical bridge rather than treating subtraction as a proof of the cohomological claim.

IV.2.6 The cone, its link and the Reeb charge

What geometric data replace compactness near a brane at a singularity? A Kähler metric cone has a radial coordinate $r > 0$ and a compact link Y with

$$C(Y) \setminus \{o\} = \mathbb{R}_{>0} \times Y, \qquad ds_C^2 = dr^2 + r^2 ds_Y^2, \qquad \xi = I(r\partial_r). \tag{IV.2.29}$$

The Reeb field ξ is tangent to Y and rotates holomorphic functions. This is geometric data on the smooth cone locus; the vertex may be singular. Ricci-flatness alone implies only $\mathrm{Hol}^0 \subseteq SU(n)$. For the Calabi–Yau/Gorenstein cone framework used below, additionally assume a globally nowhere-zero holomorphic top form Ω on that smooth locus and choose the homogeneous normalization $\mathcal{L}_\xi \Omega = in\Omega$ in complex dimension n. The link is Sasaki–Einstein when the cone metric is Ricci-flat. These metric assertions require an actual metric and cannot be inferred from a graded coordinate ring alone.

For $\mathbb{C}^n$ choose $z_a = r_a e^{i\phi_a}$ and positive coordinate Reeb weights b_a. Acting on holomorphic functions, $Q_\xi(z_a) = b_a$ and $\mathcal{L}_\xi z_a = ib_a z_a$. Since the exterior derivative commutes with Lie differentiation, each dz_a has the same charge:

$$\Omega = dz_1 \wedge \cdots \wedge dz_n, \qquad \mathcal{L}_\xi \Omega = i\Big(\sum_{a=1}^{n} b_a\Big)\Omega, \qquad \sum_a b_a = n. \tag{IV.2.30}$$

For the flat metric the Reeb field has $b_a = 1$, so the threefold top form has charge three and the fourfold top form charge four. A nonunit positive vector can define a grading and a compatible Sasakian deformation, but its top-form normalization alone does not say it is the Reeb field of a Ricci-flat cone. The weights approaching zero reach a boundary at which the positive grading and finite-volume description fail.

The link of flat $\mathbb{C}^n$ at $r = 1$ is S^{2n-1}. The cone curvature identity is transparent from the warped metric: tangential Ricci curvature of the link enters $\mathrm{Ric}_C\,|_{TY}$ as $\mathrm{Ric}_Y - (2n-2)g_Y$. Thus a Ricci-flat cone requires

$$\mathrm{Ric}_C = 0 \quad \Longrightarrow \quad \mathrm{Ric}_Y = 2(n-1)g_Y. \tag{IV.2.31}$$

The unit round S^5 has $\mathrm{Ric} = 4g$ and the unit round S^7 has $\mathrm{Ric} = 6g$, matching $n = 3, 4$. This verifies the coefficient on actual links, not the existence of an Einstein metric for an arbitrary proposed algebraic cone.

Finite scalar quotients give controlled noncompact examples. Let $\mathbb{Z}_n$ act on $\mathbb{C}^n$ by the common phase ω_n. Its determinant is $\omega_n^n = 1$, and the action is effective. Every nonidentity element fixes only the origin, so the action on the unit sphere is free. The Euclidean quotient cone has a Ricci-flat orbifold metric on its smooth locus and link $S^{2n-1}/\mathbb{Z}_n$ with inherited Einstein metric. Explicitly,

$$\mathbb{C}^3/\mathbb{Z}_3 : \quad Y = S^5/\mathbb{Z}_3, \quad \mathcal{L}_\xi\Omega = 3i\Omega; \qquad \mathbb{C}^4/\mathbb{Z}_4 : \quad Y = S^7/\mathbb{Z}_4, \quad \mathcal{L}_\xi\Omega = 4i\Omega. \tag{IV.2.32}$$

The smooth-link conclusion follows from this specific free sphere action and inherited metric. A determinant-one test for a different finite action would not establish these properties.

The geometric normalization needs translation before entering later physical dictionaries. In the height-one toric chart used for the threefold construction in Chapter VII.6, the fixed coordinate is $b_3 = 3$. The cone formulas in Martelli–Sparks–Yau use a first-coordinate height convention, $b_1 = 3$; this is a permutation of torus-coordinate conventions, not a change of charge. For the fourfold convention used later in Volume VIII, the geometric weight of a holomorphic coordinate is $b_a = 2R_a$ in the stated three-dimensional physical normalization, with $\sum b_a = 4$. One must not apply this $2R$ conversion to the threefold chart. Figure IV.2.5 places the radial and Reeb directions

on the same links. The next section uses these weights to count functions, while leaving the physical R conversion outside the geometric volume calculation.

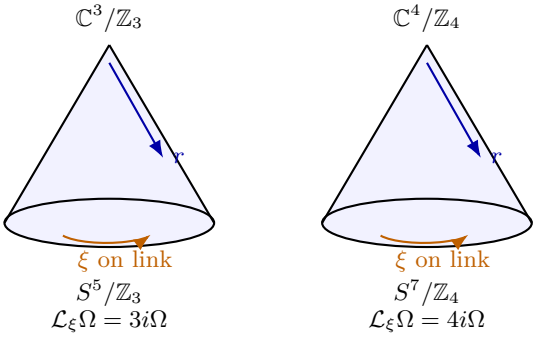


Figure IV.2.5: Two metric cones with radial direction r and tangent Reeb orbit $\xi = I(r\partial_r)$ on their links. For the flat scalar quotients, the smooth links are $S^5/\mathbb{Z}_3$ and $S^7/\mathbb{Z}_4$ and the top forms have charges three and four. The vertex is singular; the threefold toric height coordinate and the fourfold physical $2R$ conversion are separate conventions.

IV.2.7 Character poles and link volume

How can holomorphic functions report the volume of a link without an explicit integration over the metric? For a positive Reeb grading, write $Q_\xi f = qf$ and count eigenfunctions with $H_b(s) = \mathrm{Tr}_{\mathbb{C}[X]}\, e^{-sQ_\xi}$ for $s > 0$. On the polynomial ring of $\mathbb{C}^n$, the monomials $z_1^{m_1}\cdots z_n^{m_n}$ have charge $\sum_a m_a b_a$. Summing the independent geometric series yields

$$H_{\mathbb{C}^n,b}(s) = \sum_{m_a \geq 0} e^{-s\sum_a m_a b_a} = \prod_{a=1}^{n} (1 - e^{-sb_a})^{-1}, \qquad \lim_{s\to 0^+} s^n H_{\mathbb{C}^n,b}(s) = \frac{1}{\prod_a b_a}. \tag{IV.2.33}$$

The limit uses $1 - e^{-sb_a} = sb_a + O(s^2)$, and therefore requires every $b_a > 0$. For unit weights the leading coefficient is one. It is a property of the graded ring; relating it to volume requires the compatible Kähler cone and link setting of Martelli–Sparks–Yau.

An independent normalization starts from the Euclidean Gaussian integral in $2n$ real dimensions. In Cartesian coordinates it is π^n; in polar coordinates it is $\mathrm{Vol}(S^{2n-1})\int_0^\infty e^{-r^2} r^{2n-1} dr$. With $u = r^2$, the radial integral is $\Gamma(n)/2 = (n-1)!/2$. Hence

$$\mathrm{Vol}(S^{2n-1}) = \frac{2\pi^n}{(n-1)!}, \qquad \mathrm{Vol}(S^5) = \pi^3, \qquad \mathrm{Vol}(S^7) = \frac{\pi^4}{3}. \tag{IV.2.34}$$

The geometric character-volume relation in the specified Sasakian cone family, with $\mathcal{L}_\xi\Omega = in\Omega$, identifies the leading coefficient with $\mathrm{Vol}(Y_b)/\mathrm{Vol}(S^{2n-1})$ in these conventions. For the flat sphere, both are one. A formal pole by itself does not establish the family of metrics needed for this identification.

For an effective finite diagonal group Γ, invariants are selected by averaging characters. In the scalar action of $\mathbb{Z}_n$ on $\mathbb{C}^n$, the Molien average at unit weights is

$$H_{\mathbb{C}^n/\mathbb{Z}_n}(s) = \frac{1}{n}\sum_{j=0}^{n-1} \frac{1}{(1-\omega_n^j e^{-s})^n}. \tag{IV.2.35}$$

Only $j = 0$ has an order-n pole as $s \to 0^+$: all nonidentity phases have nonzero denominators. Thus

$$\lim_{s\to 0^+} s^n H_{\mathbb{C}^n/\mathbb{Z}_n}(s) = \frac{1}{n}, \qquad \frac{\mathrm{Vol}(S^{2n-1}/\mathbb{Z}_n)}{\mathrm{Vol}(S^{2n-1})} = \frac{1}{n}. \tag{IV.2.36}$$

The second equality also follows directly because this particular effective action is free on the unit sphere and the round metric descends. The agreement is an actual control of the character normalization. It would fail as a naive division by the displayed group order if a nominal group acted with a kernel. For example, present the same sign action on $\mathbb{C}^2$ using $\mathbb{Z}_4$ with generator -1: its image has order two. In the Molien sum the identity character appears twice and the leading coefficient is $1/2$, not $1/4$.

The two examples now give concrete numbers rather than only a scaling rule:

$$\begin{aligned} \mathbb{C}^3/\mathbb{Z}_3 :&\quad [s^{-3}]H = \frac{1}{3}, \quad \mathrm{Vol}(S^5/\mathbb{Z}_3) = \frac{\pi^3}{3}, \\ \mathbb{C}^4/\mathbb{Z}_4 :&\quad [s^{-4}]H = \frac{1}{4}, \quad \mathrm{Vol}(S^7/\mathbb{Z}_4) = \frac{\pi^4}{12}. \end{aligned} \tag{IV.2.37}$$

Here $[s^{-n}]H$ denotes the leading pole coefficient. If one changes positive coordinate weights while keeping $\sum b_a = n$, equation (IV.2.33) changes the leading coefficient to $1/\prod b_a$. For example, at $n = 3$ take $(b_1, b_2, b_3) = (1/2, 1, 3/2)$; the formal coefficient is $4/3$. As $b_1 \to 0^+$ with the others finite, it diverges. This indicates the boundary of a positive grading, not a new finite-volume Einstein link. The extra metric hypotheses and, for a physical dual, a separate field-theory dictionary must be checked at each use.

Figure IV.2.6 shows the route that has actually been computed: an effective action and positive Reeb weights determine a character, and a compatible cone metric permits a normalized geometric volume. A threefold central charge or fourfold free energy belongs to an additional physical argument in Chapters VII.6 or Volume VIII. A Hilbert pole cannot prove either a Sasaki–Einstein metric exists for arbitrary weights or an AdS dual exists.

IV.2.8 Exercises

The reader companion lists the exact submitted fields for Exercises 1–5, under task identifiers `FI-III-2-E1` through `FI-III-2-E5`. Rational answers use exact strings such as `"2/3"`. The numerical checker assesses these fields; the requested derivations and interpretations are written work. Exercise 6 requires a written argument and has no numerical score.

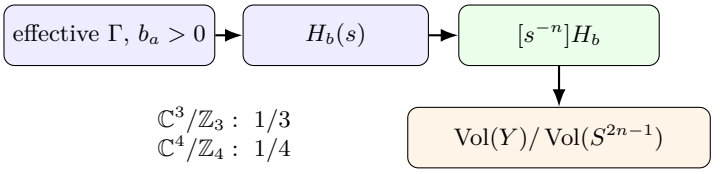


Figure IV.2.6: The unit-weight scalar quotients give leading Molien coefficients 1/3 and 1/4; the normalized smooth-link volumes agree because the effective actions are free on the spheres and inherit the round metric. A compatible cone/link metric is the condition for the general geometric volume arrow. The separate physical R and field-theory arrows are intentionally outside this geometric computation.

1. For the diagonal $\mathbb{Z}_5$ action on $\mathbb{C}^3$ with weights $(1, 1, 3)$, calculate the exponent of its action on $dz_1 \wedge dz_2 \wedge dz_3$ modulo five and whether that form is invariant. Explain why the result alone establishes neither a smooth quotient nor a global spin structure.

2. In the canonical $SU(n)$ spin lift, count invariant even and odd complex exterior components for $\mathbb{Z}_3$ weights $(1, 1, 1)$ and $\mathbb{Z}_4$ weights $(1, 3, 0)$ on $\mathbb{C}^3$. List the invariant subsets and identify the extra global and heterotic-background hypotheses before calling the components supercharges.

3. Use the Molien average at unit geometric Reeb weights for the effective scalar $\mathbb{Z}_3$ action on $\mathbb{C}^3$ and $\mathbb{Z}_4$ on $\mathbb{C}^4$. Give the leading s^{-n} coefficient and the link volume divided by π^n in each case. Show why nonidentity sectors have no leading pole. Explain why these geometric results do not establish a holographic equality.

4. At $A = 7/3$ and $\tau = 1/2 + 2i$, expand the marked torus metric (IV.2.15). Supply g_{xx}, g_{xy}, g_{yy} and $\det g_{\mathbb{R}}$ as exact rationals. Use J and the marked parallelogram to distinguish a change of area from a change of complex shape.

5. For a smooth generic quintic $Q \subset \mathbb{P}^4$, expand adjunction to obtain the coefficient of H^3 in $c_3(TQ)$, then compute $\chi(Q)$, $h^{2,1}$ and $h^{1,1}$. Show $126 - 1 - 24$ explicitly and identify which normal-sequence and Lefschetz facts are cited rather than obtained by arithmetic.

6. A colleague claims that real $c_1 = 0$ on a compact quotient implies a global holomorphic top form, exact full $SU(3)$ holonomy, four-dimensional $N = 1$ supersymmetry, and a Sasaki–Einstein AdS dual from its Hilbert series. For each arrow identify the missing hypothesis. Use the free affine torus quotient in (IV.2.5) as one counterexample and distinguish its integral Chern class from its holomorphic canonical bundle. This is a written reasoning task.

IV.2.9 Take-home message

Take-home message

For a compact Kähler manifold, real $c_1 = 0$ gives a Ricci-flat metric in each fixed Kähler class and restricted holonomy in $SU(n)$. A global holomorphic top form and full lifted holonomy are further global data. Under a specified heterotic background, invariant spinors provide geometric upper bounds on supercharges. Complex and Kähler variations are different directions: the quintic has $(h^{1,1}, h^{2,1}) = (1, 101)$ without an explicit Ricci-flat metric. On a compatible noncompact cone, positive Reeb grading and a character pole encode normalized link volume; physical R charge and dual dynamics need separate input.

The reader should now be able to test a quotient top-form character, enumerate invariant exterior spinors, separate torus area from shape, reconstruct the quintic Euler and Hodge counts, and calculate the leading Molien pole for the two scalar cone quotients. These operations feed the quotient, toric, and mirror constructions of Chapters 3, 4, and 11. The compact theorem, local deformation theorem, cohomological identifications, and cone-volume theorem have been cited at their hypotheses, not proved by the numerical examples.

Status and sources

From the Ricci form to a global volume form. The Ricci and Chern conventions continue Chapter 1. The compact fixed-class existence and uniqueness result is a cited mathematical theorem, stated at Ballmann n.d., PDF p. 94, Theorem 7.1 and Corollary 7.2; Yau 1977, PDF p. 1, Theorem 1 is Yau's announcement, while the full 1978 proof was not inspected [MATH]. The restricted/full holonomy and parallel-form framework is at Ballmann n.d., PDF pp. 63–64, eqs. (4.67)–(4.70); the compact Bochner implication for holomorphic forms is Ballmann n.d., PDF p. 90, printed p. 84, Theorem 6.11. These are cited mathematical inputs [MATH]. The free torus action, canonical sign and smooth nonholomorphic section are explicit calculations here [MATH]. They show holomorphic nontriviality with integral $c_1(K) = 0$, not nonzero integral torsion.

Top forms, quotient weights and invariant spinors. For the displayed diagonal action, the determinant and subset counts are direct calculations for the chosen $SU(n)$ lift [MATH]. The exterior/Fock spinor basis is the cited construction in Candelas et al. 1985, physical PDF pp. 14–15, printed pp. 59–60, eqs. (3.7)–(3.8); Aspinwall 1996, PDF pp. 39–40 supplies the compactification representation and reality discussion [MATH]. The ten-dimensional $N = 1$ heterotic parallel-spinor, gaugino and Bianchi conditions are physical supergravity premises from Candelas et al. 1985, physical PDF p. 9, printed p. 54, eqs. (2.39)–(2.41), physical PDF pp. 14–15, printed pp. 59–60, eqs. (3.7)–(3.10) [SUGRA]. The conditional 4/8/16 arithmetic follows from the selected representation counts [MATH]; it does not establish the supergravity premise, and no gauge bundle or full physical background is constructed.

Complex and Kähler directions in familiar spaces. The torus complex-shape example is in Hori et al. 2003, PDF p. 101, Example 6.2.1; its area-normalized metric

and numerical matrix are calculated here [MATH]. The linear contraction identification is in Hori et al. 2003, physical PDF p. 101, printed p. 81, Example 6.2.2; its bundle-level calculation here is [MATH]. Local unobstructedness under the stated compact Kähler and trivial-canonical hypotheses is a separately cited mathematical theorem from Popovici 2019, physical PDF pp. 3–4, printed pp. 674–675, Definition 1.1 and Theorem 1.2; its local convergence passage is at physical PDF p. 17, printed p. 688 [MATH]. This published modern theorem was inspected, while the historical Tian and Todorov originals and the full analytic estimates were not independently checked. Linear contraction does not prove nonlinear unobstructedness, and no finite-distance or singular extension is asserted. K3's complex positive two-plane and metric positive three-plane with scale use the cited period/metric framework in Aspinwall 1996, PDF pp. 10–15 [MATH].

Hodge structure and a quintic count. The quintic Chern and Hodge data are in Hori et al. 2003, physical PDF p. 74, printed p. 54, physical PDF p. 102, printed p. 82, Example 6.3.1 and footnote 2. Adjunction expansion, $-40 \int_Q H^3 = -200$, and $126 - 1 - 24 = 101$ are displayed calculations [MATH]; the normal-sequence vanishings, section dimensions and Lefschetz identification are cited mathematical inputs, not consequences of subtraction [MATH]. The smooth proper family, local H^3 system, Gauss–Manin connection, periods and first variation use Hori et al. 2003, physical PDF pp. 103–106, printed pp. 83–86 [MATH]. The free-lattice/torsion refinement follows from the integral pairing with cycles; it is not attributed to that source [MATH]. These family hypotheses exclude a singular-fiber inference.

The cone, its link and the Reeb charge. The cone/Reeb definitions, assumed global top form and its homogeneous normalization are the cited geometric framework in Martelli et al. 2008, physical PDF pp. 7–10, eqs. (1.4)–(1.9), physical PDF p. 20, eq. (2.17); p. 20 also distinguishes nonclosed irregular Reeb flows [MATH]. The flat-sphere and effective scalar-quotient examples are calculated here [MATH]. The threefold toric height and the fourfold geometric $2R$ conversion use the normalizations stated above. Neither conversion asserts a physical dual in this chapter.

Character poles and link volume. The general character-volume relation is a cited mathematical result under the Sasakian cone hypotheses in Martelli et al. 2008, physical PDF pp. 13–14, eqs. (1.16)–(1.17), physical PDF pp. 55–58, eqs. (6.8)–(6.22) [MATH]. The free-ring product, Gaussian sphere normalization, Molien averages and non-effective control are derived here [MATH]. The two quotient links inherit actual round quotient metrics; a general positive grading or determinant-one action does not prove Einstein metric existence. No central-charge, free-energy or holographic equality is established.

Exercises. E1–E5 assess the displayed determinant, subset, cone, torus and quintic calculations through exact short-answer fields. Their requested explanations and E6 are written mathematical and physical reasoning; the numerical checker does not grade those proofs.

References

Aspinwall, P. S. (1996). *K3 surfaces and string duality.* v5, 7 September 1999. arXiv: `hep-th/9611137`.

Ballmann, W. (n.d.). *Lectures on Kähler Manifolds.*

Candelas, P. et al. (1985). "Vacuum configurations for superstrings". In: *Nuclear Physics B* 258, pp. 46–74. DOI: 10.1016/0550-3213(85)90602-9.

Hori, K. et al. (2003). *Mirror Symmetry*. Vol. 1. Clay Mathematics Monographs. American Mathematical Society and Clay Mathematics Institute.

Martelli, D., J. Sparks, and S.-T. Yau (2008). "Sasaki–Einstein manifolds and volume minimisation". In: *Communications in Mathematical Physics* 280. arXiv v5, 23 April 2008, pp. 611–673. arXiv: hep-th/0603021.

Popovici, D. (2019). "Holomorphic Deformations of Balanced Calabi–Yau $\partial\bar{\partial}$-Manifolds". In: *Annales de l'Institut Fourier* 69.2, pp. 673–728. DOI: 10.5802/aif.3254. arXiv: 1304.0331 [math.AG].

Yau, S.-T. (1977). "Calabi's conjecture and some new results in algebraic geometry". In: *Proceedings of the National Academy of Sciences* 74.5, pp. 1798–1799. DOI: 10.1073/pnas.74.5.1798.

Chapter IV.3

ADE singularities, resolutions, and the McKay correspondence

IV.3.1 One quotient and two graphs

The surface $\mathbb{C}^2/\mathbb{Z}_2$ has a point at which the two covering coordinates and their negatives become indistinguishable. Resolving that point inserts a sphere. The same finite group also has two irreducible representations, so tensoring them with its defining representation produces a graph with two vertices. Which vertex is the sphere? This small puzzle is the quickest way to see why the representation graph and the geometry must be calculated separately. The graph includes the trivial representation; the exceptional curves do not.

The question matters for D-branes at orbifolds. A finite group labels Chan–Paton sectors after an orbifold projection, while exceptional cycles describe the resolved transverse space. The two descriptions meet in the McKay correspondence, but the projection, the metric, and the theorem about curves enter by different routes. Here we derive the character products, the smallest resolution, its quotient metric, and two instructive limits of the dictionary. General ADE and categorical results will be stated with their hypotheses, rather than inferred from these examples.

We use the Kähler normalization of Chapter 1, $J = ig_{a\bar{b}}dz^a \wedge d\bar{z}^b$ and $ds^2 = 2g_{a\bar{b}}dz^a d\bar{z}^b$. Chapter 2 explains why a determinant-one finite action preserves the holomorphic volume form on the smooth locus. That condition underlies the $SU(2)$ and $SU(3)$ examples below; it does not itself construct a smooth metric or a brane theory.

IV.3.2 Characters as a calculation tool

How can one find the sectors of an orbifold without guessing a quiver? Let $\Gamma = \mathbb{Z}_n = \langle g \rangle$ and fix $\omega = \exp(2\pi i/n)$. Its irreducible complex representations are $R_i(g) = \omega^i$, with i

understood modulo n and R_0 trivial. Their characters are $\chi_i(g^k) = \omega^{ik}$. A character records the trace of the group action, so it is directly suited to decomposing tensor products and the regular representation.

The root-of-unity sum is the entire orthogonality calculation in this abelian case. A finite geometric series gives

$$\frac{1}{n}\sum_{k=0}^{n-1}\omega^{(i-j)k} = \begin{cases} 1, & i = j \pmod n, \\ 0, & i \neq j \pmod n. \end{cases} \tag{IV.3.1}$$

Indeed, when $i \neq j$, multiplying the sum by $1-\omega^{i-j}$ leaves $1-\omega^{n(i-j)} = 0$. For $i = j$ every summand is one. This elementary calculation is the local tool; no finite-subgroup classification is needed to use it.

The regular representation $\mathbb{C}[\Gamma]$ has a basis $|g^k\rangle$ permuted by left multiplication. Its character is n at the identity and zero on every nonidentity element. Orthogonality therefore gives the multiplicity of R_i as

$$m_i = \frac{1}{n}\sum_{k=0}^{n-1}\chi_{\mathrm{reg}}(g^k)\overline{\chi_i(g^k)} = 1, \qquad \mathbb{C}[\Gamma] = \bigoplus_{i=0}^{n-1} R_i. \tag{IV.3.2}$$

The dimension check is $\sum_i (\dim R_i)^2 = n$, here just n copies of 1^2. For a nonabelian finite group the same regular decomposition has multiplicity $\dim R_i$; its dimension check is the same sum of squares.

For $n = 3$ the full calculation can be read from one table. Each column is a group element and each row an irrep.

	1	g	g^2
R_0	1	1	1
R_1	1	ω	ω^2
R_2	1	ω^2	ω

For example, the inner product of rows 1 and 2 is

$$\langle\chi_1,\chi_2\rangle = \tfrac{1}{3}(1+\omega^2+\omega^4) = \tfrac{1}{3}(1+\omega+\omega^2) = 0. \tag{IV.3.3}$$

Adding the three rows yields $(3,0,0)$, the regular character. This makes the meaning of the three labels concrete before any arrows are drawn.

There is also a useful inverse operation. Given a vector v in a $\mathbb{Z}_3$ representation, the Fourier operator

$$P_i = \frac{1}{3}\sum_{k=0}^{2}\omega^{-ik}\rho(g^k) \tag{IV.3.4}$$

projects onto the R_i sector. Multiplying two such sums and using (IV.3.1) gives $P_iP_j = \delta_{ij}P_i$, while $\sum_i P_i = I$. On the regular basis $(|1\rangle, |g\rangle, |g^2\rangle)$, for example, $P_1|1\rangle = (|1\rangle + \omega^{-1}|g\rangle + \omega^{-2}|g^2\rangle)/3$. Acting with g on this vector multiplies it by ω, so it really occupies R_1. The calculation makes the sector a subspace selected by an operator, rather than just a name in the character table. The normalization $1/3$ is essential: omitting it would yield $P_i^2 = 3P_i$ instead of a projection.

Douglas and Moore supply the physical premise that an orbifold projection decomposes Chan–Paton factors into such representation sectors. A character table by itself is a statement about finite-dimensional representations, not a derivation of a D-brane worldvolume theory. Chapter VI.2 will impose the string boundary conditions and projection; the present table gives the finite-group calculation that construction consumes. One should also resist reading the $\mathbb{Z}_3$ table as a classification of all finite subgroups of $SU(2)$. Its virtue is that every orthogonality step is visible.

IV.3.3 Tensoring and the affine McKay graph

The next question is how the same sector labels acquire edges. Let Q be the defining two-dimensional representation of a nontrivial finite $\Gamma \subset SU(2)$. Define a_{ij} by

$$Q \otimes R_i = \bigoplus_j a_{ij} R_j, \qquad a_{ij} = \frac{1}{|\Gamma|} \sum_{g \in \Gamma} \chi_Q(g) \chi_i(g) \overline{\chi_j(g)}. \tag{IV.3.5}$$

An arrow is drawn from i to j for each copy counted by a_{ij}. The formula is the character inner product of $Q \otimes R_i$ with R_j. It fixes the row and column orientation before a picture can obscure it.

Taking dimensions of the decomposition gives an immediate consistency condition. If $d_i = \dim R_i$, then

$$2d_i = \sum_j a_{ij} d_j, \qquad (2I - A)d = 0. \tag{IV.3.6}$$

The vector d is the regular dimension vector, since the regular representation has d_i copies of R_i. It is also the positive null vector of the affine Cartan matrix. The equality follows from dimensions; it does not assign a compact curve to the trivial irrep.

For $\mathbb{Z}_3 \subset SU(2)$ choose the action with weights $(1, -1)$, so $Q = R_1 \oplus R_2$. Tensoring one row at a time gives

$$QR_0 = R_1 \oplus R_2, \qquad QR_1 = R_2 \oplus R_0, \qquad QR_2 = R_0 \oplus R_1. \tag{IV.3.7}$$

The same answer follows from the character average. For example $a_{12} = \langle (\omega^k + \omega^{-k})\omega^k, \omega^{2k} \rangle = 1$ after averaging over $k = 0, 1, 2$. Thus

$$A = \begin{pmatrix} 0 & 1 & 1 \\ 1 & 0 & 1 \\ 1 & 1 & 0 \end{pmatrix}, \qquad (2I - A) \begin{pmatrix} 1 \\ 1 \\ 1 \end{pmatrix} = 0. \tag{IV.3.8}$$

Figure IV.3.1 shows the resulting affine triangle. The node R_0 is present because the tensor calculation includes every irrep. Removing it leaves two vertices joined by one edge, the finite A_2 diagram of the exceptional curves.

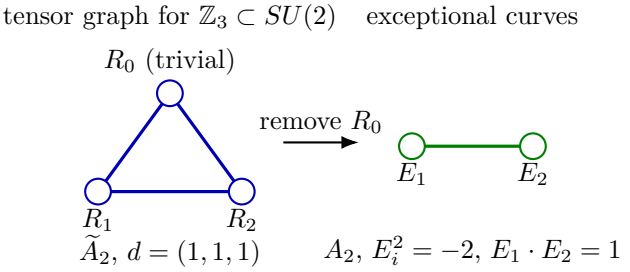


Figure IV.3.1: For the declared $(1,-1)$ action of $\mathbb{Z}_3$, tensoring with Q gives the full affine $\widetilde{A}_2$ graph. The trivial representation R_0 is the affine vertex. The finite A_2 graph on the right records two exceptional curves, each with self-intersection -2 and with mutual intersection one. The arrow indicates removal of a vertex from the representation graph, not a contraction of a curve.

The smallest case is a useful control against drawing an ordinary single edge by habit. For $\mathbb{Z}_2$ acting by $(-1,-1)$, $Q = R_1 \oplus R_1$. Hence

$$A = \begin{pmatrix} 0 & 2 \\ 2 & 0 \end{pmatrix}, \qquad 2I - A = \begin{pmatrix} 2 & -2 \\ -2 & 2 \end{pmatrix}. \tag{IV.3.9}$$

This is affine A_1 with a double edge. After deleting R_0 the finite diagram has one vertex and no edge, matching one exceptional curve. The double edge is a tensor multiplicity, not two different spheres.

The null-vector calculation supplies another check in this special case. $d = (1,1)$ gives $Ad = (2,2)$, so each tensor product still has dimension two even though its two summands coincide. If the double edge were mistakenly drawn as a single edge, its adjacency would have row sum one, and (IV.3.6) would fail. This detects an incorrectly simplified affine A_1 drawing before using it as a quiver. The same dimension test works for any finite group, though it cannot by itself establish the ADE classification.

McKay's general statement identifies the connected graphs for nontrivial finite subgroups of $SU(2)$ as affine ADE. The calculation above proves only the displayed cyclic examples. The trivial group is a separate flat case, with neither a singular point nor an exceptional curve. Chapter VI.3 uses the full affine quiver for orbifold gauge sectors; the finite graph enters when asking what a resolution contributes to geometry. For an $SU(2)$ action the adjacency is symmetric, so reversing every arrow does not test the convention. The directed example in Section IV.3.6 will.

IV.3.4 Exceptional curves and finite ADE

What replaces a singular quotient point when it is resolved? We can answer from coordinates for $\mathbb{C}^2/\mathbb{Z}_2$. To keep the two quotients in this chapter distinct, call the coordinates on the covering space (ξ_1, ξ_2). The group acts by simultaneous sign reversal. An invariant monomial has even total degree, so every invariant is a polynomial in

$$U = \xi_1^2, \qquad V = \xi_2^2, \qquad W = \xi_1\xi_2, \qquad UV - W^2 = 0. \tag{IV.3.10}$$

For the generation claim, write an even monomial $\xi_1^a \xi_2^b$. If both exponents are even, it is a product of U and V; if both are odd, remove one W and reduce to the even case. The relation is the only one because monomials can be reduced to either $U^r V^s$ or $U^r V^s W$, which have different exponent parities on the cover. Thus the invariant ring is

$$\mathbb{C}[\xi_1, \xi_2]^{\mathbb{Z}_2} \simeq \mathbb{C}[U, V, W]/(UV - W^2). \tag{IV.3.11}$$

The gradient of $F = UV - W^2$ is $(V, U, -2W)$, so the hypersurface is singular only at the origin. Away from it, the quotient is smooth.

A resolution replaces this one point by a compact curve and is an isomorphism elsewhere. The two charts of the total space of $\mathcal{O}_{\mathbb{P}^1}(-2)$ make the replacement explicit. On the first chart use base coordinate t and fiber coordinate p; map to the cone by

$$(t, p) \longmapsto (U, V, W) = (p, pt^2, pt). \tag{IV.3.12}$$

On the second chart use (s, p') and set

$$(s, p') \longmapsto (U, V, W) = (p's^2, p', p's). \tag{IV.3.13}$$

Both maps obey $UV = W^2$. On the overlap $t \neq 0$, equality of the maps forces

$$s = t^{-1}, \qquad p' = pt^2. \tag{IV.3.14}$$

This is the fiber transition of $\mathcal{O}(-2)$ in the chosen local trivializations. The total space is smooth because (t, p) and (s, p') are ordinary complex coordinates. The locus $p = 0$, equivalently $p' = 0$, is the zero section $E \simeq \mathbb{P}^1$; the two base charts cover it. For $p \neq 0$ the first map has inverse $p = U$, $t = W/U$; where $V \neq 0$ the second has inverse $p' = V$, $s = W/V$. These inverses show directly that the map changes only the origin.

At a generic point one can see the two-chart construction without abstract bundle language. Take $(U, V, W) = (1, 4, 2)$ on the cone. It lies in the first chart at $(t, p) = (2, 1)$ and in the second at $(s, p') = (1/2, 4)$. The overlap rule sends $(2, 1)$ to $(1/2, 4)$ as it should. As $p \to 0$ with t fixed, all three cone coordinates tend to zero, but distinct values of t remain distinct in the smooth total space. In the second chart the point $t = \infty$ is represented by $s = 0, p' = 0$. This shows how an entire $\mathbb{P}^1$ is contracted to one singular point.

The normal bundle to the zero section is the fiber line bundle itself. Its degree is -2, so for this smooth compact curve

$$E \cdot E = \deg N_{E/\widetilde{X}} = -2. \tag{IV.3.15}$$

There is one E, hence one finite A_1 vertex, although the affine representation graph in (IV.3.9) has two vertices. The distinction is visible without a general theorem. Figure IV.3.1 shows the same affine-versus-finite step for the next cyclic surface quotient, where two curves meet.

The sign in the normal degree can be checked against the coordinate transition rather than guessed from the cone equation. The base transition is $s = t^{-1}$. A section of the normal line has components p and p' related by $p' = t^2 p$, the standard local expression for $\mathcal{O}(-2)$ in these projective trivializations. Thus moving away from the

exceptional curve is a nontrivial bundle direction. A product $\mathbb{P}^1 \times \mathbb{C}$ would instead have $p' = p$ and normal degree zero; it could not reproduce this resolution map.

The same chart map will arise from a gauge quotient, but its charged coordinates are different from ξ_1, ξ_2. With z_i of charge $+1$ and w_i of charge -1, the holomorphic invariants on $z \cdot w = 0$ are

$$U = z_1 w_2, \qquad V = -z_2 w_1, \qquad W = z_2 w_2, \qquad UV - W^2 = 0. \tag{IV.3.16}$$

Indeed $z_1 w_1 + z_2 w_2 = 0$ gives the last relation after multiplying by $-z_2 w_2$. These are products of charged fields, not the squares of the cover coordinates in (IV.3.10). The common letters name coordinates on the same cone, not an identification of the fields before quotienting.

For a general nontrivial finite $\Gamma \subset SL(2, \mathbb{C})$, González-Sprinberg and Verdier identify nontrivial irreps with the exceptional curves of the minimal resolution. Their intersection result gives the off-diagonal adjacency; the casewise resolutions give the diagonal self-intersections -2. Together they yield the negative finite ADE Cartan pairing

$$E_i \cdot E_j = -C_{ij}^{\text{finite}}, \qquad i, j \neq 0. \tag{IV.3.17}$$

Our A_1 chart calculation illustrates this theorem but does not prove the assertion for every finite subgroup. Chapter 7 will use the finite curve configurations as geometric building blocks; the affine node must not be added to their compact intersection matrix.

IV.3.5 The hyperkahler resolution

The charts answer which smooth complex surface replaces the cone. They do not yet assign an area to its exceptional sphere. How does a level assign an area and a smooth metric to that sphere? A positive real Fayet–Iliopoulos level supplies that size in a four-real-dimensional hyperkähler quotient. Start from flat $\mathbb{H}^2 \simeq \mathbb{C}^4$ with coordinates (z_1, z_2, w_1, w_2) and real metric

$$ds^2_{\text{flat}} = 2 \sum_{i=1}^{2} (dz_i d\bar{z}_i + dw_i d\bar{w}_i), \qquad K_{\text{flat}} = |z|^2 + |w|^2. \tag{IV.3.18}$$

The common diagonal subgroup of $U(1)_0 \times U(1)_1$ acts trivially in the two-node regular construction. Divide it out first. The resulting effective $U(1)$ has a primitive ratio character, represented here by charges $(+1, +1, -1, -1)$. Its moment-map levels are

$$\mu_{\mathbb{R}} = |z_1|^2 + |z_2|^2 - |w_1|^2 - |w_2|^2 = \zeta > 0, \qquad \mu_{\mathbb{C}} = z_1 w_1 + z_2 w_2 = 0. \tag{IV.3.19}$$

This ζ is the effective level in these primitive charges. A per-node FI vector in a larger quiver requires its own conversion. The positive level forces $z \neq 0$, so the effective circle acts freely on the level set. At zero level the origin remains fixed and the quotient is singular.

The dimension count checks the quotient before a metric is computed. Flat $\mathbb{H}^2$ has eight real coordinates. The real moment map imposes one real equation and

the complex moment map two; dividing by the effective circle removes one more real direction. The result has real dimension four. Keeping the trivially acting diagonal $U(1)$ as an independent quotient would spoil both this count and the primitive charges. At $\zeta > 0$, one of z_1, z_2 is nonzero, so the two holomorphic patches used below cover the entire level-set quotient.

To solve the quotient, use the holomorphic chart $z_1 \neq 0$. A complex gauge representative can be written

$$z = (\lambda, \lambda t), \qquad w = (-pt/\lambda, p/\lambda), \qquad \lambda \in \mathbb{C}^*. \tag{IV.3.20}$$

The complex moment map vanishes identically. The charged invariants of (IV.3.16) become $(U, V, W) = (p, pt^2, pt)$, precisely the first resolution chart. The $z_2 \neq 0$ representative produces $s = 1/t$, $p' = pt^2$, so the complex surface is the two-chart $\mathcal{O}(-2)$ resolution already constructed.

Let $A = 1 + |t|^2$ and $L = |\lambda|^2$. The real moment map is a quadratic equation for the positive gauge scale,

$$AL - \frac{|p|^2 A}{L} = \zeta, \qquad x := AL = \frac{\zeta + D}{2}, \qquad D := \sqrt{\zeta^2 + 4|p|^2 A^2}. \tag{IV.3.21}$$

The norm of the negative-charge pair is $(D - \zeta)/2$. Their sum is D. Kähler reduction subtracts $\zeta \log L$ from the flat potential in this complex gauge. Since $L = x/A$, the reduced potential is

$$K_{\mathrm{red}} = D - \zeta \log\left(\frac{\zeta + D}{2}\right) + \zeta \log(1 + |t|^2). \tag{IV.3.22}$$

The subtraction has a local origin. Under a real positive complex-gauge rescaling, z grows while w shrinks. The derivative of $K_{\mathrm{flat}} - \zeta \log L$ with respect to $\log L$ is the real moment-map equation in (IV.3.21). At its stationary point, $K_{\mathrm{flat}} = x + |p|^2 A^2/x = D$. Substituting $\log L = \log x - \log A$ then gives (IV.3.22). This explains the logarithm's sign and why the Fubini–Study term survives on the zero section. Merely substituting the level solution into the flat potential without the FI subtraction would give the wrong quotient Hessian and area. On the other chart the two local potentials differ by a Kähler transform, so their Hessians define one metric. The last term restricts to the Fubini–Study potential when $p = 0$. Consequently

$$g_{t\bar{t}}\big|_{p=0} = \frac{\zeta}{(1 + |t|^2)^2}, \qquad g_{p\bar{p}}\big|_{p=0} = \frac{(1 + |t|^2)^2}{\zeta}, \qquad g_{t\bar{p}}\big|_{p=0} = 0. \tag{IV.3.23}$$

This patching can be checked at the zero section. In the $s = 1/t$ chart the base potential is $K_s = \zeta \log(1 + |s|^2)$. On the overlap,

$$K_t - K_s = \zeta \log(1 + |t|^2) - \zeta \log(1 + |t|^{-2}) = \zeta \log |t|^2. \tag{IV.3.24}$$

The right side is locally the real part of a holomorphic logarithm, so applying $i\partial\bar{\partial}$ removes it. The chart potentials therefore yield the same Kähler form even though neither potential is a global function on the compact sphere. The second coefficient

follows by expanding $D = \zeta + 2|p|^2A^2/\zeta + O(|p|^4)$ in (IV.3.22). The quotient is smooth at $p = 0$ when $\zeta > 0$; the apparent use of λ^{-1} in one chart causes no singularity there.

The period can be integrated on the first base chart, with the point at infinity supplied by the second. In polar coordinates $t = re^{i\theta}$,

$$\int_E J = i\zeta \int_{\mathbb{C}} \frac{dt \wedge d\bar{t}}{(1+|t|^2)^2} = 2\zeta \int_0^{2\pi} d\theta \int_0^{\infty} \frac{r\, dr}{(1+r^2)^2} = 2\pi\zeta. \tag{IV.3.25}$$

At $\zeta = 3/2$ and $t = 1, p = 0$, the metric coefficients in (IV.3.23) are $g_{t\bar{t}} = 3/8$ and $g_{p\bar{p}} = 8/3$, while the sphere area is 3π. This is an area in the declared real-metric normalization, not a value imported from an unconverted FI convention.

The zero-section calculation alone does not determine the full metric. Write $B = |p|^2A^2$. Differentiating the nontrivial part of (IV.3.22) gives

$$\frac{\partial K_{\mathrm{red}}}{\partial B} = \frac{2}{\zeta + D}, \qquad \frac{\partial}{\partial B}\left(B\frac{\partial K_{\mathrm{red}}}{\partial B}\right) = \frac{1}{D}. \tag{IV.3.26}$$

It follows that the horizontal quotient metric has, away from the zero section, the mixed and fiber entries

$$g_{t\bar{p}} = \frac{2pA\bar{t}}{D}, \qquad g_{p\bar{p}} = \frac{A^2}{D}. \tag{IV.3.27}$$

For a nonsymmetric point, take $\zeta = 3/2$ and $t = p = 1$. Here $A = 2$, $D = \sqrt{73}/2$, and direct differentiation of (IV.3.22) gives

$$(g_{a\bar{b}})_{(t,p)=(1,1)} = \begin{pmatrix} 137\sqrt{73}/584 & 8/\sqrt{73} \\ 8/\sqrt{73} & 8/\sqrt{73} \end{pmatrix}, \qquad \det g = 1. \tag{IV.3.28}$$

Thus a base slice or a fiber slice cannot stand in for the full metric. The off-diagonal entry measures how changing t changes the norm of the fiber coordinate through A. This is also why a diagonal-only comparison to a radial metric would miss actual quotient information.

One can see the mixed term directly from the invariant combination $B = |p|^2(1+|t|^2)^2$. At a point with $p, t \neq 0$, $\partial_t B = 2|p|^2A\bar{t}$ and $\partial_{\bar{p}}B = pA^2$. Differentiating the latter while keeping track of the B dependence of K_B yields $g_{t\bar{p}} = 2pA\bar{t}(K_B + BK_{BB})$, which becomes (IV.3.27). A calculation along $p = 0$ sets this expression to zero, but that is a property of the chosen slice. The matrix in (IV.3.28) shows that it is not a property of the resolved space. Its determinant is positive and equal to one at the stated point, giving a local nondegeneracy check independent of either diagonal entry alone.

The relation to the Eguchi–Hanson form fixes the scale. Away from $p = 0$, put $\rho^2 = 4\sqrt{B}$ and $a^2 = 2\zeta$. Then

$$K_{\mathrm{rad}} = D + \zeta \log\left(\frac{2\sqrt{B}}{\zeta + D}\right), \qquad K_{\mathrm{rad}} - K_{\mathrm{red}} = \zeta \log|p|, \tag{IV.3.29}$$

up to an irrelevant constant. The difference is locally pluriharmonic when $p \neq 0$, so the two Hessians agree there. Write $u = \sqrt{B} > 0$, so $\rho^2 = 4u$ and $D = \sqrt{\zeta^2 + 4u^2}$. Direct differentiation of $F(u) = K_{\mathrm{rad}}$ gives

$$uF'(u) = D, \qquad F'(u) + uF''(u) = \frac{4u}{D}. \tag{IV.3.30}$$

Away from $p = 0$, choose a branch of the local double cover $p = \xi_1^2$, $t = \xi_2/\xi_1$. Its two sheets differ by $(\xi_1, \xi_2) \mapsto (-\xi_1, -\xi_2)$, and $u = \sqrt{B} = |p|(1 + |t|^2) = |\xi_1|^2 + |\xi_2|^2$. These cover coordinates are distinct from the charged fields z_i, w_i. The ordinary flat polar line element is $\sum_i |d\xi_i|^2 = du^2/(4u) + u(\sigma_1^2 + \sigma_2^2 + \sigma_3^2)/4$, where $\sigma_3 = d\psi + \cos\theta\, d\phi$ and $\sigma_1^2 + \sigma_2^2 = d\theta^2 + \sin^2\theta\, d\phi^2$. Using $ds^2 = 2g_{i\bar{\jmath}} d\xi^i d\bar{\xi}^{\bar{\jmath}}$, the radial Hessian separates into

$$ds^2 = \frac{F' + uF''}{2u}\, du^2 + \frac{uF'}{2}(\sigma_1^2 + \sigma_2^2) + \frac{u(F' + uF'')}{2}\sigma_3^2 = \frac{2}{D}\, du^2 + \frac{D}{2}(\sigma_1^2 + \sigma_2^2) + \frac{2u^2}{D}\sigma_3^2. \tag{IV.3.31}$$

Define $r^2 = 2D$. Since $a^2 = 2\zeta$, this gives $r^4 = \rho^4 + a^4$, with $\rho \geq 0$ and $r \geq a$. Moreover $dr/du = 4u/(rD)$ and $f = 1 - a^4/r^4 = 4u^2/D^2$. Substitution into (IV.3.31) gives the Eguchi–Hanson real metric

$$ds^2 = f(r)^{-1} dr^2 + \frac{r^2}{4}\left(\sigma_1^2 + \sigma_2^2 + f(r)\sigma_3^2\right), \qquad f(r) = 1 - \frac{a^4}{r^4}, \quad r \geq a. \tag{IV.3.32}$$

Eguchi and Hanson use angular forms $\sigma_i^{\mathrm{EH}} = \sigma_i/2$. For example, their $\sigma_3^{\mathrm{EH}} = (d\psi + \cos\theta\, d\phi)/2$; their $r^2(\sigma_i^{\mathrm{EH}})^2$ terms therefore become our $r^2\sigma_i^2/4$ terms. Their radial relation is the same $\rho^4 = r^4 - a^4$ in these metric units. Smoothness at $r = a$ requires the Euler fiber ψ to have period 2π, giving the asymptotic link $S^3/\mathbb{Z}_2$. At the bolt, the remaining metric is $(a^2/4)(d\theta^2 + \sin^2\theta\, d\phi^2)$, hence

$$\mathrm{Area}(E) = 4\pi\frac{a^2}{4} = \pi a^2 = 2\pi\zeta, \qquad a^2 = 2\zeta. \tag{IV.3.33}$$

The equality checks the FI-to-radial parameter map derived above. At $\zeta = 3/2$ it yields $a^2 = 3$, fiber period 2π, and boundary group of order two. As $\zeta \to 0$ the sphere collapses and the quotient potential approaches the cone potential. Figure IV.3.2 shows which cycle changes and which asymptotic identification remains.

The required fiber period follows from the local radial plane rather than from a name assigned to ψ. Put $r = a + \varepsilon$ with $\varepsilon > 0$ small. Then $f(r) = 4\varepsilon/a + O(\varepsilon^2)$. Setting $R^2 = a\varepsilon$, the radial and fiber terms become

$$f^{-1} dr^2 + \frac{r^2 f}{4}\sigma_3^2 = dR^2 + R^2(d\psi + \cos\theta\, d\phi)^2 + O(R^2 dR^2, R^4). \tag{IV.3.34}$$

At fixed (θ, ϕ) this is a polar plane only when the shrinking angle has period 2π. Giving it the 4π range of the full S^3 Euler coordinate would introduce a conical defect at the bolt. At large r the same period divides the usual S^3 fiber by its central $\mathbb{Z}_2$. The smooth interior and asymptotic link constrain the same period.

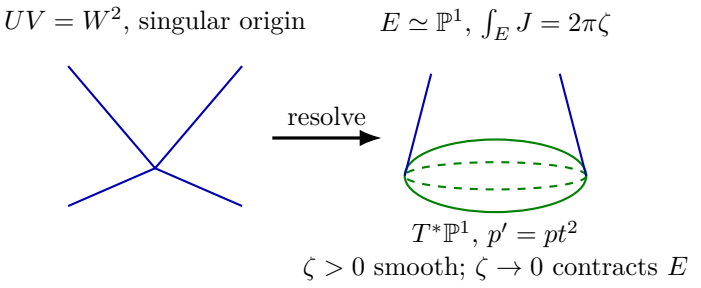


Figure IV.3.2: The two-chart resolution replaces the origin of $UV = W^2$ by one $\mathbb{P}^1$. Its normal transition is $p' = pt^2$, and the quotient Kähler period is $2\pi\zeta$. Sending the positive effective level to zero collapses this sphere; the smooth space at positive level retains the asymptotic $S^3/\mathbb{Z}_2$ link. The drawing shows topology and scale, not the full metric tensor.

The hyperkähler quotient principle applies to a free triholomorphic compact-group action at the chosen level. In this example freeness and the shifted central level were established explicitly. For general ADE, Kronheimer's ALE construction and marked-period classification are cited through the attributed review discussed in the end matter. They are not proved by the A_1 potential. Douglas and Moore connect the effective FI deformation to an orbifold D-brane construction; this physical input does not fix a string coupling, a B field, or an exact brane metric here. Chapter VI.4 can use the local curve and its period while keeping those additional choices visible.

IV.3.6 Beyond SU2

Does every three-node orbifold diagram inherit ADE symmetry? No. Put $\mathbb{Z}_3$ in $SU(3)$ with weights $(1, 1, 1)$. The determinant is $\omega^3 = 1$, but the defining representation is now $Q = 3R_1$. Using the same arrow convention and the character table from Section IV.3.2 gives

$$Q \otimes R_i = 3R_{i+1}, \qquad a_{ij} = 3\delta_{j,i+1} \quad (i, j \bmod 3). \tag{IV.3.35}$$

For instance, multiplying the R_2 character by $3\omega^k$ gives the constant character 3, so there are three arrows $2 \to 0$. This is a direct tensor-product calculation, not a choice of artistic orientation. The full adjacency and its transpose are

$$A = \begin{pmatrix} 0 & 3 & 0 \\ 0 & 0 & 3 \\ 3 & 0 & 0 \end{pmatrix}, \qquad A^{\mathsf{T}} = \begin{pmatrix} 0 & 0 & 3 \\ 3 & 0 & 0 \\ 0 & 3 & 0 \end{pmatrix}. \tag{IV.3.36}$$

They are unequal. Taking dimensions gives

$$A \begin{pmatrix} 1 \\ 1 \\ 1 \end{pmatrix} = 3 \begin{pmatrix} 1 \\ 1 \\ 1 \end{pmatrix}, \qquad (3I - A)d = 0. \tag{IV.3.37}$$

The equation resembles the $SU(2)$ dimension relation, but $3I - A$ is neither symmetric nor an ADE Cartan matrix. The $SU(2)$ McKay theorem used a two-dimensional self-dual defining representation. Its representation graph has a different mathematical type.

The row orientation can be recovered directly from the Fourier sum, which is useful when a source draws arrows with the opposite convention. For this embedding $\chi_Q(g^k) = 3\omega^k$, so

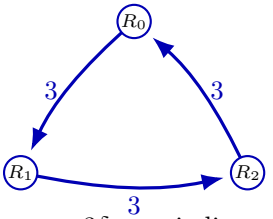
$$a_{ij} = \frac{1}{3}\sum_{k=0}^{2} 3\omega^{(1+i-j)k} = 3\,\delta_{j,i+1}. \tag{IV.3.38}$$

For $i = 0$, only the $j = 1$ sum survives. For $i = 1$, only $j = 2$ survives, and for $i = 2$ the modular condition returns to $j = 0$. This calculation produces the oriented cycle without relying on a picture. It also shows where the factor three enters: it is the multiplicity of the same character in the three coordinates, not the number of nodes in the group.

Complex conjugating the chosen representation changes the weights to $(2, 2, 2)$ and reverses every arrow. The underlying abstract group and its ordinary irreps are unchanged. In formulas the new adjacency is

$$Q^* = 3R_2, \qquad A(Q^*) = A(Q)^{\mathsf{T}}. \tag{IV.3.39}$$

This gives a useful orientation check: an arrow reversal is a change of the complex representation or of the declared row convention, not a consequence of forgetting the arrows. In a chiral orbifold problem that change matters to the field assignments. It is absent from the undirected ADE intersection graph of a surface resolution.



$Q = 3R_1$, $a_{ij} = 3\delta_{j,i+1}$, indices modulo 3

Figure IV.3.3: The declared $\mathbb{Z}_3 \subset SU(3)$ action has three coordinates of weight one. Each node has three arrows to the next node in the $0 \to 1 \to 2 \to 0$ orientation; no reverse arrows are implied. The direction is determined by $Q \otimes R_i = 3R_{i+1}$ and carries information that the symmetric $SU(2)$ ADE graph lacks.

The regular vector remains $(1, 1, 1)$ because the group is still $\mathbb{Z}_3$. What changed was the embedding, hence Q. A useful misconception is that a familiar group name alone fixes its quiver. The pair (Γ, Q) is the input. Chapter VI.6 uses directed orbifold arrows to organize chiral matter; geometry and dynamics require their own premises. In particular, this drawing does not establish a crepant resolution or a derived-category equivalence. The theorem that can do the latter job will be stated in Section IV.3.8.

For the actual linear action just used, $M = \mathbb{C}^3$ is smooth and quasiprojective, the finite group acts by automorphisms, and the determinant-one condition supplies the required local action on its canonical bundle. Thus the BKR theorem cited below has a concrete eligible input in this example. The point is logical: the directed matrix in (IV.3.36) is an independently computed representation object, while BKR supplies its own geometric and categorical conclusions from its stated hypotheses. Neither result is a derivation of a quantum worldvolume theory.

IV.3.7 Projective characters

Ordinary characters assume that a group element acts by an honest matrix representation. Which representation data survive when a commuting pair has a nontrivial phase? Discrete torsion changes the representation problem before any brane dynamics is discussed. A projective lift γ obeys

$$\gamma(g)\gamma(h) = c(g,h)\gamma(gh), \qquad c(g,h)c(gh,k) = c(h,k)c(g,hk). \tag{IV.3.40}$$

The second identity is associativity of three matrices. Replacing $\gamma(g)$ by $b(g)\gamma(g)$ changes c by a coboundary, so a table of phases depends on the lift. For commuting group elements the ratio

$$\beta(g,h) = \frac{c(g,h)}{c(h,g)} \tag{IV.3.41}$$

is unchanged by that replacement. It is the phase relevant to the commuting-sector comparison, not generally the chosen factor set itself.

For a complete small example take $\Gamma = \mathbb{Z}_2 \times \mathbb{Z}_2$ with elements (p,q), $p,q \in \{0,1\}$, and order them as $(00, 10, 01, 11)$. Define the clock and shift matrices

$$X = \begin{pmatrix} 0 & 1 \\ 1 & 0 \end{pmatrix}, \qquad Z = \begin{pmatrix} 1 & 0 \\ 0 & -1 \end{pmatrix}, \qquad XZ = -ZX, \qquad \gamma(p,q) = X^p Z^q. \tag{IV.3.42}$$

Moving Z^q past $X^{p'}$ gives the exact factor set

$$c((p,q),(p',q')) = (-1)^{qp'}. \tag{IV.3.43}$$

For clarity, its entire table in the declared order is

$$(c(a,b))_{a,b=(00,10,01,11)} = \begin{pmatrix} 1 & 1 & 1 & 1 \\ 1 & 1 & 1 & 1 \\ 1 & -1 & 1 & -1 \\ 1 & -1 & 1 & -1 \end{pmatrix}. \tag{IV.3.44}$$

Two entries locate the otherwise easy-to-miss sign. Multiplying $\gamma(10)\gamma(01) = XZ$ introduces no reordering, hence $c(10,01) = 1$. Multiplying in the opposite order gives $\gamma(01)\gamma(10) = ZX = -XZ$, hence $c(01,10) = -1$. The fourth lift is $\gamma(11) = XZ$, so $\gamma(11)^2 = -I$ even though $(11)^2 = 00$ in the group. That is allowed in a projective representation; it is the central phase retained by the factor set. The cocycle identity

can be checked without enumerating every triple. Its left exponent is $qp' + (q+q')p''$, while its right exponent is $q'p'' + q(p'+p'')$; they agree modulo two. For the two generators,

$$\beta((1,0),(0,1)) = \frac{c((1,0),(0,1))}{c((0,1),(1,0))} = \frac{1}{-1} = -1. \tag{IV.3.45}$$

A representative can change while this conclusion remains fixed. For example, choose a phase function b that is -1 on (11) and $+1$ on the other three elements. The new lift $\gamma'(g) = b(g)\gamma(g)$ has

$$c'(g,h) = \frac{b(g)b(h)}{b(gh)}\, c(g,h), \qquad c'(10,01) = -1, \quad c'(01,10) = +1. \tag{IV.3.46}$$

The two displayed entries flip, but their ratio remains -1. This is why the physical commuting-sector phase can be compared across conventions while an individual factor-set table cannot. An ordinary one-dimensional representation of this abelian group would make all matrices commute. It cannot realize $\beta = -1$. The four matrices I, X, Z, XZ span $M_2(\mathbb{C})$, so the twisted group algebra is the full 2×2 matrix algebra. It has one inequivalent simple module, of dimension two. The dimension-square check is

$$\sum_{\alpha \in \mathrm{Irr}_c(\Gamma)} (\dim \alpha)^2 = 2^2 = 4 = |\Gamma|, \tag{IV.3.47}$$

whereas ordinary $\mathbb{Z}_2^2$ has four one-dimensional irreps. The projective regular module therefore has two copies of the unique two-dimensional simple module.

There is a direct way to see why the two-dimensional module is irreducible. Any one-dimensional invariant subspace would be a simultaneous eigenspace of X and Z. If v were a common eigenvector with nonzero eigenvalues x, z, then $XZv = xzv$ but $ZXv = zxv = -XZv$, an impossibility over $\mathbb{C}$. Since the matrices span all endomorphisms of $\mathbb{C}^2$, the commutant of this action consists only of scalar matrices; there is no second inequivalent simple module of the same twisted algebra. This checks the module count using actual matrices as well as the dimension-square identity.

Douglas's Pauli-matrix construction motivates this Chan–Paton choice, and Vafa and Witten's commuting-sector phase corresponds to the invariant β. Their printed representatives need not equal (IV.3.43) entry by entry. Comparing phase tables without allowing a coboundary would manufacture a disagreement. Chapter VI.9 uses the projective sectors in a physical orbifold construction; the present matrix algebra establishes their representation count, not the resulting brane spectrum.

IV.3.8 Lie-algebra and theorem interface

ADE also appears in Lie algebra and boundary problems. Which part of that recurrence can be calculated here? For rank two, take $J_i = \sigma_i/2$, with Hermitian Pauli matrices and $[J_i, J_j] = i\epsilon_{ijk}J_k$. Work on a local interval with $s \neq 0$, away from the pole. Choose the connection gauge $A_s = 0$, so $D_s = \partial_s$ on adjoint fields. In the boundary convention of Chapter IX.4, a simple pole $X_i = J_i/s$ then solves

$$D_s X_i - \frac{i}{2}\epsilon_{ijk}[X_j, X_k] = 0, \qquad -\frac{J_i}{s^2} - \frac{i}{2s^2}\epsilon_{ijk}[J_j, J_k] = 0. \tag{IV.3.48}$$

The last equality uses $\epsilon_{ijk}\epsilon_{jkl} = 2\delta_{il}$; it fixes the sign of the pole rather than silently changing the boundary equation. The complex raising element is

$$e = J_1 + iJ_2 = \begin{pmatrix} 0 & 1 \\ 0 & 0 \end{pmatrix}, \quad f = \begin{pmatrix} 0 & 0 \\ 1 & 0 \end{pmatrix}, \quad h = \begin{pmatrix} 1 & 0 \\ 0 & -1 \end{pmatrix}. \tag{IV.3.49}$$

Multiplication gives $[h, e] = 2e$, $[h, f] = -2f$, and $[e, f] = h$. Thus the same rank-two matrices produce a nilpotent $\mathfrak{sl}_2$ orbit calculation.

Write a general traceless matrix as $N = \left(\begin{smallmatrix} a & b \\ c & -a \end{smallmatrix}\right)$. Its square is scalar,

$$N^2 = (a^2 + bc)I, \qquad \overline{\mathcal{O}_e} = \{(a, b, c) \in \mathbb{C}^3 : a^2 + bc = 0\}. \tag{IV.3.50}$$

Every nonzero nilpotent traceless 2×2 matrix is conjugate to e; the closure adds the zero matrix. Setting $U = b$, $V = -c$, $W = a$ turns the equation into $UV - W^2 = 0$. This is an isomorphism of affine surfaces with the A_1 cone. It does not identify complete Nahm moduli spaces, boundary dynamics, or the Eguchi–Hanson metric. Chapter IX.4 will address the boundary conditions that the local residue calculation does not contain.

One can check the orbit statement on a dense chart. If $b \neq 0$ and $a^2 + bc = 0$, then

$$N = \begin{pmatrix} a & b \\ -a^2/b & -a \end{pmatrix}, \qquad N \begin{pmatrix} b \\ -a \end{pmatrix} = 0, \qquad \operatorname{rank} N = 1. \tag{IV.3.51}$$

A nonzero rank-one nilpotent has a one-dimensional image equal to its kernel. Choosing a vector that maps to a generator of this line gives a basis in which its matrix is e. The $c \neq 0$ chart is analogous; the origin is obtained as the limit of scalar multiples of e under diagonal conjugation. Thus the orbit closure is the whole cone, not only its smooth locus. The equation and its singular gradient are the same as for the quotient in Section IV.3.4, but the construction that produced them is different.

Three general results explain how far the examples extend, and their hypotheses do different work. For a nontrivial finite $\Gamma \subset SL(2, \mathbb{C})$, geometric McKay identifies the nontrivial irreps with curves on the minimal resolution. Their intersections give the negative finite ADE Cartan matrix, with the trivial irrep reserved for the affine graph. This is a statement about a resolved surface and its compact curves, not about its metric.

Kronheimer's ALE results concern a fixed minimal-resolution topology and three marked Kähler classes $\alpha_i = [\omega_i]$, $i = 1, 2, 3$. For every integral two-cycle Σ of square $\Sigma \cdot \Sigma = -2$, nondegeneracy requires that at least one period $\alpha_i(\Sigma)$ be nonzero:

$$\Sigma \cdot \Sigma = -2 \quad \Longrightarrow \quad \big(\alpha_1(\Sigma), \alpha_2(\Sigma), \alpha_3(\Sigma)\big) \neq (0, 0, 0). \tag{IV.3.52}$$

A root wall is the locus where all three pairings with one such root vanish simultaneously. In the attributed review we use, a nonfree effective quotient level lies on a root wall; levels away from those walls are a sufficient regular choice. The opposite implication is not asserted. The same review states existence of complete ALE hyperkähler metrics on the fixed minimal-resolution topology for nondegenerate marked triples. It also states that an ALE hyperkähler four-manifold has the minimal-resolution topology and that a diffeomorphism matching all three Kähler cohomology classes determines the isometry class. Group type alone therefore does not fix a metric. Our A_1 area is one period in a

chosen complex structure, and the complete triple belongs to the general theorem. The original 1989 papers are not used as directly read proofs here.

In the A_1 family the positive real level already displays why period data matter. The smooth spaces at $\zeta = 1$ and $\zeta = 2$ have the same exceptional sphere and the same end $S^3/\mathbb{Z}_2$, yet (IV.3.25) gives respective sphere areas 2π and 4π. An isometry respecting the marked two-cycle cannot identify those metrics. This concrete difference does not reconstruct the full three-period classification or prove existence for every allowed marked period.

Finally, Bridgeland–King–Reid start with a nonsingular quasiprojective complex variety M and a finite group of automorphisms G. Its canonical bundle is locally G-trivial when every point has a G-invariant neighbourhood carrying a nowhere-vanishing invariant top form. Equivalently, each stabilizer acts with determinant one on the tangent space at its fixed point. Assume this and $\dim_{\mathbb{C}} M \leq 3$. A G-cluster is a G-invariant zero-dimensional subscheme $Z \subset M$ whose functions form the regular representation:

$$H^0(\mathcal{O}_Z) \simeq \mathbb{C}[G], \qquad \text{length}(Z) = |G|. \tag{IV.3.53}$$

The space $G\text{-Hilb}(M)$ parametrizes these clusters. Under the stated hypotheses, their Theorem 1.2 says that the relevant G-Hilbert scheme is irreducible, gives a crepant resolution of M/G, and has a derived-category equivalence

$$D^b(\text{Coh}(G\text{-Hilb}(M))) \simeq D^b_G(\text{Coh}(M))\,. \tag{IV.3.54}$$

Here crepant means that the resolution pulls back the canonical bundle of M/G to the canonical bundle upstairs. $\text{Coh}(Y)$ is the category of coherent sheaves on Y; D^b consists of bounded complexes of such sheaves, with quasi-isomorphic complexes identified. The subscript G on the right requires compatible G actions on the sheaves and their maps. Thus the two sides compare sheaf complexes on the resolution with equivariant sheaf complexes on M. The theorem is categorical and geometric; it is not a conclusion of the three-arrow graph in Figure IV.3.3. Chapter V.6 uses such derived categories for B-branes with additional physical interpretation. The finite-group computations here, the cited theorems, and that interpretation should remain distinct.

IV.3.9 Exercises

Each numbered task has the same public identifier and JSON fields as the reader companion. The written steps request explanations beyond the bounded submitted answers.

1. **FI-III-3-E1.** For $\Gamma = \mathbb{Z}_4 \subset SU(2)$ with weights $(1, -1)$, order R_0, R_1, R_2, R_3. Compute the 4×4 adjacency a_{ij} and primitive regular dimension vector. Derive one row by a character average and verify $(2I - A)d = 0$. Submit fields `adjacency` and `regular_vector`.

2. **FI-III-3-E2.** For the sign action on the cover coordinates (ξ_1, ξ_2), submit the exponent pairs of U, V, W in that order, the coefficients of UV and W^2 in the primitive relation whose UV coefficient is $+1$, and the normal degree of the exceptional

curve. Locate the singular point and derive the degree from the overlap map. Submit `U_exponents`, `V_exponents`, `W_exponents`, `relation_coefficients`, and `normal_degree`.

3. **FI-III-3-E3.** In the effective quotient of Section IV.3.5, set $\zeta = 3/2$, $t = 1$, $p = 0$. Compute $g_{t\bar{t}}$, $g_{p\bar{p}}$, area divided by π, the Eguchi–Hanson a^2, fiber period divided by π, and the order of the asymptotic link group. Use $ds^2 = 2g\, dz\, d\bar{z}$ and show the zero-section integral. Submit rational strings in fields `g_t`, `g_p`, `area_over_pi`, `a_squared`, `fiber_period_over_pi`, and an integer in `boundary_order`.

4. **FI-III-3-E4.** For $\mathbb{Z}_2^2$ ordered $(00, 10, 01, 11)$ and $\gamma(p, q) = X^p Z^q$, compute the 4×4 factor-set table, $\beta(10, 01)$, the irreducible projective-module dimension and number of inequivalent irreducibles. Explain how a coboundary changes a lift without changing β. Submit `factor_table`, `beta_gh`, `projective_irrep_dimension`, and `projective_irrep_count`.

5. **FI-III-3-E5.** For $\mathbb{C}^3/\mathbb{Z}_3$ with the declared $(1, 1, 1)$ weights, order nodes R_0, R_1, R_2 and compute the directed adjacency, primitive regular vector, and whether the adjacency is symmetric. Explain why this is not an ADE Cartan graph. Submit `adjacency`, `regular_vector`, and `symmetric`.

6. **FI-III-3-E6, written.** State BKR Theorem 1.2 with its standing hypotheses and distinguish its derived equivalence from both the affine $SU(2)$ representation graph and finite exceptional-curve graph. Then state the fixed-topology and marked-period limits of the attributed Kronheimer review. Explain why that restatement does not amount to a direct reading of the 1989 proofs. This task is written only.

IV.3.10 Take-home message

Take-home message

An orbifold group and its chosen linear action determine tensor-product arrows. For a nontrivial finite $SU(2)$ action the full graph is affine ADE, and the trivial irrep is its affine vertex. The minimal surface resolution instead has finite ADE exceptional curves. In the A_1 example, the invariant cone $UV = W^2$ resolves to $\mathcal{O}_{\mathbb{P}^1}(-2)$; a positive effective quotient level gives its sphere area $2\pi\zeta$ and the Eguchi–Hanson scale $a^2 = 2\zeta$ in our metric frame. Directed $SU(3)$ arrows, projective phases, the rank-two nilpotent cone, and derived equivalence answer different questions. Their common group or ADE vocabulary does not replace the hypotheses of each construction.

Status and sources

Sections IV.3.2 and IV.3.3 derive the cyclic character sums, tensor adjacency and dimension vectors under the declared actions [MATH]. The general affine ADE identification for nontrivial finite $SU(2)$ subgroups is cited from McKay (1980, physical

pp. 3–5, printed pp. 183–185) and Gonzalez-Sprinberg and Verdier (1983, physical pp. 3–5); no classification proof is given. The orbifold Chan–Paton use is a physical premise from Douglas and Moore (1996, physical pp. 8–9, eqs. (3.1)–(3.3), physical p. 13, eqs. (4.1)–(4.5)) [GEO-E]. The orbifold action and its projected quiver use the frame stated above.

Section IV.3.4 computes the A_1 invariant ring, singular point, both resolution charts and normal degree [MATH]. For general nontrivial finite $\Gamma \subset SL(2,\mathbb{C})$, the nontrivial-irrep/curve pairing and off-diagonal intersections are Gonzalez-Sprinberg and Verdier (1983, Theorem 2.2(i), physical p. 8, printed p. 415); the casewise -2 self-intersections are in Gonzalez-Sprinberg and Verdier (1983, physical pp. 33–37, printed pp. 440–444). The affine trivial node is not an exceptional curve. The flat trivial group lies outside this ADE statement.

Section IV.3.5 derives the positive-level effective $\mathbb{H}^2/U(1)$ quotient potential, its full local Hessian and period [MATH] in the Hermitian metric convention of Chapter 1. The physical orbifold/FI setting is Douglas and Moore (1996, physical pp. 35–37, eqs. (8.2)–(8.12)) [GEO-E]. The free triholomorphic quotient principle is Hitchin et al. (1987, Theorem 3.2, printed p. 549); its original online scan was read but has no local file hash. The radial metric, smooth 2π Euler-fiber period, bolt and $S^3/\mathbb{Z}_2$ asymptotics are Eguchi and Hanson (1979, physical pp. 4, 9–11, eqs. (2.2), (2.26), (2.31), (2.37)–(2.41)). The radial Hessian and coordinate change yield $r^2 = 2D$ and $a^2 = 2\zeta$ in the present units; the bolt area checks this map. The general ALE construction, fixed minimal-resolution topology and three marked Kähler-period classification are cited only through the explicit Kronheimer-attributed review in Yan (2025, Section 2.1, physical pp. 3–5) [MATH]. The two 1989 Kronheimer originals have not been directly read; no page locator or proof claim is assigned to them. Yan's duplicated moment-map component and ineffective-group notation are corrected by the stated three-component and effective-group setup. A nonfree level lying on a root wall is a necessary implication, not a converse.

Section IV.3.6 calculates the directed $(1,1,1)$ example [MATH]. Section IV.3.7 calculates one factor set, its associativity, invariant commutator and simple-module count [MATH]. The projective Chan–Paton premise is Douglas (1998, physical pp. 3–5); the commuting-sector phase is Vafa and Witten (1995, eq. (2.2), physical p. 5) [GEO-E]. Section IV.3.8 computes only the rank-two residue and nilpotent affine cone [MATH]; full Nahm boundary dynamics is outside this chapter. BKR's irreducibility, crepant resolution and derived equivalence use its smooth quasiprojective, finite-automorphism, locally canonical-trivial and dimension-at-most-three hypotheses Bridgeland et al. (2001, Theorem 1.2, physical pp. 2–5) [MATH]. No directed graph alone establishes that theorem or a full QFT identification. Downstream pointers are Chapters VI.2–VI.4, VI.6, VI.9, IX.4, IV.7 and V.6. Readers should now be able to compute cyclic tensor arrows, separate affine nodes from compact curves, reproduce the A_1 area calculation, detect an orientation or cocycle error, and state the scope of the cited theorems.

References

Bridgeland, T., A. King, and M. Reid (2001). "The McKay Correspondence as an Equivalence of Derived Categories". In: *Journal of the American Mathematical Society* 14.3, pp. 535–554. DOI: 10.1090/S0894-0347-01-00368-X. arXiv: math/9908027.

Douglas, M. R. (1998). *D-Branes and Discrete Torsion*. arXiv: hep-th/9807235.

Douglas, M. R. and G. Moore (1996). *D-Branes, Quivers, and ALE Instantons*. arXiv: hep-th/9603167.

Eguchi, T. and A. J. Hanson (1979). "Self-Dual Solutions to Euclidean Gravity". In: *Annals of Physics* 120, pp. 82–106. DOI: 10.1016/0003-4916(79)90282-3.

Gonzalez-Sprinberg, G. and J.-L. Verdier (1983). "Construction géométrique de la correspondance de McKay". In: *Annales scientifiques de l'École Normale Supérieure*. 4th ser. 16.3, pp. 409–449. DOI: 10.24033/asens.1454.

Hitchin, N. J. et al. (1987). "Hyperkähler Metrics and Supersymmetry". In: *Communications in Mathematical Physics* 108.4, pp. 535–589. DOI: 10.1007/BF01214418.

McKay, J. (1980). "Graphs, Singularities, and Finite Groups". In: *The Santa Cruz Conference on Finite Groups*. Vol. 37. Proceedings of Symposia in Pure Mathematics. American Mathematical Society, pp. 183–186.

Vafa, C. and E. Witten (1995). "On Orbifolds with Discrete Torsion". In: *Journal of Geometry and Physics* 15, pp. 189–214. DOI: 10.1016/0393-0440(94)00048-9. arXiv: hep-th/9409188.

Yan, J. (2025). "A New Gauge-Theoretic Construction of the 4-Dimensional Hyperkähler ALE Spaces". In: *Mathematische Annalen*. Source edition: arXiv v2, 7 January 2026, section 2.1. DOI: 10.1007/s00208-024-02944-3. arXiv: 2310.10979.

Chapter IV.4

Toric geometry: fans, polytopes, and GLSM realizations

IV.4.1 A conifold in three descriptions

The conifold appears first as the hypersurface $AD - BC = 0$ in $\mathbb{C}^4$. It also appears as a cone with four lattice rays and as a quotient of four homogeneous coordinates. These are three descriptions of the same affine geometry, but they remember different things. The equation exposes its functions. The lattice retains integral data. The quotient makes the two small resolutions visible when a Fayet–Iliopoulos (FI) level is varied. The useful question is therefore not merely how to draw a polygon. It is which information survives each passage between a ring, a fan, and a gauge quotient.

This chapter develops that dictionary using explicit small examples. A unit triangle gives $\mathbb{C}^3$. A square gives the conifold and its two FI chambers. Formal Hilbert series count functions on their affine rings. A fixed bipartite graph then recovers the square polygon. Finally, a four-dimensional cone shows why an integer ambient lattice is essential: the same real cone and a zero rational charge kernel can still hide a finite quotient. Chapter 5 will study conifold deformation and resolution in more detail. Chapters VII.2–VII.4 use the polygon and graph interface in actual probe constructions; this chapter establishes the underlying geometry, not their dynamics.

IV.4.2 Cones and their dual semigroups

What functions does a cone encode? Let $N \cong \mathbb{Z}^d$ be a lattice and $M = \mathrm{Hom}_{\mathbb{Z}}(N, \mathbb{Z})$ its character lattice. A vector $m \in M$ labels a torus character χ^m, with $\chi^m \chi^{m'} = \chi^{m+m'}$. A rational polyhedral cone $\sigma \subset N_{\mathbb{R}}$ is generated by finitely many lattice vectors. It is strongly convex if it contains no line. Its dual cone selects the characters regular on the

affine toric chart:

$$\sigma^\vee = \{m \in M_\mathbb{R} : \langle m, n\rangle \geq 0 \text{ for every } n \in \sigma\}, \qquad X_\sigma = \operatorname{Spec} \mathbb{C}[\sigma^\vee \cap M]. \quad \text{(IV.4.1)}$$

The last equality is the standard affine toric construction. A fan Σ is a finite collection of such cones, closed under faces, such that the intersection of any two cones is a face of each. This common-face condition lets the affine charts X_σ glue along their intersection charts. Its one-dimensional cones are rays. The primitive generator n_ρ of a ray is its first nonzero lattice point. The lattice, not just the real picture, determines which characters are allowed.

For a height-one example set $N = \mathbb{Z}^3$ and choose

$$n_0 = (0,0,1), \quad n_1 = (1,0,1), \quad n_2 = (0,1,1), \qquad V_3 = \begin{pmatrix} 0 & 1 & 0 \\ 0 & 0 & 1 \\ 1 & 1 & 1 \end{pmatrix}. \quad \text{(IV.4.2)}$$

The determinant is one. Hence these rays form a lattice basis, not just a basis over $\mathbb{Q}$. The dual basis is

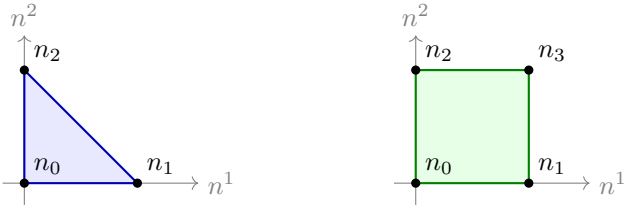
$$m_0 = (-1,-1,1), \qquad m_1 = (1,0,0), \qquad m_2 = (0,1,0), \qquad \langle m_i, n_j\rangle = \delta_{ij}. \quad \text{(IV.4.3)}$$

Write $m = \sum_i a_i m_i$. Integrality of m makes every a_i an integer, while $m \in \sigma^\vee$ makes every a_i nonnegative. Thus the semigroup has three free generators:

$$\sigma^\vee \cap M = \mathbb{N}m_0 \oplus \mathbb{N}m_1 \oplus \mathbb{N}m_2, \qquad \mathbb{C}[\sigma^\vee \cap M] = \mathbb{C}[\chi^{m_0}, \chi^{m_1}, \chi^{m_2}] \cong \mathbb{C}[u,v,w]. \quad \text{(IV.4.4)}$$

The unit triangle in Figure IV.4.1 is therefore a genuine $\mathbb{C}^3$ cone in this lattice. Its height-one section is a two-dimensional diagram; the full cone is three-dimensional.

The dual-basis step is the important part of this example. If the determinant of V_3 had absolute value greater than one, each real dual-basis vector would still exist. It need not lie in M, however. Then the nonnegative integer span of those vectors would not describe all integral characters. This is why a polygon drawn with the same Euclidean shape can define a different affine variety after the lattice is changed. For a direct check, evaluate m_0 on the three rays: $1, 0, 0$. Similarly m_1 gives $0, 1, 0$ and m_2 gives $0, 0, 1$. A negative coefficient in any character expansion would be detected by one ray, so cancellation cannot produce another regular character.



$\mathbb{C}^3$: unit triangle conifold: unit square

Figure IV.4.1: Height-one sections in the declared $N = \mathbb{Z}^3$ lattice. The unit triangle has unimodular ray matrix V_3. Adding the fourth ray $(1,1,1)$ gives the conifold square. Coordinates on the page are the first two components of rays whose third component is one.

A non-unimodular ray matrix changes this conclusion even when its real cone resembles the positive orthant. In Section IV.4.7 we will keep four real coordinate rays but enlarge the ambient lattice. The dual semigroup then loses all odd-degree cover monomials. The general local identification in (IV.4.1) is a cited toric result; the displayed free-semigroup calculation is the direct example. The distinction matters whenever a toric diagram is transferred to a brane construction: the sketch alone does not carry the character lattice.

The fan language will shortly become useful in a different way. A single affine cone retains its functions, while subdividing it into smaller cones records charts of a resolution. Gluing requires the face condition in the definition of a fan: merely listing a set of rays does not tell us which chart intersections to use. The conifold square is small enough that its two subdivisions can be compared directly.

IV.4.3 GLSM charges and saturated lattices

How can four homogeneous fields describe a three-dimensional cone? Order the conifold rays as n_0, n_1, n_2, n_3, where the first three are in (IV.4.2) and $n_3 = (1,1,1)$. Their ray map is

$$V : \mathbb{Z}^4 \longrightarrow N, \qquad V = \begin{pmatrix} 0 & 1 & 0 & 1 \\ 0 & 0 & 1 & 1 \\ 1 & 1 & 1 & 1 \end{pmatrix}. \tag{IV.4.5}$$

For $q = (q_0, q_1, q_2, q_3)$, the first two equations in $Vq = 0$ give $q_1 = q_2 = -q_3$; the third gives $q_0 = q_3$. Hence

$$\ker_{\mathbb{Z}} V = \mathbb{Z}Q, \qquad Q = (1,-1,-1,1), \qquad [\ker_{\mathbb{Z}} V : \mathbb{Z}(2Q)] = 2. \tag{IV.4.6}$$

The gcd of the entries of Q is one. This makes Q a primitive generator of the integral kernel. A rational nullspace calculation would see the line spanned by Q and $2Q$ as identical. It would miss their index. The 3×3 minor formed by the first three columns has determinant one, so these conifold rays span all of N; that ray-span index differs from the index of $2Q$ in the kernel.

This gives a practical two-stage integer calculation. First solve $Vq = 0$ over $\mathbb{Q}$ to find the dimension of the relation space. Then intersect that space with $\mathbb{Z}^4$ and take a saturated integral basis. A subgroup $L \subset \mathbb{Z}^r$ is saturated when $kq \in L$ for an integer $k \neq 0$ and $q \in \mathbb{Z}^r$ implies $q \in L$; equivalently, $\mathbb{Z}^r/L$ has no torsion. For this one-dimensional kernel, clearing denominators and dividing by the gcd produces Q. Finally, compute the gcd of the maximal 3×3 minors of V to test the span of the rays in N. The minor just exhibited makes that gcd one. In higher rank, Smith normal form performs the same integer-lattice calculation. It also distinguishes free relation directions from torsion in a cokernel.

There is a general quotient statement behind this elementary charge calculation. For a rational strongly convex fan Σ with primitive rays spanning $N_{\mathbb{R}}$, let X_Σ denote the toric variety, D_ρ its invariant prime divisors, and $\mathrm{Cl}(X_\Sigma)$ its full divisor class group.

Principal characters give the exact sequence

$$M \xrightarrow{V^T} \mathbb{Z}^{\Sigma(1)} \longrightarrow \mathrm{Cl}(X_\Sigma) \longrightarrow 0, \qquad m \longmapsto \sum_\rho \langle m, n_\rho \rangle D_\rho. \tag{IV.4.7}$$

The polynomial Cox ring $S = \mathbb{C}[x_\rho : \rho \in \Sigma(1)]$ is graded by this *full* class group, including any torsion. Let B_Σ be the irrelevant ideal generated by $x^{\widehat{\sigma}} = \prod_{\rho \notin \sigma(1)} x_\rho$ for maximal cones σ. Define $U_\Sigma = \operatorname{Spec} S \setminus V(B_\Sigma)$ and $G = \operatorname{Hom}(\mathrm{Cl}(X_\Sigma), \mathbb{C}^*)$. Each x_ρ has degree $[D_\rho]$, so a character $g \in G$ acts by

$$g \cdot x_\rho = g([D_\rho]) x_\rho. \tag{IV.4.8}$$

The class $[D_\rho]$ thus specifies any finite factor acting on that coordinate. A cone is simplicial when its ray generators are linearly independent over $\mathbb{R}$. Cox's quotient theorem then gives

$$U_\Sigma / G = X_\Sigma \quad \text{categorically;} \qquad \text{geometric iff } \Sigma \text{ is simplicial.} \tag{IV.4.9}$$

No smoothness, completeness, or projectivity assumption is used here. This is a cited theorem, not a result inferred from the conifold matrix. In a geometric quotient, distinct orbits remain distinct points. The categorical quotient need not separate them; at the affine wall below, two orbits whose closures meet have the same invariant image. For our ray matrix, the class group itself can be read from (IV.4.7). Since the rays span N, its transpose embeds M as a primitive rank-three sublattice of $\mathbb{Z}^4$. The primitive row Q annihilates that image. Ranks and the determinant-one minor show that its kernel is exactly the image, giving

$$\mathrm{Cl}(X_{\mathrm{con}}) \cong \mathbb{Z}^4 / V^T M \cong \mathbb{Z}, \qquad [a_0, a_1, a_2, a_3] \longmapsto a_0 - a_1 - a_2 + a_3. \tag{IV.4.10}$$

Thus the four Cox variables have degrees $1, -1, -1, 1$ in this particular free class group. This derivation uses the same integral data as the GLSM charge row, but the general class group may also have torsion. The latter possibility is why the full group appears in the theorem before any special $U(1)$ example. For a fan with a torus factor, such as the zero fan in $N = \mathbb{Z}$, the rays do not span $N_\mathbb{R}$: a zero-variable unaugmented Cox ring would incorrectly return a point instead of $\mathbb{C}^*$.

The conifold illustrates why the irrelevant ideal must accompany the charge row. Its four affine rays form a nonsimplicial cone, whereas the two subdivisions use different maximal cones and therefore different sets U_Σ. The same Q does not encode which pairs of coordinates may vanish. Moreover, torsion in $\mathrm{Cl}(X)$ gives a finite factor in G even when there is no continuous charge row. The fourfold in Section IV.4.7 makes that effect explicit. For the conifold toy GLSM we use the effective compact $U(1)$ with charges Q. Replacing it by the nonprimitive row $2Q$ without specifying the global group would change the effective-action question; it is not a harmless normalization.

One can see the group issue directly. The map $\lambda \mapsto (\lambda, \lambda^{-1}, \lambda^{-1}, \lambda)$ is faithful on $\mathbb{C}^*$. The map with exponents $2Q$ has kernel $\{+1, -1\}$. It has the same image in $(\mathbb{C}^*)^4$ after modding out that kernel, but it is an ineffective presentation if $\mathbb{C}^*$ itself is retained as the stated gauge group. By contrast, a torsion factor in the full Cox group can act faithfully even with no connected gauge direction. The data to record are the ray map, its integral image and kernel, the class-group grading, and the fan's excluded set.

IV.4.4 FI chambers and triangulations

What changes when the real moment level moves away from the singular conifold? Take four complex scalars x_i, no F-term constraints, and the full effective $U(1)$ action $x_i \mapsto e^{iQ_i\theta}x_i$. The classical D-flat equation, with the declared sign of the FI level, is

$$|x_0|^2 + |x_3|^2 - |x_1|^2 - |x_2|^2 = \zeta. \tag{IV.4.11}$$

At $\zeta = +2$, $x_0 = x_3 = 0$ would make the left side nonpositive, so that pair cannot vanish. At $\zeta = -2$, $x_1 = x_2 = 0$ is excluded. The exclusion also suffices for a representative on the moment level. Put $p = |x_0|^2 + |x_3|^2$ and $n = |x_1|^2 + |x_2|^2$. Along the positive real part $\rho > 0$ of the complexified action, the left side of (IV.4.11) becomes

$$f(\rho) = p\rho^2 - n\rho^{-2}. \tag{IV.4.12}$$

If $p > 0$, f rises strictly from $-\infty$ to $+\infty$ when $n > 0$. If $n = 0$, it rises from zero to $+\infty$. Thus every orbit with $p > 0$ meets each positive moment level exactly once in its positive real scaling, leaving only the compact phase to divide out. If $p = 0$, no positive level is possible. Symmetrically, for a negative level every orbit with $n > 0$ has exactly one such scaling, including $p = 0$, while $n = 0$ is excluded. This is the local classical bridge between the moment equation and the two complex quotient sets. Their irrelevant ideals are

$$\begin{aligned} B_+ &= (x_0, x_3), \quad U_+ = \mathbb{C}^4 \setminus \{x_0 = x_3 = 0\}, \\ B_- &= (x_1, x_2), \quad U_- = \mathbb{C}^4 \setminus \{x_1 = x_2 = 0\}. \end{aligned} \tag{IV.4.13}$$

For B_+ the complements of the two maximal cones are respectively x_0 and x_3. The corresponding square triangulation has diagonal joining rays 1 and 2. For B_- the complements are x_1, x_2; its diagonal joins rays 0 and 3. Figure IV.4.2 shows the two choices in the fixed ray order.

It is worth checking the fan statement rather than inferring it from the FI inequality alone. A triangle in the height-one square lifts to a three-dimensional cone. In the positive chamber the two maximal cones are $\langle n_1, n_2, n_3\rangle$ and $\langle n_0, n_1, n_2\rangle$. Their missing rays are n_0, n_3, so the Cox complement monomials are x_0, x_3. In the negative chamber the maximal cones are $\langle n_0, n_1, n_3\rangle$ and $\langle n_0, n_2, n_3\rangle$. Their missing rays are n_2, n_1. Each triangle has lattice area one half in the height plane. Its three lifted rays therefore form a unimodular basis. Consequently both resolved fans are smooth as well as simplicial. At the wall, all four rays generate a single three-dimensional cone, which is nonsimplicial. This verifies the different geometric status in (IV.4.9) for these specific fans.

The bundle can be read without guessing its name. On $x_0 \neq 0$ define

$$u = \frac{x_3}{x_0}, \qquad y_1 = x_0x_1, \quad y_2 = x_0x_2. \tag{IV.4.14}$$

All three expressions are invariant under $\mathbb{C}^*$. On $x_3 \neq 0$ take $u' = x_0/x_3$ and $y'_j = x_3x_j$. On the overlap,

$$u' = u^{-1}, \qquad y'_j = uy_j \quad (j = 1, 2). \tag{IV.4.15}$$

The pair (x_0, x_3) supplies homogeneous coordinates on $\mathbb{P}^1$. The two fiber coordinates each transform by the tautological $\mathcal{O}_{\mathbb{P}^1}(-1)$ transition. Thus the positive chamber is $\mathcal{O}(-1) \oplus \mathcal{O}(-1) \to \mathbb{P}^1$. In the negative chamber, exchange the positive pair (x_0, x_3) with the negative pair (x_1, x_2) and repeat the two charts. This yields a second copy of $\mathcal{O}(-1) \oplus \mathcal{O}(-1)$, now with $[x_1 : x_2]$ as the exceptional base. The two maps contract distinct curves to the same affine point. The calculation identifies classical quotient spaces; it does not equate their metrics or establish a quantum GLSM phase theorem.

At the numerical level $\zeta = +2$, set $x_1 = x_2 = 0$. The moment equation becomes $|x_0|^2 + |x_3|^2 = 2$. Its quotient by the common $U(1)$ phase is $\mathbb{P}^1$, the zero section of the two fibers. The point $(\sqrt{2}, 0, 0, 0)$ represents $[x_0 : x_3] = [1 : 0]$; $(0, 0, 0, \sqrt{2})$ represents the other chart endpoint. For $\zeta = -2$, setting $x_0 = x_3 = 0$ instead leaves $|x_1|^2 + |x_2|^2 = 2$ and the base $[x_1 : x_2]$. These are actual D-flat representatives, not just statements about an excluded set. The moment-level sphere depends on the field normalization; the algebraic bundle transitions do not require a metric identification.

The negative chamber's fiber coordinates can be displayed as well. On $x_1 \neq 0$ define $v = x_2/x_1$ and $z_0 = x_1 x_0$, $z_3 = x_1 x_3$. On $x_2 \neq 0$, use $v' = x_1/x_2$ and $z'_i = x_2 x_i$ for $i = 0, 3$. Then

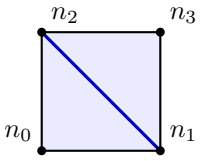
$$v' = v^{-1}, \qquad z'_0 = v z_0, \qquad z'_3 = v z_3. \tag{IV.4.16}$$

The same tautological transition appears, but its base is a different coordinate pair. This explicit swap is the local content of the two small resolutions in this quotient example.

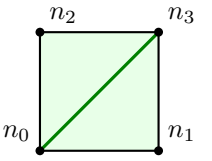
There is also a useful map from either bundle to the common affine conifold. In the positive $x_0 \neq 0$ chart, (IV.4.18) becomes

$$(A, B, C, D) = (y_1, y_2, u y_1, u y_2). \tag{IV.4.17}$$

On $x_3 \neq 0$ the corresponding expression is $(A, B, C, D) = (u' y'_1, u' y'_2, y'_1, y'_2)$, so the two formulas agree under (IV.4.15): $u' y'_j = y_j$ and $y'_j = u y_j$. In the negative chamber the $x_1 \neq 0$ map is $(A, B, C, D) = (z_0, v z_0, z_3, v z_3)$, while the $x_2 \neq 0$ map is $(v' z'_0, z'_0, v' z'_3, z'_3)$. They agree because $v' z'_i = z_i$ and $z'_i = v z_i$. If $y_1 = y_2 = 0$, the image is the origin for every $u \in \mathbb{P}^1$; this is exactly the contracted zero section. If $(A, B) \neq (0, 0)$, the affine matrix has rank one and $u = C/A = D/B$ wherever the denominators are defined. Thus the fiber away from the origin is one point on this chart. The other chart covers the cases with $(C, D) \neq (0, 0)$. This directly exhibits a proper exceptional curve in the local algebraic picture, while the affine coordinate ring stays fixed.



$\zeta > 0$: diagonal $(1, 2)$
$[x_0 : x_3]$, exclude $(x_0, x_3) = (0, 0)$



$\zeta < 0$: diagonal $(0, 3)$
$[x_1 : x_2]$, exclude $(x_1, x_2) = (0, 0)$

Figure IV.4.2: The two triangulations of the conifold square in the fixed coordinate order. The positive FI level excludes $x_0 = x_3 = 0$ and uses diagonal $(1, 2)$. The negative level excludes $x_1 = x_2 = 0$ and uses diagonal $(0, 3)$. Each internal diagonal represents the compact curve in its resolved fan.

At $\zeta = 0$ the exceptional curve shrinks. The affine cone is nonsimplicial, and its Cox quotient is categorical rather than geometric. For example, the distinct complexified orbits of $(1, 0, 0, 0)$ and $(0, 0, 0, 0)$ have the same four bilinear invariants, all zero. The first point is not D-flat at $\zeta = 0$; its orbit closure contains the origin, which is the D-flat representative of that closure class. This keeps the algebraic orbit statement separate from the real moment-level statement. Chapter 5 develops the associated small resolutions alongside deformations, while probe dynamics belongs to Volume VI.

IV.4.5 Graded coordinate rings

Which functions survive the quotient, and how many occur at a chosen degree? Give each homogeneous conifold variable formal degree one. The $U(1)$ action pairs positive variables (x_0, x_3) with negative variables (x_1, x_2). Four degree-two invariants form a rank-one matrix:

$$\begin{pmatrix} A & B \\ C & D \end{pmatrix} = \begin{pmatrix} x_0 \\ x_3 \end{pmatrix} \begin{pmatrix} x_1 & x_2 \end{pmatrix} = \begin{pmatrix} x_0x_1 & x_0x_2 \\ x_3x_1 & x_3x_2 \end{pmatrix}, \qquad AD - BC = 0. \tag{IV.4.18}$$

Every invariant monomial has as many positive as negative factors. Repeatedly pair one factor of each sign; hence the four bilinears generate the invariant ring. The only relation among a generic 2×2 rank-one matrix's entries is its determinant: for instance, on $A \neq 0$ one can solve $D = BC/A$, and the irreducible determinant hypersurface has the required dimension three. Thus the affine ring is

$$R_{\mathrm{con}} = \mathbb{C}[A, B, C, D]/(AD - BC), \qquad H_{\mathrm{con}}(t) = \frac{1 - t^4}{(1 - t^2)^4}. \tag{IV.4.19}$$

This ring is shared by both FI chambers because regular affine invariants forget which exceptional $\mathbb{P}^1$ was inserted.

We can also recover the four generators directly from the dual cone. For $m = (a, b, c) \in M$, regularity on the four rays means

$$c \geq 0, \qquad a + c \geq 0, \qquad b + c \geq 0, \qquad a + b + c \geq 0. \tag{IV.4.20}$$

Four generating characters are $(0,-1,1)$, $(-1,0,1)$, $(1,0,0)$ and $(0,1,0)$. The Cox monomial map sends χ^m to $\prod_i x_i^{\langle m,n_i\rangle}$. In this order the characters become A,B,C,D of (IV.4.18). Their one lattice relation is

$$(0,-1,1)+(0,1,0)=(-1,0,1)+(1,0,0), \qquad AD=BC. \tag{IV.4.21}$$

To see generation, take an integral (a,b,c) satisfying the four inequalities. If $a<0$, subtract $-a$ copies of $(-1,0,1)$; if $b<0$, subtract $-b$ copies of $(0,-1,1)$. The last inequality ensures the remaining third component stays nonnegative when both subtractions occur. What remains has nonnegative first two components; subtract those copies of $(1,0,0)$ and $(0,1,0)$. The residue is $(0,0,c')$ with $c'\geq 0$, and $(0,0,1)$ is the sum of either pair in (IV.4.21). This gives a direct semigroup route to the determinant ring.

We can check the Hilbert coefficients without using the presentation. At total degree $2k$, the positive exponents sum to k and the negative exponents also sum to k. Each pair has $k+1$ choices, giving

$$[t^{2k}]H_{\mathrm{con}}(t)=(k+1)^2, \qquad H_{\mathrm{con}}(t)=\sum_{k\geq 0}(k+1)^2t^{2k}. \tag{IV.4.22}$$

The first counts are $1,4,9,16,25$ at degrees $0,2,4,6,8$. Setting $q=t^2$, the identity $\sum_{k\geq 0}(k+1)^2q^k=(1+q)/(1-q)^3$ agrees with (IV.4.19), since $(1-q^2)/(1-q)^4=(1+q)/(1-q)^3$.

The generating-function identity can be derived rather than memorized. Start from $(1-q)^{-1}=\sum_{k\geq 0}q^k$. Differentiate once and multiply by q to generate kq^k; differentiate again to generate k^2q^k. Combining k^2+2k+1 yields

$$\sum_{k\geq 0}(k+1)^2q^k=\frac{q(1+q)}{(1-q)^3}+\frac{2q}{(1-q)^2}+\frac{1}{1-q}=\frac{1+q}{(1-q)^3}. \tag{IV.4.23}$$

This is a useful cross-check because it uses only composition counting, not the claim that the determinant is the full ideal of relations. The two routes agree at every coefficient, not just at a finite sample.

For example, at degree four the positive exponents may be $(2,0)$, $(1,1)$ or $(0,2)$. The negative exponents have the same three choices, making nine distinct monomials. In the generator presentation there are ten quadratic monomials in A,B,C,D, but $AD=BC$ removes one. This makes the numerator $1-t^4$ concrete: it records a degree-four relation, not the absence of degree-four functions.

A second example changes the finite group rather than the FI chamber. Let $\omega^3=1$, $\omega\neq 1$, and let the generator of $\mathbb{Z}_3$ act diagonally on (z_1,z_2,z_3) by multiplication by ω. A monomial $z_1^{a_1}z_2^{a_2}z_3^{a_3}$ is invariant exactly when $a_1+a_2+a_3\equiv 0 \pmod 3$. At degree $3k$ the exponent vectors are lattice points in a triangle slice, with

$$\#\{a_i\geq 0:\sum_i a_i=3k\}=\binom{3k+2}{2}; \qquad 1,10,28,55 \text{ for } k=0,1,2,3. \tag{IV.4.24}$$

There are ten cubic invariant monomials, but their relations are not captured by saying merely that the generators are ten in number. At degree three, the ten compositions

consist of the three cubes z_i^3, the six terms $z_i^2 z_j$ with $i \neq j$, and $z_1 z_2 z_3$. At degree six, stars and bars gives $\binom{8}{2} = 28$ without listing every monomial. A compact way to count the whole ring is the character filter:

$$H_{\mathbb{C}^3/\mathbb{Z}_3}(t) = \frac{1}{3}\sum_{j=0}^{2} \frac{1}{(1-\omega^j t)^3} = \sum_{k\geq 0} \binom{3k+2}{2} t^{3k}. \tag{IV.4.25}$$

The first equality averages monomial characters: the average of ω^{jd} is one for $3 \mid d$ and zero otherwise. With $q = t^3$, sum the quadratic coefficient in k to obtain

$$\sum_{k\geq 0} \binom{3k+2}{2} q^k = \frac{1+7q+q^2}{(1-q)^3}. \tag{IV.4.26}$$

For example the q coefficient is $3 + 7 = 10$, and the q^2 coefficient is $6 + 21 + 1 = 28$. These are counts of polynomial functions at the declared formal degree. A physical R charge or Reeb grading requires extra dynamical or geometric input. This distinction matters when the same Hilbert series is used in the mesonic counting of Chapter VII.5.

To see the numerator of (IV.4.26), expand the binomial coefficient as $(9k^2+9k+2)/2$. The familiar series for 1, k and k^2 then give

$$\sum_{k\geq 0} \frac{9k^2+9k+2}{2} q^k = \frac{9q(1+q)}{2(1-q)^3} + \frac{9q}{2(1-q)^2} + \frac{1}{1-q}. \tag{IV.4.27}$$

Putting the terms over $(1-q)^3$ gives $1 + 7q + q^2$. Unlike the conifold presentation, that numerator should not be read as the complete list of minimal relations among the ten cubic generators. A Hilbert numerator depends on the chosen denominator and can hide a more involved syzygy structure. The formal q here counts one unit per cubic invariant, while q in the conifold example counts one unit per bilinear. The comparison is meaningful only after those two declared regradings are kept straight.

IV.4.6 From a graph to toric data

How can a periodic bipartite graph produce the square we have used? Put one white and one black vertex in a fundamental cell of an oriented torus. A perfect matching covers each vertex once. Here each of the four connecting edges alone is a matching. Fix horizontal and vertical cycles whose Laurent variables are z and w. In the fixed source presentation, the four edge weights are $1, -z, -w, -zw$. With rows indexed by white and columns by black vertices, the signed adjacency matrix has a single entry:

$$K(z,w) = [1 - z - w - zw], \qquad P(z,w) = \det K(z,w) = 1 - z - w - zw. \tag{IV.4.28}$$

This is a graph calculation with a specified signing and cycle basis. The four one-edge matchings have winding exponents

$$(0,0), \quad (1,0), \quad (0,1), \quad (1,1). \tag{IV.4.29}$$

Their convex hull, the Newton polygon of P, is the unit square in Figure IV.4.3. In the same convention, the three-edge honeycomb control gives $P_{\mathbb{C}^3} = 1 - z - w$ and the unit triangle. The comparison connects the earlier cone examples to actual finite graph data, without selecting a quiver action.

The signing has a local condition, beyond the choice of torus cycles. For a bipartite torus graph with positive real unsigned edge weights, choose an edge sign $\epsilon_e = \pm 1$ so that around every face with $2k$ boundary edges,

$$\prod_{e \in \partial f} \epsilon_e = (-1)^{k+1}. \tag{IV.4.30}$$

Thus a face with two edges has sign product $+1$, while one with four has product -1. After fixing a reference matching and the two winding paths, this signing gives the same determinant sign to every matching at a fixed relative height (h_x, h_y). The two global winding-sign choices are extra data: the local face rule does not fix the sign of each height sector. They do not affect same-height sign coherence. Several ordinary matchings at the same height therefore add in magnitude. If $w_e > 0$ is the unsigned edge weight, their coefficient magnitude is

$$c_{h_x,h_y} = \sum_{M\colon h(M)=(h_x,h_y)} \prod_{e \in M} w_e > 0 \tag{IV.4.31}$$

whenever that height occurs. Their count changes a coefficient, but cannot cancel an extreme exponent. The polygon retains heights, not the individual matchings that produce them.

For the three-edge honeycomb control the analogous single entry is

$$K_{\mathbb{C}^3}(z, w) = [1 - z - w], \qquad \operatorname{Newt}(\det K_{\mathbb{C}^3}) = \operatorname{conv}\{(0,0), (1,0), (0,1)\}. \tag{IV.4.32}$$

The fourth edge in the square example adds the point $(1, 1)$. It does not change the definition of the winding axes or the row and column ordering. The edge signs are part of this example's Kasteleyn signing; an unsigned drawing would not determine the coefficients.

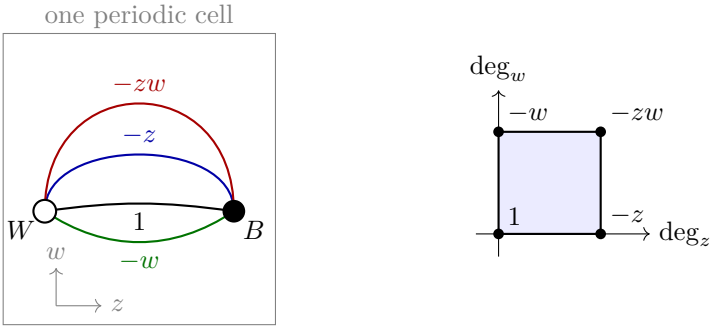


Figure IV.4.3: The fixed one-cell graph and its Newton polygon. Each of four edges joins the white vertex W to the black vertex B, with the indicated signed winding weight. The arcs separate labels; periodic boundary crossings are encoded by the weights. Horizontal z and vertical w cycles define the exponent axes. The four one-edge matchings give the four marked lattice points.

For a general bipartite torus graph with the local signing and positive weights just stated, the determinant expands into signed perfect matchings. A reference matching and winding paths determine relative height changes; their exponents give the Newton polygon. We cite this graph-to-polygon result here. Changing the reference path can multiply P by an overall Laurent monomial, translating every exponent equally. A declared $GL(2,\mathbb{Z})$ change of cycle basis changes coordinates on the polygon. By contrast, flipping the winding of one edge alone while keeping the axes fixed changes (IV.4.28); it is not an invisible convention change. The polygon by itself does not determine a unique quiver or prove worldvolume dynamics. Those physical steps are developed with their own premises in Volume VI.

Here is a concrete distinction between the allowed transformations. Multiplying the fixed polynomial by z^2w^{-1} sends every exponent (a,b) to $(a+2,b-1)$. The square translates and its edge differences stay unchanged. If instead we set $z'=zw$ and $w'=w$, then

$$z^a w^b = (z')^a (w')^{b-a}, \qquad (a,b) \longmapsto (a,b-a). \tag{IV.4.33}$$

The matrix of this shear has determinant one, so it is an integral change of cycle coordinates. Applying it to all four terms moves the square to a lattice parallelogram of the same normalized area. A change of the z winding on just the $-z$ edge, with all other terms held fixed, is neither this global shear nor a common translation. The term list in Exercise E4 therefore requires the stated cycles.

Additional complex or signed edge factors can instead make a same-height coefficient vanish at a special choice of factors. That specialization has different weight hypotheses from the positive matching count above. The fixed one-cell calculation teaches the forward map at its declared weights. An inverse algorithm requires additional graph consistency data; the same lattice square can occur in more than one graph presentation.

IV.4.7 Fourfolds and compact quotients

What does a rational ray calculation miss in a toric fourfold? Let N_4 be a rank-four lattice, $M_4 = \mathrm{Hom}_{\mathbb{Z}}(N_4, \mathbb{Z})$, and $n_i \in N_4$ primitive rays of a full-dimensional affine cone. A height-one, Gorenstein toric construction has an *integral* $m_0 \in M_4$ with $\langle m_0, n_i \rangle = 1$ for all rays. Its toric diagram lives in a three-dimensional affine hyperplane. For a ray map $V : \mathbb{Z}^r \to N_4$, the full Cox group is controlled by the cokernel of $V^T : M_4 \to \mathbb{Z}^r$. A cover monomial $x^a = \prod_i x_i^{a_i}$, $a \in \mathbb{N}^r$, is invariant precisely if its Cox degree vanishes. The general integral test is

$$a \in V^T M_4 \quad \Longleftrightarrow \quad \text{there is } m \in M_4 \text{ with } V^T m = a. \tag{IV.4.34}$$

This membership test works for any number of rays. Only when $r = 4$ and V is nonsingular over $\mathbb{Q}$ may it be shortened to

$$(V^T)^{-1} a \in M_4 \quad \text{in an integral basis of } M_4. \tag{IV.4.35}$$

A fourfold may have more than four rays, so dimension alone does not license an inverse matrix.

The test also explains what a rational charge computation can and cannot provide. A basis for $\ker_{\mathbb{Q}} V$ imposes linear equations on a. These equations are necessary for membership in $V^T M_4$. They determine its real span, but can leave congruence conditions unresolved. In the conifold example the ray image is saturated, so the single equation $Q \cdot a = 0$ is sufficient for an integral exponent. The forthcoming index-two fourfold has no rational kernel at all. There the missing condition is pure parity. In a general rectangular ray matrix, Smith normal form can reveal both the free charge equations and the finite congruences. Writing only a rational inverse, when one exists, discards the distinction between an integral character and a fractional one.

Now enlarge the standard lattice to

$$N' = \mathbb{Z}^4 + \mathbb{Z}h, \qquad h = \tfrac{1}{2}(1,1,1,1), \qquad n_i = e_i \ (i = 1, \dots, 4). \tag{IV.4.36}$$

The rays are primitive in N'. Relative to the basis (e_1, e_2, e_3, h), they form the matrix

$$V' = \begin{pmatrix} 1 & 0 & 0 & -1 \\ 0 & 1 & 0 & -1 \\ 0 & 0 & 1 & -1 \\ 0 & 0 & 0 & 2 \end{pmatrix}, \qquad |\det V'| = 2, \qquad \ker_{\mathbb{Q}} V' = 0. \tag{IV.4.37}$$

Indeed $e_4 = 2h - e_1 - e_2 - e_3$. In the smaller ambient lattice $\mathbb{Z}^4$, the same four real rays make the identity matrix and have determinant one. The rational kernel is zero in both cases. The index two is visible only after the ambient *integer* lattice is specified.

The integral dual lattice of N' is

$$M' = \{m \in \mathbb{Z}^4 : \textstyle\sum_i m_i \text{ is even}\}. \tag{IV.4.38}$$

Indeed pairing with h requires half the sum of components to be an integer. With the four standard rays, (IV.4.34) says that a monomial x^a is invariant exactly when

$\sum_i a_i$ is even. Equivalently, the finite quotient group is $\mathbb{Z}_2$ acting by $(x_1, x_2, x_3, x_4) \mapsto (-x_1, -x_2, -x_3, -x_4)$. For clarity, V'^T in the displayed basis has image consisting of vectors with even component sum; for a unit exponent its inverse has a half-integral fourth dual coordinate. Thus x_1 is excluded and x_1x_2 is included. The height functional $m_0 = (1, 1, 1, 1)$ belongs to M' and pairs to one with every e_i. The cone is a height-one toric fourfold despite its finite quotient.

The inverse criterion can be solved explicitly in this square case. Writing $V'^T m = a$ gives $m_1 = a_1$, $m_2 = a_2$, $m_3 = a_3$ and $-m_1 - m_2 - m_3 + 2m_4 = a_4$. Thus

$$m_4 = \frac{a_1 + a_2 + a_3 + a_4}{2}. \tag{IV.4.39}$$

The parity condition is now visible without invoking a general quotient classification. The four unit vectors all fail it, so all four cover coordinates carry the same nontrivial finite character. Every pair of cover coordinates passes it. This direct character test is stronger than merely reporting that $|\det V'| = 2$.

At ordinary cover degree $2k$ all four-variable monomials survive, so the invariant dimensions are

$$\begin{gathered}\dim R_{2k} = \binom{2k+3}{3}, \qquad \dim R_{2k+1} = 0, \\ (\dim R_0, \dim R_2, \dim R_4, \dim R_6) = (1, 10, 35, 84).\end{gathered} \tag{IV.4.40}$$

The finite-group projector gives an independent generating function. The identity element contributes the full cover ring; the sign element acts by $(-1)^d$ on degree-d monomials. Averaging the two characters therefore yields

$$H_{\mathrm{diag}}(t) = \tfrac{1}{2}\left(\frac{1}{(1-t)^4} + \frac{1}{(1+t)^4}\right). \tag{IV.4.41}$$

The even coefficients are $\binom{2k+3}{3}$ and the odd ones cancel. This confirms the direct dual-lattice computation while making the actual diagonal sign action explicit. Figure IV.4.4 contrasts the two ambient lattices. The geometric real cone did not change. Its allowed characters did.

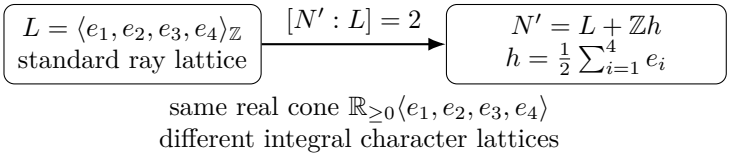


Figure IV.4.4: The same coordinate orthant with two integral ambient lattices. The additional point $h = (e_1 + e_2 + e_3 + e_4)/2$ in N' makes the ray span $\mathbb{Z}^4$ an index-two sublattice. The sketch is a lattice inclusion diagram; the determinant and dual-lattice equations establish the quotient and its diagonal action.

Even an index and a height condition do not determine the action. Consider the

independent integer matrix

$$V_{\mathrm{asym}} = \begin{pmatrix} 1 & -1 & 0 & 0 \\ 0 & 2 & 0 & 0 \\ 0 & 0 & 1 & 0 \\ 0 & 0 & 0 & 1 \end{pmatrix}, \qquad |\det V_{\mathrm{asym}}| = 2. \tag{IV.4.42}$$

Its columns are primitive: the second is $(-1, 2, 0, 0)$, whose nonzero entries have gcd one. The integer height $m_0 = (1, 1, 1, 1)$ pairs to one with every column. Solving $V_{\mathrm{asym}}^T m = a$ gives

$$m_1 = a_1, \quad m_2 = \frac{a_1 + a_2}{2}, \quad m_3 = a_3, \quad m_4 = a_4. \tag{IV.4.43}$$

Only $a_1 + a_2$ must be even. The resulting $\mathbb{Z}_2$ acts by a sign on the first two cover variables and trivially on the last two. Hence x_3 is invariant, while x_1 is not. At degree d, sum over even $j = a_1 + a_2 \le d$: there are $j + 1$ choices for the first pair and $d - j + 1$ for the last pair. This yields

$$\begin{aligned} \dim R_d &= \sum_{\substack{0 \le j \le d \\ j \text{ even}}} (j + 1)(d - j + 1), \\ (\dim R_0, \dim R_2, \dim R_4, \dim R_6) &= (1, 6, 19, 44). \end{aligned} \tag{IV.4.44}$$

Degree one already has two invariants, x_3, x_4. Both examples have index two, zero rational kernel and integral height one. Their finite characters and Hilbert counts differ. This is the boundary relevant to fourfold probe models: the algebraic compact quotient must be read from the full lattice. No M2-brane vacuum identification or inverse brane construction follows from these toric calculations alone.

The asymmetric action has a different character average:

$$H_{\mathrm{asym}}(t) = \tfrac{1}{2}\left(\frac{1}{(1-t)^4} + \frac{1}{(1+t)^2(1-t)^2} \right). \tag{IV.4.45}$$

The second denominator records two sign-changing and two fixed coordinates. Expanding the identity contribution alone would give ten degree-two cover monomials. The sign contribution has trace two at that degree, so the projector keeps $(10 + 2)/2 = 6$. This recovers the same number as the exponent-parity sum without assuming that an index-two lattice must act diagonally on every coordinate.

The first asymmetric counts can be checked before using the general sum. At degree two, $j = 0$ contributes the three monomials in x_3, x_4 and $j = 2$ contributes three in x_1, x_2, totaling six. At degree four, the sectors $j = 0, 2, 4$ contribute $5, 9, 5$, totaling nineteen. At degree six they contribute $7, 15, 15, 7$, totaling forty-four. The diagonal action instead keeps every monomial of even total degree, regardless of which variables appear. The difference between 6 and 10 at degree two already distinguishes the actions.

IV.4.8 Exercises

Use the conventions and ordered data of this chapter. For E1–E6 the named JSON fields are the numerical or finite answers checked by the companion grader; the requested derivations remain written parts of the exercise. E7 is written only.

E1. For the ordered conifold rays in (IV.4.5), solve the *integral* kernel and submit a primitive row as `{"charge":[q0,q1,q2,q3]}`. Either overall sign is allowed. Explain the index of its double.

E2. With every homogeneous variable of formal degree one, compute invariant dimensions at conifold degrees $0, 2, 4, 6, 8$. Submit the array field `coefficients` in that degree order. Derive the result both by monomial compositions and by the determinant ring.

E3. At $\zeta = +2$ and -2, identify the pair that cannot vanish simultaneously. Submit the two array fields `positive_excluded` and `negative_excluded`. Explain the two charts and fiber transition in one chamber.

E4. For the signed graph of (IV.4.28), submit four objects in the array field `terms`. Each object has integer fields `z`, `w` and `coefficient`. Keep the fixed winding cycles. Draw the Newton polygon and identify what a global cycle change does.

E5. For N' in (IV.4.36), submit the integer field `ray_span_index` and an array field `even_degree_coefficients` in degree order $0, 2, 4, 6$. Explain why the rational kernel misses the finite action.

E6. For the diagonal scalar $\mathbb{Z}_3$ action on $\mathbb{C}^3$, submit invariant dimensions at ordinary degrees $0, 3, 6, 9$ as `{"coefficients":[c0,c3,c6,c9]}`. Derive the values using both the character filter and lattice slices.

E7. Compare the diagonal and asymmetric index-two fourfolds. Then give separate examples showing why a common rational cone does not fix a compact quotient, why formal Hilbert degree is not a physical R charge, and why a Newton polygon does not establish full dimer gauge-theory dynamics. State which extra input each physical identification would need. This is a written task.

IV.4.9 Take-home message

Take-home message

Use integral rays and their dual semigroup to compute regular functions and the full quotient group. Use a primitive charge and FI level to find the conifold's two small resolutions, then count their common affine ring at a declared formal grading. Use a locally signed graph with fixed cycles to recover its Newton polygon. In four dimensions, check the ambient lattice for a finite quotient even when the rational charge kernel vanishes. Each calculation stops at geometric or combinatorial data until a physical brane construction supplies its own premises.

Status and sources

Section IV.4.2 uses the general affine semigroup identification from Cox (1995, physical p. 6, Lemma 2.2) [MATH]. The three-ray dual-basis and $\mathbb{C}^3$ calculations are explicit here

[MATH]. The threefold height-one convention is illustrated in Hanany and Kennaway (2005, physical p. 9, eqs. (3.6)–(3.7)).

Section IV.4.3 derives the primitive conifold kernel and doubled-row index [MATH]. The full divisor-class grading, irrelevant ideal, character group, categorical quotient and geometric-if-simplicial boundary are Cox (1995, physical pp. 2, 4–6, §1 and Theorem 2.1) [MATH]. Cox's ray-span hypothesis excludes the unaugmented zero-fan torus example. Sections IV.4.4 and IV.4.5 compute the two classical conifold charts, invariant ring and formal Hilbert counts [MATH]. The FI-sign premise comes from Witten (1993, physical p. 2, eqs. (1.1)–(1.3)) [GEO-E]. The physical premise is four scalars, full effective $U(1)$ and no F terms; no quantum transition or metric equality is deduced. The diagonal $\mathbb{Z}_3$ example is algebraic [MATH].

Section IV.4.6 uses the source-fixed signed one-cell graphs of Hanany and Kennaway (2005, physical p. 10, Fig. 2 and eqs. (3.8)–(3.9)) [MATH]. The general matching-height relation is cited from Franco et al. (2006, physical pp. 16–17, eqs. (3.1)–(3.3)) [MATH], cited rather than proved here. This use is graph-to-polygon only; it does not prove a unique quiver inverse or worldvolume dynamics. Section IV.4.7 derives both integral fourfold examples and their invariant counts [MATH]; its full-class-group interpretation uses Cox (1995, physical p. 5, exact sequence and Theorem 2.1). The formal degree in this chapter is not a physical R charge. The underlying conventions are the stated toric ray, quotient, orbifold, quiver and FI conventions. Downstream uses are Chapters 5, VII.1–VII.5 and VIII.6–VIII.7.

References

Cox, D. A. (1995). "The Homogeneous Coordinate Ring of a Toric Variety". In: *J. Algebraic Geom.* 4. arXiv version 2, revised 21 June 1993, pp. 17–50. arXiv: `alg-geom/9210008`.

Franco, S. et al. (2006). "Brane Dimers and Quiver Gauge Theories". In: *JHEP* 01. Source edition: arXiv version 2, p. 096. DOI: `10.1088/1126-6708/2006/01/096`. arXiv: `hep-th/0504110`.

Hanany, A. and K. D. Kennaway (2005). *Dimer models and toric diagrams*. Source edition: arXiv version 2. arXiv: `hep-th/0503149`.

Witten, E. (1993). "Phases of N=2 Theories in Two Dimensions". In: *Nucl. Phys. B* 403. Source edition: arXiv version 3, pp. 159–222. DOI: `10.1016/0550-3213(93)90033-L`. arXiv: `hep-th/9301042`.

Chapter IV.5

The conifold: deformation and small resolutions

IV.5.1 One node and three questions

The conifold is a useful meeting point of algebra, topology, and brane physics. Its equation is short, yet it admits three different questions. What are its regular functions? What replaces its singular point if a two-sphere is inserted? What changes if instead a three-sphere survives in a smooth complex deformation? A fourth question concerns the angular space seen from the node. The answers are related, but they measure different data.

Chapter 4 found the conifold as an affine toric quotient and drew its two FI chambers. Here we keep the coordinates throughout the geometry. The same matrix will exhibit the invariant ring, both projective incidence spaces, and the quadratic smoothing. The angular link then supplies a topology and, after a metric is specified, a normalised volume. Figure IV.5.1 previews the three routes. The arrows toward the node mean contraction or a limit of equations; they do not identify an FI parameter with a complex deformation parameter.

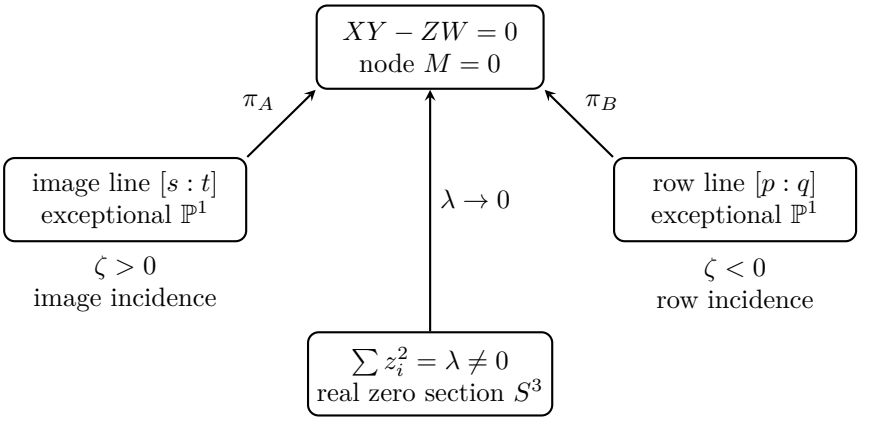


Figure IV.5.1: Three local operations starting from the same rank-one node. The two upper spaces retain different projective lines and contract them to $M = 0$. The lower space is the nonzero complex smoothing, whose displayed S^3 is a real zero section after a phase choice. The diagram specifies maps and limiting equations, not a metric or a quantum transition.

IV.5.2 The rank-one matrix cone

Why does a quotient by a single circle yield a threefold singularity? Use the ordered homogeneous variables of Chapter 4, (x_0, x_1, x_2, x_3), with primitive charge row $Q = (1, -1, -1, 1)$. Define the two positive and two negative charge vectors before forming any gauge invariants:

$$A = \begin{pmatrix} x_0 \\ x_3 \end{pmatrix}, \qquad B = \begin{pmatrix} x_1 \\ x_2 \end{pmatrix}, \qquad (A, B) \longmapsto (gA, g^{-1}B), \quad g \in \mathbb{C}^*. \tag{IV.5.1}$$

The full effective classical $U(1)$ theory considered here has four scalars, no F-term equations, and real moment-map level ζ. Its complex polynomial invariants are generated by the entries of the outer product

$$M = AB^T = \begin{pmatrix} X & Z \\ W & Y \end{pmatrix} = \begin{pmatrix} x_0x_1 & x_0x_2 \\ x_3x_1 & x_3x_2 \end{pmatrix}. \tag{IV.5.2}$$

Each entry has charge zero. Consequently every such matrix obeys

$$F(M) = \det M = XY - ZW = 0. \tag{IV.5.3}$$

The relation is necessary; to identify the whole invariant ring we must also show that no generator or relation is missing.

Take an invariant monomial $x_0^{r_0}x_3^{r_3}x_1^{s_1}x_2^{s_2}$. Charge neutrality says

$$r_0 + r_3 = s_1 + s_2 = d \geq 0. \tag{IV.5.4}$$

Pair one positive-charge factor with one negative-charge factor, then repeat d times. This factors the monomial into entries of M. Equivalently, a nonnegative 2×2 integer matrix with row sums (r_0, r_3) and column sums (s_1, s_2) records the pairings. Such a matrix exists whenever the totals agree: allocate $k_{11} = \min(r_0, s_1)$, then fill the remaining entries from the row and column sums. Thus the homomorphism

$$\mathbb{C}[X, Y, Z, W] \longrightarrow \mathbb{C}[x_0, x_1, x_2, x_3]^{\mathbb{C}^*} \tag{IV.5.5}$$

is onto.

The invariant ring is a domain of dimension three: on the dense set $x_0 \neq 0$ fix $x_0 = 1$ by the complex scaling, leaving three independent coordinates. The polynomial $XY - ZW$ is irreducible, so its principal ideal is prime of height one. An onto map from four polynomial generators to a three-dimensional domain has a height-one prime kernel. Since the kernel contains this irreducible polynomial, it equals its ideal. We have derived

$$\mathbb{C}[A, B]^{\mathbb{C}^*} \cong \frac{\mathbb{C}[X, Y, Z, W]}{(XY - ZW)}. \tag{IV.5.6}$$

This is the holomorphic polynomial invariant ring, rather than the algebra of all real functions on the moment-map quotient.

There is a useful finite-degree way to see why the determinant relation is exactly one relation at the first nontrivial degree. Assign formal degree one to each cover variable and degree two to each bilinear. At cover degree $2d$, an invariant monomial chooses degree d in the two components of A and degree d in the two components of B. Each two-variable choice has $d + 1$ monomials, so the invariant subspace has dimension

$$\dim \mathbb{C}[A, B]^{\mathbb{C}^*}_{2d} = (d + 1)^2, \qquad d = 0, 1, 2, \ldots. \tag{IV.5.7}$$

At $d = 1$, the four entries of M provide exactly four independent functions. At $d = 2$, ten quadratic words in those four entries would be available in a free polynomial ring, while the direct cover count gives nine. The single loss is $XY = ZW$. Summing the dimensions gives

$$H(q) = \sum_{d \geq 0} (d + 1)^2 q^d = \frac{1 + q}{(1 - q)^3} = \frac{1 - q^2}{(1 - q)^4}, \qquad q = t^2. \tag{IV.5.8}$$

The last form is the Hilbert series of four bilinear generators with one quadratic relation. This count checks the presentation degree by degree; the surjection and prime-kernel argument above establish it for the whole polynomial ring. The variables t and q count formal polynomial degree, as in Chapter 4. Neither has been identified with a physical R charge.

For a concrete check, $A = (2, 3)^T$ and $B = (5, 7)^T$ give

$$M = \begin{pmatrix} 10 & 14 \\ 15 & 21 \end{pmatrix}, \qquad 10 \cdot 21 - 14 \cdot 15 = 0. \tag{IV.5.9}$$

Conversely, every nonzero matrix satisfying (IV.5.3) has rank one and factors as AB^T. If $AB^T = A'B'^T \neq 0$, its column space fixes $A' = gA$ for some $g \neq 0$, and then

$B' = g^{-1}B$. The factorisation is unique modulo the complex gauge scaling. At $M = 0$ this argument fails, leaving room for different geometric completions.

The singularity is concentrated precisely there. The Jacobian is

$$(\partial_X F, \partial_Y F, \partial_Z F, \partial_W F) = (Y, X, -W, -Z), \tag{IV.5.10}$$

so the only critical point of the hypersurface is the zero matrix. Four ambient coordinates minus one equation make a complex threefold; the origin is an ordinary double point because the defining polynomial is a nondegenerate quadratic form after a linear change of coordinates.

The distinction between the cone and a probe vacuum is already visible here. A mesonic branch can use these functions when a specified brane theory supplies this quotient, but the determinant alone cannot establish the full interacting moduli space. Chapter VII.1 will give that engine its own fields and superpotential. The present ring calculation is the reusable geometric input.

IV.5.3 Two small resolutions

What can replace the node without changing the nonzero matrices? A rank-one matrix has a column image line and a row line. Retain one of those lines even when the matrix becomes zero. These choices produce two incidence spaces over the same affine cone $C = \{XY - ZW = 0\} \subset \mathbb{C}^4$.

For the image-line choice write $[s : t] \in \mathbb{P}^1$ and require both columns of M to lie in the span of $(s, t)^T$:

$$R_A = \{(M, [s : t]) \in C \times \mathbb{P}^1 : tX = sW,\ tZ = sY\}. \tag{IV.5.11}$$

On $s \neq 0$ set $u = t/s$ and take $f_1 = X$, $g_1 = Z$. The equations solve every other entry:

$$M = \begin{pmatrix} f_1 & g_1 \\ uf_1 & ug_1 \end{pmatrix}, \qquad (u, f_1, g_1) \in \mathbb{C}^3. \tag{IV.5.12}$$

On $t \neq 0$ set $v = s/t$ and take $f_2 = W$, $g_2 = Y$. Then

$$M = \begin{pmatrix} vf_2 & vg_2 \\ f_2 & g_2 \end{pmatrix}, \qquad (v, f_2, g_2) \in \mathbb{C}^3. \tag{IV.5.13}$$

On their overlap $v = u^{-1}$ and

$$(f_2, g_2) = u(f_1, g_1). \tag{IV.5.14}$$

These are the two smooth three-coordinate charts of the total space $\mathcal{O}_{\mathbb{P}^1}(-1) \oplus \mathcal{O}_{\mathbb{P}^1}(-1)$, with our stated choice of fiber coordinates. Figure IV.5.2 records the overlap rather than hiding the bundle in a name.

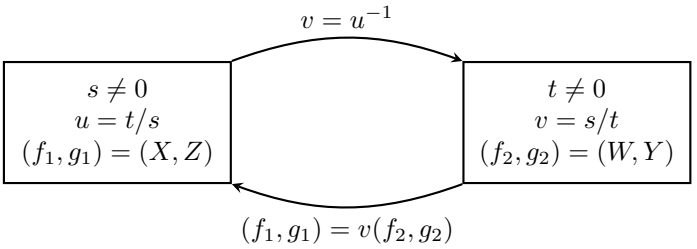


Figure IV.5.2: The image-line resolution on its two standard base charts. On the overlap $st \neq 0$, the relation fixes both fiber transitions. Setting the two fiber coordinates to zero leaves the entire projective base, which maps to the node. The row-line charts have the same transition with different matrix entries.

Retaining the row line instead means both rows are multiples of (p, q). Define

$$R_B = \{(M, [p : q]) \in C \times \mathbb{P}^1 : qX = pZ,\ qW = pY\}. \tag{IV.5.15}$$

On $p \neq 0$, $u = q/p$, take $(f_1, g_1) = (X, W)$; on $q \neq 0$, $v = p/q$, take $(f_2, g_2) = (Z, Y)$. These yield

$$M = \begin{pmatrix} f_1 & uf_1 \\ g_1 & ug_1 \end{pmatrix} \quad \text{and} \quad M = \begin{pmatrix} vf_2 & f_2 \\ vg_2 & g_2 \end{pmatrix}, \qquad v = u^{-1}, \quad (f_2, g_2) = u(f_1, g_1). \tag{IV.5.16}$$

Thus R_B is smooth with the same bundle type but a different projection to C. The two incidence conditions should not be interchanged: the first remembers the image, the second the row.

Projection $\pi_A : R_A \to C$ and $\pi_B : R_B \to C$ is proper because each incidence variety is closed in $C \times \mathbb{P}^1$, and projection from a product with projective space is proper. Over $M \neq 0$ the image and row lines are forced by M, so each map is an isomorphism there. Over $M = 0$, both incidence equations become $0 = 0$ and the fiber is $\mathbb{P}^1$. In a complex threefold this exceptional curve has codimension two, with no exceptional divisor:

$$\pi_A^{-1}(0) \cong \pi_B^{-1}(0) \cong \mathbb{P}^1, \qquad \dim_{\mathbb{C}} R_A = \dim_{\mathbb{C}} R_B = 3. \tag{IV.5.17}$$

This is why the resolutions are called small. Contracting either curve and expanding the other way gives the local conifold flop.

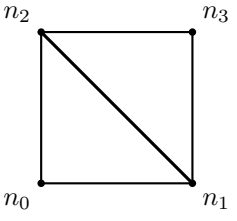
The exceptional points are not an extra collection of matrices. Every point on the zero section has the same matrix $M = 0$ under π_A or π_B; the additional datum is a line. To see the gluing directly in R_A, the point $u = 0$ in the first chart is $[s : t] = [1 : 0]$, while the point $v = 0$ in the second is $[0 : 1]$. Both have $f_i = g_i = 0$. For a finite nonzero u the two chart descriptions agree because $v = 1/u$ and both fiber coordinates obey (IV.5.14). The same check with (X, W) and (Z, Y) gives the row-line zero section in R_B. Thus the exceptional projective line is glued from two ordinary affine lines, rather than inferred solely from the incidence name.

The FI signs select the two incidence descriptions in the stated classical quotient. With the ordered charge vector in (IV.5.1), the D equation is

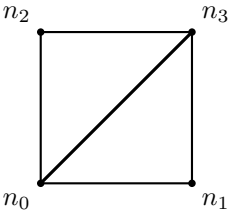
$$\mu_{\mathbb{R}} = |x_0|^2 + |x_3|^2 - |x_1|^2 - |x_2|^2 = |A|^2 - |B|^2 = \zeta. \tag{IV.5.18}$$

For $\zeta > 0$, A cannot vanish. Its line $[A] = [x_0 : x_3]$ survives at $M = 0$ and gives R_A. For $\zeta < 0$, B cannot vanish, and $[B] = [x_1 : x_2]$ gives R_B. This is an ordered charge statement; changing the order of the fields or the sign of Q without translating ζ would reverse the conclusion. The exceptional fiber can also be seen in the D-flat description. At positive level, $M = 0$ and $A \neq 0$ force $B = 0$; then $|A|^2 = \zeta$. Dividing this three-sphere by the remaining circle phase gives $S^3/U(1) = \mathbb{P}^1$. At negative level $A = 0$, $|B|^2 = -\zeta$, and the same Hopf quotient gives the row-line $\mathbb{P}^1$. In particular the endpoints $(\sqrt{\zeta}, 0)$ and $(0, \sqrt{\zeta})$ for positive level are distinct projective lines above the identical zero matrix. This is precisely the data the affine invariant ring forgets.

The square of Chapter 4 gives a second way to record which projective line was retained. With rays ordered $n_0 = (0, 0, 1)$, $n_1 = (1, 0, 1)$, $n_2 = (0, 1, 1)$, $n_3 = (1, 1, 1)$, the positive chamber uses the (n_1, n_2) diagonal, while the negative chamber uses (n_0, n_3). Figure IV.5.3 keeps the same four rays in both panels. The incidence atlases establish the geometry; the diagonal drawing is a compact record of the two triangulations and their chamber labels.



$\zeta > 0$: image line $[x_0 : x_3]$
diagonal (n_1, n_2)



$\zeta < 0$: row line $[x_1 : x_2]$
diagonal (n_0, n_3)

Figure IV.5.3: The same height-one conifold square, with its two triangulations in the fixed ray order. The diagonal and the retained projective line change together under the stated FI sign convention. This fan picture records the local birational models; it does not determine their metrics.

The nonunit example in (IV.5.9) makes the charts tangible. Its image coordinate is $u = x_3/x_0 = 3/2$. On R_A the first fiber is $(X, Z) = (10, 14)$ and the second is $(W, Y) = (15, 21)$, indeed $u(10, 14) = (15, 21)$. The row coordinate is $q/p = x_2/x_1 = 7/5$. On R_B, $(X, W) = (10, 15)$ and $(Z, Y) = (14, 21)$. These four cover coordinates are a convenient complex-orbit representative, not a claim that it satisfies the D equation for $\zeta = \pm 2$. Since both A and B are nonzero, scaling $(A, B) \mapsto (e^t A, e^{-t} B)$ changes the left side of (IV.5.18) continuously and strictly from $-\infty$ to $+\infty$, so either specified level has a unique real-scaling representative in that orbit.

The curve is a Kähler rather than a complex smoothing parameter in this local classical model. The sign of ζ chooses a chamber; the positive area of the exceptional

$\mathbb{P}^1$ is proportional to $|\zeta|$ after a metric and moment-map normalization are fixed. The dimensionless complexified Kähler coordinate also contains the B period, as set out in Chapter 1 and the book convention dictionary. No claim about a quantum phase of a general quiver follows from these charts.

IV.5.4 The deformation and its three-sphere

Can the same node be made smooth by changing its equation instead of inserting a curve? The answer is the family

$$C_\lambda^{\det} = \{M \in \mathbb{C}^4 : XY - ZW = \lambda\}. \tag{IV.5.19}$$

Its relation to the often used quadratic form is an explicit complex-linear coordinate change. Define

$$z_0 = \frac{X+Y}{2}, \quad z_1 = \frac{X-Y}{2i}, \quad z_2 = \frac{Z+W}{2i}, \quad z_3 = \frac{Z-W}{2}. \tag{IV.5.20}$$

The inverse is

$$X = z_0 + iz_1, \quad Y = z_0 - iz_1, \quad Z = iz_2 + z_3, \quad W = iz_2 - z_3. \tag{IV.5.21}$$

The first two squares sum to XY, the last two to $-ZW$. Therefore our fixed normalization is

$$C_\lambda = \left\{ z \in \mathbb{C}^4 : \sum_{i=0}^{3} z_i^2 = \lambda \right\} \cong C_\lambda^{\det}. \tag{IV.5.22}$$

Other matrix coordinates can place a factor or sign between their determinant parameter and λ. In particular the Klebanov–Strassler matrix convention writes $\sum z_i^2 = -2\det(z_{ij})$. We use (IV.5.20) whenever converting our own two equations.

The gradient of $\sum z_i^2 - \lambda$ is $2z$. A critical point would have $z = 0$, which lies on the level only when $\lambda = 0$. Hence

$$\operatorname{Crit}(C_\lambda) = \varnothing \quad (\lambda \neq 0), \qquad \operatorname{Crit}(C_0) = \{0\}. \tag{IV.5.23}$$

For a fixed nonzero complex $\lambda = |\lambda| e^{i\alpha}$, the phase rotation $z \mapsto e^{-i\alpha/2} z$ makes the right side $|\lambda|$. This is a chosen phase at a chosen parameter; it is not a global single-valued square root over the punctured parameter plane. We can now take $\lambda > 0$ real.

Write $z = x + iy$ for real $x, y \in \mathbb{R}^4$. Separating real and imaginary parts of (IV.5.22) gives

$$|x|^2 - |y|^2 = \lambda, \qquad x \cdot y = 0. \tag{IV.5.24}$$

Since $|x|^2 = \lambda + |y|^2$, x never vanishes. At $y = 0$ one obtains the real three-sphere

$$S^3_\lambda = \{x \in \mathbb{R}^4 : |x|^2 = \lambda\}, \qquad r_{\text{ambient}} = \sqrt{\lambda}. \tag{IV.5.25}$$

The displayed radius is in the algebraic coordinates of (IV.5.22). It is not a proper radius measured in a Ricci-flat metric on the smoothing.

The rest of C_λ has a useful global description, not just a near-sphere approximation. For $z = x + iy$, set

$$n = \frac{x}{\sqrt{\lambda + |y|^2}}, \qquad p = y. \tag{IV.5.26}$$

Equation (IV.5.24) implies $|n| = 1$ and $n \cdot p = 0$. Thus (n, p) is a point of TS^3, with tangent and cotangent fibers identified by the round metric. Conversely, any $|n| = 1$ and $n \cdot p = 0$ gives

$$z = \sqrt{\lambda + |p|^2}\, n + ip, \tag{IV.5.27}$$

and substitution recovers both equations in (IV.5.24). The maps are smooth mutual inverses:

$$C_\lambda \simeq TS^3 \simeq T^*S^3 \quad (\lambda > 0), \qquad S^3_\lambda \longleftrightarrow \{p = 0\}. \tag{IV.5.28}$$

This is a diffeomorphism, not an assertion that the induced ambient Euclidean metric or a Ricci-flat metric equals the canonical cotangent-bundle metric.

The zero section really captures the topology of the entire smoothing. Keep n fixed and contract the cotangent vector p linearly. Written back in the quadric coordinates, the path is

$$z_s = \sqrt{\lambda + s^2|p|^2}\, n + isp, \qquad 0 \le s \le 1, \qquad z_1 = z, \quad z_0 = \sqrt{\lambda}\, n. \tag{IV.5.29}$$

For every s, the real and imaginary parts obey (IV.5.24). Thus this is a deformation retraction onto S^3_λ, and the smoothing has the homotopy type of a three-sphere. The contraction uses the chosen positive-real presentation; it does not identify the cycles of nearby fibers by a globally single-valued phase convention around $\lambda = 0$. This makes precise the phrase *vanishing cycle*: the compact zero section is visible for every nonzero chosen level and collapses to the singular origin in the algebraic-coordinate limit.

As a check with more than the zero section, take $\lambda = 9$, $x = (5, 0, 0, 0)$, and $y = (0, 4, 0, 0)$. Their squared norms are 25 and 16, their dot product vanishes, and

$$z = (5, 4i, 0, 0), \qquad \sum_i z_i^2 = 25 - 16 = 9, \qquad n = (1, 0, 0, 0),\ p = (0, 4, 0, 0). \tag{IV.5.30}$$

The zero section instead has radius 3. If $\lambda = -9$ in these same coordinates, the all-real slice is empty: $|x|^2 = -9$ cannot hold at $y = 0$. A phase rotation gives an equivalent positive-real presentation and reveals its real three-sphere in the rotated coordinates. Thus a negative real parameter does not eliminate the smooth cycle; it changes which real slice displays it.

The deformation changes complex structure. The resolution of the previous section changes the geometry while retaining a projective curve. Their replacement cycles have different real dimensions: $\mathbb{P}^1 \cong S^2$ versus S^3. The smoothing's actual Ricci-flat metric and its proper tip scale require further metric input. Chapter 2 describes what a holomorphic top form can say without providing that metric, while Chapter VII.8 will use this geometry in a specified gauge theory. The lower route in Figure IV.5.1 records only this complex smoothing and its real zero section.

IV.5.5 The link and its normalized volume

What does an observer see on an angular section around the node? The factorisation $M = AB^T$ makes the punctured cone particularly transparent. To take both factors to unit norm, first move radially on the cone, scaling M and choosing the algebraic section

$$\|M\|_F^2 := \sum_{i,j} |M_{ij}|^2 = |A|^2|B|^2 = 1.$$

This changes the matrix, whereas the positive real complex-gauge action $(A, B) \mapsto (cA, c^{-1}B)$ leaves M and $|A||B|$ fixed. On this section choose $c^2 = |B|/|A|$; then

$$|cA|^2 = c^2|A|^2 = |A||B| = 1, \qquad |c^{-1}B|^2 = c^{-2}|B|^2 = |A||B| = 1.$$

The reciprocal gauge action cannot perform the first step: for the nonunit example below it preserves $|A|^2|B|^2 = 13 \cdot 74 = 962$. The remaining equivalence is the relative phase:

$$|A| = |B| = 1, \qquad (A, B) \sim (e^{i\alpha}A, e^{-i\alpha}B). \tag{IV.5.31}$$

Each unit vector lies on S^3. Quotienting their relative phase gives the five-manifold

$$T^{1,1} = \frac{S_A^3 \times S_B^3}{U(1)_{\text{rel}}}. \tag{IV.5.32}$$

The choice of link section fixes a coordinate scale on the algebraic cone. A cone's metric radial variable is separately normalized by writing $ds_6^2 = dr^2 + r^2 ds_{T^{1,1}}^2$; r need not equal $|M|$ or the radius in (IV.5.25).

Apply the Hopf projection to each S^3 factor. Before the relative quotient, there are two phase circles above $S_A^2 \times S_B^2$. Dividing the anti-diagonal phase leaves one circle, so the link is a circle bundle:

$$S^1 \longrightarrow T^{1,1} \longrightarrow S_A^2 \times S_B^2. \tag{IV.5.33}$$

If both base orientations are chosen so each individual Hopf bundle has positive first Chern class, the residual primitive pair is $(1, 1)$. This pair describes a bundle only after those orientations and the circle generator are stated. The geometry is drawn in Figure IV.5.4.

The period of the residual phase deserves care. On a local Hopf trivialization let β_A and β_B be 2π-periodic phase coordinates of the two factors. The relative quotient shifts them oppositely. Their sum is invariant, so one may choose

$$(\beta_A, \beta_B) \sim (\beta_A + \alpha, \beta_B - \alpha), \qquad \beta = \beta_A + \beta_B \pmod{2\pi}, \qquad \psi = 2\beta \pmod{4\pi}. \tag{IV.5.34}$$

The last equality fixes the angular coordinate used below. The factor of two explains why $\eta/2$, rather than η, is the connection for a principal circle with standard 2π period. The local phase construction is compatible with the bundle description, while the curvature integral determines its oriented Chern numbers.

To compare the topological orientation statement with the angular coordinates used for the standard Einstein metric, define

$$\eta = d\psi + \cos\theta_1\, d\phi_1 + \cos\theta_2\, d\phi_2, \qquad 0 \le \psi < 4\pi, \quad 0 \le \phi_i < 2\pi, \quad 0 \le \theta_i \le \pi. \tag{IV.5.35}$$

The principal connection for a circle of period 2π is $\mathcal{A} = \eta/2$. On conventional polar orientations $\sin\theta_i\, d\theta_i \wedge d\phi_i > 0$, its curvature is

$$d\mathcal{A} = -\frac{1}{2}\sum_{i=1}^{2} \sin\theta_i\, d\theta_i \wedge d\phi_i, \qquad \frac{1}{2\pi}\int_{S_i^2} d\mathcal{A} = \frac{-2\pi}{2\pi} = -1. \tag{IV.5.36}$$

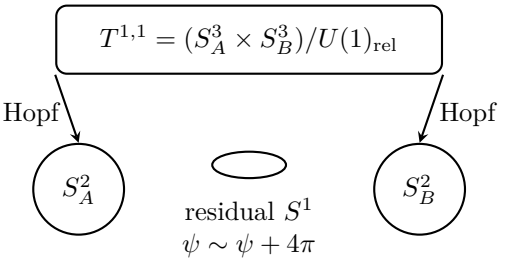


Figure IV.5.4: The relative phase quotient of two unit three-spheres. The remaining circle lies above the product of their Hopf base two-spheres. The angular coordinate ψ has period 4π in the angular convention of (IV.5.35); its principal 2π-period coordinate is $\psi/2$.

Thus this connection displays the pair $(-1,-1)$ on polar-oriented spheres. Reversing both base orientations displays $(1,1)$, agreeing with the preceding Hopf convention. These are translations of orientations, not distinct total spaces.

Topology alone does not choose a metric. In the angular convention (IV.5.35), consider

$$ds_5^2 = a\eta^2 + b\sum_{i=1}^{2}(d\theta_i^2 + \sin^2\theta_i\, d\phi_i^2). \tag{IV.5.37}$$

The sourced conifold Einstein metric has $a = 1/9$ and $b = 1/6$; in this normalization its Ricci tensor is $\mathrm{Ric} = 4g$. We use this metric statement as an input, rather than deriving its Ricci tensor. Once the metric is fixed, however, its volume is a short direct calculation.

An orthonormal coframe can be chosen as

$$e^0 = \sqrt{a}\,\eta, \qquad e^{2i-1} = \sqrt{b}\, d\theta_i, \qquad e^{2i} = \sqrt{b}\sin\theta_i\, d\phi_i \quad (i = 1, 2). \tag{IV.5.38}$$

Terms containing $d\phi_i$ in e^0 vanish when wedged with the four base one-forms. Hence

$$d\,\mathrm{vol}_5 = \sqrt{a}\, b^2 \sin\theta_1 \sin\theta_2\, d\psi\, d\theta_1\, d\phi_1\, d\theta_2\, d\phi_2 \tag{IV.5.39}$$

with the orientation chosen to make it positive. Each polar integral is 2, each azimuthal integral is 2π, and the fiber integral is 4π. Therefore

$$\mathrm{Vol}(a,b) = \sqrt{a}\, b^2 (4\pi)(4\pi)(4\pi) = 64\pi^3 \sqrt{a}\, b^2. \tag{IV.5.40}$$

For the cited Einstein coefficients this yields

$$\mathrm{Vol}(T^{1,1}) = 64\pi^3 \left(\frac{1}{3}\right)\left(\frac{1}{6}\right)^2 = \frac{16\pi^3}{27}. \tag{IV.5.41}$$

As a control, keeping the same angle periods and base coefficient but setting $a = 1/4$ gives $8\pi^3/9$. The topology and the circle bundle in (IV.5.33) are unchanged, yet the volume differs. A Euclidean unit-sphere cut through the affine equation is likewise not enough to infer the normalized Einstein volume. This metric-sensitive quantity becomes useful in the volume discussion of Chapter VII.6.

IV.5.6 Transitions and engine limits

Which parameter could a physical branch measure? The preceding constructions answer separate geometric questions. At $\zeta = +2$ the classical D equation forces $A \neq 0$, so R_A retains an image-line $\mathbb{P}^1$ over $M = 0$. At $\zeta = -2$ it forces $B \neq 0$, so R_B retains a row-line $\mathbb{P}^1$. At $\lambda = 9$ the quadric has no exceptional curve; its real zero section is an S^3 of ambient coordinate radius 3. These three statements are explicit outputs of different equations:

input	smooth local space	compact cycle
$\zeta > 0$	R_A	$\mathbb{P}^1_{\text{image}}$
$\zeta < 0$	R_B	$\mathbb{P}^1_{\text{row}}$
$\lambda \neq 0$	C_λ	S^3

(IV.5.42)

The table's rows compare geometric branches, not a one-parameter physical trajectory between them.

The two resolutions meet at the singular affine limit $\zeta = 0$. The smoothing meets the same singular equation at $\lambda = 0$. One can therefore draw the same node as their common limit, as in Figure IV.5.1, while retaining their different parameters. The complex parameter λ changes the holomorphic equation. The real level ζ changes the symplectic quotient chamber, with its associated Kähler and B-period data. Identifying either parameter with a gauge condensate requires a field-theory dictionary and dynamics beyond this local geometry.

The earlier nonunit orbit gives a direct numerical comparison without confusing a complex representative with a fixed-level vacuum. Its norms are $|A|^2 = 13$ and $|B|^2 = 74$. A positive real complex-gauge scaling $A \mapsto \sqrt{h}\, A$, $B \mapsto B/\sqrt{h}$ preserves all four entries of M but changes the moment map:

$$\mu_{\mathbb{R}}(h) = 13h - \frac{74}{h}, \qquad h > 0, \qquad \frac{d\mu_{\mathbb{R}}}{dh} = 13 + \frac{74}{h^2} > 0. \tag{IV.5.43}$$

Solving $\mu_{\mathbb{R}}(h) = \zeta$ gives one positive root for every real level,

$$13h^2 - \zeta h - 74 = 0, \qquad h_\zeta = \frac{\zeta + \sqrt{\zeta^2 + 3848}}{26}. \tag{IV.5.44}$$

The two requested levels give exact, positive and different scale factors:

$$h_{+2} = \frac{1 + \sqrt{963}}{13}, \qquad h_{-2} = \frac{-1 + \sqrt{963}}{13}, \qquad h_{+2} - h_{-2} = \frac{2}{13}. \tag{IV.5.45}$$

At $\zeta = +2$ and -2 these roots are distinct, but both represent the same nonzero matrix (IV.5.9); neither lies on an exceptional curve. The difference between the resolutions is exposed at $M = 0$, where the appropriate nonzero pair retains its line. This is a concrete reason to inspect the fiber over the node, rather than comparing only generic matrices.

For comparison, a point on the deformed zero section at $\lambda = 9$ is $z = (3, 0, 0, 0)$. The inverse linear map gives

$$M = \begin{pmatrix} 3 & 0 \\ 0 & 3 \end{pmatrix}, \qquad \det M = 9, \qquad \operatorname{rank} M = 2. \tag{IV.5.46}$$

No rank-one factorization AB^T can produce this matrix. The smoothing is therefore a change of the affine equation itself, not merely a different choice of projective line above a rank-one matrix. In the limit $\lambda \to 0$, the real zero section shrinks in these chosen ambient coordinates. This limit does not compute its proper metric diameter.

There is a specific source-supported setting where that further dictionary is supplied. Klebanov and Strassler analyse one additional D3 probe in their cascade setting. Here M denotes their integer fractional-brane/rank parameter, distinct from the 2×2 matrix used above. For $M > 1$, the $SU(M+1)$ sector has two flavors, so $N_f = 2 < N_c = M+1$. Together with a tree-level interaction, its ADS-type quantum superpotential leads to a branchwise meson constraint in the form of a deformed determinant equation. This ADS route excludes the endpoint $M = 1$. Its numerical deformation scale and branch interpretation depend on those physical premises. Chapter VII.8 will develop that example with its own fields and operators. The geometric maps in this chapter neither compute a condensate nor give a universal quantum deformation of every conifold theory.

The link supplies another useful boundary. It detects angular topology and, after a chosen Einstein normalization, the volume (IV.5.41). It does not identify the coordinate radius $\sqrt{\lambda}$ of a deformed zero section with a proper distance in a Ricci-flat smoothing. The latter asks for a metric on C_λ, whereas the former follows from its defining equation. This distinction matters when a conifold diagram is used to describe a brane throat or a confinement scale. Chapters VII.8 and XVIII.4 use additional physical and metric input for those questions.

IV.5.7 Exercises

The first four tasks have bounded JSON submissions through the companion grader. Supply the scientific reasoning separately; the grader checks the stated numerical or coordinate answer. Exercise E5 is written only.

E1. For $A = (2, 3)^T$, $B = (5, 7)^T$, compute the outer-product matrix with rows $[X, Z]$ and $[W, Y]$, and its determinant. Submit `matrix` as two length-two integer arrays and `determinant` as an integer. Explain the generator and relation argument for the invariant ring.

E2. Use that same complex-orbit representative. For the positive chamber, submit x_3/x_0 as an integer fraction array, the first image-line fiber $[X, Z]$, and the second $[W, Y]$. For the negative chamber, submit x_2/x_1, the first row-line fiber $[X, W]$, and the second $[Z, Y]$. The JSON has objects `positive` and `negative`, each with `ratio`, `first_fiber`, and `second_fiber`. Explain the two exceptional curves and off-node uniqueness. The supplied representative is not itself fixed-level D-flat.

E3. For $\sum z_i^2 = 9$ and $z = x + iy$, submit integer four-vectors `x` and `y` with squared norms 25 and 16 and zero dot product. Also submit integers `vanishing_radius_squared` and `critical_points_at_nonzero_level`. Explain both directions of the T^*S^3 map and the exceptional $\lambda = 0$ case.

E4. With ψ period 4π, compute Vol/π^3 for $(a, b) = (1/9, 1/6)$ and $(1/4, 1/6)$ in (IV.5.37). Submit each as an integer fraction array under `normalized_volume_over_pi_cubed` and `a_quarter_volume_over_pi_cubed`. Explain why the bundle topology does not choose either coefficient.

E5. Explain why neither a local FI level nor a complex smoothing parameter alone identifies a particular gauge condensate. State what the IV.5 geometry establishes and what the VII.8 dynamics must add. This is a written exercise.

IV.5.8 Take-home message

Take-home message

The conifold ring is the determinant-zero rank-one matrix ring. Its two small resolutions remember, respectively, an image line and a row line, selected by opposite FI signs in the declared classical quotient. A nonzero quadratic deformation instead has a real S^3 zero section and is diffeomorphic to T^*S^3. The link is a circle bundle over $S^2 \times S^2$; its volume requires a metric normalization. Keep coordinate radii, proper metric scales, Kähler levels and complex deformations separate when carrying this geometry into a brane construction.

After this chapter the reader should be able to: derive the holomorphic invariant ring; write both incidence atlases and their fiber transitions; construct the explicit T^*S^3 diffeomorphism; and integrate the normalized link volume while declaring its orientation and metric. The common misconception is that a picture of a shrinking cycle determines a unique quantum phase. The mathematical calculations above and the cited metric statement have different hypotheses, and the physical dictionary is supplied only by a specified engine.

Status and sources

Section IV.5.2 derives the invariant ring and isolated singularity [MATH]; compare Klebanov and Witten (1998, physical pp. 5–6, eqs. (7)–(15)) and Martelli et al. (2008, physical p. 60, eq. (7.8)). The ring is a classical holomorphic quotient under the explicitly stated fields and no-F-term premise, not a full quantum moduli-space claim.

Section IV.5.3 derives both incidence atlases, their exceptional fibers, proper projective maps and FI signs [MATH]. The classical FI interpretation uses Klebanov and Witten (1998, physical p. 7, eq. (16) and following text); the toric resolution context is Martelli et al. (2008, physical pp. 65–66, eqs. (7.27)–(7.32)). The charge and moment-map choice follows the scoped IV.4 convention and the stated FI chamber normalization. No general quantum chamber theorem is inferred.

Section IV.5.4 computes the linear map, smoothness, real cycle and T^*S^3 diffeomorphism [MATH]. The source-local deformation equation is Klebanov and Strassler (2000, physical p. 14, eq. (46)); its matrix determinant normalization differs by -2 from ours. The source's proper tip geometry in Klebanov and Strassler (2000, physical p. 19, eqs. (53)–(59)) is cited context, not a metric derived here.

Section IV.5.5 derives the quotient and Chern orientation translation [MATH], cites the $\mathrm{Ric} = 4g$ angular metric [MATH], cited rather than proved here, and integrates its normalized volume [MATH]. The metric and angular periods are Klebanov and Witten (1998, physical pp. 5–6, eqs. (9)–(10)). The topology by itself does not establish the Einstein metric. Section IV.5.6 restricts the quantum deformation attribution to the single-probe, two-flavor branch discussed in Klebanov and Strassler (2000, physical pp. 15–16, eqs. (47)–(51)). This physical input is used only on its stated branch. Its detailed dynamics belong to Chapter VII.8. Candelas and de la Ossa is an unread bibliographic pointer and is not used to support a claim here. The explicit symbolic and reader checks are bounded algebraic controls; they do not certify the cited metric, the physical premise or a general gauge-theory transition.

References

Klebanov, I. R. and M. J. Strassler (2000). "Supergravity and a Confining Gauge Theory: Duality Cascades and ChiSB-Resolution of Naked Singularities". In: *JHEP* 08, p. 052. DOI: 10.1088/1126-6708/2000/08/052. arXiv: hep-th/0007191.

Klebanov, I. R. and E. Witten (1998). "Superconformal Field Theory on Threebranes at a Calabi-Yau Singularity". In: *Nucl. Phys. B* 536, pp. 199–218. DOI: 10.1016/S0550-3213(98)00654-3. arXiv: hep-th/9807080.

Martelli, D., J. Sparks, and S.-T. Yau (2008). "Sasaki–Einstein Manifolds and Volume Minimisation". In: *Commun. Math. Phys.* 280, pp. 611–673. DOI: 10.1007/s00220-008-0479-4. arXiv: hep-th/0603021.

Chapter IV.6

Calibrated cycles and wrapped-brane BPS states

IV.6.1 A wrapped cycle asks for a volume bound

A D-brane wrapped on a small internal cycle appears pointlike in the noncompact spatial directions. Its leading rest energy depends on the volume of that cycle. A drawing of a small cycle, however, does not tell us whether a deformation can lower its volume. A closed differential form can answer the geometric part of this question without solving the full minimal-surface equation.

This chapter follows one chain of implications. A form with a pointwise bound supplies a lower bound on the volume of every representative of a homology class. A cycle that saturates the bound minimizes volume in that class. The Kähler form provides the simplest complex example; the real part of a suitably normalized holomorphic three-form provides a phase-sensitive example. A restricted D2 action turns an actual two-cycle volume into a leading particle energy. Spacetime supersymmetry and state existence require further physical input. Figure IV.6.1 marks the steps and their distinct assumptions.

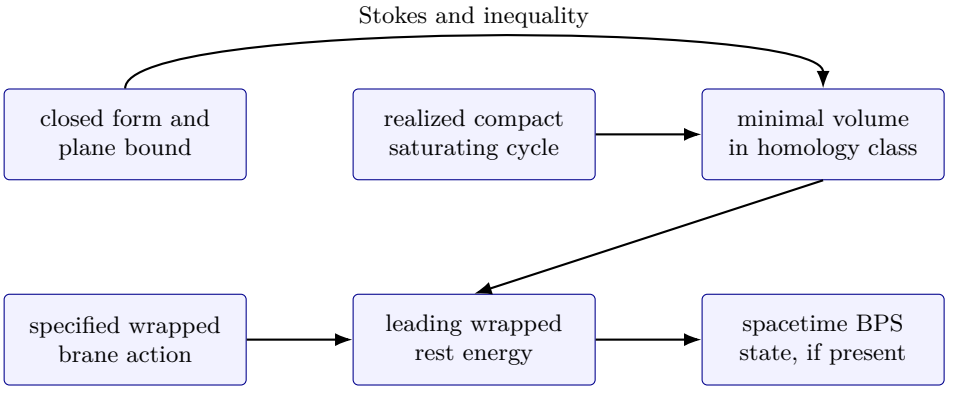


Figure IV.6.1: The geometric and physical route. Closedness and the plane inequality compare homologous cycles. A realized saturating cycle supplies a volume, which enters a specified wrapped action. A spacetime BPS statement needs a superalgebra and a supersymmetric state. The arrows indicate required input, not automatic existence of the next object.

Sections IV.6.2–IV.6.4 develop the local geometry and compact-cycle argument. Section IV.6.5 applies them to a zero-field D2 example. Section IV.6.6 asks what phase alignment says about a possible marginal threshold. The same distinctions will matter when later chapters use ADE two-cycles, three-cycle periods, and brane probes.

IV.6.2 Volume bounded by a closed form

The physical question. Suppose a wrapped cycle can move within its homology class. How can we know that its area or volume cannot decrease? The answer begins at an oriented tangent plane. Let (M, h) be a Riemannian manifold and let P be an oriented k-plane with an oriented orthonormal basis $(v_1, \dots, v_k)$. For a real k-form φ, define its value on this plane by $\varphi(P) = \varphi(v_1, \dots, v_k)$. Its comass is the supremum of the absolute values of these evaluations over unit simple k-vectors. The condition we use is the oriented, one-sided inequality

$$\varphi|_P \leq \mathrm{vol}_P \qquad \text{for every oriented tangent } k\text{-plane } P. \tag{IV.6.1}$$

A *calibration* is a closed real form satisfying this inequality. A submanifold N is calibrated when equality holds on every oriented tangent plane. The inequality is not an assertion that every plane saturates. In particular the zero form meets the inequality and is closed, yet it saturates no positive-dimensional plane.

The pointwise test can be made visible in flat $\mathbb{C}^2$. Use the standard Euclidean metric and $J = dx^1 \wedge dy^1 + dx^2 \wedge dy^2$. Let $e_{x^1}, e_{y^1}, e_{x^2}, e_{y^2}$ be the corresponding unit coordinate vectors. Orient a plane with

$$v_1 = e_{x^1}, \qquad v_2 = ce_{y^1} + se_{x^2}, \qquad c^2 + s^2 = 1. \tag{IV.6.2}$$

The parameter c measures how much of the second tangent lies in the complex line of v_1. Direct evaluation gives the real Gram and form matrices

$$G_{ab} = h(v_a, v_b) = \begin{pmatrix} 1 & 0 \\ 0 & c^2 + s^2 \end{pmatrix}, \qquad J(v_a, v_b) = \begin{pmatrix} 0 & c \\ -c & 0 \end{pmatrix}. \tag{IV.6.3}$$

Consequently the oriented area density is $\sqrt{\det G} = 1$ while $J(v_1, v_2) = c$. For $c = 3/5$ and $s = 4/5$, the gap is $1 - 3/5 = 2/5$. This plane is a concrete nonsaturating competitor. At $c = 1, s = 0$, the plane is a complex line with its complex orientation and the bound is saturated. If we reverse the order of its basis, the area stays one while the form evaluation becomes -1. Figure IV.6.2 keeps the two vectors and the orientation arrow visible.

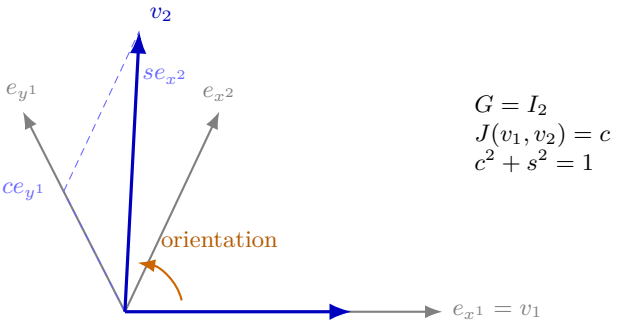


Figure IV.6.2: An oriented tangent plane in standard flat $\mathbb{C}^2$. The first tangent is e_{x^1}; the second has components $ce_{y^1} + se_{x^2}$, with $c^2 + s^2 = 1$. The orange orientation arc indicates the ordered pair (v_1, v_2). Tilting toward e_{x^2} preserves unit Gram area but lowers the J evaluation from 1 to c. The schematic projection separates the y^1 and x^2 directions for legibility.

The local inequality has a global consequence, provided that the cycle actually exists. Let N be a smooth compact oriented boundaryless calibrated k-cycle. Let N' be another smooth compact oriented boundaryless cycle in the same real homology class. There is a real $(k+1)$-chain B with $\partial B = N' - N$. Closedness gives

$$\int_{N'} \varphi - \int_N \varphi = \int_{\partial B} \varphi = \int_B d\varphi = 0. \tag{IV.6.4}$$

On N the tangent-plane equality converts the integral into its volume. On N' the plane bound gives an inequality. Combining both steps yields

$$\mathrm{Vol}(N) = \int_N \varphi = \int_{N'} \varphi \leq \mathrm{Vol}(N'). \tag{IV.6.5}$$

Thus an already realized compact calibrated cycle minimizes volume among compact representatives of its real homology class. Neither Stokes' theorem nor the pointwise inequality constructs N for a prescribed class. The boundaryless, compact, homologous and closedness assumptions are precisely what allow the middle equality.

For a Kähler two-form there is a useful direct check of the plane bound. The metric and complex structure obey $J(u,v) = h(Iu,v)$, with I an isometry. If u and v are an oriented orthonormal pair, Cauchy–Schwarz gives

$$J(u,v) = h(Iu,v) \le \|Iu\|\|v\| = 1. \tag{IV.6.6}$$

Equality requires $v = Iu$ in this orientation. In the tilted example $u = e_{x^1}$, so $Iu = e_{y^1}$ and v_2 agrees with it only when $c = 1$. This proves the local two-plane bound for a Hermitian metric; it does not replace the separate closedness hypothesis or prove the higher-degree $J^k/k!$ theorem.

There is a second useful distinction. A nonclosed form can still have a unit pointwise bound, but then $\int_{N'} \varphi - \int_N \varphi = \int_B d\varphi$ need not vanish. A closed form whose plane inequality is strict on the actual cycle gives a lower bound without proving that cycle minimizes anything. The worked tilt illustrates the latter possibility at one point. Chapter 1 supplies the Kähler form that can saturate the bound globally on a holomorphic curve; the next section computes the factor in its area formula.

IV.6.3 Kähler calibrations

The physical question. A holomorphic curve is a natural wrapped two-cycle in a complex target. Which period measures its geometric area in the book's metric convention? Write one complex coordinate $z = x + iy$ and a positive constant Hermitian coefficient g. The real metric and Kähler form are

$$ds^2 = 2g\, dz\, d\bar{z} = 2g(dx^2 + dy^2), \qquad J = ig\, dz \wedge d\bar{z}. \tag{IV.6.7}$$

The factor two in the real metric matters. Since $dz = dx + i\, dy$ and $d\bar{z} = dx - i\, dy$, exterior multiplication gives

$$dz \wedge d\bar{z} = -2i\, dx \wedge dy, \qquad J = 2g\, dx \wedge dy. \tag{IV.6.8}$$

A rectangle oriented by (∂_x, ∂_y) has induced Gram matrix $\mathrm{diag}(2g, 2g)$. Its area density is $\sqrt{(2g)^2} = 2g$, exactly $J(\partial_x, \partial_y)$. The opposite orientation makes $\int J$ negative while its area stays positive. The complex orientation is therefore part of the equality.

For comparison with the standard flat complex geometry often used in the calibration theorem, $ds^2 = |dz|^2$ corresponds here to $g = 1/2$. It then gives $J = dx \wedge dy$, not half of that form. This conversion prevents a spurious factor of two when a theorem stated in the standard flat frame is applied to the book's notation.

Consider the flat product threefold

$$X = \big(\mathbb{C}/(L_x\mathbb{Z} + iL_y\mathbb{Z})\big) \times \big(\mathbb{C}/(\mathbb{Z} + i\mathbb{Z})\big)^2, \qquad L_x, L_y > 0, \tag{IV.6.9}$$

with the first factor carrying the metric in (IV.6.7). Let C be that first complex torus at fixed points in the other factors. Coordinates $x \in [0, L_x]$, $y \in [0, L_y]$ cover a fundamental cell, with opposite edges identified. Because C is compact and has no boundary, it is an actual cycle to which the preceding Stokes argument can apply. Its period and area are

$$\int_C J = \int_0^{L_x} dx \int_0^{L_y} dy\, 2g = 2gL_xL_y = \mathrm{Area}(C). \tag{IV.6.10}$$

For $g = 3/2$, $L_x = 2$, and $L_y = 5$, the metric matrix is $\mathrm{diag}(3, 3)$, its determinant is 9, and the coordinate cell has area 10. Thus the geometric area and J period are both $3 \cdot 10 = 30$. The number 30 is not a dimensionless Kähler coordinate; it is an area in these length units.

The homology comparison can also be seen with an explicit nonsaturating torus. Keep the same first-factor coordinates, but displace the embedding in the real x^2 direction of the second factor by $x^2 = \epsilon \sin(2\pi x/L_x)$, where ϵ is small enough for a simple graph in its coordinate chart. Leave y^2 and the third factor fixed. This periodic graph is compact and smoothly homotopic to C by scaling ϵ to zero. Let $g_2 = 1/2$ on the second factor, so its real coordinate metric is Euclidean. The induced real metric and the restricted Kähler form become

$$G_{C_\epsilon} = \begin{pmatrix} 2g + (2\pi\epsilon/L_x)^2 \cos^2(2\pi x/L_x) & 0 \\ 0 & 2g \end{pmatrix}, \qquad J|_{C_\epsilon} = 2g\, dx \wedge dy. \tag{IV.6.11}$$

The graph has no y^2 tangent, so the second factor contributes no two-form evaluation. Nevertheless its extra x^2 slope increases the area density wherever the cosine is nonzero. In particular,

$$\begin{aligned} \mathrm{Area}(C_\epsilon) &= L_y \int_0^{L_x} dx\, \sqrt{2g\,[2g + (2\pi\epsilon/L_x)^2 \cos^2(2\pi x/L_x)]} \\ &> 2gL_xL_y = \int_{C_\epsilon} J \qquad (\epsilon \neq 0). \end{aligned} \tag{IV.6.12}$$

Its J period remains fixed by homology while its area grows. This is the compact counterpart of the tilted tangent plane, with no assumption that a new calibrated representative appears.

The complexified coordinate used for worldsheet instantons is a different object. With the book's unit-periodic B convention,

$$t_C = \frac{1}{4\pi^2\alpha'} \int_C (B + iJ), \qquad \mathrm{Im}\, t_C\big|_{B=0} = \frac{2gL_xL_y}{4\pi^2\alpha'}. \tag{IV.6.13}$$

At $\alpha' = 4$ in the worked cell this is $30/(16\pi^2)$, whereas the area remains 30. The distinction will matter when the same curve is inserted into a D2 action. The string tension $T_{\mathrm{F1}} = 1/(2\pi\alpha')$ and the normalization of t_C are inherited conventions; no equality between t_C and a D2 mass is being asserted.

For a Kähler manifold of complex dimension m, the geometric theorem extends this example. On an oriented complex k-plane the form $J^k/k!$ equals its real $2k$-volume form, and its value on any other oriented $2k$-plane is no larger than the volume form. The theorem applies for $1 \leq k \leq m$ with the Kähler metric and complex orientation. Closedness of J implies closedness of $J^k/k!$ because

$$d\left(\frac{J^k}{k!}\right) = \frac{k}{k!}\, dJ \wedge J^{k-1} = 0. \tag{IV.6.14}$$

The general plane inequality is the Kähler calibration theorem, cited rather than proved here. Our explicit two-dimensional Gram calculation shows its $k = 1$ equality in

one coordinate chart, not a proof for every higher-dimensional plane. A holomorphic representative, if it exists and is compact, therefore minimizes volume in its real homology class. Merely specifying a $(1,1)$ class or a period does not supply such a representative. This is the first link from complex geometry to wrapped-brane masses; Chapter 3 will use shrinking ADE two-cycles, while the next section replaces J by a phase-sensitive three-form.

IV.6.4 Special Lagrangians

The physical question. A real three-cycle in a complex threefold is not a complex curve. How can an oriented real tangent three-plane saturate a geometric volume bound? Begin in standard flat $\mathbb{C}^3$, with $z^j = x^j + iy^j$, metric $ds^2 = \sum_j |dz^j|^2$, and

$$J = \sum_{j=1}^{3} dx^j \wedge dy^j, \qquad \Omega_{\text{unit}} = dz^1 \wedge dz^2 \wedge dz^3. \tag{IV.6.15}$$

Here Ω_{unit} has unit comass relative to this flat metric. The real form $\varphi_\theta = \mathrm{Re}(e^{-i\theta}\Omega_{\text{unit}})$ has unit comass and is closed because Ω_{unit} is constant. The phase θ selects which oriented real planes can saturate its bound. The statement requires both the metric normalization and closedness; holomorphic notation alone does not fix either property for an arbitrarily rescaled form.

Take real coordinates u_1, u_2, u_3 on a diagonal plane and embed it by

$$z^j = e^{i\theta_j} u_j = (c_j + i s_j) u_j, \qquad c_j^2 + s_j^2 = 1, \qquad j = 1,2,3. \tag{IV.6.16}$$

Its positively oriented tangent basis is $v_j = c_j e_{x^j} + s_j e_{y^j}$. In the real ambient ordered basis $(e_{x^1}, e_{y^1}, e_{x^2}, e_{y^2}, e_{x^3}, e_{y^3})$, the tangent matrix is

$$V = \begin{pmatrix} c_1 & 0 & 0 \\ s_1 & 0 & 0 \\ 0 & c_2 & 0 \\ 0 & s_2 & 0 \\ 0 & 0 & c_3 \\ 0 & 0 & s_3 \end{pmatrix}, \qquad G = V^T V = \mathrm{diag}(c_1^2 + s_1^2, c_2^2 + s_2^2, c_3^2 + s_3^2) = I_3. \tag{IV.6.17}$$

The oriented volume density is therefore $\sqrt{\det G} = 1$. Each tangent lies in a different complex coordinate line. Every pair is annihilated by J, including the three off-diagonal pairs. In matrix form,

$$\big(J(v_a, v_b)\big)_{a,b=1}^{3} = \begin{pmatrix} 0 & 0 & 0 \\ 0 & 0 & 0 \\ 0 & 0 & 0 \end{pmatrix}, \qquad J|_P = 0. \tag{IV.6.18}$$

The complex Jacobian of the map $u \mapsto z$ is diagonal. Its determinant gives the three-form evaluation without suppressing the phase,

$$\Omega_{\text{unit}}(v_1, v_2, v_3) = \det \mathrm{diag}(c_1 + i s_1, c_2 + i s_2, c_3 + i s_3) = \prod_{j=1}^{3} (c_j + i s_j) = e^{i(\theta_1 + \theta_2 + \theta_3)}. \tag{IV.6.19}$$

Thus φ_θ evaluates to $\cos(\theta_1+\theta_2+\theta_3-\theta)$. The chosen orientation saturates precisely when the phase difference is 0 modulo 2π. The J condition and the phase condition perform different jobs. The first says the plane is Lagrangian; the second selects its oriented special-Lagrangian phase.

A numerical example makes the determinant nontrivial. Choose the three unit factors

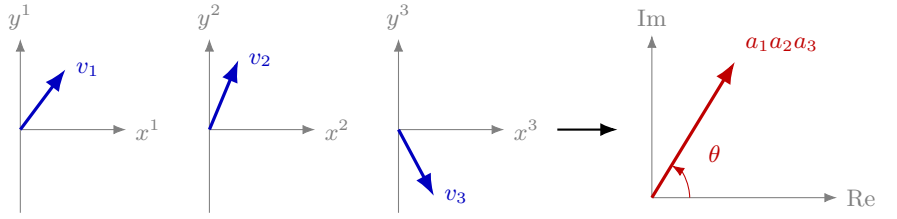
$$a_1=\frac{3+4i}{5},\qquad a_2=\frac{5+12i}{13},\qquad a_3=\frac{8-15i}{17}. \tag{IV.6.20}$$

Each has modulus one. Multiplying the first two gives $(-33+56i)/65$; multiplying by the third gives

$$a_1a_2a_3=\frac{(-33+56i)(8-15i)}{1105}=\frac{576+943i}{1105},\qquad 576^2+943^2=1105^2. \tag{IV.6.21}$$

Both real and imaginary parts are nonzero. The Gram volume is still one and the entire J matrix is still zero. If $\theta=\arg(576+943i)$, then φ_θ evaluates to one. If we kept the same plane but chose $\theta=0$, its value would be $576/1105<1$. This is an explicit check that the phase cannot be dropped from the volume statement.

The exercise later uses a simpler exact phase. Factors $(3+4i)/5$, $(3-4i)/5$, and i multiply to i. Their J pairings vanish, and $\mathrm{Re}(-i\Omega_{\mathrm{unit}})$ saturates the oriented unit volume. Figure IV.6.3 records the phase and orientation convention without trying to draw the full six-dimensional ambient space.



$a_1=(3+4i)/5$ $\quad a_2=(5+12i)/13$ $\quad a_3=(8-15i)/17$

Figure IV.6.3: Phase of the unit-normalized three-form on a diagonal oriented plane. Each real tangent v_j lies in its own (x^j,y^j) complex line, so the pairwise J values vanish. Their complex factors multiply to the phase shown at right. Reversing the orientation changes the signed form evaluation by a minus sign and shifts its phase by π; the positive Gram volume stays one.

Orientation reversal replaces (v_1,v_2,v_3) by, for example, (v_2,v_1,v_3). Its real Gram determinant remains one, but the determinant in (IV.6.19) changes sign. The phase therefore shifts by π. The same reversal changes an oriented brane charge and signed period, not the positive energy of the object. In the standard phase-zero statement, $J|_P=0$ and $\mathrm{Im}\,\Omega_{\mathrm{unit}}|_P=0$ must be accompanied by the orientation for which $\mathrm{Re}\,\Omega_{\mathrm{unit}}|_P$ is positive. Otherwise the opposite orientation satisfies the vanishing equations but does not saturate the same phase-zero calibration.

A nonzero holomorphic rescaling illustrates why normalization is physical information. Replace Ω_{unit} by $c\Omega_{\mathrm{unit}}$ for constant $c \in \mathbb{C}^*$. The period scales by c, and $\mathrm{Re}(e^{-i\theta}c\Omega_{\mathrm{unit}})$ has comass $|c|$ rather than one. One must divide by the metric norm and adjust the phase before using a unit volume inequality. A varying holomorphic top-form multiplier remains closed in complex dimension three, but dividing by its generally varying metric norm need not preserve closedness. Both properties must be checked for the resulting real form. The flat calculation proves none of the global existence assertions for a special-Lagrangian representative. The general phase-zero characterization and the calibrated volume theorem are cited mathematical results. In the following section the safely realized complex torus, rather than an assumed special-Lagrangian three-cycle, supplies the explicit D2 energy.

IV.6.5 Wrapped brane central charges

The physical question. Once a geometric cycle realizes a volume bound, what mass follows for a wrapped brane? Start with a deliberately narrow background. Let a static D2 occupy noncompact time and the smooth spatial torus C of Section IV.6.3. Use an unwarped product metric, constant dilaton $g_s > 0$, vanishing background B and worldvolume F, and no induced lower charges or curvature terms. The leading string-frame DBI action has the metric-only form

$$S_{\mathrm{DBI}} = -\tau_2 \int dt\, d^2\sigma \, \sqrt{-\det P[G]_{\alpha\beta}}, \qquad \tau_2 = \frac{1}{(2\pi)^2 \alpha'^{3/2} g_s}. \tag{IV.6.22}$$

Here $P[G]$ denotes the induced worldvolume metric and τ_2 includes the constant inverse string coupling. This is the same rest-tension convention used throughout the book. A more general DBI action would include $B + 2\pi\alpha' F$, but those fields have been set to zero in this calculation.

Use worldvolume coordinates (t, x, y) and the static embedding of C. The induced matrix and its determinant are explicit,

$$P[G]_{\alpha\beta} = \mathrm{diag}(-1, 2g, 2g), \qquad -\det P[G] = (2g)^2. \tag{IV.6.23}$$

The action becomes $-\int dt\, M_{\mathrm{lead}}$ with

$$M_{\mathrm{lead}} = \tau_2 \int_0^{L_x} dx \int_0^{L_y} dy\, 2g = \tau_2 \,\mathrm{Area}(C) = \tau_2 \int_C J. \tag{IV.6.24}$$

The last equality uses the complex orientation and the fact that this particular C is holomorphic. In another orientation, the signed J period changes sign but the square root in the DBI energy does not. A brane and its orientation-reversed charge carrier need not preserve the same supersymmetries even though both have nonnegative rest energy.

For the earlier cell, $g = 3/2$, $L_x = 2$, $L_y = 5$, $\alpha' = 4$, and $g_s = 1/2$. The metric gives $\mathrm{Area}(C) = 30$. Since $\alpha'^{3/2} = 8$, the tension factor is $\tau_2 = 1/[4(2\pi)^2]$. Therefore

$$M_{\mathrm{lead}} = \frac{30}{4(2\pi)^2}, \qquad (2\pi)^2 M_{\mathrm{lead}} = \frac{15}{2}. \tag{IV.6.25}$$

This computation uses the physical area 30, not $\operatorname{Im} t_C = 30/(16\pi^2)$. The two quantities serve different roles. The latter is a dimensionless worldsheet coordinate, while the former is the metric factor in this zero-field D2 action. It is also clear which step would fail in a warped background: the induced time and spatial metric factors could no longer be replaced by the constant matrix above.

The calibration argument constrains the leading geometric energy for a fixed homology class of realized compact competitors. In the restricted background, each candidate has $M_{\mathrm{lead}} = \tau_2 \,\mathrm{Area}$ and positive τ_2, so (IV.6.5) implies

$$M_{\mathrm{lead}}(C') \geq \tau_2 \int_{C'} J = \tau_2 \int_C J = M_{\mathrm{lead}}(C) \tag{IV.6.26}$$

when C' is compact, homologous and compared in the same restricted action. This is a geometric energy comparison. It does not by itself identify the right-hand side with an exact spacetime central charge or prove that the full quantum theory contains a one-particle BPS state.

The graph torus from Section IV.6.3 lets us see an energy difference rather than only an inequality. Put $k = 2\pi/L_x$. At fixed positive g, L_x, L_y, expand for small slope $|\epsilon k|/\sqrt{2g}$:

$$\sqrt{2g\,[2g + \epsilon^2 k^2 \cos^2(kx)]} = 2g + \frac{\epsilon^2 k^2}{2}\cos^2(kx) + O(\epsilon^4).$$

Integrating over x and y, with the average of $\cos^2(kx)$ equal to $1/2$, and multiplying the area difference by τ_2 gives

$$\mathrm{Area}(C_\epsilon) - \mathrm{Area}(C) = \frac{\epsilon^2 k^2 L_x L_y}{4} + O(\epsilon^4), \qquad M_{\mathrm{lead}}(C_\epsilon) - M_{\mathrm{lead}}(C) = \tau_2 \frac{\pi^2 \epsilon^2 L_y}{L_x} + O(\epsilon^4). \tag{IV.6.27}$$

The first nonzero correction is positive. This local expansion agrees with the exact strict inequality in (IV.6.12). It is a restricted classical fluctuation energy; it is not a calculation of the quantum spectrum or a stability chamber.

The dimensions also check the normalization. Since $[\alpha'] = \mathrm{length}^2$ and g_s is dimensionless, $[\tau_2] = \mathrm{length}^{-3}$. Multiplying by $[\mathrm{Area}(C)] = \mathrm{length}^2$ gives $[M_{\mathrm{lead}}] = \mathrm{length}^{-1}$. The dimensionless period t_C cannot replace the area in this action without an additional length scale. This dimensional check is particularly useful when translating a source that absorbs α' into its Kähler coordinates.

A BPS equality in spacetime needs a supersymmetric embedding in a specified compactification, a charge map into its superalgebra, a common normalization of that algebra, and control of background fields and induced charges. State existence and stability add dynamical questions. It is useful to name the source frames precisely. The three-cycle conditions in Becker, Becker and Strominger describe a supersymmetric *Euclidean M2-brane* map. Their normalized $e^{-K}\Omega$ and associated period bound are in that source's units and do not identify our flat Ω_{unit} or the Lorentzian D2 tension above. Their comparison with an IIB D3 wrapped on a three-cycle to form a four-dimensional black hole is conditional on the physical identification discussed there. A Euclidean instanton action, a D3 black-hole mass and a Lorentzian wrapped D2 particle mass are different observables.

The large-volume D2 discussion in the mirror-symmetry source likewise uses its own λ and Kähler units. It supports the area dependence for its setup, but it does not supply the coefficient in (IV.6.22) without translation. Chapter III.9 supplies brane boundary and supersymmetry language; it should not be replaced by a volume formula alone. The later ADE applications need the relevant compactification, charges and light-state dynamics. The next section tests what can be learned from complex periods before those ingredients are available.

IV.6.6 Marginality and limitations

The physical question. When can the charges of two objects lie at a marginal BPS threshold? First do the calculation for two complex numbers $Z_1 = a + ib$ and $Z_2 = c + id$. The ordinary triangle inequality reads

$$|Z_1 + Z_2| \leq |Z_1| + |Z_2|. \tag{IV.6.28}$$

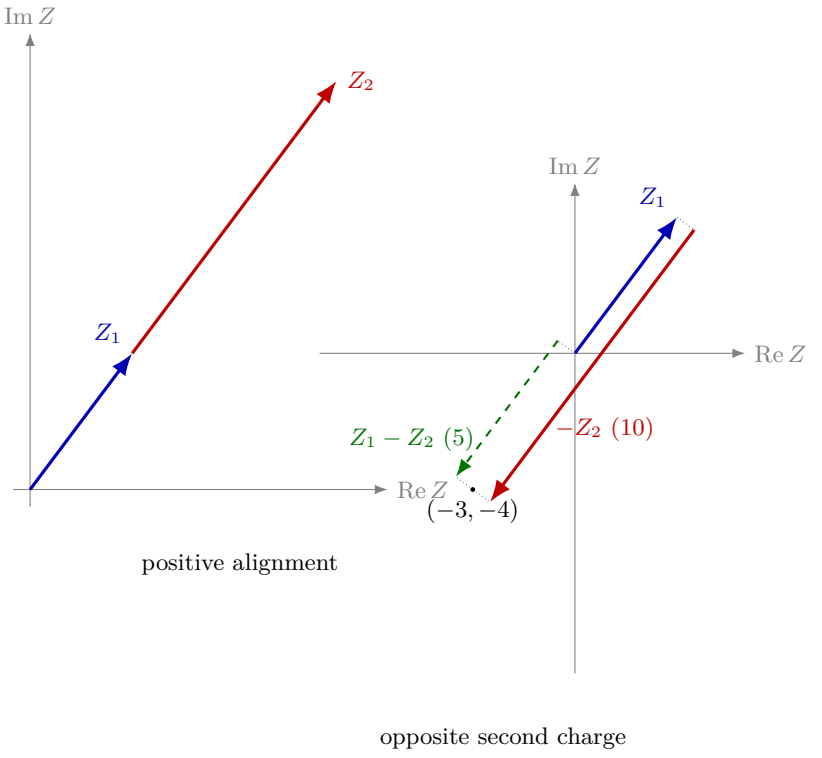


Figure IV.6.4: Complex-period arithmetic. Left, $(0,0) \to (3,4) \to (9,12)$ gives $|Z_1 + Z_2| = 15$. Right, the red head-to-tail $-Z_2$ runs from $(3,4)$ to $(-3,-4)$ with length 10; the green resultant from $(0,0)$ to $(-3,-4)$ has length 5. Both shafts are offset to expose the blue Z_1, with dotted connectors to their true endpoints. Neither panel implies stability.

For nonzero Z_1, Z_2, square both sides. Equality is equivalent to $\mathrm{Re}(Z_1\overline{Z}_2) = |Z_1||Z_2|$. Written in real components, the dot and oriented area are

$$D = ac + bd, \qquad A = ad - bc, \qquad D^2 + A^2 = (a^2 + b^2)(c^2 + d^2). \tag{IV.6.29}$$

The identity shows that equality requires $A = 0$ and $D > 0$. The first condition makes the two arrows collinear. The positive dot product rules out opposite directions. If either $Z_i = 0$, equality is automatic but the zero complex number has no phase, so it should not be called positively phase-aligned.

Take $Z_1 = 3 + 4i$ and $Z_2 = 6 + 8i$. The first has length $\sqrt{3^2 + 4^2} = 5$; the second has length $\sqrt{6^2 + 8^2} = 10$. Their area is $3 \cdot 8 - 4 \cdot 6 = 0$, and their dot product is $3 \cdot 6 + 4 \cdot 8 = 50 > 0$. Their sum is $9 + 12i$ and has length 15, so the inequality saturates:

$$|Z_1 + Z_2| = |9 + 12i| = 15 = 5 + 10 = |Z_1| + |Z_2|. \tag{IV.6.30}$$

Figure IV.6.4 draws these numbers as arrows in the same complex plane. Its second panel reverses the second charge. The second arrow then has length ten and points the

other way. The resulting sum is $Z_1 - Z_2 = -3 - 4i$, with positive modulus five, not a negative mass and not the threshold sum fifteen.

The same conclusion can be seen directly from the squared gap,

$$(|Z_1| + |Z_2|)^2 - |Z_1 + Z_2|^2 = 2\big(|Z_1||Z_2| - \mathrm{Re}(Z_1\overline{Z}_2)\big) \geq 0. \tag{IV.6.31}$$

To interpret the equality as a threshold, suppose a specified spacetime theory has an additive charge map $Z(\gamma_1 + \gamma_2) = Z(\gamma_1) + Z(\gamma_2)$, with $Z_i = Z(\gamma_i)$, and two constituent BPS states whose masses saturate $M_i = |Z_i|$ in the same normalization. Then the actual two-particle threshold obeys

$$M_1 + M_2 = |Z_1| + |Z_2| \geq |Z(\gamma_1 + \gamma_2)|. \tag{IV.6.32}$$

For nonzero constituents, equality with the total-charge BPS bound holds precisely when their phases align positively. A putative one-particle BPS state of charge $\gamma_1 + \gamma_2$ would have mass $|Z(\gamma_1 + \gamma_2)|$ if it exists; equality of the bounds neither constructs that state nor establishes its normalizability or stability. If a constituent does not saturate its BPS bound, the displayed first equality does not hold. A formal pair of geometric periods does not supply the charge map, constituent states or their masses.

Two nearby algebraic cases sharpen the equality condition. If the second charge is reversed, its new complex number is $-Z_2 = -6 - 8i$. The oriented area with Z_1 is still zero, but the dot product is now $-50 < 0$. The arrows are collinear and opposed, so

$$|Z_1 + (-Z_2)| = |-3 - 4i| = 5 = \big||Z_2| - |Z_1|\big|, \qquad |Z_1| + |-Z_2| = 15. \tag{IV.6.33}$$

The modulus five is a charge-sum modulus. It is not a negative energy, and the equality in (IV.6.28) is now strict. If instead one input is zero, the triangle equality holds trivially,

$$|Z_1 + 0| = |Z_1| + 0, \qquad \arg 0 \text{ is undefined.} \tag{IV.6.34}$$

There is no second phase to align. A zero central charge in a physical model could have other consequences, but the complex-number identity alone does not decide them.

For a genuinely noncollinear comparison, keep $Z_1 = 3 + 4i$ and take $Z_3 = 4 + 3i$. Both moduli equal five. The oriented area is $3 \cdot 3 - 4 \cdot 4 = -7$, while the dot product is $3 \cdot 4 + 4 \cdot 3 = 24$. Direct addition gives

$$|Z_1 + Z_3| = |7 + 7i| = \sqrt{98} < 10 = |Z_1| + |Z_3|. \tag{IV.6.35}$$

The strict gap is geometric. Two vectors at different phases cannot add to the sum of their lengths. This comparison checks the sign in the dot-product test without invoking a stability model.

The aligned numbers above give a definite missing-premise case. Suppose a geometric calculation supplies periods $3 + 4i$ and $6 + 8i$ for two proposed charges, with no compactification or spectrum specified. It establishes $|Z_1 + Z_2| = 15 = |Z_1| + |Z_2|$ as complex arithmetic. It supplies neither two physical constituent states with masses 5 and 10 in one BPS normalization nor an additive spacetime charge map. Thus 15 is not yet an established two-particle mass threshold. Even after those premises are supplied, the equation would only put the two-particle threshold at the total-charge

bound; a normalizable one-particle BPS state and its stability in a chosen chamber remain undetermined. A local phase-zero patch or a pair of periods also does not establish smooth compact representatives of the proposed classes. The Euclidean M2 example discussed above computes an instanton action with all three worldvolume directions internal; it does not supply the timelike worldline of the Lorentzian D2 particle. Exercise E5 asks the reader to identify these distinct missing steps in writing.

The common misconception is to turn a local calibration or two aligned arrows into an existence theorem for a BPS state. The proved geometric implication goes in the narrower direction. A realized compact calibrated cycle minimizes volume among compact homologous competitors. A specified leading brane action then assigns a restricted energy. A sourced supersymmetry construction can connect that object to a spacetime BPS bound. Later chapters add the relevant charge and dynamical dictionaries for ADE vanishing cycles and wrapped-brane states; this chapter supplies the geometric test and the boundary of what it can establish.

IV.6.7 Exercises

The first four exercises have exact-answer fields in the reader companion. State the intermediate argument on paper even when submitting only the requested fields. The fifth exercise is written reasoning.

E1. In standard flat $\mathbb{C}^2$, orient the plane by e_{x^1} and $(3/5)e_{y^1} + (4/5)e_{x^2}$. Compute the real Gram and J matrices. Submit the J pullback, area and whether J saturates the bound as `pullback`, `volume` and `saturates`.

E2. For the flat holomorphic torus with $g = 3/2$, $L_x = 2$, $L_y = 5$, $\alpha' = 4$, $g_s = 1/2$, $B = F = 0$ and constant dilaton, submit $\int_C J$, area and $(2\pi)^2$ times the leading wrapped D2 rest mass as `J_period`, `area` and `mass_times_4pi2`. Explain why $\operatorname{Im} t_C$ is a different quantity.

E3. For the oriented diagonal plane in flat $\mathbb{C}^3$ with unit factors $(3+4i)/5$, $(3-4i)/5$, i, compute the Gram matrix, the three J cross-pairings and the complex determinant of Ω_{unit}. Submit its real and imaginary parts as `omega_re`, `omega_im`, and the pairings as `J_12`, `J_13`, `J_23`. State the phase of the saturating real form.

E4. For $Z_1 = 3 + 4i$ and $Z_2 = 6 + 8i$, compute the dot and oriented-area conditions. Submit positive alignment, $|Z_1|$, $|Z_2|$, $|Z_1 + Z_2|$ and $|Z_1 - Z_2|$ as `aligned_positive`, `abs_z1`, `abs_z2`, `abs_sum` and `anti_abs_sum`. Explain the zero-period and opposite-charge cases without asserting stability.

E5. Explain which additional geometric and physical premises are needed before a locally calibrated cycle and aligned periods imply an actual stable BPS object. Distinguish a Euclidean membrane instanton from a Lorentzian D2 particle. Identify a cited theorem, a local calculation and a physical premise in your answer.

IV.6.8 Take-home message

Take-home message

A closed form bounded by oriented volume turns a realized compact saturating cycle into a volume minimizer in its real homology class. In the book's metric convention, a holomorphic flat torus has $\int_C J = \mathrm{Area}(C) = 2gL_xL_y$. A unit-normalized holomorphic three-form detects the phase of an oriented Lagrangian three-plane. In the stated zero-field, constant-dilaton D2 model, the leading rest energy is $\tau_2\,\mathrm{Area}(C)$. Spacetime BPS equality and an actual stable state require a supersymmetric charge map and dynamical input. Positive period alignment is a necessary threshold condition, not that input.

After this chapter the reader should be able to test an oriented plane inequality, reproduce the compact Stokes argument, translate the book's Kähler metric into area, evaluate a diagonal special-Lagrangian phase, and separate a leading action calculation from a state-existence claim. The geometric theorem used for higher complex dimension and the flat special-Lagrangian characterization are cited at their stated hypotheses; they are not consequences of the finite examples alone. Chapter 7 will use intersection and period data in K3 geometry, while later wrapped-brane constructions must supply their own superalgebra, charge and stability information.

Status and sources

Section IV.6.2 uses the calibration definition and compact real-homology minimization theorem [MATH], cited rather than proved here, in Joyce (2002, physical PDF pp. 24–25, Section 6.2 and Proposition 6.1). The tilted-plane Gram and form computation is explicit algebra [MATH]. Closedness, compactness, orientation and an already realized representative are required. The zero calibration is allowed by the definition but does not calibrate a positive-dimensional submanifold.

Section IV.6.3 uses the convention $ds^2 = 2g_{a\bar{b}}dz^a d\bar{z}^b$ and $J = ig_{a\bar{b}}dz^a \wedge d\bar{z}^b$. The metric-factor translation, torus area and dimensionless-period distinction are local calculations [MATH]. The periodic graph perturbation, its induced Gram matrix, unchanged J period and strict area excess are further local calculations in this flat torus. These flat-torus calculations do not prove a general calibration theorem. The general $J^k/k!$ plane inequality is a cited Kähler theorem [MATH], cited rather than proved here, from Joyce (2002, physical PDF p. 26, Section 6.4). The t_C normalization is the dimensionless period defined above; the torus does not establish existence in an arbitrary class.

Section IV.6.4 calculates the unit flat diagonal-plane Gram, J and complex determinant [MATH]. The phase-zero characterization with its orientation is cited at its flat hypotheses from Joyce (2002, physical PDF pp. 27–28, Section 7 and Proposition 7.3). Unit comass belongs to the declared flat metric; a rescaled holomorphic form needs its own metric norm and closedness check. This section supplies no global representative theorem.

Section IV.6.5 uses the metric-only induced action of Johnson (2000, physical PDF pp. 70–71, Section 3.10, eqs. (179)–(183)), translated to the physical tension τ_2. The restricted area energy and numerical value are action and arithmetic calculations [MATH]

under the stated zero-field, constant-dilaton, unwarped assumptions. The small-slope density expansion and integrated graph-energy excess are additional local algebra applied to that same restricted action, distinct from the cited calibration theorem. The large-volume D2 area discussion in Hori et al. (2003, physical PDF p. 626, Section 32.3) uses different units. The Euclidean M2 conditions and normalized period in Becker et al. (1995, physical PDF pp. 9, 12, eqs. (2.17)–(2.18), (2.32)) and conditional IIB D3 black-hole discussion on physical pp. 16–17 are source-frame statements, taken as physical premises. They provide no universal Lorentzian D2 central-charge coefficient or state-existence theorem here.

Section IV.6.6 derives the positive-alignment and opposite-charge arithmetic [MATH]. The conditional central-charge interpretation uses the A-brane period context in Hori et al. (2003, physical PDF p. 873, Section 39.5) and the source-specific three-cycle discussion in Becker et al. (1995, physical PDF pp. 16–17, Section 2.6), taken as physical premises. A common spacetime superalgebra and charge normalization, realized cycles and stable states remain separate physical premises, not a decoupling-limit claim. No wall-crossing rule, quantum-exact mass, projector formula or full spectrum is derived. The chapter's four bounded exercise tasks check only the displayed algebra and restricted action; E5 tests the missing-premise explanation in writing.

References

Becker, K., M. Becker, and A. Strominger (1995). *Fivebranes, Membranes and Non-Perturbative String Theory*. Version 3. arXiv: `hep-th/9507158`.

Hori, K. et al. (2003). *Mirror Symmetry*. Vol. 1. Clay Mathematics Monographs. American Mathematical Society and Clay Mathematics Institute.

Johnson, C. V. (2000). *D-Brane Primer*. Version 3. arXiv: `hep-th/0007170`.

Joyce, D. (2002). *Lectures on Calabi–Yau and special Lagrangian geometry*. Version 3. arXiv: `math/0108088`.

Chapter IV.7

K3 surfaces and heterotic/type-II duality

IV.7.1 Two spheres at a singularity

Resolve a local $\mathbb{C}^2/\mathbb{Z}_3$ singularity inside a K3 surface. The exceptional set contains two rational curves that meet at one point. If their areas decrease to zero, a type IIA string sees a place where new charged particles may become light. The intersection of the curves fixes an A_2 root pattern. Yet a metric picture alone does not specify the string background. A period of the NS two-form can remain on each shrinking sphere, and the proposed heterotic description needs a separate nonperturbative identification.

We will follow one pair of curves through three descriptions. The integral K3 lattice records their intersection. A marked metric and a B field decide whether the geometric collapse also reaches the relevant string locus. Finally, a heterotic charge lattice has the same A_2 root form after a sign translation. Figure IV.7.5 will collect the last comparison. The lattice equality is useful because it gives a concrete test of the proposed duality; it does not supply the duality itself.

The chapter develops five capabilities. We will compute pairings in the K3 lattice, distinguish lattice roots from represented curves, read the metric and B periods separately, derive a restricted wrapped-D2 energy, and compare its root pattern with heterotic weight-one charges. Chapters 2 and 3 provide the complex and local quotient geometry. Chapter 8 turns to elliptic fibrations and Kodaira fibers. Special geometry belongs to Chapter V.3.

IV.7.2 The K3 topological data

The physical question. A K3 has many two-cycles. Which arithmetic structure tells us which cycles can intersect and which signs to expect? Let S be a smooth compact K3 with its complex orientation. It is a simply connected compact complex Kähler surface with trivial canonical bundle. For integral oriented two-cycle classes $x, y \in H_2(S, \mathbb{Z})$,

their algebraic intersection $x \cdot y$ is the signed count of transverse intersection points after moving representatives. This pairing is topological. It does not measure the area of either representative.

The K3 classification gives a free rank-22 lattice with an even unimodular form of signature $(3, 19)$. We use a standard integral presentation

$$H_2(S, \mathbb{Z}) \simeq E_8(-1) \oplus E_8(-1) \oplus U \oplus U \oplus U, \qquad U = \begin{pmatrix} 0 & 1 \\ 1 & 0 \end{pmatrix}. \tag{IV.7.1}$$

Here $E_8(-1)$ is the negative of the positive E_8 root-lattice pairing. The signs in U refer to eigenvalues of the intersection matrix, not to the positivity of a geometric area. The classification and its K3 identification are cited results. The finite consequences of the displayed form can be checked directly.

Choose a simple-root basis $u_1, \ldots, u_8$ in each negative E_8 block. Our fixed basis has $u_i^2 = -2$ and $u_i \cdot u_j = 1$ for the seven edges

$$(1, 2), (2, 3), (3, 4), (4, 5), (5, 6), (6, 7), (3, 8), \tag{IV.7.2}$$

with every other distinct simple-root pairing zero. In this basis the positive Cartan matrix C_{E_8} has diagonal 2, minus one on these edges, and zero elsewhere. Thus the negative block is $-C_{E_8}$. The choice of simple basis is a declaration of coordinates in the lattice, not a claim that all eight vectors are effective curves at an arbitrary K3 point.

The rank and inertia now follow block by block. Each negative E_8 contributes eight negative directions. A U block has eigenvectors $e + f$ and $e - f$ with eigenvalues $+1$ and -1. Therefore

$$\operatorname{rank} Q = 8 + 8 + 3(2) = 22, \qquad (n_+, n_-) = (3, 16 + 3) = (3, 19). \tag{IV.7.3}$$

The determinant of C_{E_8} is one. Each U has determinant -1, so $\det Q = (-1)^3 = -1$. For any integral vector v, its square is a sum of even diagonal contributions and twice every off-diagonal contribution. Hence $v^2 \in 2\mathbb{Z}$. These elementary checks exhibit the claimed evenness and unimodularity of this presented matrix; they do not derive the classification of all K3 surfaces.

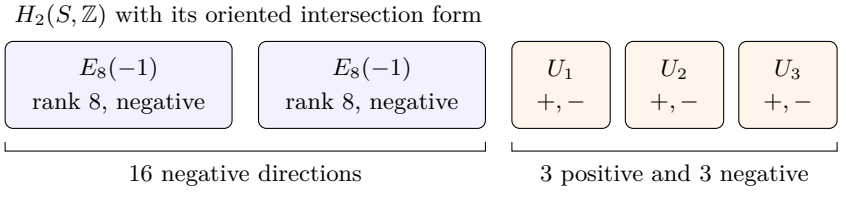


Figure IV.7.1: The marked K3 intersection lattice in the declared block basis. Each negative E_8 block contributes eight negative directions. Each hyperbolic plane U_i contributes one positive and one negative direction, giving signature $(3, 19)$. The boxes represent orthogonal lattice summands, not disjoint regions of a K3 surface.

Figure IV.7.1 also explains a common sign puzzle. A nonzero two-sphere may have positive area but negative self-intersection. Area depends on a metric and an orientation;

self-intersection depends on the normal bundle and the oriented topology. One must not turn $x^2 < 0$ into a negative physical volume.

The first U block gives a reusable calculation. Let $e^2 = f^2 = 0$ and $e \cdot f = 1$. For integers p, q,

$$(pe + qf)^2 = p^2e^2 + 2pq(e \cdot f) + q^2f^2 = 2pq. \tag{IV.7.4}$$

Take $r = e - f$ and $s = e + 2f$. Their squares and mutual pairing are

$$r^2 = -2, \qquad s^2 = 4, \qquad r \cdot s = (e - f) \cdot (e + 2f) = 2 - 1 = 1. \tag{IV.7.5}$$

Both vectors are integral, and the first is a root by its square. The second shows why pairwise intersection and self-intersection must be calculated independently. A positive-square class is not an exceptional (-2) curve merely because it meets one. Exercise 1 asks the reader to reproduce all three numbers. In Chapter 3, local quotient geometry supplies actual exceptional curves. The topological lattice here supplies only their possible intersection arithmetic.

IV.7.3 Roots and collapsing curves

The physical question. How does the intersection form turn an observed pair of exceptional spheres into an A_2 configuration? Call an integral class r a negative root when $r^2 = -2$. For arbitrary roots r_i, the matrix $-r_i \cdot r_j$ is their negative Gram matrix. It is a finite ADE Cartan matrix when the r_i are a simple-root basis of a negative-definite ADE root lattice, as for the selected adjacent pair below, or the corresponding specified exceptional-curve configuration. A different selection of roots need not be a simple system. The geometric interpretation also requires actual curves in a specified complex structure and Kähler chamber.

Take adjacent simple vectors $r_1 = u_1$ and $r_2 = u_2$ in our negative E_8 basis. Equation (IV.7.2) gives

$$G_{\mathrm{geom}} = \big(r_i \cdot r_j\big) = \begin{pmatrix} -2 & 1 \\ 1 & -2 \end{pmatrix}, \qquad A = -G_{\mathrm{geom}} = \begin{pmatrix} 2 & -1 \\ -1 & 2 \end{pmatrix}. \tag{IV.7.6}$$

The determinant of G_{geom} is $4 - 1 = 3 > 0$, while its trace is -4. Both eigenvalues are therefore negative; explicitly they are -1 and -3. The same arithmetic makes $r_1 + r_2$ another root:

$$(r_1 + r_2)^2 = r_1^2 + 2r_1 \cdot r_2 + r_2^2 = -2 + 2 - 2 = -2. \tag{IV.7.7}$$

The three positive-root choices in the abstract A_2 system are r_1, r_2 and $r_1 + r_2$. This statement is about the lattice. If two irreducible exceptional curves C_1, C_2 realize r_1, r_2, their sum is the class of the reducible effective cycle $C_1 + C_2$. It need not be a third irreducible sphere.

The additivity can be tested in both topology and geometry. For a Kähler form J in the chamber where the two curves are represented,

$$[C_1 + C_2]^2 = -2, \qquad \int_{C_1+C_2} J = \int_{C_1} J + \int_{C_2} J = A_1 + A_2. \tag{IV.7.8}$$

The first equality follows from the Gram matrix. The second follows from integration over the sum of oriented cycles. Both component areas are positive in the interior of this chamber, so the reducible cycle has positive area there despite its negative square. To make its total area vanish along this path, both nonnegative component areas must tend to zero. This is a geometric restriction that the abstract root sum does not reveal.

An actual smooth holomorphic rational curve has the same square for a geometric reason. For a smooth compact holomorphic curve C of genus g in a smooth K3, the adjunction formula is

$$2g - 2 = (K_S + C) \cdot C = C^2, \qquad K_S = 0. \tag{IV.7.9}$$

Thus $C \simeq \mathbb{P}^1$ implies $C^2 = -2$. The implication runs from a represented smooth rational curve to its square. Reversing it requires information about type $(1,1)$, effectivity, the chamber, and the chosen sign of the class. The cited K3 period and curve results can supply such information under their hypotheses; the finite matrix in Equation (IV.7.6) alone cannot.

For a concrete local geometry, resolve $\mathbb{C}^2/\mathbb{Z}_3$ with the action $(z_1, z_2) \mapsto (\omega z_1, \omega^{-1} z_2)$, where $\omega^3 = 1$. Three invariant coordinate functions obey

$$x = z_1^3, \qquad y = z_2^3, \qquad z = z_1 z_2, \qquad xy = (z_1 z_2)^3 = z^3. \tag{IV.7.10}$$

The hypersurface $xy = z^3$ has the quotient singularity at the origin. Its minimal resolution has two exceptional $\mathbb{P}^1$ curves meeting transversely once. Adjunction gives each diagonal entry -2, and the one transverse complex intersection gives off-diagonal entry $+1$. This realizes Equation (IV.7.6) in the local resolution. A single $\mathbb{C}^2/\mathbb{Z}_2$ exceptional curve instead gives the A_1 matrix (-2).

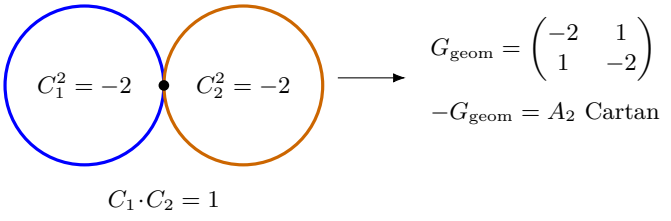


Figure IV.7.2: A schematic pair of exceptional rational curves in the local A_2 resolution. The circles and their drawn tangency encode incidence only, not an embedding or a planar transverse crossing. The dot records one transverse intersection of the complex curves, contributing $+1$ in the complex orientation. The finite two-node matrix omits the affine McKay node of the quotient description.

There is a useful representation distinction in Figure IV.7.2. The finite Dynkin diagram has one node for each exceptional curve in the resolution. The affine McKay diagram has an additional node tied to a different representation-theoretic construction. Its 3×3 affine A_2 Cartan matrix is singular with null vector $(1,1,1)$, while both it and the 2×2 finite matrix have rank two. The extra node changes the matrix size, not its

rank here; the affine matrix is not the intersection matrix of just these two compact exceptional curves.

For a fixed complex structure, choose the Kähler form J inside a chamber where C_1, C_2 are represented. The calibrated area of each holomorphic curve is $A_i = \int_{C_i} J > 0$. A degeneration can approach a boundary where these periods tend to zero. This is more information than the abstract identities $r_i^2 = -2$. The difference matters later: the heterotic root test will be an arithmetic and moduli condition, whereas a geometric picture of a shrinking sphere must also identify the represented curves. Chapter 3 supplies the local resolution; a later gauge-theory construction uses the possible light states, with their dynamics supplied separately.

IV.7.4 Metric and B-field moduli

The physical question. If a sphere has zero metric area, has the string background reached the enhancement locus? We first need to separate two kinds of period. A marked Ricci-flat K3 metric determines a positive oriented three-plane $\Sigma \subset H^2(S, \mathbb{R})$ spanned by its three self-dual harmonic two-forms. In one compatible complex structure, it is spanned by J, $\operatorname{Re}\Omega$, and $\operatorname{Im}\Omega$, after suitable normalization. The intersection pairing is positive on Σ. For a class r to be orthogonal to the whole plane means

$$r \perp \Sigma \quad \Longleftrightarrow \quad \int_r J = \int_r \operatorname{Re}\Omega = \int_r \operatorname{Im}\Omega = 0. \tag{IV.7.11}$$

The complex periods vanish when the class is of type $(1,1)$ in that complex structure. The J period then measures the area of a represented holomorphic curve in the chosen orientation. The marked K3 metric theorem relates roots perpendicular to Σ to orbifold degenerations. Its source setting includes a marked metric and the geometric quotient limit; Equation (IV.7.11) is not a claim that every negative root is an effective curve at every smooth point.

The U root $r = e - f$ from Equation (IV.7.5) gives a concrete counterexample to an immediate curve inference. Its square remains -2 as the complex structure varies. Choose a marked period for which $\int_r \Omega \neq 0$, and normalize Ω so that this period is one. Then

$$\begin{aligned} &r^2 = -2, \qquad \int_r \Omega = 1, \\ &r \notin H^{1,1}(S) \quad \Longrightarrow \quad r \text{ is not a holomorphic curve class.} \end{aligned} \tag{IV.7.12}$$

The implication uses the Hodge type of a holomorphic curve, not a claim that every normalized period defines the same K3. The period theory supplies complex structures off the root's $(1,1)$ locus. Even when the complex period vanishes, one must still identify the effective sign and the Kähler chamber before drawing a represented shrinking sphere.

For example, the represented A_2 curves of the previous section have $\int_{C_i} \Omega = 0$. If a metric path sends both $\int_{C_i} J$ to zero, then both classes become orthogonal to Σ at the boundary. The two separate periods matter. Shrinking only C_1 gives an A_1 local pattern, while the two-curve A_2 pattern requires the two periods to vanish together in a compatible chamber. A numerical matrix by itself gives neither path.

The full string moduli problem has a positive four-plane Π in an extended lattice of signature $(4,20)$. In a chosen geometric large-volume or cusp frame, the metric three-plane is accompanied by volume and B-field information. To make the relation precise, choose a primitive isotropic vector w and a second null vector w^* with $w\cdot w^*=1$. Choose the $H^2(S,\mathbb{R})$ subspace orthogonal to both. Set $\Sigma'=\Pi\cap w^\perp$; its projection into $w^\perp/\mathbb{R}w\simeq H^2(S,\mathbb{R})$ is the metric three-plane Σ. Choose $B'\in\Pi$ orthogonal to Σ' and normalized by $B'\cdot w=1$. The positive form on Π makes this choice unique: the functional $v\mapsto v\cdot w$ is nonzero on Π, its kernel is Σ', and its orthogonal complement inside Π is a line fixed by the normalization. In the chosen splitting,

$$B'=\alpha w+w^*+\mathcal{B},\qquad \mathcal{B}\in H^2(S,\mathbb{R}),\qquad \Pi=\operatorname{span}(\Pi\cap w^\perp,B'). \tag{IV.7.13}$$

Here $\mathcal{B}$ is the source-normalized dimensionless B class; its period over a curve is the book's $L^{-1}\int_C B$ in the chosen lift. Without orthogonality one could add Σ' vectors to B', changing $\mathcal{B}$ at fixed Π. For fixed $\Pi=\operatorname{span}(w+w^*,s_1,s_2,s_3)$ with positive orthonormal $s_i\perp w,w^*$, every $B'_t=w+w^*+ts_1$ has $B'_t\cdot w=1$, but projects to ts_1; orthogonality selects $t=0$. This continuous ambiguity is not a large-gauge shift. The real parameter α, together with $\mathcal{B}$, carries the volume information in this cusp description. For a pure two-cycle root $r\in H^2(S,\mathbb{Z})$, Poincaré dual to C, the two components of its orthogonality condition are

$$r\perp\Pi\quad\Longleftrightarrow\quad r\perp\Sigma\quad\text{and}\quad r\cdot B'=r\cdot\mathcal{B}=\frac{1}{L}\int_C B=0 \tag{IV.7.14}$$

in this fixed pure-two-cycle lift. The last equality follows because $r\cdot w=r\cdot w^*=0$. For a root already perpendicular to Σ, adding any vector of Σ' to a provisional B' would leave $r\cdot B'$ unchanged; the restricted root test therefore survives that provisional ambiguity, even though the full B-field dictionary does not. Under an integral B shift, the corresponding extended-lattice charge representative changes as well; the invariant statement for the selected cycle sector is trivial holonomy modulo the integral period. Thus the geometric condition $r\perp\Sigma$ and the additional B condition are distinct. Away from the selected geometric cusp, one should use the full four-plane criterion rather than silently extending this simple curve picture to every stringy point.

The dimensions check the fourth direction. The tangent space to a positive p-plane in signature (p,q) is a space of linear maps from that plane to its negative orthogonal complement, so it has dimension pq. In the geometric split, the metric three-plane has $3\cdot19=57$ parameters at fixed volume. A real B class contributes 22 more and the volume one more. The full positive four-plane has

$$\dim \mathrm{Gr}_3^+(3,19)+22+1=3\cdot19+22+1=80=4\cdot20=\dim \mathrm{Gr}_4^+(4,20). \tag{IV.7.15}$$

This local parameter count explains why the positive four-plane is the right size to hold the metric, B field and scale together. It is not a statement that the geometric coordinates cover every boundary or that every point admits the same chosen cusp frame.

Let C be one specified oriented curve. We use the book's dimensionless period unit

$$L=(2\pi)^2\alpha',\qquad a=\frac{1}{L}\int_C J=\frac{A}{L},\qquad [b]=\left[\frac{1}{L}\int_C B\right]\in\mathbb{R}/\mathbb{Z}. \tag{IV.7.16}$$

Here A is the metric area for a represented holomorphic curve, and $[b]$ is the periodic NS holonomy class. Writing $[b]$ rather than a real number matters because a large B-field shift changes a chosen lift by an integer. The source's dimensionless B normalization and the book's length-squared B field are related by this common L unit. The flux calculation below will choose a real lift $b \in \mathbb{R}$ explicitly.

For this one curve, an integral large-gauge shift changes the lift but not its holonomy phase:

$$b \longmapsto b + k, \quad k \in \mathbb{Z}, \qquad e^{2\pi i(b+k)} = e^{2\pi i b}. \tag{IV.7.17}$$

For example $b = 0$ and $b = 1$ represent the same point of the period circle, whereas $b = 1/2$ gives phase -1. This is why a numerical comparison between 0 and $1/2$ is invariant under the allowed shifts, even though the particular real lift is a choice.

The two conditions can now be compared without pretending that either follows from the other. In the selected geometric setting,

$$\begin{aligned} \text{represented metric collapse:} \quad & a \longrightarrow 0, \\ \text{trivial cycle holonomy:} \quad & [b] = 0 \in \mathbb{R}/\mathbb{Z}. \end{aligned} \tag{IV.7.18}$$

At $a = 0$ and $[b] = 1/2$, the metric curve is collapsed but the B holonomy is nontrivial. At $a = 0$ and $[b] = 0$, the two conditions coincide. The familiar orbifold conformal-field-theory point often has a half-period on exceptional cycles, so the two points need not be the same string background. The cited discussion makes this distinction in its geometric frame; it does not classify every enhancement locus at small volume.

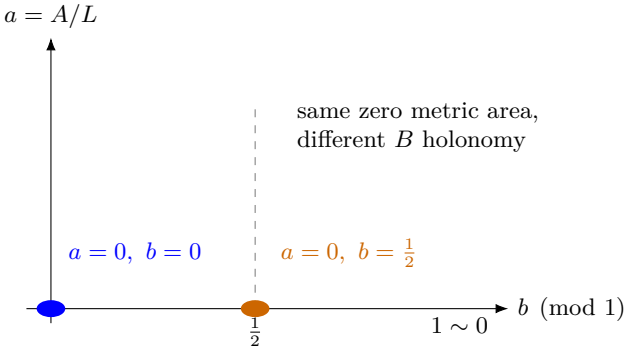


Figure IV.7.3: The area and B periods of one specified oriented curve in the local geometric frame. The horizontal coordinate is periodic modulo integers and the vertical coordinate is nonnegative. The two marked points have zero area but distinct B holonomy. Their separation remains meaningful when the circle is drawn as an interval with endpoints identified.

Figure IV.7.3 represents a two-coordinate slice, not the full K3 moduli space. It makes the pitfall visible: no change of the metric area can force $[b]$ to move horizontally. Conversely a large B shift changes the lift but leaves the point on the horizontal circle unchanged. Chapter 1 fixed the meaning of the Kähler period; Chapter II.6 discussed

orbifold backgrounds. The next section tests the same distinction with a controlled D2 action.

IV.7.5 Wrapped states

The physical question. What energy scale does a D2 wrapped on a particular smooth curve carry as its area decreases? We will calculate a leading single-brane action in a restricted regime. The curve C has a smooth finite-area representative and a static worldvolume. The dilaton is constant, spatial derivatives are small in string units, and the pullback of $B + 2\pi\alpha' F$ is a constant multiple of the induced area form. These hypotheses make the determinant exactly integrable within the leading abelian DBI action. They do not extend that action to a singular zero-area cycle.

Let T_{D2} include the constant dilaton factor, so the static energy from DBI has the form

$$M = T_{D2} \int_C \sqrt{\det\bigl(g + \mathcal{F}\bigr)}, \qquad \mathcal{F} = B + 2\pi\alpha' F. \tag{IV.7.19}$$

The determinant is spatial and uses the induced metric g. The two-form F is the worldvolume gauge curvature. In our declared orientation its flux integer is $n = (2\pi)^{-1} \int_C F \in \mathbb{Z}$. Choose a real lift $b = L^{-1} \int_C B$ of the periodic holonomy of Equation (IV.7.16). Then

$$\int_C \mathcal{F} = \int_C B + 2\pi\alpha' \int_C F = Lb + 4\pi^2\alpha' n = L(b + n). \tag{IV.7.20}$$

The explicit $4\pi^2\alpha'$ is why the flux integer enters with coefficient one. In particular, using $\int F = n$ would miss a factor of 2π.

Use a positively oriented orthonormal tangent frame on C. The restricted constant-proportionality assumption says $\mathcal{F} = q \,\mathrm{vol}_C$ for one real constant q. Thus the spatial matrix, its determinant, and its square root are

$$g + \mathcal{F} = \begin{pmatrix} 1 & q \\ -q & 1 \end{pmatrix}, \qquad \det(g + \mathcal{F}) = 1 + q^2, \qquad \sqrt{\det(g + \mathcal{F})} = \sqrt{1 + q^2}. \tag{IV.7.21}$$

Since q is constant, $qA = \int_C \mathcal{F} = L(b + n)$. Substitution into Equation (IV.7.19) gives

$$\begin{aligned} M &= T_{D2} A \sqrt{1 + \left[\frac{L(b+n)}{A}\right]^2} = T_{D2} L \sqrt{a^2 + (b+n)^2}, \\ m^2 &:= \left(\frac{M}{T_{D2} L}\right)^2 = a^2 + (b+n)^2. \end{aligned} \tag{IV.7.22}$$

This derivation uses $A > 0$ for the orthonormal frame and constant q. It is a finite-area equality within the specified leading action. The expression at $a = 0$ below means the limit of its right-hand side, not a new DBI derivation on a singular curve.

The chosen real lift is partly a description of the B field. Under an integral large-gauge change, one may relabel it together with the worldvolume flux:

$$(b, n) \longmapsto (b + k, n - k), \quad k \in \mathbb{Z}, \qquad (b + k) + (n - k) = b + n. \tag{IV.7.23}$$

This joint transformation leaves $\mathcal{F}$ and Equation (IV.7.22) fixed. Shifting b alone while keeping the same integer n would compare different physical branches in this frame. At $B = 0$, the Wess–Zumino term contains $\mu_2 \int C_1 \wedge 2\pi\alpha' F$, where C_1 is the RR one-form and μ_2, μ_0 are the D2 and D0 RR charge coefficients. Its integral over C is $\mu_2 Ln = \mu_0 n$ in the chosen orientation and normalization. Thus n also labels induced D0 flux charge in that frame. The full conserved charge in a general B background has further global subtleties that this local calculation does not classify.

Now calculate a nontrivial point. Set $a = 3/4$, $b = 1/2$ and $n = 0$. From Equation (IV.7.22),

$$m^2 = \left(\frac{3}{4}\right)^2 + \left(\frac{1}{2}\right)^2 = \frac{9}{16} + \frac{4}{16} = \frac{13}{16}, \qquad m = \frac{\sqrt{13}}{4}. \tag{IV.7.24}$$

Keeping the same lift and flux sector, the formal collapse limit gives $m^2 \to 1/4$. This is a residual scale in the leading diagnostic. By contrast, $b = 1, n = -1$ gives $b + n = 0$ and $m^2 = a^2$, which tends to zero. The two limits differ although both have zero metric area. Figure IV.7.4 displays their finite-area branches; its plotted half-period curve uses $n = 0$.

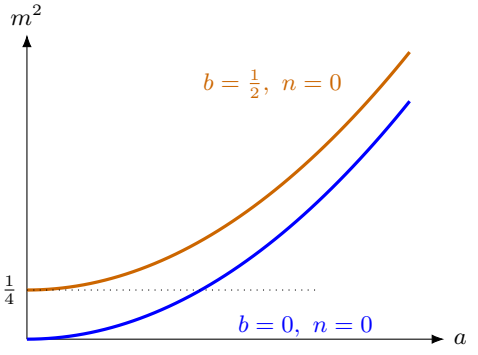


Figure IV.7.4: Scaled leading DBI mass squared as a function of positive scaled area a. The blue branch has $b = 0, n = 0$ and the orange branch has $b = 1/2, n = 0$. The nonzero orange intercept is the formal $a \to 0$ limit of a smooth-action expression, not an exact mass computed at the singular cycle.

At fixed flux label, Equation (IV.7.22) is the answer. If the question instead allows comparison of every integer flux sector, elementary nearest-integer arithmetic yields a different quantity:

$$\min_{n\in\mathbb{Z}} m_n^2 = a^2 + \min_{n\in\mathbb{Z}} (b+n)^2 = a^2 + \operatorname{dist}(b,\mathbb{Z})^2. \tag{IV.7.25}$$

For $b = 1/2$, both $n = 0$ and $n = -1$ give the same residual $1/4$ at $a \to 0$. For $b = 1$, the minimum uses $n = -1$ and gives zero. But at $b = 1$ with *fixed* $n = 0$, the collapse limit of m^2 is one. This contrasting example prevents a hidden minimization over induced D0 charge. The all-sector minimum is only a comparison of leading smooth-action branches;

it does not establish that every branch has a stable state or that a singular-limit state is exactly massless.

If $\mathcal{F}$ is not a constant multiple of area, its integral alone cannot replace the local determinant. In an orthonormal frame write $\mathcal{F} = q(x)\mathrm{vol}_C$. The action is then $T_{D2}\int_C \sqrt{1+q(x)^2}\,dA$, while $\int_C q(x)dA = L(b+n)$. These are different operations. For example, two equal-area patches with values $q_1 = 0$ and $q_2 = 2$ have mean $\bar{q} = 1$, but mean density $(1+\sqrt{5})/2$ rather than $\sqrt{2}$. The constant-pullback hypothesis is exactly what permitted Equation (IV.7.22). Chapter III.3 introduced the DBI action; the present calculation isolates the period and flux issue needed in later enhancement discussions.

IV.7.6 Heterotic/type-II comparison

The physical question. What can a matching A_2 matrix actually tell us about heterotic strings on T^4 and type IIA strings on K3? The proposed six-dimensional identification is a nonperturbative premise. We can test a necessary local consequence by comparing the roots that can support enhanced gauge symmetry. The sign and chirality conventions have to be stated before placing the two matrices side by side.

In the heterotic torus description, use an even charge lattice of signature $(4, 20)$ and a positive four-plane V selected by the moduli. Witten's source convention assigns V to right-moving charges and the negative complement $V^\perp$ to left-moving, antiholomorphic charges. A lattice vector $P \in V^\perp$ with $P^2 = -2$ has chiral conformal weight

$$d_P = -\frac{P^2}{2} = 1. \tag{IV.7.26}$$

This is the source's weight-one operator criterion. Aspinwall uses the opposite left/right names for the bosonic and supersymmetric sectors, while retaining the negative-square-two lattice criterion in his pairing. The book's heterotic gauge-root convention instead uses a positive Euclidean norm $h^2 = 2$ for the same root directions. We therefore compare $h^2 = -P^2$ on the selected negative subspace. Changing the words left and right without translating the quadratic-form sign would make the comparison inconsistent.

The concrete rank-two test uses the geometric roots r_1, r_2 of Equation (IV.7.6). In the heterotic positive Euclidean coordinate model, take

$$h_1 = (1,-1,0), \qquad h_2 = (0,1,-1), \qquad h_1^2 = h_2^2 = 2, \quad h_1 \cdot h_2 = -1. \tag{IV.7.27}$$

The last dot product is $1\cdot 0 + (-1)\cdot 1 + 0\cdot(-1) = -1$. Thus

$$G_{\mathrm{het}} = \begin{pmatrix} 2 & -1 \\ -1 & 2 \end{pmatrix} = -\begin{pmatrix} -2 & 1 \\ 1 & -2 \end{pmatrix} = -G_{\mathrm{geom}}. \tag{IV.7.28}$$

The sum $h_1 + h_2 = (1, 0, -1)$ also has positive square two. The chosen pair therefore has the same finite A_2 Cartan data as the negative K3 root block after sign reversal. This equality is exact arithmetic in declared bases. It does not identify an individual heterotic particle with an individual D2 state without the nonperturbative map and

the required moduli and charge-sector conditions. Figure IV.7.5 keeps the sign reversal beside the separate geometric and heterotic conditions.

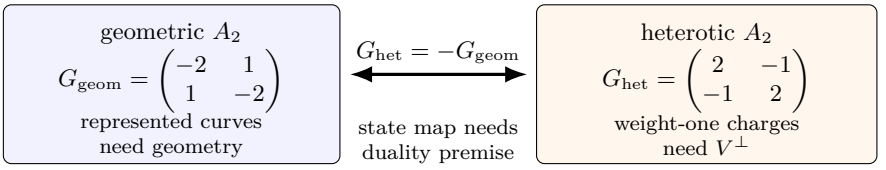


Figure IV.7.5: The restricted A_2 comparison. The geometric intersection form is negative, while the book's heterotic gauge-root norm is positive. Their matrices differ by one overall sign. Represented curves and heterotic weight-one operators require their own moduli conditions; a physical state identification additionally assumes the heterotic/type-IIA duality.

There is a small but informative closure check. In the two-dimensional span of h_1, h_2, the square of $xh_1 + yh_2$ is $2(x^2 - xy + y^2)$. For integer x, y, setting this square to two gives the six roots

$$2(x^2 - xy + y^2) = 2, \qquad \{(x, y)\} = \{(\pm 1, 0), (0, \pm 1), (1, 1), (-1, -1)\}. \tag{IV.7.29}$$

The geometric span has the same six negative-square-two vectors after reversing the form. Only two simple vectors are represented by the two irreducible exceptional curves in the pictured resolution. The other positive root is their reducible sum in that chamber. Counting roots is therefore a finite lattice statement with a clear geometric interpretation, rather than a count of six separate exceptional spheres.

There is one more lattice distinction hidden by the small matrix. The vectors r_1, r_2 generate the A_2 *root lattice* R. The dual lattice of vectors pairing integrally with both roots is the *weight lattice* R^*. Since the Cartan determinant is three,

$$[R^* : R] = |\det A| = 3. \tag{IV.7.30}$$

One can see the difference explicitly. Define $\lambda_1 = (2h_1 + h_2)/3$. Then $\lambda_1 \cdot h_1 = 1$ and $\lambda_1 \cdot h_2 = 0$, so $\lambda_1 \in R^*$, but its coefficients in the simple-root basis are not integers, so $\lambda_1 \notin R$. The two simple sphere classes and their sum therefore generate roots, not the entire weight lattice. Witten's discussion uses the phrase "weight lattice" for the lattice generated by the collapsing spheres. The displayed intersection matrix supports the root-lattice reading locally. This wording point does not determine the primitive closure of those classes in full K3 homology or the global form of a gauge group.

The second fundamental weight makes the index visible without relying only on a determinant. With $\lambda_2 = (h_1 + 2h_2)/3$ one finds

$$\lambda_1 \cdot (h_1, h_2) = (1, 0), \qquad \lambda_2 \cdot (h_1, h_2) = (0, 1), \qquad \lambda_1^2 = \lambda_2^2 = \frac{2}{3}. \tag{IV.7.31}$$

Neither λ_i lies in the integer span of h_1, h_2. Their fractional coefficients identify additional weight classes, not additional shrinking spheres in the two-curve resolution.

In particular, merely changing the label on R from "roots" to "weights" would change the lattice by index three.

The proposed heterotic/type-IIA identification becomes physically consequential only if its nonperturbative premise is supplied. At the selected geometric cusp, an A_2 collapse and suitable B periods give a candidate geometric realization of the root pattern. On the heterotic side, the orthogonality condition $P \in V^{\perp}$ makes the corresponding negative-two charges weight-one operators. Equation (IV.7.28) is the compatibility calculation between these descriptions. It is neither a proof that every K3 root is represented nor a derivation of the full duality. Chapter II.5 supplies the positive heterotic lattice convention; Chapter II.9 introduces the proposed duality generator. Future gauge constructions can use this local root interface while keeping their state and coupling premises explicit.

IV.7.7 Exercises

The first four exercises have bounded answer submissions. Enter each rational value as a canonical JSON string such as `"-2"` or `"13/16"`; enter logical answers as JSON booleans. The public question file gives the exact fields. The last exercise is a written explanation. These tasks use the same basis, normalization and branch choices as the chapter.

1. In the first U block take $e^2 = f^2 = 0$ and $e \cdot f = 1$. Put $r = e - f$ and $s = e + 2f$. Calculate r^2, s^2 and $r \cdot s$ by expanding the pairing, then submit the three fields of E1. State in words why a negative square does not mean a negative geometric area.

2. In the declared negative E_8 basis take adjacent simple vectors r_1, r_2 with diagonal entries -2 and mutual pairing $+1$. Compute both squares, their pairing, and $(r_1 + r_2)^2$. Submit the four E2 fields. Explain whether the sum must be a third irreducible exceptional curve when r_1, r_2 are represented by two curves.

3. Apply the finite-area leading DBI expression $m^2 = a^2 + (b+n)^2$ at $a = 3/4$, chosen real lift $b = 1/2$, and fixed $n = 0$. Submit the squared mass, its formal $a \to 0$ limit, and whether that limit is massless. Then submit whether $a = 0, b = 1, n = -1$ gives a zero limit in the same diagnostic. Say why these answers do not certify a singular-cycle BPS state.

4. For positive Euclidean heterotic roots $h_1 = (1, -1, 0)$ and $h_2 = (0, 1, -1)$, calculate the two squares and their mutual product. Compare them with the off-diagonal entry of Equation (IV.7.6). Submit the six E4 fields, including whether the matrices match after one sign reversal and whether that arithmetic proves duality.

5. Give two concrete counterexamples to the inference that a negative-two lattice class is already a collapsing sphere. Use the U root with a nonzero holomorphic period as one case and the A_2 root sum represented by a reducible cycle as the other. Then explain why Equation (IV.7.28) cannot by itself identify heterotic and type IIA particles. Name the needed geometric and physical premises. This is a written task, E5, without a numerical submission.

Take-home message. The K3 lattice fixes a negative root intersection pattern, represented rational curves give that pattern geometric content, and B holonomy decides whether a metric collapse reaches the corresponding string locus in the chosen frame. The heterotic positive root matrix matches after a sign change. An actual spectrum match needs the separate nonperturbative duality premise. A reader can now calculate pairings, diagnose the area/B distinction, evaluate a fixed-flux D2 branch, and state exactly what the local A_2 comparison establishes.

Status and sources

Section IV.7.2 uses the cited [MATH] classification of the intersection lattice of a smooth compact K3 with its standard orientation, from Aspinwall (1996, PDF pp. 10–11, Section 2.3, eqs. (19)–(25)); its classification proof is not supplied here. The displayed block arithmetic and U example are separate [MATH] calculations in the displayed basis.

Section IV.7.3 uses cited [MATH] results: adjunction for an actual smooth holomorphic rational curve on a smooth K3 and the two-curve exceptional configuration of the minimal $\mathbb{C}^2/\mathbb{Z}_3$ resolution, from Aspinwall (1996, PDF pp. 21–23, eq. (53), Theorem 4). General classification proofs are not supplied. Quotient coordinates, the selected A_2 Gram and root sum are local [MATH] calculations; representation and chamber remain separate hypotheses.

Section IV.7.4 uses cited [MATH] marked-period and geometric-degeneration results for a marked Ricci-flat K3 metric, represented root classes and a chosen chamber, from Aspinwall (1996, Section 2.3, Theorem 2, PDF pp. 21–23, Theorem 4); no Torelli or degeneration theorem is proved here. The off-$(1,1)$ implication and plane dimensions are conditional [MATH] consequences. The identification of a positive string four-plane with metric, volume and B data, and the physical enhancement reading, are source-stated physical premises in the chosen geometric cusp, from Aspinwall (1996, PDF pp. 28–31, 44–45, eqs. (62), (66), (68), (95)–(96)) and Witten (1995, v2, PDF pp. 44–45, Section 4.6). Equation (66) requires $B' \perp \Sigma'$ and $B' \cdot w = 1$. The complement's uniqueness, restricted root orthogonality and phase comparison are conditional [MATH] steps; counting 80 parameters alone does not derive the physical identification. The period units are as defined above.

Section IV.7.5 takes the leading single-D2 DBI and WZ actions as source-stated physical inputs from Myers (1999, PDF p. 2, eqs. (1), (3)) and Johnson (2000, PDF p. 80, eq. (207)), with a smooth finite-area static cycle, constant dilaton and low derivatives. The determinant, integrated constant-proportional pullback, joint shift and finite-area mass, then the variable-pullback contrast and all-sector minimum, are conditional [MATH] consequences. Zero area is a limit of this leading expression, not an exact singular-cycle mass or a derivation of state existence.

Section IV.7.6 uses the sourced perturbative heterotic weight-one criterion [WS] for charges perpendicular to the positive four-plane in the declared T^4 worldsheet sector, from Witten (1995, v2, PDF pp. 44–46, Section 4.6). Aspinwall's opposite chirality labels Aspinwall (1996, PDF p. 44, eq. (95)) are translated to the opposite chirality convention used here. The selected A_2 sign, six roots and root/weight index are [MATH]; Witten's sphere-generated "weight lattice" is read locally as roots, without a global-

group inference. The heterotic/type-IIA K3 identification is a separate nonperturbative premise, as in Chapter II.9, not a consequence of the Gram equality. Existence and stability of particular wrapped states require additional physical input and are not concluded by that premise and arithmetic alone. E1–E4 have bounded graded fields, while their written explanations and E5 are not graded by the numerical interface.

References

Aspinwall, P. S. (1996). *K3 Surfaces and String Duality*. arXiv: hep-th/9611137.

Johnson, C. V. (2000). *D-Brane Primer*. arXiv: hep-th/0007170.

Myers, R. C. (1999). "Dielectric-Branes". In: *Journal of High Energy Physics* 1999.12, p. 022. DOI: 10.1088/1126-6708/1999/12/022. arXiv: hep-th/9910053.

Witten, E. (1995). "String Theory Dynamics in Various Dimensions". In: *Nuclear Physics B* 443, pp. 85–126. DOI: 10.1016/0550-3213(95)00158-O. arXiv: hep-th/9503124.

Chapter IV.8

Elliptic fibrations and the Kodaira classification

IV.8.1 The curve and the construction

An elliptic curve can vary from point to point in a compactification. Most fibers are smooth tori. At special base points a cycle can shrink and the fiber becomes singular. Such degenerations are central to the geometric description of seven-branes. Their resolved curves also supply part of the geometric information used to identify nonabelian gauge algebras. To use this description, we must first learn what the equation of the varying curve actually determines.

There are several objects in this question. A cubic equation defines a possibly singular Weierstrass model. A regular surface over a transverse base curve can have a reducible special fiber even when the cubic at the same base point is irreducible. Along a discriminant divisor in a larger base, the components can be permuted. Finally, relating that geometry to a physical gauge algebra requires a compactification and a physical interpretation of the resolved geometry. We will follow these objects in this order. An order of vanishing alone cannot replace all four steps.

The first calculation uses a family whose two Weierstrass coefficients are both nonzero at the degeneration. A cancellation in the discriminant makes the distinction between a coefficient order and a fiber type visible. A further tuning changes the discriminant order without changing the central cubic. We then examine minimality, selected Tate forms and covers over the function field of a divisor. These calculations prepare the F-theory constructions in Volume X-A. They also identify which geometric information is complementary to the seven-brane charge transport of X.2.

By the end of the chapter, the reader should be able to compute an exact discriminant order through cancellations; apply a selected Kodaira or Tate row with its hypotheses; distinguish a divisorial nonminimality from a point blowup; factor the displayed covers over the correct field; and explain why the resulting local algebra leaves the global gauge group undetermined. Chapter 7 supplies the K3 setting in which these questions already arise. Chapters 1 and 2 supply the local complex geometry and the line-bundle

language.

We derive the cubic discriminant, the local cancellation examples, the weighted bundle change and the selected cover factorizations. The Kodaira surface classification and the relation between covers and resolved components are cited results. We do not prove the classification or the existence of a global resolution. The physical gauge-algebra dictionary is an additional input. Keeping that boundary visible lets the same local calculation serve several later constructions without asserting a full compactification from a polynomial.

IV.8.2 An elliptic curve varies

The first question is where a fiber stops being smooth. Work over the complex numbers and in characteristic zero throughout. An elliptic fibration with section is a family of genus-one curves together with a chosen point in each fiber. The section fixes the origin of the group law on a smooth fiber. On a local base patch, trivialize the relevant line bundles and write the short Weierstrass equation as

$$y^2 = P(x), \qquad P(x) = x^3 + fx + g. \tag{IV.8.1}$$

Here x, y are affine fiber coordinates, while f, g are functions of the base coordinates in this trivialization. They are coefficients of the family, not additional fiber coordinates. The local formula does not assert that a genus-one fibration without a section admits this model.

It is necessary to include the point at infinity. Let $[X : Y : Z]$ be homogeneous coordinates on the local projective plane, with $x = X/Z$ and $y = Y/Z$ on $Z \neq 0$. The projective cubic is

$$F(X, Y, Z) = Y^2Z - X^3 - fXZ^2 - gZ^3 = 0, \qquad O = [0 : 1 : 0]. \tag{IV.8.2}$$

On $Z = 0$, the equation forces $X = 0$, so O is the only point omitted by the affine chart. At that point $\partial F/\partial Z = Y^2 = 1$ in the $Y = 1$ chart. The projective curve is therefore smooth at O, independently of f and g. A singularity of the fiber, if present, occurs in the finite chart. This is why the section can remain well defined when the finite cubic degenerates.

For the affine equation, put $H(x, y) = y^2 - P(x)$. At a singular point both partial derivatives vanish. The complete condition is

$$H = H_x = H_y = 0 \quad \Longleftrightarrow \quad y = 0, \qquad P(x) = 0, \qquad P'(x) = 3x^2 + f = 0. \tag{IV.8.3}$$

Thus smoothness is a repeated-root question for a cubic. If r is that common root, substituting $f = -3r^2$ into $P(r) = 0$ gives

$$f = -3r^2, \qquad g = 2r^3, \qquad 4f^3 + 27g^2 = -108r^6 + 108r^6 = 0. \tag{IV.8.4}$$

The vanishing combination detects the collision even if neither coefficient vanishes. To verify its normalization and the converse, eliminate the common root by a resultant.

For a monic cubic and its derivative, the Sylvester determinant gives

$$\operatorname{Res}(P,P') = \det \begin{pmatrix} 1 & 0 & f & g & 0 \\ 0 & 1 & 0 & f & g \\ 3 & 0 & f & 0 & 0 \\ 0 & 3 & 0 & f & 0 \\ 0 & 0 & 3 & 0 & f \end{pmatrix} = 4f^3 + 27g^2 \equiv \Delta. \tag{IV.8.5}$$

One can evaluate this determinant without expanding all permutations. Subtract three times the first row from the third, and three times the second row from the fourth. The first two columns then reduce the determinant to

$$\det \begin{pmatrix} -2f & -3g & 0 \\ 0 & -2f & -3g \\ 3 & 0 & f \end{pmatrix} = (-2f)(-2f^2) + 3g(9g) = 4f^3 + 27g^2. \tag{IV.8.6}$$

A resultant is zero precisely when the polynomials have a common root over the algebraic closure. Equations (IV.8.3) and (IV.8.5), together with the infinity check, therefore establish that the projective cubic is smooth precisely when $\Delta \neq 0$. This test concerns the fiber. It does not test regularity of the total space of the family.

There are three frequently encountered scalars. If r_i are the roots of P, its monic polynomial discriminant is $\operatorname{disc}(P) = \prod_{i<j}(r_i - r_j)^2$. The sign in the resultant relation is $(-1)^{3(3-1)/2} = -1$. Consequently

$$\operatorname{disc}(P) = -\Delta, \qquad \Delta_{\mathrm{EC}} = -16\Delta = 16\operatorname{disc}(P). \tag{IV.8.7}$$

Here Δ_{EC} denotes the conventional elliptic-curve normalization. This chapter uses $\Delta = 4f^3 + 27g^2$ in every order and coefficient calculation. Multiplication by a nonzero constant preserves a vanishing order, but it changes every quoted coefficient. A sign error can be invisible in a table of orders and still spoil a worked expansion.

Now take a base coordinate t and the concrete family

$$f(t) = -12 + 3t, \qquad g(t) = 16 - 6t. \tag{IV.8.8}$$

Both functions are units at $t = 0$. Expanding the two terms of the discriminant separately gives

$$\begin{aligned} 4(-12+3t)^3 &= -6912 + 5184t - 1296t^2 + 108t^3, \\ 27(16-6t)^2 &= 6912 - 5184t + 972t^2. \end{aligned} \tag{IV.8.9}$$

The constant and linear terms cancel. The remaining polynomial is

$$\Delta(t) = -324t^2 + 108t^3 = 108t^2(t-3). \tag{IV.8.10}$$

For example, at $t = 1$ the coefficients are $f = -9$, $g = 10$, and $\Delta = -216 \neq 0$. The cubic has three distinct roots, since $P(x) = (x-2)(x^2+2x-5)$ there. At $t = 0$, however,

$$P_0(x) = x^3 - 12x + 16 = (x-2)^2(x+4). \tag{IV.8.11}$$

The singular point is $(x, y) = (2, 0)$. Translate $x = 2 + \xi$, retaining y as the second affine coordinate. Its local equation becomes

$$y^2 = \xi^2(6 + \xi), \qquad y^2 - 6\xi^2 = 0 \quad \text{to quadratic order.} \tag{IV.8.12}$$

The tangent cone has the distinct lines $y = \sqrt{6}\,\xi$ and $y = -\sqrt{6}\,\xi$. The central fiber is a nodal cubic. Its two local branches are not two irreducible projective components: $x + 4$ is not a square in $\mathbb{C}[x]$, so $y^2 - (x - 2)^2(x + 4)$ does not factor into two polynomials linear in y. The repeated root of P_0 produces a node of one cubic, rather than a pair of smooth projective curves.

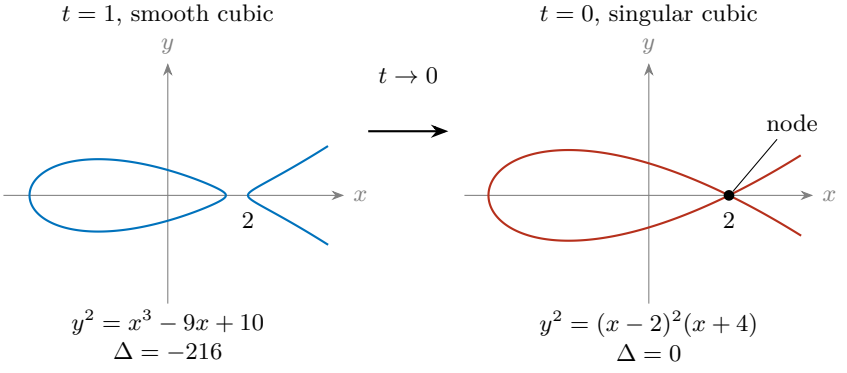


Figure IV.8.1: Real affine slices of the same complex projective family $y^2 = x^3 + (-12 + 3t)x + 16 - 6t$. The left panel has $t = 1$ and $\Delta = -216$; the right has $t = 0$ and a node at $(2, 0)$. The finite plots show both signs of y. Their unbounded branches meet the projective point $O = [0 : 1 : 0]$, which is outside these affine plots and is smooth in both fibers. The horizontal arrow specializes the base parameter; it is not a resolution map. These are Weierstrass curves, not the resolved I_2 component configuration.

Figure IV.8.1 shows this distinction in a real slice. The complex curve has more information than the drawing, but the collision and the two nodal tangents can already be seen. At a smooth base value the fiber is a compact complex genus-one curve after adding O. The affine plot alone is neither the compact torus nor its full complex topology. In particular, the number of visible real arcs cannot be used to count complex resolved components.

For the displayed family, the total affine surface has equation $y^2 - x^3 + (12 - 3t)x - 16 + 6t = 0$. Its t derivative is $-3x + 6$, which also vanishes at $(x, y, t) = (2, 0, 0)$. The surface model is singular there. A regular surface over the same base requires another model. This is the first point at which Chapter 3's distinction between a singular space and its resolution becomes necessary. The discriminant has located the bad fiber; it has not drawn the fiber of that regular model.

IV.8.3 Orders and minimal models

How much can the order of a discriminant zero tell us? The answer uses both a valuation and a geometric hypothesis. In a local coordinate t transverse to a smooth base locus, write a nonzero function as a power of t times a unit. Define

$$h(t) = t^m h_0(t), \quad h_0(0) \neq 0 \quad \Longrightarrow \quad \operatorname{ord}_t h = m, \qquad \operatorname{ord}_t 0 = \infty. \tag{IV.8.13}$$

The local ring in this transverse direction is a discrete valuation ring. The rule for a sum is an inequality, not an equality. Applied to the Weierstrass discriminant it says

$$\operatorname{ord}_t \Delta \geq \min\{3 \operatorname{ord}_t f,\, 2 \operatorname{ord}_t g\}. \tag{IV.8.14}$$

When the two candidate leading orders agree, their coefficients can cancel. Our first example has minimum zero and actual order two. The physical lesson is that the locus and strength of the degeneration depend on the relation between the coefficients, not merely on their individual zeros.

To see a second cancellation without changing the central curve, introduce a constant c and replace only g:

$$f = -12 + 3t, \qquad g = 16 - 6t + ct^2. \tag{IV.8.15}$$

The cubic power of f is unchanged. The complete square of g is

$$g^2 = 256 - 192t + (36 + 32c)t^2 - 12ct^3 + c^2t^4. \tag{IV.8.16}$$

Multiplying by 27 and adding the first line of (IV.8.9) gives the full polynomial

$$\Delta = (-324 + 864c)t^2 + (108 - 324c)t^3 + 27c^2t^4. \tag{IV.8.17}$$

There is no higher tail: f^3 has degree three in t and g^2 has degree four. This matters when a leading coefficient is tuned away. An expression for just the first two coefficients would leave the rest of the family unspecified.

The order-two coefficient vanishes at a unique value of c:

$$-324 + 864c = 0 \quad \Longrightarrow \quad c = \frac{3}{8}. \tag{IV.8.18}$$

Substitution gives

$$\Delta|_{c=3/8} = -\frac{27}{2}t^3 + \frac{243}{64}t^4 = -\frac{27}{2}t^3\left(1 - \frac{9}{32}t\right). \tag{IV.8.19}$$

Thus the exact order is three, with coefficient $-27/2$. The value $c = 1/3$, for comparison, leaves $-36t^2$ and still has order two. The fraction $3/8$ is fixed by the cancellation. Both $c = 0$ and $c = 3/8$ have the same central equation (IV.8.11). The central nodal curve therefore cannot distinguish these two degenerations.

We now state the setting in which an order triple can be read as a Kodaira fiber type. Consider a proper flat genus-one surface fibration with a section over a smooth complex

curve. Assume that the generic fiber is smooth, so its discriminant is not identically zero. Use a regular relatively minimal surface model. Relative minimality means that no fiber contains an exceptional smooth rational curve of self-intersection -1 which can be contracted in the surface. It excludes *vertical* (-1)-curves. A section maps onto the base and is horizontal; it is not excluded by this condition. Under these hypotheses the cited Kodaira classification identifies the special fiber from the minimal Weierstrass data. We use selected rows in Table IV.8.1. We do not prove that classification.

Fiber	ord f	ord g	ord Δ	Monodromy or scope
I_n, $n \geq 1$	0	0	n	split (surface)
II	≥ 1	1	2	irreducible cusp
III	1	≥ 2	3	split (surface)
IV	≥ 2	2	4	split (surface)
I_0^*	≥ 2	≥ 3	6	split (surface)
II*	≥ 4	5	10	split (surface)
Nonminimal input	≥ 4	≥ 6	≥ 12	change of model required

Table IV.8.1: Selected order rows of the cited surface classification, with the exact discriminant order shown. The last line is a boundary for the Weierstrass input, not an additional fiber of a regular relatively minimal surface. Over a positive-dimensional divisor the residue field need not be algebraically closed. The split, semi-split and non-split refinements in Tables IV.8.2 and IV.8.3 then carry additional information.

A useful horizontal control is a section of self-intersection -1 on an elliptic surface. Its intersection with a generic fiber is one, whereas a vertical curve maps to a point on the base. Contracting that section is not a contraction within a fiber. Thus its self-intersection does not contradict relative minimality. Replacing the required phrase by "no (-1)-curves anywhere" would rule out legitimate sectioned examples. Regularity, relative minimality and the location of a curve are separate conditions.

Under the surface hypotheses, our $c = 0$ and $c = 3/8$ data give I_2 and I_3, respectively. These are fibers of the regular relatively minimal model. The I_2 fiber consists of two rational components meeting at two points; I_3 has three rational components in a cycle. In both cases each component has multiplicity one. Figure IV.8.2 records their incidences. The central Weierstrass nodal cubic is the same in the two families, but its surrounding surface and the resolved fiber are different. Calling the nodal cubic itself an I_2 configuration would identify objects with different numbers of irreducible components.

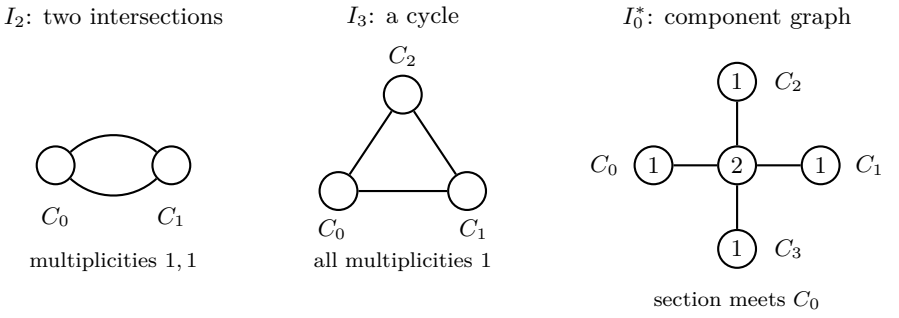
For an example on the other side of the table, take

$$f = 2t^4, \quad g = 3t^5, \qquad \Delta = 32t^{12} + 243t^{10} = t^{10}(243 + 32t^2). \tag{IV.8.20}$$

The unit $243 + 32t^2$ has nonzero constant term. The exact triple is $(4, 5, 10)$ and the cited row is II*, subject to the stated surface hypotheses. Increasing the exponent of g by one gives

$$f = 2t^4, \quad g = 3t^6, \qquad \Delta = (32 + 243)t^{12} = 275t^{12}. \tag{IV.8.21}$$

The second triple is $(4, 6, 12)$. It reaches the nonminimal threshold on the original model.



Vertices represent rational curves. Numerals inside the I_0^* vertices are multiplicities. Cubic-cover orbits act on C_1, C_2, C_3; C_0 is distinguished by the section.

Figure IV.8.2: Incidence graphs of cited resolved transverse fibers, conditional on a regular relatively minimal model. A vertex represents a whole rational component, not a point on the original cubic; an edge represents an intersection. In I_2 the two edges are two distinct intersections. All I_2 and I_3 multiplicities are one. In I_0^* the central component has multiplicity two, the four outer ones multiplicity one. The section meets C_0, leaving C_1, C_2, C_3 as the three outer components relevant to the cubic-cover permutation. They can form three, two or one orbits. The drawings are not a construction of a global resolution and are distinct from Figure IV.8.1.

It cannot be assigned the same relatively minimal fiber by continuing the preceding row beyond its hypotheses.

Why does a formal removal of common factors require care globally? Let $\mathcal{L}$ be the Weierstrass line bundle on a fixed smooth base B. The weights of the local fiber coordinates imply

$$x \sim \mathcal{L}^2, \qquad y \sim \mathcal{L}^3, \qquad f \in H^0(B, \mathcal{L}^4), \qquad g \in H^0(B, \mathcal{L}^6). \tag{IV.8.22}$$

The symbol $\sim$ here describes the transition weight in local trivializations. Suppose a Cartier divisor D has local equation $s = 0$ and $f = s^4 \widetilde{f}$, $g = s^6 \widetilde{g}$. The change $x = s^2 \widetilde{x}$, $y = s^3 \widetilde{y}$ gives, away from $s = 0$,

$$\widetilde{y}^2 = \widetilde{x}^3 + \frac{f}{s^4}\widetilde{x} + \frac{g}{s^6}, \qquad \widetilde{\Delta} = \frac{\Delta}{s^{12}}. \tag{IV.8.23}$$

This expression extends a different Weierstrass model across D. Since s is a local representative of the divisor section, the transformed coefficients have weights

$$\widetilde{f} \in H^0\big(B, (\mathcal{L}(-D))^4\big), \quad \widetilde{g} \in H^0\big(B, (\mathcal{L}(-D))^6\big), \quad \widetilde{\mathcal{L}} = \mathcal{L}(-D). \tag{IV.8.24}$$

For example, removing t^4, t^6 from (IV.8.21) gives $\widetilde{f} = 2$, $\widetilde{g} = 3$, $\widetilde{\Delta} = 275$ locally. The substitution is singular at $t = 0$; it is not an invertible coordinate transformation on the original special fiber. If the original Calabi–Yau construction used $\mathcal{L} = K_B^{-1}$, then $\mathcal{L}(-D)$ need not equal K_B^{-1}. Local removal does not preserve that fixed-base

construction automatically. This is the line-bundle issue from Chapter 2 in an explicit degeneration.

A point in a base of complex dimension two poses a different problem. Use local coordinates (z, u) and take

$$f = z^4, \qquad g = u^6, \qquad \Delta = 4z^{12} + 27u^{12}. \tag{IV.8.25}$$

At the origin, orders in the maximal ideal (z, u) give $(4, 6, 12)$. There is no common divisor of z^4 and u^6 in this local ring: the prime factors z and u are distinct. The fixed-base divisor removal above cannot be applied there. Blow up the base point and examine only the chart $u = zh$, where h is the new exceptional-direction coordinate. The pullbacks and formal fiber scaling are

$$f = z^4, \quad g = z^6h^6, \quad x = z^2x', \quad y = z^3y', \qquad (y')^2 = (x')^3 + x' + h^6. \tag{IV.8.26}$$

After dividing by z^6, the transformed coefficients and discriminant are

$$f' = 1, \qquad g' = h^6, \qquad \Delta' = 4 + 27h^{12}. \tag{IV.8.27}$$

At a generic point of the exceptional locus $z = 0$, this discriminant is nonzero. At its twelve simple complex zeros in the h chart, further local analysis is needed. We have computed one chart, not constructed a global resolved compactification. The base has changed as well as the fiber equation. For a blowup of a smooth surface at a point, its canonical bundle obeys

$$K_{B'} = \pi^* K_B + E, \tag{IV.8.28}$$

where E is the exceptional divisor. Thus an arbitrary point blowup or its inverse cannot be described as preserving the canonical bundle without a corresponding calculation. A tensor-branch interpretation requires still more physical information.

Finally, when B has higher dimension and D is a smooth discriminant divisor, the generic point of D has a residue field such as $\mathbb{C}(u)$. A transverse parameter still gives a discrete valuation. To use the surface classification in this direction, we assume a flat sectioned model, smooth generic fiber and an available regular relatively minimal resolved transverse model. This is a conditional transverse use of the theorem. It is not an existence theorem for a global resolution of the higher-dimensional total space. In particular, the point calculation above cannot be promoted to a classification of all codimension-two fibers. With this boundary fixed, we can ask which local coefficient forms retain the information that orders alone discard.

IV.8.4 Reading a Tate model

The purpose of a Tate form is to organize local equations so that certain orders and residual polynomials become accessible. It is not a universal global coordinate system. Work near a smooth divisor $D = \{t = 0\}$ in a base patch. The Tate equation is

$$y^2 + a_1xy + a_3y = x^3 + a_2x^2 + a_4x + a_6. \tag{IV.8.29}$$

The subscripts denote the Weierstrass weights of the coefficients. Each a_i is a base function after local trivialization. Bounds on its t order specify a local ansatz. Additional cancellations and residual conditions determine which generic fiber that ansatz actually produces. The existence of such a convenient form over one patch does not establish its existence everywhere on D or across intersections of divisors.

Table IV.8.2 copies the selected coefficient bounds and discriminant orders from the source Tate table. We display the output as a conditional local Lie algebra rather than a global gauge group. The surface and resolved-transverse hypotheses of the previous section still apply to the fiber interpretation. The physical interpretation of the last column is stated separately in Section IV.8.6.

Fiber	a_1	a_2	a_3	a_4	a_6	Δ	Monodromy; local algebra
IV	1	1	1	2	2	4	non-split; $\mathfrak{sp}(1)$
IV	1	1	1	2	3	4	split; $\mathfrak{su}(3)$
I_0^*	1	1	2	2	3	6	non-split; $\mathfrak{g}_2$
I_0^*	1	1	2	2	4	6	semi-split; $\mathfrak{so}(7)$
I_0^*	1	1	2	2	4	6	split; $\mathfrak{so}(8)$

Table IV.8.2: Selected local Tate ansatze. Entries in the a_i columns are lower bounds on $\operatorname{ord}_t a_i$; the displayed $\operatorname{ord}_t \Delta$ is the exact generic order required for the indicated type. The two final rows have identical bounds and require different residual factorization. The split I_0^* row in particular needs the finite square test derived below. The last column uses the additional physical dictionary, not coefficient orders alone.

To read the two final rows, set

$$\begin{aligned} &a_1 = O(t), && a_2 = t\alpha + O(t^2), \quad a_3 = O(t^2), \\ &a_4 = t^2\beta + O(t^3), && a_6 = O(t^4). \end{aligned} \tag{IV.8.30}$$

Here α and β are the leading restrictions to D. For the explicit examples D has local coordinate u and its function field is $\mathbb{C}(u)$. The notation $O(t^m)$ means membership in the mth power of the transverse ideal, with coefficients allowed in that field. We require

$$\beta(\alpha^2 - 4\beta) \neq 0 \quad \text{in } \mathbb{C}(u). \tag{IV.8.31}$$

This will ensure that the leading cubic is separable and that its root at zero does not coincide with another root. A zero at an isolated value of u is a separate exceptional locus, not a zero of the rational function as an element of the field.

We first remove the terms linear in y. Define the new coordinate $y_c = y + (a_1x + a_3)/2$. This translation is invertible in characteristic zero and gives the exact equation

$$y_c^2 = x^3 + \left(a_2 + \frac{a_1^2}{4}\right)x^2 + \left(a_4 + \frac{a_1a_3}{2}\right)x + \left(a_6 + \frac{a_3^2}{4}\right). \tag{IV.8.32}$$

The added terms have orders at least two, three and four, respectively. They do not change the leading orders one and two of the first two coefficients. Substitute $x = tX$. The right hand side is

$$t^3\big[X^3 + \alpha X^2 + \beta X\big] + O(t^4) = t^3X(X^2 + \alpha X + \beta) + O(t^4). \tag{IV.8.33}$$

Every correction from completing the square contributes at least t^4: $a_1^2x^2$ has order four, a_1a_3x order four, and the constant terms order four. This establishes which cubic the stated bounds expose.

Equation (IV.8.33) is a leading-polynomial calculation, not a claim that one can introduce $y_c/t^{3/2}$ as a single-valued coordinate. No fractional-power change of fiber coordinate is used. The residual polynomial in X is the object used in the cited component-cover criterion. We have derived that polynomial from the Tate ansatz; we have not constructed the resolution by this substitution.

The root $X = 0$ is already defined over $\mathbb{C}(u)$. The remaining quadratic has roots

$$X_\pm = \frac{-\alpha \pm \sqrt{\alpha^2 - 4\beta}}{2}. \tag{IV.8.34}$$

The cubic has three factors over the field precisely when the square root belongs to the field. If it does not, it has the one linear factor and one irreducible quadratic. Condition (IV.8.31) excludes repeated roots in both cases. The finite residual square test obtained from the original Tate coefficients is therefore

$$\left.\frac{a_2^2 - 4a_4}{t^2}\right|_{t=0} = \alpha^2 - 4\beta. \tag{IV.8.35}$$

The power of t in this formula follows from $a_2^2 - 4a_4 = t^2(\alpha^2 - 4\beta) + O(t^3)$. Dividing by t^4 would generically produce a pole, not a restriction to D. The precise source-text discrepancy is recorded in the chapter-end apparatus.

To compare this factor test with a short Weierstrass cover, translate the residual variable by $X = Y - \alpha/3$. The variable Y here belongs to the residual cubic; it is not the original fiber coordinate y or y_c. Direct expansion gives

$$X^3 + \alpha X^2 + \beta X = Y^3 + pY + q, \qquad p = \beta - \frac{\alpha^2}{3}, \quad q = \frac{2\alpha^3}{27} - \frac{\alpha\beta}{3}. \tag{IV.8.36}$$

This is an invertible translation over $\mathbb{C}(u)$. It preserves the number and degrees of irreducible factors. It also fixes the sign translation between the quadratic residual and the short-cubic scalar. Indeed,

$$4p^3 = 4\beta^3 - 4\alpha^2\beta^2 + \frac{4}{3}\alpha^4\beta - \frac{4}{27}\alpha^6, \tag{IV.8.37}$$

while

$$27q^2 = \frac{4}{27}\alpha^6 - \frac{4}{3}\alpha^4\beta + 3\alpha^2\beta^2. \tag{IV.8.38}$$

Adding these expressions cancels the two highest powers of α and leaves

$$4p^3 + 27q^2 = -\beta^2(\alpha^2 - 4\beta), \qquad \operatorname{disc}_X\big(X(X^2 + \alpha X + \beta)\big) = \beta^2(\alpha^2 - 4\beta). \tag{IV.8.39}$$

The leading cubic has nonzero discriminant precisely under (IV.8.31). The sign matches (IV.8.7); calling the quadratic discriminant itself the book short-Weierstrass discriminant would lose the factor $-\beta^2$.

A full worked split case is $\alpha = u + 1$, $\beta = u$. The residual and factorization are

$$\alpha^2 - 4\beta = (u+1)^2 - 4u = (u-1)^2, \qquad X(X^2 + (u+1)X + u) = X(X+1)(X+u). \tag{IV.8.40}$$

Its polynomial discriminant is $u^2(u-1)^2$, nonzero as a rational function. At $u = 0$ or $u = 1$ roots collide, so the generic conclusion does not apply at those points. At the ordinary value $u = 2$, the roots are $0, -1, -2$, their squared difference product is 4, and the book scalar is -4. The translated coefficients are $p = -1$, $q = 0$, giving the same scalar. This numerical specialization checks the normalization; the explicit rational factors establish the generic splitting.

For a semi-split example choose $\alpha = 0$, $\beta = -u$. Then

$$X(X^2 - u), \qquad \alpha^2 - 4\beta = 4u, \qquad \operatorname{disc}_X = 4u^3, \qquad 4p^3 + 27q^2 = -4u^3. \tag{IV.8.41}$$

A rational square has even valuation at $u = 0$, whereas $4u$ has valuation one. The quadratic is therefore irreducible over $\mathbb{C}(u)$. The cubic has two irreducible factors, and its leading discriminant is nonzero away from $u = 0$. At the closed point $u = 1$ the polynomial becomes $X(X-1)(X+1)$ over $\mathbb{C}$. That pointwise factorization does not change the generic semi-split answer. The next section explains why the field in this statement is part of the geometry. The pitfall in using the last two Tate rows is now explicit: the coefficient bounds coincide, while the residual square class can differ.

IV.8.5 Covers over the divisor

The physical question behind a split label is whether resolved fiber components can be distinguished consistently as one moves along the discriminant divisor. A picture over one closed complex point cannot answer that question. Let u vary along a smooth divisor D, let t be its transverse coordinate, and work at the generic point of D. For our examples the residue field and a convenient arithmetic subfield are

$$K = \mathbb{C}(u), \qquad K_0 = \mathbb{Q}(u) \subset K. \tag{IV.8.42}$$

A function in K is a ratio of polynomials in u with complex coefficients. It need not have a rational square or cube root. The complex constants are algebraically closed; the rational function field is not. An algebraic cover specified by a polynomial in an indeterminate ψ records the multivalued roots over D.

For a separable polynomial, its irreducible factors over K specify the connected generic parts of the finite cover. We count distinct factors only in the separable examples below. The identification of this cover with permutations of particular resolved components is part of the cited Kodaira/Tate analysis. It is not a consequence of factoring an arbitrary polynomial. The relevant leading discriminants must be nonzero in K. Their zeros at special u mark exceptional loci outside the generic analysis.

Two field comparisons prevent misleading answers. First,

$$\psi^2 - 2 \text{ is irreducible over } \mathbb{Q}(u), \qquad \psi^2 - 2 = (\psi - \sqrt{2})(\psi + \sqrt{2}) \text{ over } \mathbb{C}(u). \tag{IV.8.43}$$

Thus factorization over K_0 alone is insufficient. Second, after fixing an ordinary complex value $u = u_0$, a nondegenerate quadratic or cubic always factors over $\mathbb{C}$. Such a

specialization discards the question of whether roots can be chosen as rational functions of u. We will justify every nonsplitting statement over K itself.

The needed obstruction is elementary. At a point $u = a$, let $v_a(R)$ be the order of a rational function R, negative for a pole. If $R = A/B$ with common factors removed, then

$$v_a(R^m) = m\big(v_a(A) - v_a(B)\big) \in m\mathbb{Z}. \tag{IV.8.44}$$

A simple zero or pole is therefore impossible for a rational mth power with $m > 1$. This argument works with complex coefficients. It is the extra mathematical step needed when exact polynomial arithmetic is performed over K_0.

For type IV take the short Weierstrass ansatz

$$f = t^2F(u), \qquad g = t^2q(u), \qquad \Delta = t^4\big(27q(u)^2 + 4t^2F(u)^3\big). \tag{IV.8.45}$$

Here F and q are nonzero in K. The exact generic orders are $(2, 2, 4)$, so the cited IV row applies under the geometric hypotheses already stated. In a chosen trivialization its cover is

$$\psi^2 - q(u) = 0. \tag{IV.8.46}$$

It has two factors if q is a square in K, and one if it is not. The assumption $q \neq 0$ ensures separability. The exceptional zeros of q must not be silently included in this generic row.

Take $F = 1$ and first set $q = (u + 2)^2$. The complete discriminant and the cover factorization are

$$\Delta = t^4\big(27(u + 2)^4 + 4t^2\big), \qquad \psi^2 - (u + 2)^2 = (\psi - u - 2)(\psi + u + 2). \tag{IV.8.47}$$

For $u \neq -2$ the two roots are distinct. There are two generic cover components, so the branch is split. At $u = 0$, for example, the leading coefficient of Δ/t^4 is 432, and the cover roots are ± 2. At $u = -2$ the leading coefficient vanishes and the roots coincide. The generic label has reached its boundary; a statement about that point needs another calculation.

Next take $q = u^2 + 2$, retaining $F = 1$. Now

$$\Delta = t^4\big(27(u^2 + 2)^2 + 4t^2\big), \qquad \psi^2 - u^2 - 2 = 0. \tag{IV.8.48}$$

The roots of $u^2 + 2$ in the complex u plane are $a_\pm = \pm i\sqrt{2}$. Each is simple, since its derivative $2a_\pm$ is nonzero. If $R(u)^2 = u^2 + 2$ in K, then

$$2v_{a_+}(R) = v_{a_+}(u^2 + 2) = 1, \tag{IV.8.49}$$

which is impossible. A quadratic over a field is reducible precisely when it has a root there, so this cover is irreducible over K. It is non-split. Its leading discriminant coefficient is nonzero outside $u = \pm i\sqrt{2}$. At $u = 0$ the two complex roots are $\pm\sqrt{2}$. Those numerical roots coexist with generic irreducibility. The obstruction concerns varying u, not solving a quadratic at one point.

For I_0^*, use a different transverse scaling:

$$f = t^2A(u), \qquad g = t^3B(u), \qquad \Delta = t^6d(u), \qquad d(u) = 4A(u)^3 + 27B(u)^2. \tag{IV.8.50}$$

The assumption is $d \neq 0$ in K. Its exact generic discriminant order is six. The cited component cover is

$$\psi^3 + A(u)\psi + B(u) = 0. \tag{IV.8.51}$$

Its three, two or one irreducible factors distinguish split, semi-split and non-split branches. A separable cubic with two factors must have a linear factor and an irreducible quadratic. This is exactly the pattern exposed by the semi-split Tate example, after the translation to a short cubic.

For a split example choose the cubic through its rational roots:

$$\begin{aligned}(\psi - u)(\psi - 1)(\psi + u + 1) &= \big(\psi^2 - (u+1)\psi + u\big)(\psi + u + 1) \\ &= \psi^3 - (u^2 + u + 1)\psi + u(u+1).\end{aligned} \tag{IV.8.52}$$

The sum of the three roots $u, 1, -u-1$ is zero, as a short cubic requires. Thus $A = -(u^2 + u + 1)$ and $B = u(u+1)$, and direct substitution or the squared root differences gives

$$d(u) = -(u-1)^2(u+2)^2(2u+1)^2. \tag{IV.8.53}$$

This is the book scalar, with the minus sign relative to the polynomial discriminant. It is nonzero generically. The roots collide at $u = 1, -2$ or $-1/2$, so those values are excluded. At $u = 0$, the roots are $0, 1, -1$, $A = -1$, $B = 0$ and $d = -4$. Although g vanishes on that slice, the exact discriminant order remains six; the cover is still separable there. One coefficient alone is not the generic condition.

The semi-split example is

$$\psi(\psi^2 - u) = \psi^3 - u\psi, \qquad A = -u, \quad B = 0, \quad d = -4u^3. \tag{IV.8.54}$$

The root $\psi = 0$ is rational. If the quadratic had a rational root R, then $2v_0(R) = v_0(u) = 1$. It therefore stays irreducible even over $K = \mathbb{C}(u)$. The count is two, with a nonzero leading scalar away from $u = 0$. The zero function B has infinite order in the transverse parameter; this is compatible with the $\operatorname{ord} g \geq 3$ entry of the row. A local classification table can allow an infinite coefficient order while requiring a finite exact discriminant order.

Finally take

$$\psi^3 - u = 0, \qquad A = 0, \quad B = -u, \quad d = 27u^2. \tag{IV.8.55}$$

A reducible cubic over a field must have a linear factor. Such a factor would give $R^3 = u$ for a rational function R, implying

$$3v_0(R) = 1. \tag{IV.8.56}$$

No such integer valuation exists. The cubic is irreducible over K. It has one generic component and is non-split, with $u = 0$ excluded. The derivative is $3\psi^2$; it has no common root with $\psi^3 - u$ when u is nonzero in the field. Thus the cubic is separable, as the nonzero scalar also shows. At $u = 1$ the specialized polynomial has the three complex cube roots of unity. Those roots do not supply a rational function $u^{1/3}$ on D.

Figure IV.8.2 makes the component information visible. In the resolved I_0^* fiber a section distinguishes one outer component. The other three are the ones whose

permutation is encoded by the cited cubic cover. Three rational roots leave them individually distinguished. A rational root and an irreducible quadratic leave one fixed and exchange the other two. An irreducible cubic gives one orbit of three. Counting these orbits is a geometric operation; assigning the result a physical Lie algebra requires the next step.

These examples establish more than a factor count over rational coefficients, and less than a full classification of all degenerations. The explicit factors establish the split cases over $\mathbb{C}(u)$. Valuations at simple complex zeros establish the nonsplit factors there. All leading scalars are nonzero functions, with the exceptional points listed. This is the information needed before using the local dictionary in Volume X-A. At an intersection of discriminant divisors, or at a zero of a leading scalar, a generic-divisor answer cannot be reused as a matter calculation. The nearby Chapter 7 K3 examples provide a useful surface comparison: their base is a curve, so a discriminant component is a closed point and carries no along-divisor function-field variation of this kind.

IV.8.6 From fiber geometry to physics

What does a cover factorization contribute to a QFT construction? It identifies a component-permutation pattern in the geometric setting for which the cover criterion holds. In an appropriate F-theory compactification, a suitable flat resolved generic-divisor geometry and the cited gauge-algebra dictionary turn that pattern into a local nonabelian Lie algebra. The physical dictionary is an additional premise. Neither a polynomial discriminant nor an incidence graph derives the physical spectrum of a compactification by itself.

Table IV.8.3 applies this dictionary to the exact examples already calculated. The three I_0^* examples have the same Kodaira discriminant order six. Nevertheless they lead to three different conditional algebras. The two type-IV examples similarly have the same order four and different conditional algebras. This is a concrete failure of the proposed shortcut from an order triple to a unique physical answer.

Fiber	Generic cover factors	Monodromy	Local algebra
IV	2	split	$\mathfrak{su}(3)$
IV	1	non-split	$\mathfrak{sp}(1) \simeq \mathfrak{su}(2)$
I_0^*	3	split	$\mathfrak{so}(8)$
I_0^*	2	semi-split	$\mathfrak{so}(7)$
I_0^*	1	non-split	$\mathfrak{g}_2$

Table IV.8.3: The cited local F-theory Lie-algebra dictionary for the selected generic fibers, under its compactification and resolved-geometry premises. Factor counts refer to separable covers over $\mathbb{C}(u)$, not to closed-point factors over $\mathbb{C}$. No entry specifies a global gauge group, finite quotient or matter spectrum.

The component permutation is often described as a folding of the resolved configuration. The split I_0^* case preserves the three outer labels individually. The semi-split case identifies a pair under transport, and the non-split case puts all three in one orbit. The cited physical interpretation gives the three algebras in the table. This use

of the component graph differs from constructing an arbitrary invariant subalgebra by drawing fewer vertices. The geometry, its component transport and the physical compactification must all match the stated setting.

There is another monodromy in the same elliptic fibration. Away from the discriminant, a smooth complex fiber has the rank-two integral cycle lattice $H_1(E_b, \mathbb{Z})$. Choosing an oriented basis identifies the intersection-preserving transport around a loop in the base complement with an element of $SL(2, \mathbb{Z})$. This transport acts on one-cycles of a smooth fiber. X.2 fixes the charge-column convention needed when that action is expressed in seven-brane charges. We introduce no new matrix convention here.

Component monodromy instead follows the irreducible components of a resolved singular fiber as u varies along the discriminant divisor. The base paths and the transported objects differ. Figure IV.8.3 separates them. A loop in the u plane around a simple zero of u changes a local choice of $\sqrt{u}$ to $-\sqrt{u}$ in the semi-split cover. That exchange concerns two component labels. A loop in the transverse t plane around $t = 0$ acts on the cycles of a smooth nearby elliptic fiber. The two operations can belong to one geometry, but neither is the definition of the other.

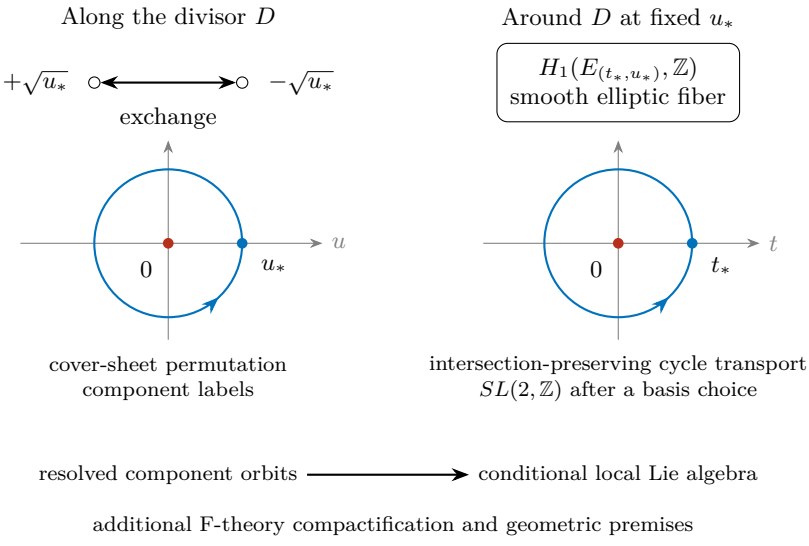


Figure IV.8.3: Two different transports in a local base with divisor $D = \{t = 0\}$. Left: the u coordinate runs along D; a loop about an exceptional point permutes the cover roots $+\sqrt{u}$ and $-\sqrt{u}$. The points shown above the base are cover sheets, not elliptic one-cycles. Right: at a fixed ordinary u_*, a loop in the punctured transverse t disc transports $H_1(E, \mathbb{Z})$ and gives an $SL(2, \mathbb{Z})$ action after choosing a basis. The lower arrow records a separate conditional F-theory interpretation of the resolved component orbits. The figure does not identify the permutation with a cycle-transport matrix or assert a global resolution.

To see exactly what remains unknown globally, take the split IV example with $q = (u + 2)^2$. Its explicit rational factors establish the split cover, and the conditional

local algebra is $\mathfrak{su}(3)$. This algebra alone admits a simply connected group $SU(3)$ and a quotient by its center. Choosing a global gauge group requires the charge and representation content that distinguishes these possibilities. Global section information and its relation to charge quantization can constrain the choice. The local function q has not specified those global data. With several factors, a common finite quotient can also correlate them, so deciding one factor in isolation still need not decide the whole group.

Now take the non-split IV example with $q = u^2 + 2$. Its simple-zero obstruction gives the conditional local algebra $\mathfrak{sp}(1)$. The order triple is the same as in the split example, but the algebra changes. Neither example determines representations localized at the excluded special points. A collision of roots or a zero of the leading scalar announces a new geometric question; it does not supply a matter multiplet or its multiplicity. Those conclusions need codimension-two geometry, a physical compactification and the relevant spectrum calculation. Written Exercise E6 asks the reader to keep these three levels of reasoning separate.

The distinction is useful for later construction work. XIV, Chapters 3 and 5 use the generic-divisor tools before examining more singular loci. X.2 supplies the complementary seven-brane transport language. Chapters 2, 3 and 7 of the present volume supply bundles, resolutions and K3 surfaces. Passing between these subjects requires the object that each operation actually uses: a minimal Weierstrass equation, a regular transverse fiber, a cover over a function field or a chosen physical compactification. Preserving those objects prevents an ADE label from carrying more physical information than the construction has supplied.

IV.8.7 Exercises

Use $\Delta = 4f^3 + 27g^2$ throughout. Exercises E1–E5 accept bounded scientific submissions through the companion questions. The public `questions.json` specifies the exact fields and bounds. Each submission has exactly the keys `task` and `answer`. Write rational coefficients as strings such as `"3/8"`, and orders as JSON integers. E6 is a written reasoning problem; it has no numerical acceptance criterion. The algebra names in the submission interface are identifiers for the conditional local algebras in Table IV.8.3.

1. **E1. A cancellation with unit coefficients.** For $f = -12 + 3t$ and $g = 16 - 6t$, expand both terms of the discriminant separately and add them. Submit `ord_f`, `ord_g`, `ord_delta`, `delta_t2` and `delta_t3`. The last two entries are rational strings. Explain in writing why nonzero $f(0)$ and $g(0)$ do not imply a smooth fiber. Locate the finite singular point and distinguish its local branches from projective components. These written explanations are not part of the bounded submission.

2. **E2. A further tuning.** Replace g in E1 by $16 - 6t + (3/8)t^2$. Compute the entire discriminant, including its highest-degree term. Submit `ord_delta`, `delta_t2` and `delta_t3`. Include the canceled coefficient. As a written check, state why no powers beyond degree four can occur, and explain how the central cubic can stay

unchanged while the cited resolved fiber type changes. The submitted fields test the specified order and coefficients; they do not certify that explanation.

3. **E3. Two type-IV covers.** For $f = t^2F(u)$ with generic nonzero F and $g = t^2q(u)$, compare $q = (u+2)^2$ and $q = u^2+2$, in that order. Factor their covers over $\mathbb{C}(u)$ or prove the required irreducibility. Exact arithmetic may use $\mathbb{Q}(u)$, but justify the extension to complex constants. Submit `cover_components`, `split` and `algebra`, each an array of length two. The split entries are booleans; the algebra entries use `su3` or `sp1`. The algebra interpretation assumes the physical premises of Section IV.8.6. State in writing the exceptional values of u and explain why factorization at $u = 0$ does not settle the generic question.

4. **E4. Three cubic covers.** For I_0^* candidates $f = t^2A(u)$, $g = t^3B(u)$, compare $(\psi - u)(\psi - 1)(\psi + u + 1)$, $\psi(\psi^2 - u)$ and $\psi^3 - u$, in that order. Expand the first cover to recover A, B. For each cover check that the leading book scalar is a nonzero rational function, locate its zeros and establish the generic factor count over $\mathbb{C}(u)$. Submit arrays `cover_components`, `monodromy` and `algebra`, each of length three. Use `split`, `semi-split` or `non-split` for monodromy, and `so8`, `so7` or `g2` for the conditional algebras. The valuation arguments and exceptional-locus explanations are written parts, beyond these three submitted arrays.

5. **E5. The nonminimal boundary.** Compute the exact discriminants for $(f, g) = (2t^4, 3t^5)$ and $(2t^4, 3t^6)$, in that order. Submit `boundary_orders` and `nonminimal_orders` as arrays of three orders each. Use the boolean `boundary_nonminimal` for the first threshold test and `second_nonminimal` for the second. The threshold is $(\operatorname{ord} f, \operatorname{ord} g, \operatorname{ord} \Delta) \geq (4, 6, 12)$ componentwise on the original model. In writing, compare fixed-base removal along a common divisor with the point model $f = z^4, g = u^6$. Reconstruct the $u = zh$ chart and state what its transformed discriminant does and does not establish globally.

6. **E6. What geometry determines.** Explain, using one split and one non-split fiber example, why a Kodaira order triple alone does not determine the generic-divisor local F-theory algebra. Identify the further global information needed before asserting a global gauge group. Separate a cited classification statement, an algebraic calculation and a physical premise. Discuss the excluded special points, the possible finite quotient and the absence of a matter calculation. Explain why the semi-split component exchange is not itself an $SL(2, \mathbb{Z})$ matrix on elliptic cycles. This is a written task.

IV.8.8 Take-home message

Take-home message

The book discriminant is the cubic resultant $4f^3 + 27g^2$. Cancellations can raise its order while leaving the central nodal cubic unchanged. A Kodaira label describes the fiber of a regular relatively minimal surface under its stated hypotheses. A Tate ansatz exposes further residual factorization, which must be evaluated over the generic divisor field. In the selected examples this factorization separates the split, semi-split and non-split branches. The conditional local F-theory algebras use a further physical dictionary. They determine neither the global gauge group nor matter. Component permutation along the divisor and cycle transport around it retain different objects and paths.

Status and sources

§8.1–8.2: cubic and discriminant. The sectioned short-Weierstrass equation and scalar use the normalization defined above. The resultant calculation, infinity check, unit-coefficient cancellation and central node are mathematical calculations [MATH]. They are direct calculations, not a resolution theorem. The inspected equation and order anchors are Katz et al. 2011, arXiv v1, physical PDF pp. 5–6, equations (2.2)–(2.4), with the cubic in its later equations (2.7), (5.3), (6.1) and (A.1). Its printed (2.1) on physical p. 5 has x^2, not x^3. We have not silently quoted that printed equation as the cubic. The later explicit cubic forms supply the working object. The sign relation to the monic polynomial discriminant and the factor -16 are stated explicitly in (IV.8.7).

§8.3: orders and minimality. The full tuned polynomial and the orders in the II^* and nonminimal examples are direct calculations [MATH]. Their classification is cited from Katz et al. 2011, v1, physical p. 6, Table 1, not proved here. The surface and conditional higher-base hypotheses concern the cited classification [MATH], read with Weigand 2018, v1, physical pp. 26–29, Section 4.1–4.2 and Table 4.1. The resolved I_n and I_0^* component pictures also use Aspinwall 1996, v5, physical pp. 78–81, equations (138)–(140), Figure 9 on physical p. 80 and Table 4 on physical p. 81. The printed page labels in that edition are offset from the physical PDF pages. Its source-specific j normalization is not imported. Kodaira's original paper was not inspected; the theorem is cited through these inspected accounts.

The bundle transformation is a mathematical result [MATH], with the source comparison Weigand 2018, v1, physical pp. 27–28, equations (4.10)–(4.12). The fixed-base statement changes $\mathcal{L}$ to $\mathcal{L}(-D)$; the local (z^4, u^6) point calculation is a distinct base blowup. Neither is a global resolution existence claim. Relative minimality excludes only vertical (-1)-curves. We do not use the blanket canonical-bundle-preserving blowdown wording on physical p. 26 of Weigand 2018; the point blowup formula is (IV.8.28).

§8.4: Tate ansatze. The quoted classification table and the finite-residue calculation are separate mathematical results [MATH]. The five rows in Table IV.8.2 are copied from Katz et al. 2011, v1, physical p. 23, Table 2, with the qualifications on physical pp. 22–24. Its global-form obstruction is stated on physical pp. 21–22. The source

prints group names; here these entries are used only for conditional local Lie algebras, with the monodromy column retained. Under the quoted I_0^* semi-split/split orders, the leading cubic, quadratic residue, translation and nonzero discriminant are calculated in (IV.8.33)–(IV.8.41).

There is a second literal source discrepancy. The SO(8) asterisk condition on physical pp. 23–24 of that v1 prints $(a_2^2 - 4a_4)/z^4|_{z=0}$, where its z is our transverse t. For its own orders $a_2 = z\alpha + O(z^2)$, $a_4 = z^2\beta + O(z^3)$, this quotient has a generic z^{-2} pole. In the explicit split example it is $(u-1)^2/z^2$. Equation (IV.8.35) derives the finite z^2 denominator from the leading quadratic. We report the printed inconsistency and the separate derivation; we do not attribute a published erratum to the authors. Neither source-text discrepancy is used to alter the stated scientific problem.

§8.5: generic covers. The type-IV criterion is a cited result [MATH], cited from Katz et al. 2011, v1, physical p. 17, Section 5, equation (5.3). The I_0^* cover uses its equations (6.1)–(6.2) and Weigand 2018, v1, physical p. 27, Table 4.1. The selected quadratic and cubic factor counts, separability and valuation arguments are mathematical calculations [MATH]. Their field is $\mathbb{C}(u)$, with $\mathbb{Q}(u)$ used only for exact arithmetic of the displayed rational-coefficient examples. The nonsquare and noncube conclusions include independent arguments over complex constants in the text. No general factorization theorem over the geometric field is inferred from finite rational-coefficient tests.

§8.6: physical interpretation. The conditional local F-theory gauge-algebra map [GEO-E] is given in Katz et al. 2011, v1, physical pp. 5–6 and 17, and Weigand 2018, v1, physical pp. 26–29, Table 4.1 and Section 4.2. No independent covering dictionary route is claimed here. The global-group limitation [GEO-E] is discussed in Katz et al. 2011, physical p. 5, footnote 2. A local algebra, a global quotient, a matter spectrum and a QFT decoupling limit are separate questions. The cycle-transport interface points to Chapter X.2; no new seven-brane matrix convention is introduced. Volume XIV, Chapters 3 and 5, uses these constructions.

Exercises and limits. Five bounded exercises consume submitted coefficients, orders, cover counts and conditional labels. Written E6 and the written portions of E1–E5 test interpretation outside numerical grading. Exact algebra and bounded answer checks do not certify the surface theorem, a global resolution or the physical compactification premise. The mathematical calculations and cited theorems remain separate from the physical interpretations.

References

Aspinwall, P. S. (1996). *K3 Surfaces and String Duality*. arXiv v5, physical PDF pp. 78–81, including Table 4 on physical p. 81. arXiv: `hep-th/9611137`.

Katz, S. et al. (2011). *Tate's algorithm and F-theory*. Source edition: arXiv v1, physical PDF pp. 5–6, 17, 21–24. arXiv: `1106.3854 [hep-th]`.

Weigand, T. (2018). *TASI Lectures on F-theory*. Source edition: arXiv v1, physical PDF pp. 26–29. arXiv: `1806.01854 [hep-th]`.

Chapter IV.9

M-theory on special holonomy: G_2 and Spin(7)

IV.9.1 Geometry that preserves supersymmetry

An observer in four dimensions can inherit supersymmetry from eleven dimensions even when the seven hidden directions are curved. The surviving supersymmetry parameters must fit together over the entire internal space. Parallel transport around a loop therefore has to preserve an internal spinor. Exceptional holonomy provides two ways to meet this requirement: a seven-dimensional internal space can leave four real supercharges in four dimensions, and an eight-dimensional internal space can leave two in three dimensions. Both are called minimal supersymmetry in their respective external dimensions.

This statement raises a geometric question before it raises a field-theory question. What does the internal metric preserve, and how can we recognize it without solving explicitly for the spinor? For G_2 the useful tensor is a real three-form. For Spin(7) it is a real four-form called the Cayley form. These tensors determine a metric and select oriented planes whose volume they measure exactly. The same geometry consequently governs parallel spinors and distinguished cycles.

Neither conclusion supplies the interactions of a particular quantum field theory. A smooth compact internal space retains an external metric and a finite Einstein gravity coupling. Its holonomy constrains supersymmetry, while its smooth reduction usually gives abelian fields and neutral matter. A proposed interacting local theory needs further geometric and physical information. We will keep that distinction visible by first calculating what the forms and spinors determine, then asking what a compact reduction actually retains.

The route uses the holonomy language of Chapter 2 and the real calibration of Chapter 6. Volume II, Chapter 8 supplies the eleven-dimensional supergravity setting. The general stabilizer, torsion-free and comass results used below are mathematical theorems whose proofs we cite rather than reproduce. We do derive finite plane evaluations, real spinor products, and the compact volume-minimization argument.

Joyce's compact existence theorems enter with their stated scope; a list of coordinate planes cannot replace their analytic construction.

By the end, the reader should be able to evaluate an exceptional form on an ordered nonunit frame, distinguish a torsion-free structure from exact exceptional holonomy, count real supercharges with a declared spin lift, apply volume minimization to an existing compact calibrated cycle, and identify the missing inputs in a local-QFT proposal. A recurring misconception will be that a holonomy name determines all of these conclusions at once. Each step below needs its own hypotheses.

IV.9.2 The invariant forms and their metrics

Which geometric object packages the metric information needed by the supersymmetry question? Start at one tangent space. Let $x^1, \dots, x^7$ be oriented Cartesian coordinates on $\mathbb{R}^7$. Write $e_i = \partial/\partial x^i$ and $dx^{i_1 \cdots i_k} = dx^{i_1} \wedge \cdots \wedge dx^{i_k}$ with increasing indices. Our Euclidean metric and orientation are

$$g_0 = \sum_{i=1}^{7} dx^i \otimes dx^i, \qquad \mathrm{vol}_7 = dx^{1234567}. \tag{IV.9.1}$$

The G_2 normal form in this frame is

$$\varphi_0 = dx^{123} + dx^{145} + dx^{167} + dx^{246} - dx^{257} - dx^{347} - dx^{356}. \tag{IV.9.2}$$

Its stabilizer in $GL(7, \mathbb{R})$ is the compact group G_2. This is a cited stabilizer theorem. In particular, the stabilizer preserves both g_0 and the orientation. The signs in (IV.9.2) belong to this specific frame. A different-looking normal form can represent the same geometry after a change of coframe, but coefficients cannot be transferred without that change.

A three-form φ on a seven-dimensional real vector space is called positive here if there is an isomorphism A to this model with $\varphi = A^*\varphi_0$. Define its metric by $g_\varphi = A^* g_0$. This does not depend on the chosen A: if A and B give the same three-form, their relative transformation preserves φ_0, hence lies in G_2 and preserves g_0. Thus

$$\varphi = A^*\varphi_0 \quad \Longrightarrow \quad g_\varphi = A^* g_0, \qquad \mathrm{vol}_\varphi = A^* \mathrm{vol}_7. \tag{IV.9.3}$$

This argument explains why the adjective positive is substantive. It specifies an orbit on which the tensor determines a positive-definite metric. It does not mean that every component of the form is positive.

A useful example connects this real expression to Chapter 2. Set $t = x^1$ and introduce, explicitly,

$$z^1 = x^2 + ix^3, \qquad z^2 = x^4 + ix^5, \qquad z^3 = x^6 + ix^7. \tag{IV.9.4}$$

In this Euclidean frame let $\omega = dx^{23} + dx^{45} + dx^{67}$ and $\Theta = dz^1 \wedge dz^2 \wedge dz^3$. There is no rescaling of the metric or of Θ. Expanding the three factors gives

$$\mathrm{Re}\,\Theta = dx^{246} - dx^{257} - dx^{347} - dx^{356}, \qquad \varphi_0 = dt \wedge \omega + \mathrm{Re}\,\Theta. \tag{IV.9.5}$$

For example, the term with dx^2, idx^5, and idx^7 has coefficient $i^2 = -1$, which fixes the sign on 257. The $SU(3)$ action on the three complex coordinates preserves ω and Θ and fixes t. It therefore preserves φ_0. This gives a concrete reason for the $SU(3)$ subgroup control used later, with its coordinate and phase conventions exposed.

For the eight-dimensional model now use oriented Cartesian coordinates $x^1, \dots, x^8$, with $g_0 = \sum_i (dx^i)^2$ and orientation $dx^{12345678}$. The Cayley form is

$$\begin{aligned}\Omega_0 = {} & dx^{1234} + dx^{1256} + dx^{1278} + dx^{1357} - dx^{1368} - dx^{1458} - dx^{1467} \\ & - dx^{2358} - dx^{2367} - dx^{2457} + dx^{2468} + dx^{3456} + dx^{3478} + dx^{5678}.\end{aligned} \tag{IV.9.6}$$

Its stabilizer in $GL(8,\mathbb{R})$ is the compact Spin(7) in its real eight-dimensional orthogonal representation. An admissible Cayley form means a form in the $GL(8,\mathbb{R})$ orbit of (IV.9.6). As before, the preserved model metric and orientation descend to a uniquely induced metric and orientation on that orbit.

For a second explicit complex-coordinate translation, put $w^a = x^{2a-1} + ix^{2a}$ for $a = 1, \dots, 4$. Define $\omega = dx^{12} + dx^{34} + dx^{56} + dx^{78}$ and $\Theta = dw^1 \wedge dw^2 \wedge dw^3 \wedge dw^4$. Direct expansion yields

$$\begin{aligned}\tfrac{1}{2}\omega^2 &= dx^{1234} + dx^{1256} + dx^{1278} + dx^{3456} + dx^{3478} + dx^{5678}, \\ \operatorname{Re}\Theta &= dx^{1357} - dx^{1368} - dx^{1458} - dx^{1467} - dx^{2358} - dx^{2367} - dx^{2457} + dx^{2468}.\end{aligned} \tag{IV.9.7}$$

The factor $1/2$ cancels the two equal cross terms in $\omega\wedge\omega$. Consequently $\Omega_0 = \omega^2/2 + \operatorname{Re}\Theta$. This is the local form of the $SU(4) \subset \mathrm{Spin}(7)$ relation. The real metric here is $\sum_a |dw^a|^2$; in the complex metric convention of Chapter 1 its coefficients are $g_{a\bar{b}} = \delta_{a\bar{b}}/2$.

There is a significant difference between the two exceptional tensors. The orbit dimension is the dimension of the linear group minus that of its stabilizer. In seven dimensions,

$$\dim GL(7,\mathbb{R}) - \dim G_2 = 49 - 14 = 35 = \binom{7}{3} = \dim \Lambda^3(\mathbb{R}^7)^*. \tag{IV.9.8}$$

The positive orbit is open. Small enough changes of a positive form at a point remain in it. In eight dimensions instead,

$$\dim GL(8,\mathbb{R}) - \dim \mathrm{Spin}(7) = 64 - 21 = 43, \qquad \binom{8}{4} - 43 = 70 - 43 = 27. \tag{IV.9.9}$$

The admissible Cayley orbit has codimension 27 in the space of all four-forms. A general small change of its coefficients need not be admissible. Thus one must first know that a four-form defines a Spin(7) structure before using its induced metric or the torsion-free theorem below. Closedness alone cannot repair a failure of algebraic admissibility.

These orbit counts explain what information the normal forms carry. They do not construct a global metric on a chosen compact manifold. The next step uses the forms for a calculation that requires no such construction: measuring their value relative to the actual volume of an oriented plane. Figure IV.9.1 will display a projected view of that comparison rather than a picture of seven-dimensional space.

IV.9.3 Oriented planes and the Gram determinant

How can an invariant form distinguish cycles if its value depends on the lengths of the vectors used to span them? The answer is to compare the form value to the volume of the same ordered frame. Let $v_1, \dots, v_k$ be linearly independent tangent vectors and write their coordinate rows as a $k \times n$ matrix V. For a k-form $\alpha = \sum_I c_I dx^I$, with increasing index sets $I = (i_1, \dots, i_k)$, alternating multilinearity gives

$$\alpha(v_1, \dots, v_k) = \sum_I c_I \det V_I, \qquad (V_I)_{ab} = v_a^{i_b}. \tag{IV.9.10}$$

There is no additional $k!$: the wedge monomials already evaluate by determinants. In the Euclidean model the Gram matrix is $H_{ab} = v_a \cdot v_b$. The squared volume and the normalized form value are

$$\mathcal{V}(V)^2 = \det H = \det(VV^{\mathsf{T}}), \qquad r_\alpha(V) = \frac{\alpha(v_1, \dots, v_k)}{\sqrt{\det H}}. \tag{IV.9.11}$$

The positive square root measures the ordered frame with the orientation it defines. A degenerate frame has $\det H = 0$ and does not define a k-plane, so the ratio is then undefined.

The basis independence is worth deriving. Replace the rows by $V' = AV$ with $A \in GL(k, \mathbb{R})$. Determinants and the Gram matrix transform as

$$\alpha(V') = \det A \, \alpha(V), \qquad H' = AHA^{\mathsf{T}}, \qquad \mathcal{V}(V') = |\det A| \mathcal{V}(V). \tag{IV.9.12}$$

The ratio is unchanged by an orientation-preserving basis change and changes sign under orientation reversal. This is the correct quantity for an oriented plane. A nonunit frame is perfectly suitable.

Take $V = (e_1, 2e_2, 3e_3)$ in $\mathbb{R}^7$. Only the 123 minor in (IV.9.10) survives, and its coefficient in φ_0 is $+1$. Thus

$$\varphi_0(e_1, 2e_2, 3e_3) = \det \begin{pmatrix} 1 & 0 & 0 \\ 0 & 2 & 0 \\ 0 & 0 & 3 \end{pmatrix} = 6, \quad H = \operatorname{diag}(1, 4, 9), \quad \mathcal{V}^2 = 36. \tag{IV.9.13}$$

Its ratio is $r_{\varphi_0} = 1$. The ordered frame (e_1, e_2, e_4) instead has Gram matrix $\mathbb{1}_3$ and zero form value, because the coefficient of 124 is zero. Both planes have nonzero volume; the form distinguishes them.

Tilt the first vector while keeping the same ordered second and third vectors. For $V = (e_1 + e_4, 2e_2, 3e_3)$, the only possible contributions arise from indices 123 and 234. The latter coefficient is absent in φ_0. Therefore

$$\varphi_0(e_1 + e_4, 2e_2, 3e_3) = 6, \qquad H = \operatorname{diag}(2, 4, 9), \qquad \mathcal{V}^2 = 72, \qquad r_{\varphi_0} = \frac{1}{\sqrt{2}}. \tag{IV.9.14}$$

The value 6 by itself did not reveal the tilt. The larger geometric volume does. For the orientation-reversed frame (e_3, e_2, e_1) there is one interchange of the first and third rows. Hence

$$\varphi_0(e_3, e_2, e_1) = -1, \qquad \mathcal{V}^2 = 1, \qquad r_{\varphi_0} = -1. \tag{IV.9.15}$$

A squared equality $\varphi_0(V)^2 = \mathcal{V}^2$ consequently loses essential information. The positive orientation is part of the saturation condition.

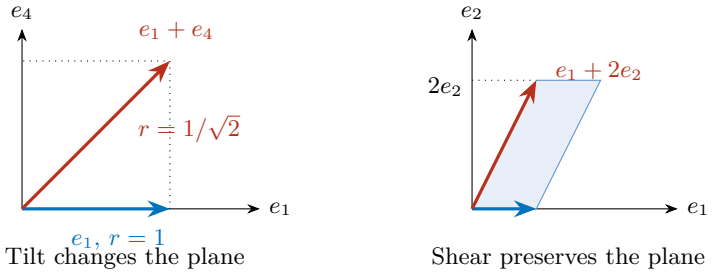


Figure IV.9.1: A two-direction projection of the associative-plane calculation. The left panel suppresses the common ordered transverse pair $(2e_2, 3e_3)$. The right panel displays e_1, e_2 and suppresses only $3e_3$. The blue first vector gives $r_{\varphi_0} = 1$; the red vector $e_1 + e_4$ gives $1/\sqrt{2}$. The right panel shears the second vector within the original plane. The shear changes the Gram entries but preserves its determinant and the oriented form value. Lines represent actual vector components in the displayed e_1, e_4 or e_1, e_2 plane, not a rendering of the full ambient space.

The tilted frame happened to have orthogonal rows. To see why the full Gram determinant is necessary, shear the original associative frame to

$$u_1 = e_1, \qquad u_2 = e_1 + 2e_2, \qquad u_3 = 3e_3, \qquad A = \begin{pmatrix} 1 & 0 & 0 \\ 1 & 1 & 0 \\ 0 & 0 & 1 \end{pmatrix}. \tag{IV.9.16}$$

Here A relates it to $(e_1, 2e_2, 3e_3)$ and has determinant one. The only contributing minor is again 123, now with rows $(1, 0, 0)$, $(1, 2, 0)$, $(0, 0, 3)$, so its determinant is 6. Directly computing the inner products gives

$$H = \begin{pmatrix} 1 & 1 & 0 \\ 1 & 5 & 0 \\ 0 & 0 & 9 \end{pmatrix}, \qquad \det H = 9(5-1) = 36, \qquad \prod_{a=1}^{3} \|u_a\|^2 = 1 \cdot 5 \cdot 9 = 45. \tag{IV.9.17}$$

Thus $r_{\varphi_0} = 6/6 = 1$. Replacing the Gram determinant by the product of squared norms would incorrectly give $6/\sqrt{45}$. Figure IV.9.1 shows why: the second vector has acquired a component along the first. That component increases its length but contributes no new volume. A shear is a change of spanning frame, unlike the tilt, which changes the plane itself.

The Cayley calculation uses the same determinant rule with four rows. For $(e_1, 2e_2, e_3, 3e_4)$, only the 1234 minor contributes. For (e_1, e_2, e_3, e_5), the 1235 coefficient vanishes. The two results are

ordered frame	$\Omega_0(V)$	$\mathcal{V}^2$	r_{Ω_0}
$(e_1, 2e_2, e_3, 3e_4)$	6	36	1
(e_1, e_2, e_3, e_5)	0	1	0

(IV.9.18)

The first determinant is $1 \cdot 2 \cdot 1 \cdot 3 = 6$, while its Gram determinant is $1 \cdot 4 \cdot 1 \cdot 9 = 36$. These factors are evaluations on the specified frame, not a rescaling of the Cayley form.

A mixed example tests the terms farther along in (IV.9.6). Choose $V = (e_1 + e_2, 2e_4, 3e_6, e_8)$. Only the 1468 and 2468 minors can be nonzero. Their two submatrices are both diagonal with entries $(1, 2, 3, 1)$. The coefficient of 1468 is zero and that of 2468 is $+1$, so

$$\Omega_0(V) = 0 \cdot 6 + 1 \cdot 6 = 6, \qquad H = \operatorname{diag}(2, 4, 9, 1), \qquad \mathcal{V}^2 = 72, \qquad r_{\Omega_0} = \frac{1}{\sqrt{2}}. \tag{IV.9.19}$$

This plane has a positive but nonsaturating form value. The calculation uses both an absent component and a present component, so reading off just one coordinate coefficient would fail.

The interpretation becomes geometric in Section IV.9.6: $r = 1$ selects an associative or Cayley oriented plane. The general all-plane bound is a separate cited theorem. No finite set of evaluations proves comass one. Chapter 6 used the same distinction for real and Kähler calibrations; here the new ingredient is the exceptional form, not a new definition of volume.

IV.9.4 Torsion-free structures and exact holonomy

When does a pointwise exceptional tensor answer the global parallel-transport question? On a manifold X, a smooth positive three-form gives a G_2 structure, and a smooth admissible Cayley four-form gives a Spin(7) structure. In each case the form induces its metric g. Let ∇ be the Levi-Civita connection of that metric. Torsion-free means that the defining tensor is parallel under ∇. It is stronger than the algebraic existence of the structure.

Parallel transport P_γ around a loop γ based at p preserves a parallel tensor. For instance, $\nabla\varphi = 0$ gives

$$P_\gamma^* \varphi_p = \varphi_p \quad \text{for every loop } \gamma, \qquad \operatorname{Hol}_p(g) \subset \operatorname{Stab}(\varphi_p) = G_2. \tag{IV.9.20}$$

Conversely, a holonomy-invariant tensor at one point extends by parallel transport without path dependence. This is the invariant-tensor principle from Chapter 2. The equality with G_2 at the right refers to the tensor stabilizer; it does not replace the inclusion for the metric holonomy by an equality.

The useful differential tests are cited torsion-free theorems. For a positive G_2 form and its induced metric they state

$$\nabla\varphi = 0 \quad \Longleftrightarrow \quad d\varphi = 0, \quad d(*_\varphi \varphi) = 0. \tag{IV.9.21}$$

The Hodge star $*_\varphi$ is computed with g_φ and its orientation. It cannot be borrowed from an unrelated background metric. For an admissible Cayley form with its own induced metric the theorem instead states

$$\nabla\Omega = 0 \quad \Longleftrightarrow \quad d\Omega = 0, \qquad \operatorname{Hol}(g_\Omega) \subset \operatorname{Spin}(7). \tag{IV.9.22}$$

The different differential tests do not erase the algebraic restriction on Ω. Applying the second equivalence to an arbitrary closed four-form would omit a hypothesis. Neither equivalence is proved by the finite plane computations of the preceding section.

A full geometric example exposes the inclusion. Put the constant form (IV.9.2) on $T^7 = \mathbb{R}^7/\mathbb{Z}^7$ with its induced Euclidean metric. The one-forms dx^i descend globally. Their derivatives vanish, as do derivatives of all constant wedge products. In this same oriented orthonormal frame,

$$*_\varphi\varphi_0 = dx^{4567} + dx^{2367} + dx^{2345} + dx^{1357} - dx^{1346} - dx^{1256} - dx^{1247}. \tag{IV.9.23}$$

For example, $dx^{123} \wedge dx^{4567} = \mathrm{vol}_7$ fixes the first sign. All terms in both forms have constant coefficients. The connection in the global Cartesian frame is zero, giving

$$d\varphi_0 = d(*_\varphi\varphi_0) = 0, \qquad \nabla\varphi_0 = 0, \qquad \mathrm{Hol}(T^7, g_0) = \{1\} \subsetneq G_2. \tag{IV.9.24}$$

This torsion-free G_2 structure has trivial holonomy. Similarly the constant Cayley form descends to flat T^8 and is closed, although its metric holonomy is trivial. A torus is therefore a counterexample to identifying torsion-free exceptional structure with exact exceptional holonomy.

There are also curved subgroup examples. Let Y be a Calabi–Yau threefold with exact $SU(3)$ holonomy, metric h, and compatible parallel ω, Θ in the normalization of Section IV.9.2. With t a local arc-length coordinate on a circle, the globally defined one-form dt gives

$$g = dt^2 + h, \qquad \varphi = dt \wedge \omega + \mathrm{Re}\,\Theta, \qquad d\varphi = -dt \wedge d\omega + \mathrm{Re}(d\Theta) = 0. \tag{IV.9.25}$$

Both factors are parallel, so the product tensor is parallel. The tangent circle direction stays fixed; the product metric has holonomy $SU(3) \subsetneq G_2$. A Calabi–Yau fourfold with exact $SU(4)$ holonomy gives a second control:

$$\begin{aligned} \Omega &= \tfrac{1}{2}\omega \wedge \omega + \mathrm{Re}\,\Theta, \\ d\Omega &= d\omega \wedge \omega + \mathrm{Re}(d\Theta) = 0, \qquad \mathrm{Hol}(g) = SU(4) \subsetneq \mathrm{Spin}(7). \end{aligned} \tag{IV.9.26}$$

These formulas use parallel forms with the compatible metric normalization, not arbitrarily normalized holomorphic volume forms. They exhibit actual contained holonomy; they are not perturbative approximations to exact exceptional holonomy.

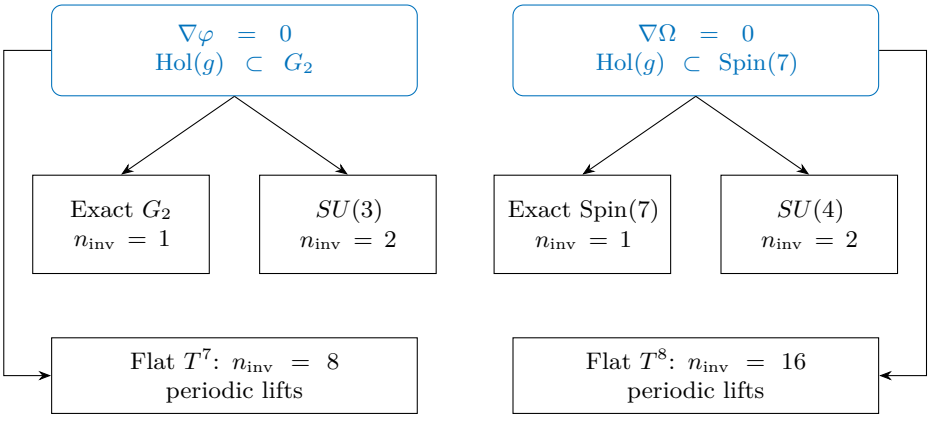


Figure IV.9.2: Contained holonomy permits several different invariant-spinor counts. The top boxes describe torsion-free structures and their induced metrics. Each downward arrow selects a possible actual holonomy, rather than asserting that the differential equation forces that selection. The integers are real internal invariant dimensions. Circle and torus examples use periodic spin lifts in every compact flat direction. The $SU(4)$ count includes both internal chiral modules relevant to the eleven-dimensional reduction.

Exact exceptional holonomy is realized by compact metrics, but its existence requires more than these examples. Joyce's original G_2 theorem concerns the specified compact simply connected seven-dimensional resolution M in section 2.2 of that construction. It gives a 43-dimensional family of metrics with full G_2 holonomy. The number 43 here is a metric-family dimension on that particular M, unrelated to the pointwise Cayley-orbit dimension 43 found earlier.

The original Spin(7) construction supplies at least 95 topologically distinct compact simply connected eight-dimensional manifolds admitting metrics with full Spin(7) holonomy. In its exact-holonomy step, torsion-free existence is supplemented by simple connectivity and $\widehat{A}(M) = 1$, where $\widehat{A}(M)$ is the spin Dirac index. These are cited existence results for specified constructions. They are neither classifications of all exceptional-holonomy manifolds nor deductions from counting spinors. We will use them only to know that the exact-holonomy cases in Figure IV.9.2 are populated. Their analytic existence proofs lie beyond this chapter.

The next section applies the distinction to supersymmetry. The pitfall has a physical cost: replacing an inclusion by equality can discard extra parallel spinors and therefore assign too little supersymmetry to the external theory.

IV.9.5 Real spinors and external supercharges

How many supersymmetry parameters survive a compactification with one parallel internal spinor? Fix the physical assumptions before multiplying dimensions. We use eleven-dimensional supergravity with a vanishing four-form field strength, an unwarped direct-product metric, and an external Minkowski factor. This is a conditional background ansatz; Section IV.9.7 will explain an obstruction to choosing zero flux. In this ansatz the gravitino supersymmetry equation reduces to parallel transport of the parameter:

$$M_{11} = \mathbb{R}^{1,d-1} \times X^{11-d}, \qquad G = 0, \qquad \nabla_M \epsilon = 0. \tag{IV.9.27}$$

For a product connection write $\epsilon(x,y) = \sum_a \zeta_a(x) \otimes \eta_a(y)$ in the corresponding real spin representations. The internal factors obey $\nabla_X \eta_a = 0$, while the external factors are constant in the Minkowski frame. Thus the relevant vector space of parameters is the external spinor space tensored with the internal invariant space.

Let n_{ext} denote the real dimension of the minimal external spinor and n_{inv} the real dimension of the internal invariant space in this reduction. A basis of one tensor factor paired with a basis of the other gives

$$Q_{\mathbb{R}} = n_{\mathrm{ext}} n_{\mathrm{inv}}, \qquad n_{\mathrm{ext}} = 4 \text{ in } 4d, \qquad n_{\mathrm{ext}} = 2 \text{ in } 3d. \tag{IV.9.28}$$

These are real dimensions, with the Lorentzian Majorana reality of Volume 0. The eleven-dimensional parameter has 32 real components. A complexified calculation can find invariants, but one must return to that real representation before multiplying.

For the seven-dimensional internal spin module, the restriction to full G_2 is

$$S_7|_{G_2} = \mathbf{1}_{\mathbb{R}} \oplus \mathbf{7}_{\mathbb{R}}, \qquad n_{\mathrm{inv}} = 1, \qquad Q_{\mathbb{R}} = 4 \cdot 1 = 4. \tag{IV.9.29}$$

The nontrivial seven-dimensional representation contributes no invariant. This is $4d$ $\mathcal{N} = 1$. For the eight-dimensional internal space both real chiral modules enter the eleven-dimensional decomposition. Choose the Spin(7) embedding that fixes a positive-chirality spinor. Its restrictions are

$$S_8^+\big|_{\mathrm{Spin}(7)} = \mathbf{1}_{\mathbb{R}} \oplus \mathbf{7}_{\mathbb{R}}, \qquad S_8^-\big|_{\mathrm{Spin}(7)} = \mathbf{8}_{\mathbb{R}}, \qquad Q_{\mathbb{R}} = 2(1+0) = 2. \tag{IV.9.30}$$

This is $3d$ $\mathcal{N} = 1$. Changing the chirality naming convention exchanges the two modules, with no change of the real total. Full holonomy matters in both equations. A subgroup can fix vectors in a representation that had none for the larger group.

For the $SU(3)$ control, restrict the $\mathbf{7}$ in (IV.9.29) to the real representation on $\mathbb{R} \oplus \mathbb{C}^3$ used in (IV.9.4). If $(\mathbf{3})_{\mathbb{R}}$ denotes the underlying real rank-six representation, then

$$\mathbf{7}_{\mathbb{R}}|_{SU(3)} = \mathbf{1}_{\mathbb{R}} \oplus (\mathbf{3})_{\mathbb{R}}, \qquad S_7|_{SU(3)} = \mathbf{1}_{\mathbb{R}} \oplus \mathbf{1}_{\mathbb{R}} \oplus (\mathbf{3})_{\mathbb{R}}. \tag{IV.9.31}$$

There are two real invariants. On $S^1 \times Y$, with Y of exact $SU(3)$ holonomy and the periodic lift on the circle, the result is $Q_{\mathbb{R}} = 4 \cdot 2 = 8$. It is $4d$ $\mathcal{N} = 2$, despite the existence of a torsion-free G_2 form on the product.

The $SU(4)$ control makes the complex-real distinction particularly visible. A complex model for the positive chiral spin representation in eight Euclidean dimensions is the even exterior algebra of $\mathbb{C}^4$. Its restriction is

$$S^+_{8,\mathbb{C}} = \Lambda^{\text{even}}\mathbb{C}^4 = \Lambda^0\mathbb{C}^4 \oplus \Lambda^2\mathbb{C}^4 \oplus \Lambda^4\mathbb{C}^4, \qquad 8 = 1 + 6 + 1. \tag{IV.9.32}$$

The degree-zero and degree-four pieces are complex singlets; the middle piece has no $SU(4)$ invariant. Let s_0, s_4 span the two singlet lines. Choose their phases so the antilinear real structure ρ has $\rho(s_0) = s_4$ and $\rho(s_4) = s_0$. A fixed vector then has the form

$$\rho(as_0 + bs_4) = \bar{b}s_0 + \bar{a}s_4, \qquad \rho(v) = v \iff b = \bar{a}, \qquad v = as_0 + \bar{a}s_4. \tag{IV.9.33}$$

One complex parameter a supplies two real parameters, not four. The odd exterior algebra has degrees one and three and no $SU(4)$ singlet. Therefore the full internal invariant dimension is two and $Q_{\mathbb{R}} = 2 \cdot 2 = 4$, or $3d\ \mathcal{N} = 2$. The phase choice just made specifies a basis for the real structure; it is not a new independent spinor.

For flat T^7 and T^8, choose periodic spin lifts along every lattice direction. All constant internal spinors then descend. The internal dimensions are respectively 8 and $8 + 8 = 16$, so

$$T^7: \quad Q_{\mathbb{R}} = 4 \cdot 8 = 32, \qquad T^8: \quad Q_{\mathbb{R}} = 2 \cdot (8 + 8) = 32. \tag{IV.9.34}$$

This recovers the eleven-dimensional count and checks that no extra complex doubling has entered. Figure IV.9.2 compares these flat, subgroup and exact cases.

The lift condition is physical information beyond vector holonomy. On a flat circle of length L, a local parallel spinor is constant because $\partial_t\eta = 0$. Its global boundary condition can still be periodic or antiperiodic:

$$\eta(t + L) = \sigma\eta(t), \qquad \sigma \in \{+1, -1\}, \qquad \partial_t\eta = 0 \implies (1 - \sigma)\eta = 0. \tag{IV.9.35}$$

For $\sigma = +1$ the constant survives. For $\sigma = -1$ it must vanish. Vector parallel transport is trivial in both cases. In particular, putting an antiperiodic lift on any one of the torus circles eliminates these global constant parallel spinors. Our positive torus and $S^1 \times Y$ counts always select the periodic lifts explicitly. This does not alter the conditional counts supplied as assumptions in Exercise 3.

These results determine a supersymmetry count under (IV.9.27). They say nothing yet about nonabelian gauge bosons or charged matter. The next two sections explain the separate cycle and reduction questions that use the same geometry. Chapter 10 will take up the flux interface, where the simple parallel-spinor equation need not remain the correct equation.

IV.9.6 Calibrated cycles and volume minimization

What global statement follows from the positive saturation seen in the plane examples? Recall a real calibration from Chapter 6. On a Riemannian manifold (X, g) a degree-k

form α is closed and obeys a one-sided bound on every oriented tangent k-plane. In an oriented spanning frame this reads

$$d\alpha = 0, \qquad \alpha(v_1, \ldots, v_k) \le \mathcal{V}(V) \quad \text{for all independent ordered } V. \tag{IV.9.36}$$

The comass at a point is the supremum of the absolute value on orthonormal k-frames. Since both orientations are tested, the bound implies comass at most one. A submanifold is calibrated when equality with positive oriented volume holds at every tangent plane. Closedness is the global ingredient that will make the integral depend only on homology.

For the model metric the forms φ_0, $*_\varphi\varphi_0$, and Ω_0 have comass one by the cited exceptional-calibration theorem. On torsion-free structures they are parallel and closed. The corresponding calibrated submanifolds are called associative, coassociative, and Cayley, of dimensions three, four, and four respectively. For example,

$$\varphi_0(e_1, e_2, e_3) = 1, \qquad (*_\varphi\varphi_0)(e_4, e_5, e_6, e_7) = 1, \qquad \Omega_0(e_1, e_2, e_3, e_4) = 1. \tag{IV.9.37}$$

Each frame is orthonormal with the stated order. The equality tests identify these particular planes using the general theorem. They do not establish the bound on all planes. An arbitrary multiple $c\alpha$ does not retain unit comass: its comass is $|c|$ times the original one in the fixed metric. A frame rescaling in Section IV.9.3 rescaled the numerator and volume together; a form rescaling is a different operation.

Now assume that $N \subset X$ is an already existing compact oriented boundaryless calibrated submanifold. Let N' be a compact oriented boundaryless competitor of the same dimension in the same real homology class. These are the theorem hypotheses, rather than conclusions supplied by a homology label. Equality on N gives

$$\operatorname{Vol}(N) = \int_N \operatorname{vol}_N = \int_N \alpha. \tag{IV.9.38}$$

Because $[N'] = [N]$ in $H_k(X, \mathbb{R})$, their difference is the boundary of a real chain B; write $N' - N = \partial B$. Stokes' theorem and closedness yield

$$\int_{N'} \alpha - \int_N \alpha = \int_{\partial B} \alpha = \int_B d\alpha = 0. \tag{IV.9.39}$$

The one-sided bound on every tangent plane of the competitor then gives

$$\int_{N'} \alpha \le \int_{N'} \operatorname{vol}_{N'} = \operatorname{Vol}(N'), \qquad \operatorname{Vol}(N) \le \operatorname{Vol}(N'). \tag{IV.9.40}$$

This is global volume minimization among these competitors, not just stationarity under an infinitesimal deformation. The proof fails at identifiable places if the hypotheses are removed. Without closedness the chain integral need not vanish. Without calibration of N, its volume need not equal its form integral. For a noncompact pair, boundary conditions and convergence need separate treatment.

A realized compact example makes the distinction from existence precise. Take the flat torus $T^7 = \mathbb{R}^7/\mathbb{Z}^7$ with metric and φ_0 as above. The subset with $x^4 = x^5 = x^6 =$

$x^7 = 0$ is an embedded T^3. Give it the orientation dx^{123}. Its coordinate parametrization uses $0 \le x^1, x^2, x^3 < 1$, so

$$\varphi_0|_{T^3} = dx^{123} = \mathrm{vol}_{T^3}, \qquad \int_{T^3} \varphi_0 = \int_0^1 \int_0^1 \int_0^1 dx^1 dx^2 dx^3 = 1. \tag{IV.9.41}$$

Thus $\mathrm{Vol}(T^3) = 1$. Every compact oriented real-homologous competitor has volume at least one by (IV.9.40). The torus is already given as a subset, so this example does not infer existence from the inequality. It also does not require exact G_2 holonomy; the contained flat case suffices.

There is a useful graph competitor with a bent embedding in the same class that can be computed completely. Let $f(s) = a\sin(2\pi s)$, with real a, and parametrize a graph by

$$F(s_1, s_2, s_3) = (s_1, s_2, s_3, f(s_1), 0, 0, 0) \pmod{\mathbb{Z}^7}, \quad (s_1, s_2, s_3) \in T^3. \tag{IV.9.42}$$

The first three coordinates make this an embedding. Multiplying f by a parameter from zero to one gives an isotopy from the coordinate torus, so the oriented graph is homologous to it. Its tangent rows are $e_1 + f'(s_1)e_4, e_2, e_3$. Only 123 contributes to the pulled-back form, whereas the Gram matrix has diagonal entries $1 + (f')^2, 1, 1$. Therefore

$$F^*\varphi_0 = ds^{123}, \qquad F^*g_0 = \big(1 + (f')^2\big)(ds_1)^2 + (ds_2)^2 + (ds_3)^2, \qquad \det H = 1 + (f')^2. \tag{IV.9.43}$$

The induced metric is intrinsically flat. Locally set $du = \sqrt{1 + (f\prime)^2}\, ds_1$. In this arc-length coordinate the metric is $du^2 + ds_2^2 + ds_3^2$. Globally the first circle has a larger length when $a \neq 0$. The embedding bends, although its intrinsic curvature vanishes. The integral of the form stays one, but the volume becomes

$$\mathrm{Vol}(F(T^3)) = \int_0^1 \sqrt{1 + 4\pi^2 a^2 \cos^2(2\pi s_1)}\, ds_1 \ge 1. \tag{IV.9.44}$$

For $a \neq 0$, the integrand exceeds one on a set of positive measure, so the inequality is strict. Where $f' \neq 0$, the tangent ratio is $1/\sqrt{1 + (f')^2} < 1$. This connects the tilted plane calculation directly to a compact geometric deformation with a realized reference cycle.

In flat T^8 the coordinate T^4 along 1234 similarly has Ω_0 integral and volume one, with its standard orientation. Reversing the orientation of either torus changes the form integral to minus one while the positive volume remains one. It is then no longer calibrated by that same form. The orientation dependence from (IV.9.15) persists globally.

Calibrated cycles are useful geometric candidates in wrapped-brane questions because they control volume in a fixed class. A wrapped state, its charge normalization, and its survival in a decoupling limit require additional physical premises. This chapter does not derive those premises from minimization. Chapter 6 provides the shared calibration logic; the next section instead asks what the bulk metric itself contributes to the lower-dimensional theory.

IV.9.7 Compact reduction and the zero-flux premise

Does a smooth compact exceptional-holonomy space already remove gravity? To answer, keep the product ansatz of Section IV.9.5 and take the size of X large compared with the eleven-dimensional Planck length. We consider the low-energy zero-mode approximation. Let κ_{11} denote the eleven-dimensional gravitational coupling in the Einstein term and $V_X = \int_X \sqrt{g_X}\, d^{11-d}y$ the finite internal volume. For a direct product, the external-curvature part of the action reduces as

$$\begin{aligned} S_{11} &\supset \frac{1}{2\kappa_{11}^2} \int_{M_d \times X} \sqrt{-g_d}\sqrt{g_X}\, R_d\, d^d x\, d^{11-d} y \\ &= \frac{V_X}{2\kappa_{11}^2} \int_{M_d} \sqrt{-g_d}\, R_d\, d^d x. \end{aligned} \tag{IV.9.45}$$

Here R_d is the external scalar curvature; only that term is needed to read the gravitational coupling. There is no internal-dependent warp factor in this calculation. Defining the effective coupling by $S_d \supset (2\kappa_d^2)^{-1} \int \sqrt{-g_d} R_d$ gives

$$\frac{1}{\kappa_d^2} = \frac{V_X}{\kappa_{11}^2}, \qquad \kappa_d^2 = \frac{\kappa_{11}^2}{V_X}. \tag{IV.9.46}$$

At finite nonzero V_X the coupling is finite and nonzero. The lower-dimensional metric sector is retained. Its constant internal profile is normalizable; normalizing that profile makes the compactness condition visible:

$$\psi_0(y) = V_X^{-1/2}, \qquad \int_X \sqrt{g_X}\, |\psi_0|^2 = V_X^{-1} V_X = 1. \tag{IV.9.47}$$

A very large compact volume weakens the gravitational coupling. It does not remove the metric sector from the finite-volume effective theory. The internal norm does not count external propagating polarizations. In four-dimensional Einstein gravity there are two local massless graviton polarizations; in pure three-dimensional Einstein gravity there are none. The three-dimensional theory still has a finite gravitational coupling and gravitational constraints, so this absence does not by itself give a gravity-free matter QFT.

For example, compare two uniformly scaled seven-dimensional compact metrics, g_X and $\widetilde{g}_X = 4 g_X$, with the same κ_{11}. All internal lengths double. The volume form in seven dimensions picks up the factor 2^7, and (IV.9.46) gives

$$\widetilde{V}_X = 2^7 V_X = 128 V_X, \qquad \widetilde{\kappa}_4^2 = \frac{\kappa_4^2}{128}. \tag{IV.9.48}$$

This is a relative scaling example, not a specification of a new Planck convention. The same uniform scaling also lowers the Kaluza–Klein mass scale. A statement about weak gravity must consequently be accompanied by the energy range in which a lower-dimensional effective theory is being used.

Let L be a characteristic internal length, ℓ_{11} the eleven-dimensional Planck length, and E an external energy. In a smooth large-volume reduction the intended regime is

$$\frac{L}{\ell_{11}} \gg 1, \qquad E \ll m_{\mathrm{KK}} \sim L^{-1}. \tag{IV.9.49}$$

The first inequality suppresses curvature corrections in a geometry without additional small curvature radii. The second suppresses excited Kaluza–Klein modes. Taking L to infinity at fixed E closes the second window rather than producing an automatic local QFT limit. Figure IV.9.3 separates the volume argument from the local-sector problem.

The smooth spectrum also illustrates the limit of the holonomy count. In the smooth large-volume regime, a compact full-G_2 reduction gives four-dimensional $\mathcal{N} = 1$ supergravity coupled to $b_2(X)$ abelian vector multiplets and $b_3(X)$ neutral chiral multiplets in the stated zero-flux regime. Here $b_k(X) = \dim H^k(X, \mathbb{R})$ is the kth Betti number. Abelian vectors arise by expanding the three-form potential on harmonic two-forms, while its harmonic three-form modes pair with metric moduli. This is a reduction statement under the physical ansatz, not a consequence of the single invariant spinor alone. The smooth compact Spin(7) case similarly retains three-dimensional supergravity with abelian fields and neutral matter in this regime. Neither statement supplies a nonabelian singular sector.

The zero-flux premise itself needs a topological check. Use the flux units of the sourced membrane path-integral condition. Let G be the internal four-form field strength in those units and let $\lambda = p_1(X)/2$ be the integral spin characteristic class, with p_1 the first Pontryagin class. The shifted quantization condition is

$$\left[\frac{G}{2\pi}\right] - \frac{\lambda}{2} \in H^4(X, \mathbb{Z}), \qquad \lambda = \frac{p_1(X)}{2}. \tag{IV.9.50}$$

This condition is cited from the membrane anomaly analysis. We do not derive or independently match its anomaly coefficient. It is a constraint on the permitted background, rather than a correction to the arithmetic of Section IV.9.5.

For an integral four-cycle Σ, define the real flux period $g_\Sigma = \int_\Sigma G/(2\pi)$ and the integer $\ell_\Sigma = \langle \lambda, [\Sigma] \rangle$. The period test is

$$g_\Sigma - \frac{\ell_\Sigma}{2} \in \mathbb{Z}. \tag{IV.9.51}$$

If $\ell_\Sigma = 3$, then $G = 0$ would give $-3/2$, which is not an integer. The allowed periods instead have the form $g_\Sigma = 3/2 + n$ with $n \in \mathbb{Z}$. For example, $n = -1$ gives $g_\Sigma = 1/2$, and the shifted period is -1. This single odd period rules out the zero-flux product ansatz on that background.

If $\ell_\Sigma = 4$, the zero period gives $0 - 4/2 = -2 \in \mathbb{Z}$. Thus even periods remove this particular obstruction. They do not solve the full vacuum equations, tadpoles or possible torsion conditions. In particular, verifying a collection of free-cycle periods does not settle information invisible to those periods. We use evenness only in this necessary-condition sense. Turning on an allowed nonzero flux generally requires revisiting the metric and supersymmetry equations; the present chapter does not build a flux vacuum.

The physical conclusion is precise. A consistent smooth compact zero-flux background, when available, gives a gravity-coupled effective theory with a conditional supersymmetry count. An odd λ period can invalidate that background before the count is applied. Chapter 10 develops the flux and warping interface. A local interacting QFT requires a different set of geometric and scaling questions, to which we now turn.

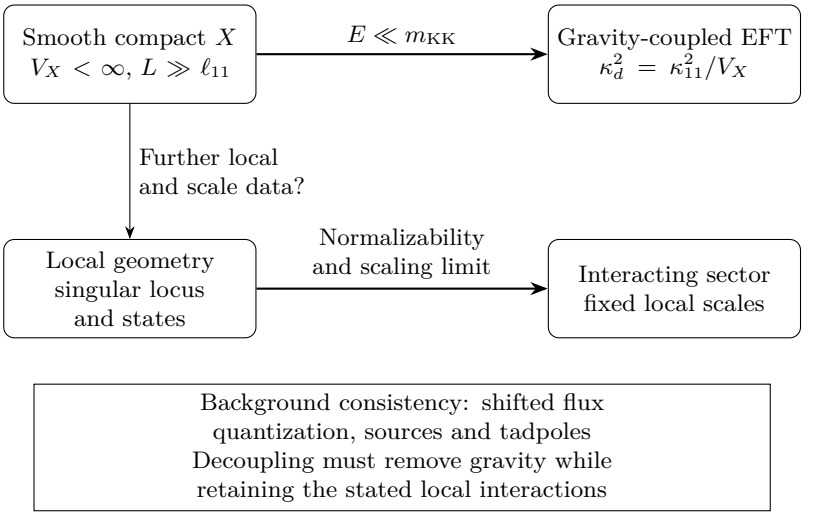


Figure IV.9.3: The compact calculation and the local-QFT problem require different scale information. The upper route integrates over a smooth compact X and retains a normalizable internal metric profile and finite Einstein coupling at finite V_X. The lower route asks for specified singular geometry, a localized state sector and a limit keeping its interactions while gravitational effects vanish. The boxes on the lower route list required inputs, not a completed construction. Enlarging the whole compact space also lowers m_{KK}, so the downward arrow is labelled as a further question rather than a decoupling theorem.

IV.9.8 What a local interacting theory still needs

Consider a proposed construction stated only as follows: take M-theory on a smooth compact Spin(7) manifold and obtain an interacting decoupled $3d$ $\mathcal{N} = 1$ QFT. The holonomy label can support the two-real-supercharge count under the specified flux and spin assumptions. It leaves the rest of the proposal undetermined. Equation (IV.9.47) normalizes the constant internal metric profile, and (IV.9.46) gives the finite three-dimensional Einstein coupling. This retains gravity and its constraints, even though the massless three-dimensional Einstein sector has no local graviton polarization. The smooth reduction described above gives abelian gauge fields and neutral matter. Calling this a local interacting construction would skip both the identification of the interacting states and the removal of gravity.

A worked response begins by replacing the label with an actual local geometry. One must specify the singular locus, its transverse model and the way it sits in the internal space. If branes or wrapped states are invoked, their cycles, boundary conditions and charges must be identified. The role of an ADE singularity in established nonabelian constructions motivates this requirement, but the generic Cayley form is not a universal map from singularities to gauge theories. Its fourteen coefficients do not specify a singular spectrum.

Next ask which modes are dynamical for the observer. A mode localized near a singularity must have the appropriate finite kinetic norm in the proposed limit. A mode whose norm diverges may instead behave as an externally prescribed coupling. Merely finding a geometric deformation or a formal harmonic representative does not decide this distinction on a noncompact space. The metric near infinity, allowed boundary conditions, and state wavefunctions are therefore part of the proposal. These questions identify the degrees of freedom before assigning interactions to them.

Then check the background conditions for that actual geometry. The shifted class in (IV.9.50) must be meaningful in the chosen global or relative setting. Flux, sources and tadpole conditions must be mutually compatible. The example with an odd λ period shows why an unsupported choice $G = 0$ can already be inconsistent. The even-period example only removes that one obstruction and cannot replace the remaining background conditions.

Finally specify what is held fixed in a scaling limit. The interaction scale of the localized sector must remain finite while gravitational effects vanish in the observables of interest. One must also account for bulk and Kaluza–Klein modes, rather than assuming that the uniform large-volume rescaling isolates the desired sector. Equations (IV.9.48) and (IV.9.49) show the competing changes in the simplest smooth scaling. A successful singular limit may involve different local and bulk scales; those scales have to be given by the construction.

This completes the worked explanation needed for the written Exercise 5. It identifies four missing links: local geometry, states and normalizability, background consistency, and a scaling argument for the target interactions. It does not supply them for an unspecified manifold. The same caution applies to a G_2 label in four dimensions. The compact existence theorems establish metrics, while the holonomy calculation constrains supersymmetry. Neither determines a particular interacting QFT.

This is the boundary of the present foundations chapter. Later construction chapters can use the explicit forms, spinor counts and cycle inequalities as inputs once their own local geometry is fixed. The Spin(7) outlook in Volume VII does not supply an M-theory exceptional-holonomy construction by itself. Chapter 10 continues with the background flux interface; the singular-sector dynamics remains a separate construction problem.

IV.9.9 Exercises

Use the oriented Euclidean forms (IV.9.2) and (IV.9.6). The first four exercises have bounded submitted-answer checks. Exact form values and squared volumes are submitted as rational strings, including integers written as strings. Calibration flags are JSON booleans. Supercharge totals are JSON integers. The public question file gives the exact fields and the common envelope with `task` and `answer`; no additional field is needed. Each exercise also asks for an explanation to be written by the reader. Those explanations are not certified by the bounded numerical comparison.

1. **E1. Nonunit associative frame.** Evaluate φ_0 on $(e_1, 2e_2, 3e_3)$ and (e_1, e_2, e_4), in that order. Compute their Gram determinants and determine whether each

oriented plane is calibrated. Submit `values`, `volume_squared` and `calibrated`, each an array of length two. Write out the contributing minors and explain why the length of a spanning vector does not alter the calibrated-plane condition.

2. **E2. Cayley frame and absent component.** Repeat the calculation for Ω_0 on $(e_1, 2e_2, e_3, 3e_4)$ and (e_1, e_2, e_3, e_5). Use the same three field names and array order as in E1. Explain why a zero form value on one plane is compatible with a nonzero form whose comass is one. Distinguish the finite evaluation from the all-plane theorem.

3. **E3. Conditional real spinor products.** Assume the zero-flux unwarped product ansatz. Take one real invariant internal spinor for exact G_2 and one for exact Spin(7). Use four real components for a minimal $4d$ spinor and two for a minimal $3d$ spinor. For flat T^7, T^8 take eight and sixteen real internal constant spinors. For $S^1 \times CY_3$ of exact $SU(3)$ holonomy and CY_4 of exact $SU(4)$ holonomy take two real internal invariants each. These supplied dimensions are assumptions of the task. Submit the totals as `g2_real`, `spin7_real`, `torus7_real`, `torus8_real`, `su3_product_real` and `su4_product_real`. In writing, identify the periodic spin lifts used by the positive flat and circle controls, and explain the complex-real distinction for the $SU(4)$ singlets.

4. **E4. Tilt and orientation.** For $(e_1 + e_4, 2e_2, 3e_3)$ and (e_3, e_2, e_1), compute φ_0, the squared volume, and the oriented calibration condition. For the tilted frame submit `tilted_value`, `tilted_volume_squared` and `tilted_calibrated`. For the reversed frame submit `reversed_value`, `reversed_volume_squared` and `reversed_calibrated`. Explain why testing equality after squaring would accept the wrong orientation. As a written extension, repeat the Gram calculation on the sheared associative frame (IV.9.16); state why a product of norms gives the wrong volume.

5. **E5. Written construction analysis.** A proposal claims that a smooth compact Spin(7) manifold by itself constructs an interacting decoupled $3d$ $\mathcal{N} = 1$ QFT. Explain the theory actually obtained in the smooth large-volume reduction. Identify the additional singular or local geometry, states, normalizability, flux consistency and scaling information needed for a specific interacting theory. Use the internal metric-profile normalization and the odd/even λ period examples to separate a supercharge count, an allowed background, a spectrum and a decoupling limit. This is a written reasoning task without a numerical acceptance criterion.

IV.9.10 Take-home message

Take-home message

A positive G_2 three-form and an admissible Cayley four-form determine their metrics and orientations. Their torsion-free conditions give contained exceptional holonomy. Exact holonomy, together with a specified spin lift and the zero-flux product ansatz, fixes the real spinor count: four real supercharges in four dimensions for full G_2, and two in three dimensions for full Spin(7). The Gram determinant and the sign of the form evaluation identify calibrated oriented planes. Closedness then proves volume minimization for an already realized compact calibrated cycle. Smooth compact reduction retains gravity. Specifying an interacting local QFT requires further geometry, state and scaling information.

Status and sources

Sections 9.2–9.3. The chapter-local oriented coordinate forms are those of Joyce (2004, physical PDF p. 4, eqs. (1)–(2)). The stabilizers and induced metrics are cited mathematical results [MATH], not inferred from finite coordinate evaluations. The complex-coordinate expansions, minor evaluations, frame-change identity and Gram calculations are derived specializations. The G_2 positive orbit is open of dimension 35; the Cayley orbit has dimension 43 and codimension 27, as in Joyce (1996a, physical PDF p. 4, section 1.1). That source's Cayley components agree with the 2004 components after $\tau_i = dx^i$ and term reordering. The 1996 G_2 coframe is different and is not used for plane values here.

Section 9.4. Torsion-free equivalences use Joyce (2004, physical PDF pp. 4–5, Propositions 2.4 and 2.6), with each form's induced metric and orientation. Product controls use the same source, physical PDF p. 6, Propositions 2.9–2.11. These are cited [MATH] statements. Compact full-holonomy existence is Joyce (1996b, physical PDF p. 12, Theorem 2.3.1, for the specified M of section 2.2) and Joyce (1996a, physical PDF p. 9, Theorem 2.1.2 and its preceding exact-holonomy argument). The former gives the stated 43-dimensional family; the latter gives at least 95 topologically distinct compact simply connected examples. Proofs and classification are not supplied by the chapter.

Section 9.5. The zero-field parallel-spinor criterion, external dimensions and exceptional counts follow Acharya and Gukov (2004, physical PDF pp. 10–11, section 2.2, Table 2 and eqs. (2.10)–(2.11)), with the stated Lorentzian, real-supercharge and spinor-embedding conventions. The spinor count is a supergravity consequence [SUGRA] under the stated product premises. Real subgroup restrictions and periodic lift controls specify the representation and global spin assumptions. They are not a spectrum or a flux-vacuum theorem.

Section 9.6. The all-plane calibration results are cited [MATH] inputs from Joyce (2004, physical PDF pp. 18–20 and p. 25, Proposition 5.2, Definition 5.3, Proposition 5.4, Definition 5.12 and Proposition 5.13). The compact minimization proof is reproduced with the realized-representative hypothesis. The torus and its graph competitor are

explicit derived examples. No finite component test proves comass, and no homology class is asserted to possess a calibrated representative merely because it is a class.

Sections 9.7–9.8. The smooth compact spectrum and retained supergravity are sourced [SUGRA] claims from Acharya and Gukov (2004, physical PDF pp. 29–32, section 4); the volume factor follows by direct reduction of the Einstein term. The shifted quantization condition is the sourced membrane path-integral constraint [ANOM] in that work, physical PDF p. 32, eq. (4.62). Its power here is one sourced shifted-class integrality condition evaluated per cycle, with zero independently matched anomaly coefficients. Odd periods obstruct $G = 0$; evenness removes only that obstruction, not tadpoles, torsion or the full vacuum conditions. The missing local-construction inputs follow the scope of the same work, physical PDF p. 1, p. 32 and p. 35, section 5.1. This is a candidate geometric route [GEO-E], without a specific QFT identification or an asserted [DEC] limit.

Scope and exercises. The plane, real-spinor and shear examples establish the stated calculations. The general calibration results and physical premises have the separate hypotheses given above. Singular dynamics requires further input.

References

Acharya, B. S. and S. Gukov (2004). *M Theory and Singularities of Exceptional Holonomy Manifolds*. arXiv: `hep-th/0409191v2`.

Joyce, D. D. (1996a). "Compact 8-Manifolds with Holonomy Spin(7)". In: *Inventiones Mathematicae* 123, pp. 507–552.

Joyce, D. D. (1996b). "Compact Riemannian 7-Manifolds with Holonomy G_2. I". In: *Journal of Differential Geometry* 43, pp. 291–328.

Joyce, D. D. (2004). *The Exceptional Holonomy Groups and Calibrated Geometry*. arXiv: `math/0406011v1`.

Chapter IV.10

Fluxes and warping

IV.10.1 A number on a surface

A flux integral can remain nonzero while its measuring surface moves through a region without branes. A second measurement can change if the region between the two surfaces contains distributed charge. Neither measurement determines a metric. These three facts are the starting point for understanding flux backgrounds. A period specifies part of a field configuration. A sourced equation relates measurements at different locations. Boundary data and the remaining equations determine whether that configuration can be a physical solution.

This chapter follows that progression in a small set of explicit calculations. First we recover integer flux coordinates from nonprimitive measuring cycles. Then we balance a five-form flux across an oriented shell. A radial boundary problem shows how a localized source hides in a singular solution. The M-theory membrane anomaly supplies a distinct quantum restriction on magnetic periods. Finally, a symplectic pairing turns flux and period data into a candidate superpotential, whose physical use requires more than ordinary differentiation.

The background fields are those of Volume II, Chapter 8. The charge qualifications of Volume III, Chapter 5 remain in force. Chapter 2 supplies the Calabi–Yau setting; Volume V, Chapter 3 develops period calculations further. The present aim is to prepare a reader to use these ingredients in a construction. It is not to catalogue compact flux vacua. In particular, the existence of a positive warp profile on a ball says nothing by itself about gravity decoupling or stabilization of all moduli.

By the end, the reader should be able to reconstruct free flux coefficients with their units, distinguish a shell balance from a compact tadpole, solve a radial equation with both central and outer data, test the shifted magnetic lattice, and differentiate the flux pairing while naming the physical data still needed. Each of these operations has a worked example below.

IV.10.2 Flux and free cohomology

What can a period measurement recover about a field? The answer begins with a distinction between a differential form and its cohomology class. Let X be an oriented internal manifold, and let H_3 be a real closed three-form in a region without magnetic sources. Locally one can write $H_3 = dB_2$. A globally defined B_2 would make every closed-cycle period vanish. Nonzero periods therefore require patches for the potential, even when the curvature is a globally defined form.

We work first with the free part of integral homology. Torsion is removed in forming this lattice. Choose basis cycles C_a and closed real forms η_a whose periods are dual to them. In the relevant subspace their normalization is

$$dH_3 = 0, \qquad \partial C_a = 0, \qquad \int_{C_a} \eta_b = \delta_{ab}. \tag{IV.10.1}$$

The integral lattice is extra physical information. In the constant-axiodilaton, untwisted chart used here, the three-form unit is

$$U_3 = (2\pi)^2 \alpha', \qquad \frac{1}{U_3} \int_{C_a} H_3 = n_a \in \mathbb{Z}. \tag{IV.10.2}$$

This quantum period condition is an input to the effective theory. The classical equation $dH_3 = 0$ does not derive it. That equation would also allow arbitrary real multiples of any closed form.

Assume that the chosen cycles span all the free directions under discussion. The representative of the class can then be written

$$H_3 = U_3 \sum_a n_a \eta_a + d\Lambda_2, \tag{IV.10.3}$$

where Λ_2 is globally defined for the exact difference between the chosen representative and H_3. Integrating this difference over a closed cycle gives

$$\int_{C_a} d\Lambda_2 = \int_{\partial C_a} \Lambda_2 = 0, \qquad \int_{C_a} H_3 = U_3 n_a. \tag{IV.10.4}$$

The exact part can affect a local field without changing these numbers. Periods determine the real cohomology class, not its local representative or its energy-minimizing metric.

In practice, the available measuring cycles need not be a primitive integral basis. Let their classes be $C'_i = \sum_a M_{ia} C_a$, with integral M. Define the dimensionless period vector $p_i = \int_{C'_i} H_3/U_3$. Linearity gives the reconstruction problem

$$\boldsymbol{p} = M\boldsymbol{n}, \qquad \boldsymbol{n} = M^{-1}\boldsymbol{p} \quad (\det M \neq 0). \tag{IV.10.5}$$

Invertibility over the rationals does not make M an integral basis change. For a square full-rank matrix, the sublattice generated by its rows has index $|\det M|$. Only $\det M = \pm 1$ gives another integral basis. A measurement on a proper sublattice must pass the reconstruction test $M^{-1}\boldsymbol{p} \in \mathbb{Z}^r$.

For a concrete realization of the free cycles, take $T^6 = (\mathbb{R}/\mathbb{Z})^6$ with oriented coordinates $x^1, \ldots, x^6$. Let $A = T^3_{123}$ and $B = T^3_{456}$, with the complementary coordinates held fixed. Their dual forms in this two-dimensional subspace are

$$\eta_A = dx^1 \wedge dx^2 \wedge dx^3, \qquad \eta_B = dx^4 \wedge dx^5 \wedge dx^6, \qquad \int_A \eta_A = \int_B \eta_B = 1. \quad \text{(IV.10.6)}$$

The mixed periods vanish. This specifies actual cycles and forms, but does not claim that the resulting torus with flux is a solution of all the field equations.

Choose the nonunit scale $\alpha' = 5\ell_0^2/2$ and free coordinates $\boldsymbol{n} = (3, -2)^t$. Numerical periods below are expressed in the reference area unit ℓ_0^2. Measure on $C_1 = A + 2B$ and $C_2 = -A + B$. The matrix and its action are

$$M = \begin{pmatrix} 1 & 2 \\ -1 & 1 \end{pmatrix}, \qquad M \begin{pmatrix} 3 \\ -2 \end{pmatrix} = \begin{pmatrix} -1 \\ -5 \end{pmatrix}, \qquad \det M = 3. \quad \text{(IV.10.7)}$$

Since $U_3/\pi^2 = 4\alpha' = 10\ell_0^2$, the actual measured periods are

$$\frac{1}{\pi^2 \ell_0^2} \begin{pmatrix} \int_{C_1} H_3 \\ \int_{C_2} H_3 \end{pmatrix} = 10 \begin{pmatrix} -1 \\ -5 \end{pmatrix} = \begin{pmatrix} -10 \\ -50 \end{pmatrix}. \quad \text{(IV.10.8)}$$

The factor ten is necessary. Treating the numbers $-10, -50$ as flux coordinates would mix the normalization unit with the topology. Dividing by U_3 first and then inverting gives

$$\boldsymbol{n} = \frac{1}{3} \begin{pmatrix} 1 & -2 \\ 1 & 1 \end{pmatrix} \begin{pmatrix} -1 \\ -5 \end{pmatrix} = \frac{1}{3} \begin{pmatrix} 9 \\ -6 \end{pmatrix} = \begin{pmatrix} 3 \\ -2 \end{pmatrix}. \quad \text{(IV.10.9)}$$

More generally, integrality of both p_1, p_2 on these measuring cycles is not sufficient. The inverse requires $p_1 + p_2$ to be divisible by three. For example, $(p_1, p_2) = (1, 0)$ would reconstruct $(1/3, 1/3)$ and fail the stated free-lattice quantization. Figure IV.10.1 displays the index geometrically.

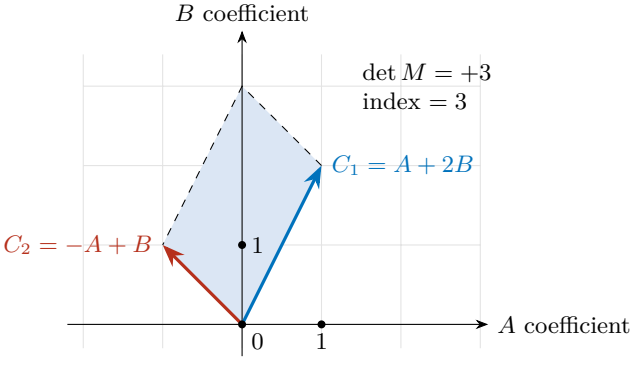


Figure IV.10.1: The coefficient lattice of the oriented cycles A, B. The two measuring cycles span a parallelogram of signed area $+3$ relative to the unit square. Their span has index three in the full free lattice. The arrows are homology coefficients, not trajectories in the torus. Unit-period forms are dual to A, B, not to the two longer arrows.

The absolute determinant controls the index, but the signed determinant controls the inverse. To separate these roles, keep the same flux and change the measuring matrix to

$$M_- = \begin{pmatrix} 2 & 3 \\ 1 & -2 \end{pmatrix}, \qquad \det M_- = -7, \qquad \boldsymbol{p}_- = M_- \boldsymbol{n} = \begin{pmatrix} 0 \\ 7 \end{pmatrix}. \tag{IV.10.10}$$

The new raw periods divided by $\pi^2 \ell_0^2$ are $(0, 70)$. The determinant-line invariant is $C_1' \wedge C_2' = -7A \wedge B$ in the exterior square of this coefficient lattice. It records reversed orientation as well as multiplicity. The reconstruction uses that sign:

$$M_-^{-1} \boldsymbol{p}_- = -\frac{1}{7} \begin{pmatrix} -2 & -3 \\ -1 & 2 \end{pmatrix} \begin{pmatrix} 0 \\ 7 \end{pmatrix} = \begin{pmatrix} 3 \\ -2 \end{pmatrix}. \tag{IV.10.11}$$

Replacing -7 with its absolute value in the inverse would give $(-3, 2)$, a different flux. The two examples express the same class in different measuring coordinates. An index alone cannot recover orientation.

Two kinds of information remain invisible. First, suppose C is a torsion three-cycle, so that $kC = \partial D$ for some positive integer k. Closure gives

$$k \int_C H_3 = \int_D dH_3 = 0, \qquad \int_C H_3 = 0. \tag{IV.10.12}$$

Real periods therefore do not detect torsion. This does not say that the quantum field has no torsion data. It says that a real form cannot measure them.

Second, even zero curvature does not fix a connection. On a circle with coordinate $x \in \mathbb{R}/\mathbb{Z}$, a unit-charge probe coupled to $A = a\,dx$ has

$$dA = 0, \qquad \exp\left(i \oint A \right) = e^{ia}, \qquad a \sim a + 2\pi m, \quad m \in \mathbb{Z}. \tag{IV.10.13}$$

For example, $a = \pi$ and $a = 0$ have the same curvature but opposite holonomies. This elementary example explains why specifying real flux periods is less information than specifying the full gauge field. Volume III, Chapter 5 discusses the related charge-classification limits. Here we retain the free periods needed for the next operation: using fluxes as terms in a sourced Bianchi identity.

IV.10.3 Bianchi identities and sources

Why can the flux through a surface change when no localized brane crosses it? A modified Bianchi identity permits the gauge fields themselves to carry distributed charge. We now use the source normalization of the GKP type-IIB framework. Work on a chart with constant $\tau = C_0 + ie^{-\Phi}$, no fivebrane sources, and closed H_3, F_3. The improved self-dual five-form obeys the sourced equation

$$d\widetilde{F}_5 = H_3 \wedge F_3 + 2\kappa_{10}^2 T_3 j_6. \tag{IV.10.14}$$

The current j_6 is a six-form distribution whose integral gives localized D3-charge units. This equation includes the source prescription appropriate to the self-dual field. It is a physical input, not the result of freely varying an unconstrained five-form action.

In this source convention, the constants are

$$2\kappa_{10}^2 = (2\pi)^7\alpha'^4, \qquad T_3 = (2\pi)^{-3}\alpha'^{-2}, \qquad 2\kappa_{10}^2 T_3 = (2\pi)^4\alpha'^2 = U_3^2. \tag{IV.10.15}$$

The κ_{10} here is the source action constant. It must not be identified with the physical asymptotic gravitational coupling containing g_s^2 used in Volume II, Chapter 8. Define normalized forms and a surface flux by

$$\widehat{H}_3 = H_3/U_3, \quad \widehat{F}_3 = F_3/U_3, \quad f_5 = \widetilde{F}_5/U_3^2, \quad m(S) = \int_S f_5. \tag{IV.10.16}$$

The normalized identity is then

$$df_5 = \widehat{H}_3 \wedge \widehat{F}_3 + j_6. \tag{IV.10.17}$$

No assertion of integrality on an arbitrary measuring surface has entered this definition of $m(S)$.

Let $\mathcal{S}$ be a shell bounded by two homologous measuring surfaces. Orient each sphere outward from the common center. The boundary orientation of the shell reverses the inner one:

$$\partial\mathcal{S} = S_{\text{out}} - S_{\text{in}}, \qquad m_{\text{out}} - m_{\text{in}} = \int_{\mathcal{S}} \widehat{H}_3 \wedge \widehat{F}_3 + q_{\text{local}}, \quad q_{\text{local}} = \int_{\mathcal{S}} j_6. \tag{IV.10.18}$$

The normal pointing out of the shell at its inner boundary points toward the center. This is why adding the two center-outward fluxes would be incorrect. The charge difference measures everything in the intervening region, not just a count of localized branes.

We can understand the bulk sign using a closed compact symplectic subpair. Choose oriented three-forms α, β with

$$\int \alpha \wedge \beta = +1, \qquad \beta \wedge \alpha = -\alpha \wedge \beta, \qquad \alpha \wedge \alpha = \beta \wedge \beta = 0. \tag{IV.10.19}$$

For fluxes $\widehat{H}_3 = h_A\alpha - h_B\beta$ and $\widehat{F}_3 = f_A\alpha - f_B\beta$, both cross terms contribute:

$$\begin{aligned} \widehat{H}_3 \wedge \widehat{F}_3 &= -h_A f_B\, \alpha \wedge \beta - h_B f_A\, \beta \wedge \alpha \\ &= (h_B f_A - h_A f_B)\, \alpha \wedge \beta. \end{aligned} \tag{IV.10.20}$$

With $h = (1, 4)$ and $f = (3, -2)$ this compact pairing gives

$$N_{\text{flux}} = 4 \cdot 3 - 1 \cdot (-2) = 12 + 2 = 14. \tag{IV.10.21}$$

This is a calculation on the stated free symplectic sublattice. A generic shell has a boundary; it is not the same compact space. For the shell example, we *supply* the integrated distributed contribution to be fourteen. We have not extended the compact

cohomology classes to a relative-cohomology problem on that shell. Its bulk integral need not be an integer in general.

Take $q_{\text{local}} = -9$ and $m_{\text{in}} = 7/3$. Substitution in the oriented balance gives

$$\Delta m = 14 - 9 = 5, \qquad m_{\text{out}} = \frac{7}{3} + 5 = \frac{22}{3}. \tag{IV.10.22}$$

Figure IV.10.2 keeps these same source and boundary numbers visible. The fractional surface flux is compatible with a Maxwell measurement. It does not represent a fractional assignment of gauge-group rank. Reversing the orientation of the whole integration region reverses the entire signed equation, rather than just changing the inner sign.

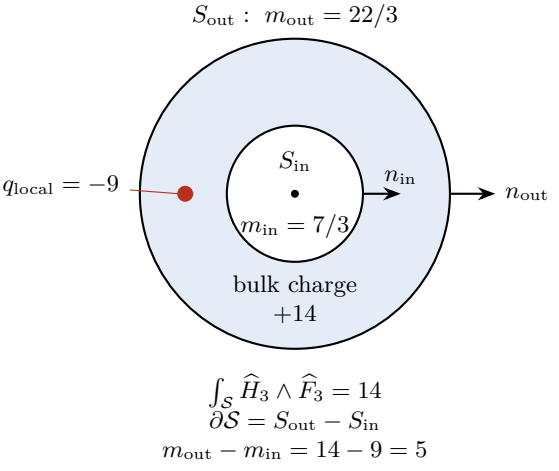


Figure IV.10.2: A cross-section of the six-dimensional shell $\mathcal{S}$. Both labeled normals point away from the center. The induced boundary of the shaded region uses the opposite of n_{in} and therefore gives $S_{\text{out}} - S_{\text{in}}$. The distributed contribution is supplied as fourteen and the red localized contribution as minus nine. A surface flux increases by five even though the localized charge is negative. This diagram specifies an integrated balance, not a global metric or a compact extension of the fluxes.

On a closed compact six-dimensional space X, there is no outer surface to carry the imbalance. Treating the Bianchi identity distributionally, its pairing with the constant test function gives

$$0 = \int_X df_5 = \int_X \widehat{H}_3 \wedge \widehat{F}_3 + Q_{\text{local}}. \tag{IV.10.23}$$

Thus the same stipulated total bulk contribution would instead require

$$Q_{\text{local}} = -14. \tag{IV.10.24}$$

Using only -9 on a compact space would leave total charge 5, contradicting the integrated identity. This identifies a missing source contribution. It does not construct an object with charge -14 or show that its tension, embedding, and supersymmetry

conditions are compatible. Cancellation is a necessary global condition, not an existence result.

To interpret these numbers, distinguish three notions of charge. Brane-source charge is localized and gauge invariant, but can fail to be conserved when other brane currents are present. Maxwell charge includes distributed gauge-field contributions. It is gauge invariant and conserved in the appropriate current equation, but its distribution is not localized on branes. Page charge combines a field strength with potential-dependent terms. It can be localized and conserved in a chosen representative, with small-gauge invariance under additional global conditions. Large gauge transformations can change that representative's charge. These are different useful measurements of a system with Chern–Simons couplings.

A local conservation statement in our restricted model is compatible with that distinction. If $dH_3 = dF_3 = 0$ and the normalization is constant, differentiating the Bianchi identity gives

$$0 = d^2\widetilde{F}_5 = dH_3 \wedge F_3 - H_3 \wedge dF_3 + U_3^2 dj_6, \qquad dj_6 = 0. \tag{IV.10.25}$$

The first equality uses the sign $(-1)^3$ in differentiating the product. Allowing magnetic currents removes this argument. One cannot promote the restricted closure of j_6 to universal source-charge conservation.

For a separate illustration of Page charge, use Marolf's IIA D4 chart. It has an RR one-form potential A_1 and a four-form field strength $\widetilde{F}_4$. In that chart the Page form and integrated charge are

$$d(\widetilde{F}_4 + A_1 \wedge H_3) = *j_{D4}^{\mathrm{Page}}, \qquad Q_{D4}^{\mathrm{Page}}(S) = \int_S (\widetilde{F}_4 + A_1 \wedge H_3). \tag{IV.10.26}$$

Here S is a closed four-dimensional integration surface. If the potential is globally defined on S and H_3 is closed there, a small transformation $A_1 \mapsto A_1 + d\Lambda_0$ changes the charge by

$$\delta Q_{D4}^{\mathrm{Page}} = \int_S d\Lambda_0 \wedge H_3 = \int_S d(\Lambda_0 H_3) = 0. \tag{IV.10.27}$$

A global exact derivative was essential to the last step. A large transformation or a patch singularity need not satisfy it. This D4 expression is not an IIB five-form formula. Volume III, Chapter 5 and Volume VIII, revised Chapter 4 use their own specified charge frames. A flux number can constrain a construction only after its charge prescription and the rank dictionary have been supplied. The next section asks what further information is needed even for a much simpler scalar field equation.

IV.10.4 Warped metrics and boundary data

What fixes a warp factor once an equation for it is known? The physical reason to ask is that the metric contains more information than a flux class. In the GKP Einstein-frame ansatz, four-dimensional Poincaré symmetry is retained while the internal position changes the relative scales of the external and internal metrics. With $A(y)$ the warp

exponent, define a positive function $h = e^{-4A}$. Then

$$ds_{10}^2 = e^{2A}\eta_{\mu\nu}dx^\mu dx^\nu + e^{-2A}\widetilde{g}_{mn}dy^m dy^n = h^{-1/2}\eta_{\mu\nu}dx^\mu dx^\nu + h^{1/2}\widetilde{g}_{mn}dy^m dy^n. \tag{IV.10.28}$$

The opposite powers are the familiar D3 pattern of Volume II, Chapter 8. Specifying them is an ansatz, not a solution. The internal metric, flux, axiodilaton, and sources must still solve their equations together.

We isolate the boundary-value issue in a stipulated scalar model. Let r be the radius in flat $\mathbb{R}^6$, with the positive Euclidean volume orientation. On the punctured ball $0 < r < R$, impose a constant density s:

$$\Delta_6 h = \frac{1}{r^5}\frac{d}{dr}(r^5 h') = -s, \qquad \lim_{r\to 0} r^5 h' = -4b, \qquad h(R) = v. \tag{IV.10.29}$$

The central flux parameter b and the outer value v are distinct data. Since h is dimensionless, $[b] = L^4$ and $[s] = L^{-2}$. This model does not identify an arbitrary constant s with an allowed three-form energy density in a compact IIB solution.

The radial Laplacian follows from the flat measure $r^5 dr\, d\Omega_5$. Multiplying the equation by r^5 and integrating once gives

$$(r^5 h')' = -sr^5, \qquad r^5 h' = -\frac{s}{6}r^6 + C_1. \tag{IV.10.30}$$

The small-sphere condition sets $C_1 = -4b$. A second integration separates the pole from the smooth response:

$$h' = -\frac{s}{6}r - \frac{4b}{r^5}, \qquad h(r) = a + \frac{b}{r^4} - \frac{s}{12}r^2. \tag{IV.10.31}$$

The remaining integration constant is determined at the outer boundary:

$$a = v - \frac{b}{R^4} + \frac{sR^2}{12}. \tag{IV.10.32}$$

Thus the constant mode is fixed by outer data, whereas the singular harmonic term is fixed by central data. A differential equation without those two conditions would leave both coefficients undetermined.

The pole is harmonic away from the origin, but has a distributional source there. To compute its coefficient, first normalize the sphere volume. The Gaussian integral in six dimensions can be evaluated in Cartesian and polar coordinates:

$$\pi^3 = \int_{\mathbb{R}^6} e^{-|y|^2} d^6y = \mathrm{Vol}(S^5)\int_0^\infty e^{-r^2} r^5 dr = \mathrm{Vol}(S^5)\frac{\Gamma(3)}{2} = \mathrm{Vol}(S^5). \tag{IV.10.33}$$

The sphere at radius ϵ has area $\pi^3\epsilon^5$. In the declared orientation, $*dh$ on that sphere is $h'(\epsilon)\epsilon^5 d\Omega_5$. Consequently the outward Gauss integral is

$$\int_{S^5_\epsilon} *dh = \pi^3\epsilon^5 h'(\epsilon) = -4\pi^3 b - \frac{\pi^3 s}{6}\epsilon^6 \longrightarrow -4\pi^3 b. \tag{IV.10.34}$$

The smooth density contributes a term that vanishes as the ball shrinks. The nonzero limit comes entirely from the pole. With $\delta_0^{(6)}$ normalized to integrate to one, the equation on the full ball is

$$\Delta_6 h = -s - 4\pi^3 b\,\delta_0^{(6)}. \tag{IV.10.35}$$

This is an equality of distributions. In six dimensions r^{-4} is locally integrable because the measure makes its radial integral proportional to $\int r\,dr$. It can therefore be differentiated distributionally, even though its value at the center is singular. Ordinary differentiation on $r > 0$ alone would miss the second term in (IV.10.35).

For example, integrate the full equation over B_R. Its volume is $\pi^3 R^6/6$, so both the smooth and point contributions enter:

$$\int_{S^5_R} *dh = -\frac{\pi^3 s R^6}{6} - 4\pi^3 b = \pi^3 R^5 h'(R). \tag{IV.10.36}$$

The pole coefficient is thereby fixed by a measurable flux, not by guessing the value of h near a singular point. It has not been converted into D3-charge units; that would require the full physical relation between the five-form, the metric, and the sources.

Now solve a nonunit example completely. Set $R = 2$, $v = 5/2$, $s = 18/5$ and $b = 7/3$ in reference-length units. Thus r in the following numerical formulas means r/ℓ_0, with $s\ell_0^2 = 18/5$ and $b/\ell_0^4 = 7/3$. If $h = a + b/r^4 + cr^2$, then

$$c = -\frac{18/5}{12} = -\frac{3}{10}, \qquad a = \frac{5}{2} - \frac{7/3}{16} + \frac{(18/5)4}{12} = \frac{600 - 35 + 288}{240} = \frac{853}{240}. \tag{IV.10.37}$$

The reconstructed solution and central flux are

$$h(r) = \frac{853}{240} + \frac{7}{3r^4} - \frac{3}{10}r^2, \qquad \frac{1}{\pi^3}\lim_{\epsilon\to 0}\int_{S^5_\epsilon} *dh = -\frac{28}{3}. \tag{IV.10.38}$$

One can verify the outer condition without decimal rounding:

$$h(2) = \frac{853}{240} + \frac{7}{48} - \frac{6}{5} = \frac{853 + 35 - 288}{240} = \frac{5}{2}. \tag{IV.10.39}$$

For this example positivity holds throughout the punctured ball. Both terms in the derivative are negative:

$$h'(r) = -\frac{28}{3r^5} - \frac{3}{5}r < 0, \qquad h(r) \geq h(2) = \frac{5}{2} > 0 \quad (0 < r \leq 2). \tag{IV.10.40}$$

The inequality follows from monotonicity and the specified positive outer value. It is not true for every formal choice of a, b, s. In particular a negative pole would drive h negative sufficiently near the center. A metric interpretation would then fail in that region.

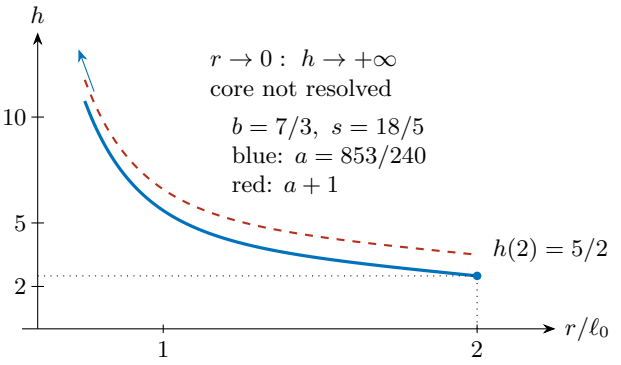


Figure IV.10.3: The exact profile (IV.10.38), drawn for $0.75 \le r/\ell_0 \le 2$. The blue curve reaches the imposed value $5/2$ at the outer boundary. The red curve adds one to a, leaving the equation and central flux unchanged while changing that boundary value. Both curves retain the same pole and constant density. The central region is omitted from the plot; the singularity is not resolved.

Figure IV.10.3 exhibits a first ambiguity of the differential equation. Adding a constant changes neither $\Delta_6 h$ nor the pole flux, but it changes $h(R)$. A different ambiguity appears if the central condition is dropped while the outer condition is kept. With δb arbitrary, set

$$\delta h = \delta b\,(r^{-4} - R^{-4}), \qquad \delta h(R) = 0, \qquad \delta\left(\int_{S^5_\varepsilon} *dh\right) = -4\pi^3 \delta b. \tag{IV.10.41}$$

This change preserves the punctured-domain differential equation and outer value. It changes the point source. Thus outer Dirichlet data alone do not fix the charge hidden at the origin.

Two limits provide distinct checks on the solution. Setting $s = 0$ leaves $h = a + b/r^4$ and its point source intact. Setting $b = 0$ leaves a regular center, with $h = a - sr^2/12$ and zero small-sphere flux. Removing the distributed term and removing the pole are different physical changes. Volume II, Chapter 8 uses the harmonic limit; full deformed-conifold dynamics requires the additional fields and geometry treated in Volume VII, Chapter 8.

Finally, test the full source on a closed connected compact manifold. There is no boundary through which a net scalar flux can escape. For a distributional solution on such a manifold, the constant function gives

$$\langle \Delta h, 1\rangle = \langle h, \Delta 1\rangle = 0, \qquad 0 = \int_X (-s)\, d\,\mathrm{vol} - 4\pi^3 b. \tag{IV.10.42}$$

If $s > 0$ and $b > 0$, the right-hand side would be strictly negative. The ball solution cannot simply be used globally on a compact space with only these sources. Additional compensating terms would be necessary. This constant-function test is analogous to the integrated five-form tadpole, but the two are not identical equations in a general

background. Even a zero integral does not establish a positive warp factor, the Einstein and dilaton equations, or supersymmetry. Those conditions require the physical system that the scalar example deliberately leaves unspecified.

IV.10.5 Shifted magnetic quantization

Can a physically allowed magnetic period be half-integral? In M-theory the answer depends on the ambient tangent bundle. The membrane couples to a three-form potential, but its fermion functional integral can also change sign during transport around a closed family of configurations. A well-defined quantum amplitude requires the two ambiguities to cancel. This is a global quantum constraint. It is not derivable by solving the classical field-strength equations.

Let Y be an orientable spin spacetime and let C be a closed oriented four-cycle lying in a region without magnetic sources. To translate the membrane-normalized field G_{W} into the book's four-form, use

$$G_{\mathrm{W}} = T_{\mathrm{M2}} F_4^{\mathrm{book}}, \qquad T_{\mathrm{M2}} = \frac{1}{(2\pi)^2 \ell_p^3}, \qquad q_C = \frac{1}{2\pi}\int_C G_{\mathrm{W}} = \frac{1}{(2\pi)^3 \ell_p^3}\int_C F_4^{\mathrm{book}}. \tag{IV.10.43}$$

The symbol λ_{char} will denote a characteristic class, not the $2\pi\alpha'$ shorthand sometimes used in D-brane actions. On a spin spacetime the half Pontryagin class is integral. Define its period by

$$\lambda_{\mathrm{char}} = \frac{p_1(TY)}{2}, \qquad \lambda_C = \int_C \lambda_{\mathrm{char}} \in \mathbb{Z}. \tag{IV.10.44}$$

The cited membrane-anomaly result states that the magnetic class obeys

$$\left[\frac{G_{\mathrm{W}}}{2\pi}\right] - \frac{\lambda_{\mathrm{char}}}{2} \;\in\; \mathrm{im}\big(H^4(Y,\mathbb{Z}) \to H^4(Y,\mathbb{R})\big). \tag{IV.10.45}$$

The displayed form is its free real-class consequence. It does not select a torsion lift or flat holonomy. In particular, a list of real periods is not a specification of the entire quantum gauge field.

The sign condition explains the half shift. For a closed swept four-cycle of the membrane family in the anomaly argument, the combined ambiguity is

$$(-1)^{\lambda_C} \exp\left(i\int_C G_{\mathrm{W}}\right) = 1, \qquad \exp(2\pi i q_C) = (-1)^{\lambda_C}. \tag{IV.10.46}$$

Here the fermion sign is a cited global result; we have not derived its determinant from a finite set of period examples. The elementary consequence is

$$q_C = n_C + \frac{\lambda_C}{2}, \qquad n_C = q_C - \frac{\lambda_C}{2} \in \mathbb{Z}. \tag{IV.10.47}$$

For odd λ_C, the unshifted q_C is half-integral. For even λ_C, it is integral. Figure IV.10.4 distinguishes the two cosets. The lattice is affine: choosing an origin for the integer coordinate is part of writing the shift explicitly.

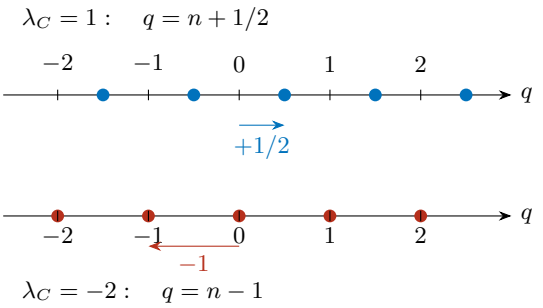


Figure IV.10.4: Allowed free magnetic periods on a supplied oriented four-cycle. Blue points show $q \in \mathbb{Z} + 1/2$ for $\lambda_C = 1$. Red points show $q \in \mathbb{Z} - 1 = \mathbb{Z}$ for $\lambda_C = -2$. The arrows translate the integer coordinate n to the measured period q. The horizontal axes are period coordinates, not positions in spacetime. This arithmetic diagram presupposes the global membrane anomaly law.

The class is ambient. If a smooth four-cycle is embedded in Y, its restricted tangent bundle splits as $TY|_C = TC \oplus N_C$. Additivity of the first Pontryagin class gives

$$p_1(TY)|_C = p_1(TC) + p_1(N_C), \qquad \lambda_C = \frac{1}{2}\int_C \big(p_1(TC) + p_1(N_C)\big). \tag{IV.10.48}$$

Dropping the normal bundle changes the characteristic period unless its contribution vanishes under an additional hypothesis. A spin ambient space does not license an arbitrary intrinsic-cycle replacement. For a singular cycle even this tangent-normal description needs care; our arithmetic below only presupposes supplied ambient periods on closed cycles.

Work a nonunit example with three supplied pairs:

$$\boldsymbol{\lambda} = (1, -2, 4), \qquad \boldsymbol{q} = (7/2, -1, -1). \tag{IV.10.49}$$

Apply the shift separately to every cycle:

$$\begin{aligned} n_1 &= \frac{7}{2} - \frac{1}{2} = 3, \\ n_2 &= -1 - \frac{-2}{2} = 0, \\ n_3 &= -1 - \frac{4}{2} = -3. \end{aligned} \tag{IV.10.50}$$

Thus the declared free integer coordinates are $(3, 0, -3)$. On the first cycle the two anomalous phases cancel directly:

$$(-1)^1 e^{2\pi i(7/2)} = (-1)(-1) = 1. \tag{IV.10.51}$$

On the even-λ cycles, the sign is already positive and the flux phases are unity. These are conditional period tests. We have not constructed an embedding of three four-cycles with exactly those characteristic periods in a common compactification.

The zero-flux test is informative. If $q_C = 0$ on a cycle with $\lambda_C = 1$, the candidate integer coordinate is $-1/2$ and the phase in (IV.10.46) is -1. The flux is disallowed by the stated law. If instead $\lambda_C = -2$, the same $q_C = 0$ gives $n_C = 1$ and is allowed. Geometry can therefore obstruct a naively flux-free magnetic sector.

Orientation must be changed consistently. Reversing the cycle changes both periods, not the characteristic class of the ambient spacetime:

$$q_{-C} = -q_C, \qquad \lambda_{-C} = -\lambda_C, \qquad n_{-C} = -q_C + \frac{\lambda_C}{2} = -n_C. \tag{IV.10.52}$$

For the first example the reversed data are $q = -7/2$, $\lambda = -1$, and $n = -3$. Negating only the flux period would mix two orientations. The declared integer coordinates also depend on the sign chosen for the shift. Since λ_C is integral,

$$\mathbb{Z} + \frac{\lambda_C}{2} = \mathbb{Z} - \frac{\lambda_C}{2}, \qquad \left(q_C + \frac{\lambda_C}{2}\right) - \left(q_C - \frac{\lambda_C}{2}\right) = \lambda_C. \tag{IV.10.53}$$

The opposite sign describes the same allowed coset but changes its integer labels. It is therefore wrong to call it a different set of allowed periods, and also wrong to substitute its labels into a calculation that has fixed $n = q - \lambda/2$.

This four-cycle test concerns magnetic flux. It does not compute an electric charge on a seven-cycle, a tadpole, or a gauge rank. It is distinct from the D-brane worldvolume anomaly discussed in Volume III, Chapter 5. For an actual M-theory construction one must supply the spacetime, the cycles, the ambient class, and the full global field data. The present calculation tells the reader exactly how to test the free periods once those objects exist. We return next to IIB, where the free three-form periods enter an interaction through a different pairing.

IV.10.6 Flux superpotentials and their limits

How can flux periods produce an interaction for geometric moduli? A three-form flux can be paired with the holomorphic three-form of a Calabi–Yau threefold. Changing the complex structure changes the holomorphic form while leaving an integral flux class fixed. The pairing therefore becomes a function of the moduli. Its role as a physical superpotential is a result of the effective-action derivation, not a consequence of symplectic linear algebra alone.

Use a smooth proper compact Calabi–Yau threefold family on a regular moduli patch. Work in its free symplectic lattice, or the retained sublattice when the orientifold projection requires one. Fix cycles A^I, B_J with $A^I \cap B_J = \delta^I{}_J$ and dual forms with the following signs:

$$\int_{A^J} \alpha_I = \delta_I{}^J, \qquad \int_{B_J} \beta^I = -\delta^I{}_J, \qquad \int_X \alpha_I \wedge \beta^J = \delta_I{}^J. \tag{IV.10.54}$$

The other cycle periods and same-type wedge pairings vanish. Write the periods of the holomorphic form as $X^I = \int_{A^I} \Omega$ and $\mathcal{F}_I = \int_{B_I} \Omega$. The minus sign in the dual B period then requires

$$\Omega = X^I \alpha_I - \mathcal{F}_I \beta^I, \qquad \widehat{F}_3 = f_A^I \alpha_I - f_{B,I} \beta^I, \qquad \widehat{H}_3 = h_A^I \alpha_I - h_{B,I} \beta^I. \tag{IV.10.55}$$

Repeated indices are summed. The symbol $\mathcal{F}_I$ is a period, while F_3 is the RR field strength. Their roles must remain distinct. The integral flux coordinates are held fixed when the complex structure varies in a locally transported cycle frame.

On the constant-τ chart without fivebrane sources, define $G_3 = F_3 - \tau H_3$. We choose the body ordering of the GKP superpotential and remove the three-form unit:

$$w = \frac{W_{\text{body}}}{U_3} = \int_X \Omega \wedge \frac{G_3}{U_3}, \qquad \operatorname{Im}\tau > 0. \tag{IV.10.56}$$

This fixes a relative normalization for the pairing; it does not assign an absolute four-dimensional mass normalization. Let $g_A^I = f_A^I - \tau h_A^I$ and $g_{B,I} = f_{B,I} - \tau h_{B,I}$. Expanding the two nonvanishing cross terms gives

$$\begin{aligned} w &= \int_X (X^I \alpha_I - \mathcal{F}_I \beta^I) \wedge (g_A^J \alpha_J - g_{B,J} \beta^J) \\ &= -X^I g_{B,I} + \mathcal{F}_I g_A^I = \sum_I \big[(f_A^I - \tau h_A^I)\mathcal{F}_I - (f_{B,I} - \tau h_{B,I}) X^I \big]. \end{aligned} \tag{IV.10.57}$$

The positive coefficient of $\mathcal{F}_I$ comes from reversing $\beta \wedge \alpha$. This is the same odd-degree wedge rule that fixed the sign of the distributed charge.

The ordering must be kept through every derivative. For two three-forms, the opposite order is globally related by

$$W_{\text{appendix}} = \int_X G_3 \wedge \Omega = -W_{\text{body}}, \qquad D_a W_{\text{appendix}} = -D_a W_{\text{body}}. \tag{IV.10.58}$$

A common sign leaves zero equations and $|W|^2$ unchanged. It does not permit copying the value of W from one convention and the derivative from the other. The exact source locations for these two orderings are recorded at the chapter end.

First perform ordinary variations. At fixed flux coordinates and fixed τ, the derivative with respect to one complex-structure coordinate z is

$$\partial_z w = \sum_I \left[(f_A^I - \tau h_A^I)\partial_z \mathcal{F}_I - (f_{B,I} - \tau h_{B,I})\partial_z X^I \right]. \tag{IV.10.59}$$

In the CY/orientifold chart the periods depend on z, not on the separately varying τ. Thus

$$\partial_\tau w = \sum_I (-h_A^I \mathcal{F}_I + h_{B,I} X^I). \tag{IV.10.60}$$

For a varying axiodilaton with monodromy these globally untwisted expansions need not apply. One must then supply the bundle-valued flux description rather than reuse the present chart unchanged.

A formal projected period pair makes every coefficient and derivative visible. Supply one pair

$$X = c_\Omega, \qquad \mathcal{F} = c_\Omega (z^2 + z/2), \qquad c_\Omega = \frac{5}{2}, \qquad f = (3, -2), \quad h = (1, 4). \tag{IV.10.61}$$

These polynomial functions are stipulated for an algebra calculation. They are not asserted to be a polarized integral period variation of a realized Calabi–Yau family. The common factor c_Ω rescales the holomorphic form; it does not change the flux unit U_3.

Before fixing τ, the polynomial is

$$w = \frac{5}{2}\left[(3-\tau)(z^2+z/2)+2+4\tau\right]. \tag{IV.10.62}$$

At $\tau = 1+2i$, the two flux combinations are $g_A = 2-2i$ and $g_B = -6-8i$. The coefficients in ascending order of degree follow separately:

$$w(z) = (15+20i) + \left(\frac{5}{2} - \frac{5}{2}i\right) z + (5-5i)z^2. \tag{IV.10.63}$$

The linear coefficient is half the quadratic coefficient because the supplied period contains $z^2 + z/2$. A constant-term comparison alone would not detect an incorrect quadratic coefficient.

Evaluate the polynomial at $z = 2/3$ by retaining each contribution:

$$\begin{aligned} w(2/3) &= 15 + 20i + \left(\frac{5}{3} - \frac{5}{3}i\right) + \left(\frac{20}{9} - \frac{20}{9}i\right) \\ &= \frac{170}{9} + \frac{145}{9}i. \end{aligned} \tag{IV.10.64}$$

Ordinary z differentiation gives

$$\partial_z w = \left(\frac{5}{2} - \frac{5}{2}i\right) + 2(5-5i)z, \qquad \partial_z w\big|_{z=2/3} = \frac{55}{6} - \frac{55}{6}i. \tag{IV.10.65}$$

For ∂_τ one must differentiate (IV.10.62) before substituting a numerical τ. At the same point,

$$\partial_\tau w = \frac{5}{2}\left[4 - (z^2+z/2)\right], \qquad \partial_\tau w\big|_{z=2/3} = \frac{5}{2}\left(4 - \frac{7}{9}\right) = \frac{145}{18}. \tag{IV.10.66}$$

Substituting τ first and then differentiating the resulting polynomial as though it still carried an independent τ would lose this information. All three coefficients, the value, and both derivatives are distinct outputs of the same pairing.

For a physical F term, ordinary derivatives are insufficient. In four-dimensional $\mathcal{N} = 1$ supergravity the Kähler covariant derivative is

$$D_a W = \partial_a W + K_a W, \qquad K_a = \partial_a K. \tag{IV.10.67}$$

Even $\partial_a W = 0$ would give $D_a W = K_a W$, which can be nonzero. No K or complete field space was supplied for the polynomial example, so it does not determine a physical F-term solution.

For the sourced leading large-radius CY/orientifold effective description, the complex-structure identity is $\partial_z \Omega = k_z \Omega + \chi_z$, where χ_z has type $(2,1)$ and $K_z = -k_z$. Its

physical and geometric hypotheses are part of that description. In the chosen body ordering, the cancellation is explicit:

$$D_z W_{\text{body}} = \int_X (k_z \Omega + \chi_z) \wedge G_3 - k_z W_{\text{body}} = \int_X \chi_z \wedge G_3. \tag{IV.10.68}$$

For $K_\tau = -1/(\tau - \bar{\tau})$ and real F_3, H_3, use $\bar{G}_3 = F_3 - \bar{\tau} H_3$ to derive

$$\begin{aligned} D_\tau W_{\text{body}} &= -\int_X \Omega \wedge H_3 + \frac{1}{\bar{\tau} - \tau} \int_X \Omega \wedge G_3 \\ &= \frac{1}{\bar{\tau} - \tau} \int_X \Omega \wedge \bar{G}_3. \end{aligned} \tag{IV.10.69}$$

Both expressions reverse sign if copied into appendix ordering. Their derivation uses more information than the ordinary variations: the allowed Hodge decomposition and the physical Kähler potential. Volume V, Chapter 3 develops the period side of this structure.

The no-scale radius provides a concrete limit on what F-term information can establish. Restrict to the classical single-radius effective framework, with $\rho = x + iy$, $y > 0$, and a factorized Kähler potential of the sourced form

$$K = -3 \log[-i(\rho - \bar{\rho})] + K_{\text{other}} = -3 \log(2y) + K_{\text{other}}, \qquad \partial_\rho W = 0. \tag{IV.10.70}$$

Here K_{other} is independent of ρ, and W is the physical flux superpotential with a consistently chosen normalization. Derivatives in complex coordinates give

$$K_\rho = -\frac{3}{\rho - \bar{\rho}}, \qquad K_{\bar{\rho}} = \frac{3}{\rho - \bar{\rho}}, \qquad K_{\rho\bar{\rho}} = -\frac{3}{(\rho - \bar{\rho})^2} = \frac{3}{4y^2}. \tag{IV.10.71}$$

The inverse metric and its contraction are therefore

$$K^{\rho\bar{\rho}} = \frac{4y^2}{3}, \qquad K^{\rho\bar{\rho}} K_\rho K_{\bar{\rho}} = \frac{4y^2}{3} \frac{9}{4y^2} = 3. \tag{IV.10.72}$$

For example, at $y = 2$ the inverse metric is $16/3$ and $K_\rho K_{\bar{\rho}} = 9/16$. Their product is still three. This nonunit radius check tests the cancellation without choosing a compactification.

Let $\mathcal{C} > 0$ stand for the fixed overall normalization of the four-dimensional potential. With a running over all retained chiral fields and i omitting ρ, the no-scale contraction removes the negative term:

$$\begin{aligned} V &= \mathcal{C} e^K \left(K^{a\bar{b}} D_a W \overline{D_b W} - 3|W|^2 \right), \\ K^{\rho\bar{\rho}} |D_\rho W|^2 = 3|W|^2, &\qquad V = \mathcal{C} e^K K^{i\bar{j}} D_i W \overline{D_j W}. \end{aligned} \tag{IV.10.73}$$

Positive definiteness of the retained Kähler metric makes the remaining potential nonnegative. The cancellation does *not* make an arbitrary off-shell potential independent of the radius. At fixed other fields in this factorized example, set $P = K^{i\bar{j}} D_i W \overline{D_j W}$. It is independent of y, but

$$V(y) = \mathcal{C} e^{K_{\text{other}}} \frac{P}{(2y)^3}, \qquad P > 0 \implies \frac{V(4)}{V(2)} = \frac{1}{8}. \tag{IV.10.74}$$

This is an off-shell comparison, not a pair of vacua. It explicitly displays the surviving radius dependence.

On the special solution locus with $D_i W = 0$ for every other retained field, the same expression instead gives $V = 0$ for every y within this approximation. The radius remains free. If $W \neq 0$, then

$$D_\rho W = -\frac{3W}{\rho - \bar{\rho}} \neq 0. \tag{IV.10.75}$$

Thus vanishing potential on that locus need not mean unbroken supersymmetry. If $W = 0$ as well, this derivative vanishes. Neither case stabilizes the radius by the displayed potential alone.

The physical claim about a radius belongs to the special GKP solution class, not every function with the same algebraic contraction. Write ρ_3^{loc} for the local D3-charge density in the source stress-tensor and volume convention. The localized sources must satisfy the cited bound

$$\frac{1}{4}(T^m{}_m - T^\mu{}_\mu)^{\mathrm{loc}} \geq T_3 \rho_3^{\mathrm{loc}}. \tag{IV.10.76}$$

This is a physical source condition, not a consequence of a tadpole integral. For the compact special solutions, the bound is actually saturated. The reason uses more than charge cancellation. Subtracting the five-form Bianchi constraint from the Einstein constraint gives a Laplacian whose right-hand side is a sum of nonnegative terms: a squared departure from imaginary self-duality, a squared warp/potential gradient, and the source-bound difference. The integral of the Laplacian vanishes on the closed internal space. Under the cited source prescription and bound, each nonnegative contribution must therefore vanish. This enforces imaginary self-duality $*_6 G_3 = i G_3$, the five-form/warp relation, and equality in (IV.10.76). The remaining internal metric and axiodilaton equations must still hold.

This equality is essential in the large-radius action reduction: the topological flux-charge contribution cancels the localized-source tension only when the total D3 tadpole cancels *and* the sources saturate the bound. An anti-D3 satisfies the inequality but does not saturate it, so the inequality by itself does not supply that cancellation. This is a useful counterexample to dropping the equality condition. The classical rescaling argument applies to the special solution class with these hypotheses. The cited effective-action reduction takes a large-radius limit with constant warp factor and vanishing five-form in that reduction. It is not a derivation of a fully corrected effective action for arbitrarily strong warping. Corrections can change the no-scale structure and its residual modulus.

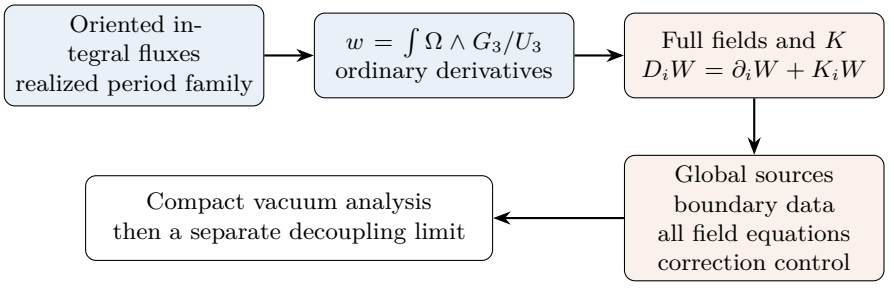


Figure IV.10.5: Data needed to turn a period pairing into a compact-vacuum analysis. The upper arrow is the algebra derived in this section. The lower stages require the physical field space, Kähler potential, global sources, boundary conditions, and equations. A formal polynomial pair does not provide the realized period family in the top box. Gravity decoupling is a further question after a consistent background is specified.

Figure IV.10.5 summarizes the missing physical work. The shell calculation must be replaced by a global source configuration and its actual tadpole. The ball must be replaced by a solution on the intended internal space with its correct boundary or compact compatibility conditions. Full periods and the complete allowed fields must replace the polynomial subpair. One then needs K, covariant equations, and control of curvature, coupling, and corrections. If the target is a decoupled QFT, a gravity-decoupling limit must also be exhibited. These are the questions faced by later constructions, including the four-form interface of XV and the compactification setting of Volume XV. The present five computations identify necessary data and consequences without turning them into an unconstructed vacuum.

IV.10.7 Exercises

The first five exercises have exact submitted-answer versions. Rational entries are exact strings such as `"7/3"`; integer coordinates are JSON integers. For a complex number, the submitted pair is its real and imaginary parts in that order. The public question file specifies every field and its ordering. The written exercise asks for physical reasoning and has no automated numerical acceptance.

1. **III10-E1. Free periods on nonprimitive cycles.** On the six-torus of Section IV.10.2, take $\alpha' = 5\ell_0^2/2$ and $H_3 = U_3(3\eta_A - 2\eta_B)$. Measure on $C_1 = A + 2B$ and $C_2 = -A + B$. Compute the periods divided by $\pi^2\ell_0^2$, then recover the primitive coordinates using the signed inverse. Submit `periods_over_pi2` and `integral_coefficients`. Explain in writing why the integrality of periods on these two measuring cycles alone does not guarantee integrality on A, B.

2. **III10-E2. An oriented shell and a compact constraint.** Use $\partial\mathcal{S} = S_{\text{out}} - S_{\text{in}}$ and the supplied integrated bulk term $h_B f_A - h_A f_B$, with $h = (1, 4)$ and $f = (3, -2)$. There is no asserted relative-cohomology extension of compact

classes onto the shell. Let its localized contribution be -9 and incoming surface flux $7/3$. Compute `flux_charge`, `delta`, and `outgoing`. Separately compute `compact_total_local_required` on a closed compact space with the same total bulk contribution. Explain why the two localized-charge requirements differ.

3. **III10-E3. A pole and an outer boundary.** In reference-length units impose $\Delta_6 h = -18/5$ on $0 < r < 2$, $\lim_{r\to 0} r^5 h' = -28/3$, and $h(2) = 5/2$. Determine a, b, c in $h = a + b/r^4 + cr^2$. Use $\mathrm{Vol}(S^5) = \pi^3$ to determine the outward small-sphere flux divided by π^3. Submit `a`, `b`, `c`, and `central_flux_over_pi3`. Explain why differentiating only at $r > 0$ fails to recover the full source, and test the source against 1 on a closed compact space.

4. **III10-E4. The shifted magnetic lattice.** On three supplied closed four-cycles in orientable spin spacetime, take $q = (7/2, -1, -1)$ and the ambient characteristic periods $\lambda = (1, -2, 4)$. Determine $n = q - \lambda/2$ and submit `shifted_integers`. These are hypothetical cycle data, not a constructed embedding. Explain which simultaneous signs change on reversing the first cycle, and why replacing $p_1(TY)|_C$ by $p_1(TC)$ requires information about the normal bundle.

5. **III10-E5. Every coefficient of a formal pairing.** Use $X = c_\Omega$, $\mathcal{F} = c_\Omega(z^2 + z/2)$, $c_\Omega = 5/2$, $f = (3, -2)$, and $h = (1, 4)$. With the body ordering of Section IV.10.6, find all three coefficients at $\tau = 1 + 2i$ in ascending degree. Evaluate w, $\partial_z w$, and $\partial_\tau w$ at $z = 2/3$. Hold flux and c_Ω fixed, and differentiate in τ before its substitution. Submit `coefficients`, `value`, `dz`, and `dtau` as rational-string complex pairs. Explain why these ordinary derivatives do not determine a covariant F-term solution or certify a realized CY period family.

6. **III10-E6. Written analysis of a proposed vacuum.** A proposal supplies integral three-form periods, a positive radial warp function on a ball, the shifted four-cycle test, and a formal critical point of a flux pairing. Explain why it has not constructed a compact vacuum or a decoupled QFT. Identify missing source/tadpole and boundary data, torsion or flat information, the realized period family, full fields and K, validity and correction control, and a decoupling limit. Give two explicit mechanisms by which an asserted implication can fail. Use the compact constant-function test and the classical no-scale radius as concrete comparisons. Distinguish off-shell radius dependence from the special zero-potential solution locus. This exercise is written-only.

IV.10.8 Take-home message

Take-home message

A quantized free period is quantum input whose coordinates can be reconstructed by signed integral-lattice arithmetic. A sourced Bianchi identity balances distributed and localized charge with the boundary orientation fixed. A warp equation needs both source and boundary data; a pole can hide a delta function from punctured differentiation. The membrane anomaly shifts magnetic periods by an ambient half characteristic class. A flux superpotential pairs a realized period family with a fixed flux class. Its ordinary derivatives become physical F terms only after the Kähler potential and full field space are supplied. In the classical special no-scale class a radius remains free. None of these steps alone supplies a compact vacuum, stabilization, or a decoupled QFT.

The calculations prepare the reader to use the fields of Volume II, Chapter 8 and the charge distinctions of Volume III, Chapter 5 in geometric constructions. Chapter 2 and Volume V, Chapter 3 supply the geometric and period hypotheses. Volume VII, Chapter 8 requires the full flux geometry rather than the scalar ball model. The rank questions of Volume VIII, revised Chapter 4 require their specified Page prescription. The common lesson is to identify what is measured, what is supplied as physical input, and which further equations a construction still has to solve.

Status and sources

§IV.10.2. The period unit and integer-flux premise are those of Giddings et al. (2002, physical PDF p. 9, eq. (2.25)), in the effective framework [SUGRA]; quantization is a supplied quantum premise, not derived from classical equations. Conditional free-period reconstruction, exact-term and torsion integrals, circle holonomy, and signed matrix inversion are [MATH]. The index is $|\det M|$; the inverse retains $\det M$. The six-torus provides cycles, not a flux solution. The negative-determinant example adds explicit arithmetic within this scope; finite positive-determinant controls alone do not establish that sign property.

§IV.10.3. The self-dual five-form source equation and units are Giddings et al. (2002, physical PDF p. 8, eqs. (2.23)–(2.24), footnotes 5–6) [SUGRA]. The self-dual pseudo-action and electric source prescription are cited. The constant is not the asymptotic g_s^2 gravitational coupling. Stokes, exterior products, and the conditional shell/compact balances are [MATH]. The shell bulk integral is supplied, without asserting a compact-to-relative extension. Charge distinctions and the separate D4 Page chart follow Marolf (2000, physical PDF p. 3 and pp. 8–9, eqs. (4.1)–(4.2)) [SUGRA]. The small-gauge argument assumes global potential and gauge parameter on the closed integration surface and closed H_3. No universal Page-charge or rank theorem is inferred.

§IV.10.4. The Einstein-frame metric ansatz is Giddings et al. (2002, physical PDF p. 5, eqs. (2.2)–(2.6)) [SUGRA]. The flat-ball equation is separately stipulated. Its integrations, sphere normalization, distributional pole, positivity example, and compact constant-function obstruction are [MATH]. They do not derive the IIB source normalization or

identify the scalar density with a general physical flux density. Special GKP solutions additionally use the localized bound (2.26) on *physical PDF p. 9*, and (2.30)–(2.36) on pp. 10–11. The latter include the ISD, internal metric and axiodilaton conditions. The corrected physical-p. 9 locator is used here; no source equation is altered.

§IV.10.5. The shifted class is the cited result of Witten (1997, physical PDF p. 2, eqs. (1.1)–(1.2), pp. 6–7, §2.2, eqs. (2.3)–(2.5)) [ANOM]. Its power is one global $\mathbb{Z}_2$ determinant-sign constraint and zero locally matched anomaly-polynomial coefficients. The three example periods are not three anomaly matches. Ambient $p_1(TY)$ and the stated physical membrane units are essential. Shift arithmetic, orientation and coset equivalence are conditional [MATH]. No common embedding, differential refinement, torsion lift, electric seven-cycle charge or rank is asserted.

§IV.10.6. The physical leading flux superpotential and the one-radius effective setting are Giddings et al. (2002, physical PDF pp. 12–14, eqs. (2.37)–(2.43), pp. 29–31, eqs. (A.7), (A.12)–(A.18)) [SUGRA]. In v2, body (2.40), physical p. 13, prints $\int \Omega \wedge G_3$; appendix (A.17), physical p. 31, prints $\int G_3 \wedge \Omega$. We use the body order. Both appendix derivative formulas acquire a minus, as in (IV.10.68) and (IV.10.69). Body (2.44) uses the appendix ordering for the zero equations; the zeros are unchanged. This records a literal ordering discrepancy, not a claimed published erratum.

The symplectic expansion, polynomial coefficients, ordinary variations, inverse-metric contraction and off-shell scaling are [MATH] conditional on their displayed inputs. The period-family and Hodge hypotheses are cited, not proved. The polynomial is a formal projected pair, not a realized CY variation. The compact nonnegative constraint in GKP (2.30), physical pp. 10–11, forces saturation of the source bound in the special solution class. The large-radius reduction explicitly uses constant warping and vanishing five-form; the source-tension cancellation after (A.14), physical p. 30, additionally uses both the total D3 tadpole and that saturation. The bound alone is insufficient, as the anti-D3 example on physical p. 9 demonstrates. It does not derive an all-orders warped Kähler potential. The physical residual-radius statement concerns the classical special solutions, with the other $D_i W = 0$ and the stated source and field equations. Corrections and gravity decoupling are separate. No compact-vacuum or general stabilization result follows from these examples.

The calculations use the displayed metric, symplectic period frame, and physical membrane units. Exercises 1–5 use the stated assumptions, and Exercise 6 asks for a written interpretation. These deductions do not establish a quantum field theory identification.

References

Giddings, S. B., S. Kachru, and J. Polchinski (2002). "Hierarchies from Fluxes in String Compactifications". In: *Phys. Rev. D* 66. v2, physical PDF pp. 5, 8–14 and 29–31; equation ordering discrepancy in (2.40) versus (A.17) retained, p. 106006. DOI: 10.1103/PhysRevD.66.106006. arXiv: hep-th/0105097.

Marolf, D. (2000). *Chern-Simons terms and the Three Notions of Charge*. v1, physical PDF p. 3 and pp. 8–9, equations (4.1)–(4.2) and their global-potential qualifications. arXiv: hep-th/0006117.

Witten, E. (1997). "On Flux Quantization in M-Theory and the Effective Action". In: *J. Geom. Phys.* 22. v2, physical PDF p. 2, equations (1.1)–(1.2); pp. 6–7, section 2.2, equations (2.3)–(2.5), pp. 1–13. DOI: 10.1016/S0393-0440(96)00042-3. arXiv: hep-th/9609122.

Chapter IV.11

Mirror symmetry

IV.11.1 Which mirror dictionary

A closed string on a circle has two ways to carry an integral charge. It can move around the circle, or it can wind around it. Exchanging these charges turns a small circle into a large one. Once the circle belongs to a supersymmetric torus, the same operation changes which target-space variables appear complex to one chirality of the worldsheet theory. A transformation that began as radius inversion can therefore exchange complex structure with Kähler structure. This is the most direct physical entry into mirror symmetry.

The word mirror also appears in calculations that compare much less, or demand much more. An equality of protected rings compares selected observables after a topological twist. A categorical statement compares boundary objects, morphisms and their compositions. A full quantum-string equivalence would compare the complete theories, including the nonperturbative objects needed to interpret their branes. These comparisons have different hypotheses. Knowing one ring does not reconstruct the operator products of an untwisted theory, and knowing the topology of a torus does not supply a metric with three Killing vectors.

We will follow two concrete routes. The first starts with a free supersymmetric torus. We keep the string length explicit, map its local operators, and interpret a flat connection on a smooth fiber as a point on its dual torus. A constant positive matrix then gives a complete local model in which the complex structure, Kähler form, normalized holomorphic volume form and fiberwise duality can all be calculated. The second route starts with the quantum twisted superpotential of a specified gauged linear sigma model. Its charge constraint produces a Laurent polynomial whose coefficient invariant and singular points we can determine exactly. The result of this second calculation is a curve in an algebraic torus.

These routes meet at the geometric idea that a mirror can exchange position with flat-connection data, while quantum information changes the classical geometry. The original Strominger–Yau–Zaslow proposal gives this idea a global setting. Its global premise will be stated where we use it. The constant local model supplies a calculation

of the smooth part; the Laurent example supplies an algebraic dictionary useful for later toric constructions. Neither calculation alone constructs a general quantum mirror.

Chapter 2 supplies the Calabi–Yau geometry, Chapter 4 the toric charge relation and Chapter 6 the calibration condition. Volume II, Chapter 3 supplies physical T-duality. The preceding chapter, Chapter 10, *Fluxes and warping*, explains why a geometric background and a dynamical solution carry different information. That distinction remains useful here. Volume V develops topological twists, periods, mirror computations and categories in their own domains.

By the end of this chapter the reader should be able to distinguish the principal mirror statements, follow the free-field mirror map including its fermions and operators, construct the character torus with physical units, calculate and dualize a constant special-Lagrangian product, and recover the invariant and node condition of the conifold Laurent curve. The common misconception to avoid is that any one of these successful comparisons establishes every other version of mirror symmetry.

IV.11.2 Free fields and chiral reflection

How can a radius inversion change the supersymmetric meaning of a complex coordinate? We first determine what the transformation does to the complete free fields. Let X be a physical coordinate of period $2\pi R$, with $R > 0$, and write $X = R\theta$, where θ has period 2π. The string parameter $\alpha' > 0$ has units of length squared. The Euclidean bosonic action, before including worldsheet fermions, is

$$S_\theta = \frac{R^2}{4\pi\alpha'} \int_\Sigma d\theta \wedge *d\theta. \tag{IV.11.1}$$

The coefficient is dimensionless. In particular, replacing R by its numerical value in string units without saying so would obscure the dual radius.

A first-order form introduces a real one-form b with the normalized action

$$S_1 = \frac{\alpha'}{4\pi R^2} \int_\Sigma b \wedge *b + \frac{i}{2\pi} \int_\Sigma b \wedge d\theta. \tag{IV.11.2}$$

Gaussian elimination of b gives (IV.11.1). In the opposite order, integrating over the single-valued part of θ makes b closed. The winding sectors of θ do more than impose closedness: their integral sum restricts the periods of b to $2\pi\mathbb{Z}$. Thus $b = d\widetilde{\theta}$ locally, with $\widetilde{\theta}$ again an angle of period 2π. Substitution yields

$$S_{\widetilde{\theta}} = \frac{\alpha'}{4\pi R^2} \int_\Sigma d\widetilde{\theta} \wedge *d\widetilde{\theta}, \qquad R' = \frac{\alpha'}{R}. \tag{IV.11.3}$$

The integral-period step is essential. A noncompact Lagrange multiplier would not reconstruct the compact dual theory. This is the global ingredient of the periodic Gaussian argument; its measure and string interpretation are the physical T-duality input from Volume II, Chapter 3.

For the positive momentum–winding exchange used here, the physical left- and right-moving momenta are

$$p_L = \frac{n}{R} + \frac{wR}{\alpha'}, \qquad p_R = \frac{n}{R} - \frac{wR}{\alpha'}, \qquad (n, w) \in \mathbb{Z}^2. \tag{IV.11.4}$$

Inserting $R' = \alpha'/R$, $n' = w$ and $w' = n$ gives

$$p'_L = \frac{wR}{\alpha'} + \frac{n}{R} = p_L, \qquad p'_R = \frac{wR}{\alpha'} - \frac{n}{R} = -p_R. \tag{IV.11.5}$$

The sum and difference of the chiral squares expose the two roles of the charges,

$$p_L^2 + p_R^2 = 2\left(\frac{n^2}{R^2} + \frac{w^2R^2}{\alpha'^2}\right), \qquad \frac{\alpha'}{4}(p_L^2 - p_R^2) = nw. \tag{IV.11.6}$$

The first combination enters the energy; the signed second one enters level matching. Both survive the exchange. Equality of these two numbers is a useful check, but to identify a free conformal field theory we also need the map of local operators.

Write $X = X_L + X_R$ after continuation to the usual chiral description. The field transformation is $X'_L = X_L$ and $X'_R = -X_R$ in the dualized direction. It preserves the chiral Gaussian contractions. A general lattice vertex has the form

$$V_k = c_k \,{:}\exp\bigl(ip_L(k)X_L + ip_R(k)X_R\bigr){:}\,, \qquad k = (n, w). \tag{IV.11.7}$$

Here c_k is a lattice cocycle: its multiplication phases ensure the required mutual locality of the vertex operators. For a product of circles, the contraction part of an operator product is

$$V_k(z,\bar z)V_\ell(0) \sim \epsilon(k,\ell)\, z^{\alpha' p_L(k)\cdot p_L(\ell)/2}\bar z^{\alpha' p_R(k)\cdot p_R(\ell)/2} V_{k+\ell}(0). \tag{IV.11.8}$$

Let T exchange n_1, w_1 and leave the other charges fixed. Choose the dual cocycle by pullback,

$$\epsilon'(Tk, T\ell) = \epsilon(k,\ell), \qquad \frac{\alpha'}{2}\bigl(p_L(k)\cdot p_L(\ell) - p_R(k)\cdot p_R(\ell)\bigr) = n\cdot w_\ell + w\cdot n_\ell. \tag{IV.11.9}$$

Both contraction exponents and the integral locality pairing are preserved by the simultaneous reflection. Pullback also preserves the cocycle associativity condition. A different cocycle representative can introduce rephasing of individual operators; it does not change the operator algebra. Oscillator descendants follow by the same reflection of every right-moving derivative. Charge-conserving Gaussian multipoint functions then have the same pairwise factors. This explains why the free map is stronger than an accidental match of conformal weights.

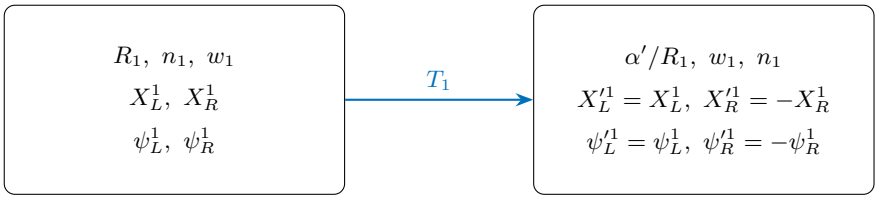
Supersymmetry forces the same transformation on the fermion in that real direction. For a flat complex torus with orthonormal real tangent labels $1, 2$, choose the usual complex combinations. Then

$$\begin{aligned} &\psi'^1_L = \psi^1_L, \quad \psi'^2_L = \psi^2_L, \qquad \psi'^1_R = -\psi^1_R, \quad \psi'^2_R = \psi^2_R, \\ &\Psi'_R = -\overline{\Psi_R}, \qquad \Psi_R = \psi^1_R + i\psi^2_R. \end{aligned} \tag{IV.11.10}$$

Reflecting the boson without its fermion would fail to map the supercurrent. The real right-moving stress tensor and $\mathcal{N} = 1$ supercurrent contain paired quadratic factors and remain invariant. The right-moving complex fermion number changes sign. Accordingly the two right-moving $\mathcal{N} = 2$ supercurrents exchange, up to constant phases, while the

left-moving pair remains fixed. Figure IV.11.1 displays this map before any geometric interpretation.

$$p'_L = p_L, \qquad p'_R = (-p_{R,1}, p_{R,2})$$



$$\Psi'_R = -\overline{\Psi_R}, \qquad J'_R = -J_R$$
$$\epsilon'(Tk, T\ell) = \epsilon(k, \ell)$$

Figure IV.11.1: First-circle duality acts on the same state and its free fields. The right-moving first real boson and fermion both reflect, preserving their real supercurrent and reversing the complex right-moving charge. The second real direction is a spectator. The charge map is integral and the cocycle is pulled back along it.

In supersymmetry language this is the mirror automorphism: it conjugates one chiral set of supercharges and exchanges vector and axial R-symmetries. A chiral multiplet becomes twisted chiral under this identification. There is a useful independent Gaussian derivation on a cylinder. In the source normalization where the radius is dimensionless, let $r = R/\sqrt{\alpha'}$. Introduce a real superfield B_{s} and a twisted chiral field Θ with D-term

$$\mathcal{L}_1 = \int d^4\vartheta \left[\frac{r^2}{4} B_{\mathrm{s}}^2 - \frac{1}{2}(\Theta + \overline{\Theta}) B_{\mathrm{s}} \right]. \tag{IV.11.11}$$

The symbol B_{s} here is an auxiliary superfield, not the target two-form. Integrating out Θ imposes the superspace constraints solved locally by $B_{\mathrm{s}} = \Phi + \overline{\Phi}$ for a chiral Φ. Up to D-terms integrating to zero, this gives

$$\mathcal{L} = \int d^4\vartheta \, \frac{r^2}{2} \Phi \overline{\Phi}. \tag{IV.11.12}$$

Eliminating B_{s} first instead gives $B_{\mathrm{s}} = (\Theta + \overline{\Theta})/r^2$ and

$$\widetilde{\mathcal{L}} = \int d^4\vartheta \left[-\frac{(\Theta + \overline{\Theta})^2}{4r^2} \right] = \int d^4\vartheta \left[-\frac{\Theta\overline{\Theta}}{2r^2} \right]. \tag{IV.11.13}$$

The sign is the source superspace convention for a twisted chiral kinetic term, not a negative physical target metric. Writing $\Phi| = u + i\theta$ and $\Theta| = \eta + i\widetilde{\theta}$, the real-field relation reads $\eta = r^2 u$. The physical target metric, with units restored, is

$$d\tilde{s}^2 = \alpha' r^{-2}(d\eta^2 + d\widetilde{\theta}^2) = R^2 du^2 + \frac{\alpha'^2}{R^2} d\widetilde{\theta}^2. \tag{IV.11.14}$$

Angular duality leaves the spectator radial coefficient unchanged. We use this superspace derivation rather than infer a component identity from an ambiguous printed line; the precise source discrepancy is recorded in Status and sources.

For a numerical state that will also test the geometric dictionary, fix a length unit and take $\alpha' = 6$, radii $(R_1, R_2) = (4, 3)$ and charges $n = (2, -1)$, $w = (-3, 2)$. Applying (IV.11.4) separately to both circles gives

$$p_L = \left(\frac{2}{4} - \frac{3\cdot 4}{6}, -\frac{1}{3} + \frac{2\cdot 3}{6}\right) = \left(-\frac{3}{2}, \frac{2}{3}\right), \qquad p_R = \left(\frac{5}{2}, -\frac{4}{3}\right). \tag{IV.11.15}$$

First-circle duality sends the full state to

$$R' = \left(\frac{3}{2}, 3\right), \quad n' = (-3, -1), \quad w' = (2, 2), \quad p'_L = \left(-\frac{3}{2}, \frac{2}{3}\right), \quad p'_R = \left(-\frac{5}{2}, -\frac{4}{3}\right). \tag{IV.11.16}$$

For instance $p'_{R,1} = (-3)/(3/2) - 2(3/2)/6 = -5/2$. The second component has not reflected. The zero-mode contributions to the two conformal weights are

$$h_0 = \frac{6}{4}\left(\frac{9}{4} + \frac{4}{9}\right) = \frac{97}{24}, \qquad \bar{h}_0 = \frac{6}{4}\left(\frac{25}{4} + \frac{16}{9}\right) = \frac{289}{24}, \qquad h_0 - \bar{h}_0 = -8 = n \cdot w. \tag{IV.11.17}$$

Oscillator levels and the relevant sector complete the physical-state condition; this example need not be a level-matched oscillator ground state. A second application restores the radii, charges, reflected oscillators and fermions. With the cocycle choices transported consistently, it restores the free operator algebra as well. The sourced spin-structure and GSO map is still needed to embed this free statement into a chosen string theory.

The physical conclusion is now precise. The free supersymmetric torus realizes a mirror automorphism through a field transformation, with the global winding sum supplying the compact dual coordinate. The important pitfall is to replace that argument by weight matching alone. Volume V, Chapter 1 will retain selected observables under a twist; here we have first identified the untwisted free fields whose complex supersymmetry is exchanged.

IV.11.3 Complex structure and dual positions

What geometric quantities are exchanged by the first-circle map, and where does a flat connection go? Begin with a rectangular two-torus, vanishing target B field and positive radii. With the first period chosen to be real, its complex coordinate and periods are

$$z = R_1\theta_1 + iR_2\theta_2, \qquad z \sim z + 2\pi R_1 \sim z + 2\pi i R_2. \tag{IV.11.18}$$

Dividing the second period by the first defines its complex structure. The Kähler coordinate on this slice follows from the dimensionless area in the book normalization,

$$\tau = i\frac{R_2}{R_1}, \qquad J = R_1 R_2\, d\theta_1 \wedge d\theta_2, \qquad \rho = \frac{i}{4\pi^2\alpha'}\int_{T^2} J = i\frac{R_1 R_2}{\alpha'}. \tag{IV.11.19}$$

Thus ρ is the book complexified Kähler period for this $B = 0$ torus. The factor $4\pi^2$ comes from integrating both angles. A radius has units of length whereas both τ and ρ are dimensionless.

Dualize the first circle and retain the same positive angular periods in the dual geometry. Then

$$\tau' = i\frac{R_2}{\alpha'/R_1} = i\frac{R_1R_2}{\alpha'} = \rho, \qquad \rho' = i\frac{(\alpha'/R_1)R_2}{\alpha'} = i\frac{R_2}{R_1} = \tau. \tag{IV.11.20}$$

This is the geometric meaning of the supersymmetry conjugation in the preceding section. It compares a shape parameter with an area parameter in different sigma models. It does not identify the two metrics on the same target. The declared first period matters: a commonly used source chart divides by the second period and implements the analogous exchange by dualizing the second circle. Its denominator cannot be copied into (IV.11.20) while keeping our first-circle map.

In the nonunit example above the calculation becomes

$$(\tau,\rho) = \left(\frac{3i}{4}, 2i\right), \qquad (\tau',\rho') = \left(2i, \frac{3i}{4}\right), \qquad \int J = 48\pi^2, \quad \int J' = 18\pi^2. \tag{IV.11.21}$$

The areas differ, but after dividing by $4\pi^2\alpha' = 24\pi^2$ they give 2 and 3/4, exactly the imaginary parts of ρ and ρ'. This is also a check on the units and period convention. We have derived the exchange only for the rectangular $B = 0$ slice. A tilted metric or a nonzero two-form needs the more general torus dictionary of Volume II, Chapter 3.

The next geometric question concerns the degrees of freedom that become positions. Let L be an actually realized smooth T^3, with fixed oriented cycles γ_i and angular coordinates θ_i of period 2π. On a trivial line bundle take a flat unitary connection in the real-potential convention

$$A = \sum_{i=1}^{3} a_i\, d\theta_i, \qquad F = dA = 0, \qquad \mathrm{Hol}_{\gamma_i}(A) = \exp(2\pi i a_i). \tag{IV.11.22}$$

A large gauge transformation generated by an integral character changes a_i by an integer. For a general integral cycle $k_1\gamma_1 + k_2\gamma_2 + k_3\gamma_3$, multiplicativity of holonomy gives

$$\chi_a(k) = \exp(2\pi i\, k\cdot a), \qquad a \in \mathbb{R}^3/\mathbb{Z}^3, \qquad \widehat{L} = \mathrm{Hom}(H_1(L,\mathbb{Z}), U(1)) \simeq T^3. \tag{IV.11.23}$$

This construction is the character torus. The group $H_1(L,\mathbb{Z}) = \mathbb{Z}^3$, its generator basis and the flat unitary hypothesis are doing the work. A statement that $b_1 = 3$ alone would retain only the rank of the free part; it would not prove that an arbitrary three-cycle is a torus or eliminate torsion sectors. In this example the trivial-bundle assumption and the topology of T^3 keep those extra questions absent.

The mathematical classification (IV.11.23) gives a torus without fixing its physical radii. To supply those, use the local isometric T-duality identification and choose

positive dual angles. For a product fiber with physical radii R_i, it reads

$$R_i' = \frac{\alpha'}{R_i}, \qquad \frac{\widetilde{\theta}_i}{2\pi} = a_i \pmod{\mathbb{Z}}, \qquad \widetilde{X}_i = R_i'\widetilde{\theta}_i = 2\pi R_i'(a_i \bmod 1) \pmod{2\pi R_i'}. \tag{IV.11.24}$$

The source boundary-coordinate comparison can be checked in physical coordinates: $A_{X_i} = a_i/R_i$ and the positive endpoint map is $\widetilde{X}_i = 2\pi\alpha' A_{X_i}$. It gives exactly (IV.11.24). A negative-potential convention reverses the corresponding angle. Once the potential sign and circle orientation have been fixed, that reversal is a translation of conventions rather than a missing physical minus sign.

For $\alpha' = 6$ and original radii $(4, 3, 5)$, take $a = (1/3, -2/5, 7/6)$. Reducing each entry modulo the integral lattice gives

$$a \bmod 1 = \left(\frac{1}{3}, \frac{3}{5}, \frac{1}{6}\right), \qquad R' = \left(\frac{3}{2}, 2, \frac{6}{5}\right), \qquad \frac{\widetilde{X}}{2\pi} = \left(\frac{1}{2}, \frac{6}{5}, \frac{1}{5}\right). \tag{IV.11.25}$$

For example $-2/5 + 1 = 3/5$, so the second physical position divided by 2π is $2(3/5) = 6/5$. The third is $(6/5)(1/6) = 1/5$. All three are in their fundamental physical intervals $[0, R_i')$. The positions are positive in the chosen orientation even when the initial representative of a holonomy parameter was negative.

One can check the same point without any radius. A cycle with $k = (2, -1, 3)$ measures

$$k \cdot a = \frac{2}{3} + \frac{2}{5} + \frac{7}{2} = \frac{137}{30}, \qquad k \cdot (a \bmod 1) = \frac{2}{3} - \frac{3}{5} + \frac{1}{2} = \frac{17}{30}. \tag{IV.11.26}$$

The difference is 4, and the two holonomies are identical. This calculation explains why one must reduce angles modulo integers rather than regard a_i as unrestricted physical positions. It also checks all three components of the character simultaneously. Figure IV.11.2 places the reduced fractions alongside their circumferences.

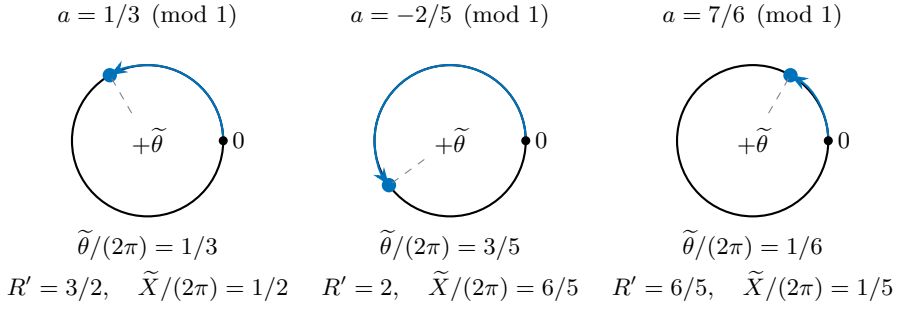


Figure IV.11.2: Three factors of the character torus in the nonunit example. Each circle is parametrized counterclockwise from the marked origin by $\widetilde{\theta}_i/(2\pi)$. Blue points represent the reduced fractions. The physical circumference is $2\pi R_i'$, so equal angular fractions on unequal circles would still represent unequal physical distances. The circles are shown at a common drawing radius to keep the fractional coordinates legible.

A flat connection therefore supplies precisely the extra angular coordinates needed to accompany deformations of a smooth fiber. The geometric group calculation and the physical position map are separate statements: the first classifies flat line systems, while the second uses T-duality. This is the local ingredient of the SYZ picture. Chapter 6 supplies the condition selecting special-Lagrangian fibers, which we now realize in a metric. Volume V, Chapter 6 will ask for the additional boundary operations required for a categorical comparison; a point of $\widehat{L}$ by itself does not give that category or a brane spectrum.

IV.11.4 A special Lagrangian product

What must a smooth fiber satisfy before its flat connections can be used in the mirror picture? The fiber must first be Lagrangian, and its holomorphic volume form must have a constant phase relative to its metric volume. We can build a local geometry in which both assertions can be derived in full. This will also fix the normalization needed to speak about a calibration rather than just a complex period.

Let $U \subset \mathbb{R}^3$ be an open base patch. Its coordinates x_i and the fiber angles $\theta_i \in \mathbb{R}/(2\pi\mathbb{Z})$ are dimensionless. Choose a constant real symmetric positive-definite matrix H. The product metric is

$$ds^2 = \alpha' \left(dx^T H\, dx + d\theta^T H^{-1} d\theta \right), \qquad B = 0. \tag{IV.11.27}$$

Constancy makes this a flat local metric with genuine fiber isometries. Positive definiteness gives a positive length for every nonzero real tangent vector and permits the inverse and positive square root of H. No metric equation or global existence assertion is hidden in the choice: we are constructing this particular local product.

The complex coordinates and Hermitian coefficient in the book convention are

$$z = x + iH^{-1}\theta, \qquad g_{a\bar{b}} = \frac{\alpha'}{2} H_{ab}, \qquad ds^2 = 2 g_{a\bar{b}}\, dz^a d\bar{z}^b. \tag{IV.11.28}$$

To verify this directly, expand $dz = dx + iH^{-1}d\theta$. Symmetry of H cancels the imaginary cross terms in the metric, leaving $\alpha' H$ on the base and $\alpha' H^{-1}$ on the fiber. The same expansion for the Kähler form gives

$$J = i\frac{\alpha'}{2} H_{ab}\, dz^a \wedge d\bar{z}^b = \alpha' \sum_{i=1}^{3} dx_i \wedge d\theta_i, \qquad dJ = 0. \tag{IV.11.29}$$

The factor $1/2$ in g matters. Doubling g would double both the metric and J and spoil the volume normalization below. On a fiber L_{x_0} with $x = x_0$, every dx_i pulls back to zero; hence $J|_{L_{x_0}} = 0$.

The metric volume also fixes the magnitude of the holomorphic three-form. Introduce orthonormal real coframes

$$e = \sqrt{\alpha'}\, H^{1/2} dx, \qquad f = \sqrt{\alpha'}\, H^{-1/2} d\theta, \qquad ds^2 = e^T e + f^T f. \tag{IV.11.30}$$

Since $e + if = \sqrt{\alpha'} H^{1/2} dz$, the unit-normalized form is

$$\Omega_{\text{unit}} = \bigwedge_{i=1}^{3} (e^i + if^i) = \alpha'^{3/2} \sqrt{\det H}\, dz^1 \wedge dz^2 \wedge dz^3. \tag{IV.11.31}$$

For this constant geometry the form is closed. Its normalization can also be checked against the oriented ambient volume,

$$\frac{i}{8} \Omega_{\text{unit}} \wedge \overline{\Omega}_{\text{unit}} = \frac{J^3}{3!}. \tag{IV.11.32}$$

This identity uses the orientation determined by J^3. It is a statement about the metric normalization of a differential form, not about the arbitrary holomorphic scale of a period vector.

Orient the fiber by $d\theta_1 \wedge d\theta_2 \wedge d\theta_3 > 0$. Its tangent Gram matrix and positive volume form are

$$K_{ij} = \langle \partial_{\theta_i}, \partial_{\theta_j} \rangle = \alpha' (H^{-1})_{ij}, \qquad \text{vol}_L = \frac{\alpha'^{3/2}}{\sqrt{\det H}}\, d\theta_1 \wedge d\theta_2 \wedge d\theta_3. \tag{IV.11.33}$$

On this fiber, $dz = iH^{-1} d\theta$. Taking its determinant gives

$$\Omega_{\text{unit}}|_L = \alpha'^{3/2} \sqrt{\det H}\, i^3 \det(H^{-1})\, d\theta_1 \wedge d\theta_2 \wedge d\theta_3 = -i\ \text{vol}_L\,. \tag{IV.11.34}$$

Thus the phase of this positively oriented fiber is $-\pi/2$, and

$$\phi_{-\pi/2} = \text{Re}(i\Omega_{\text{unit}}), \qquad \phi_{-\pi/2}|_L = \text{vol}_L\,. \tag{IV.11.35}$$

A real rescaling of Ω would leave the Lagrangian condition unchanged but would alter this equality. The phase and the normalization have different jobs.

For completeness, the flat local comass bound follows directly in the coframe (IV.11.30). For an oriented orthonormal real three-frame v_j, form the complex matrix $Z_{ij} = (e^i + if^i)(v_j)$. Each column has complex norm one. Hadamard's determinant inequality then gives $|\det Z| \le 1$, so $\text{Re}(i\Omega_{\text{unit}})$ evaluates to at most one on that frame. Together with closedness, this proves that the displayed form is a calibration on the patch. Chapter 6 states the geometric minimization theorem: an existing compact calibrated cycle minimizes ordinary volume in its real homology class, under the stated metric and closedness hypotheses. We are not constructing every representative of that class or deriving its quantum BPS spectrum.

Now choose the genuinely mixed example

$$H = \begin{pmatrix} 4 & 1 & 0 \\ 1 & 3 & 1 \\ 0 & 1 & 2 \end{pmatrix}, \qquad \alpha' = 6. \tag{IV.11.36}$$

The leading principal minors are 4, $4 \cdot 3 - 1 = 11$ and

$$\det H = 4(3 \cdot 2 - 1) - 1(1 \cdot 2 - 0) = 20 - 2 = 18. \tag{IV.11.37}$$

All are positive, so Sylvester's criterion establishes positive definiteness. The cofactor matrix is

$$\operatorname{cof}(H) = \begin{pmatrix} 5 & -2 & 1 \\ -2 & 8 & -4 \\ 1 & -4 & 11 \end{pmatrix}, \qquad H^{-1} = \frac{1}{18}\begin{pmatrix} 5 & -2 & 1 \\ -2 & 8 & -4 \\ 1 & -4 & 11 \end{pmatrix}. \tag{IV.11.38}$$

For example the $(1,3)$ cofactor comes from $\det\left(\begin{smallmatrix} 1 & 3 \\ 0 & 1 \end{smallmatrix}\right) = 1$; the $(2,3)$ cofactor carries the minus sign and gives -4. These are the offdiagonal terms that a diagonal-radius intuition would miss.

Multiplication verifies the inverse without relying on a list of entries. The first row of $H\operatorname{cof}(H)$ is $(20-2, -8+8, 4-4) = (18,0,0)$. The remaining rows are

$$(5-6+1, -2+24-4, 1-12+11) = (0,18,0), \qquad (-2+2, 8-8, -4+22) = (0,0,18). \tag{IV.11.39}$$

Dividing by 18 gives the identity. All entries of the fiber metric are therefore constrained by one geometric inverse relation, rather than chosen independently.

The physical base and fiber blocks, and the Hermitian coefficient, are

$$G_B = \begin{pmatrix} 24 & 6 & 0 \\ 6 & 18 & 6 \\ 0 & 6 & 12 \end{pmatrix}, \qquad G_F = \begin{pmatrix} 5/3 & -2/3 & 1/3 \\ -2/3 & 8/3 & -4/3 \\ 1/3 & -4/3 & 11/3 \end{pmatrix}, \qquad g = 3H. \tag{IV.11.40}$$

As a direct tangent-vector check, $v = (1,2,-1)$ satisfies $\operatorname{cof}(H)v = (0,18,-18)$, and hence

$$v^T G_F v = \frac{1}{3}(0 + 36 + 18) = 18. \tag{IV.11.41}$$

Keeping only diagonal entries would instead give $5/3 + 4(8/3) + 11/3 = 16$. The mixed terms affect a measurable length, not just the appearance of the matrix. The same issue will matter when we invert the fiber metric.

The complex coordinates in this example display the mixing explicitly,

$$\begin{aligned} z^1 &= x_1 + \frac{i}{18}(5\theta_1 - 2\theta_2 + \theta_3), \\ z^2 &= x_2 + \frac{i}{18}(-2\theta_1 + 8\theta_2 - 4\theta_3), \\ z^3 &= x_3 + \frac{i}{18}(\theta_1 - 4\theta_2 + 11\theta_3). \end{aligned} \tag{IV.11.42}$$

Finally $\det G_F = 6^3/18 = 12$, so $\sqrt{\det G_F} = 2\sqrt{3}$ and $\operatorname{Vol}(L) = (2\pi)^3\, 2\sqrt{3}$. Meanwhile the coefficient of $dz^1 \wedge dz^2 \wedge dz^3$ in Ω_{unit} is $6^{3/2}\sqrt{18} = 36\sqrt{3}$. On the fiber its determinant factor is $-i/18$, giving $-2i\sqrt{3}$ times the angular volume form, exactly as in (IV.11.34). Figure IV.11.3 shows the corresponding normalized tangent plane.

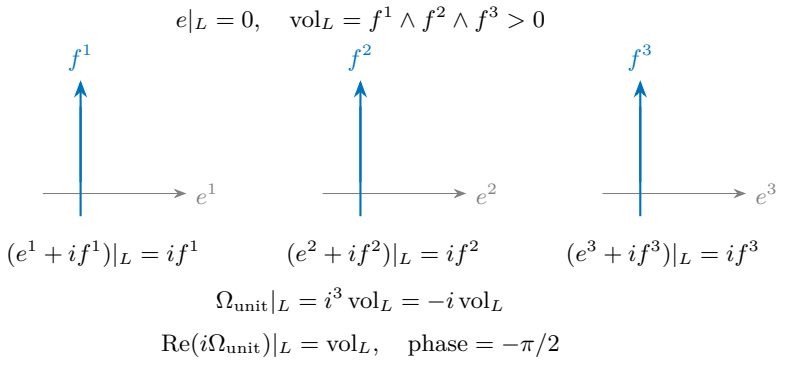


Figure IV.11.3: In the normalized coframes the fiber has $e = 0$ and positive ordered tangent directions f_1, f_2, f_3. Each complex one-form restricts to if_i, so their product has phase $i^3 = -i$. The three displayed planes are tangent-space factors after orthonormalization, not a claim that the integral fiber lattice diagonalizes in that frame. The actual angular Gram matrix remains $6H^{-1}$.

The calculation makes the special-Lagrangian condition concrete: vanishing J selects the tangent type, while the normalized Ω fixes the signed phase relative to positive volume. A varying or arbitrarily rescaled form would require fresh closure and normalization checks. The pitfall is to read a complex determinant as an energy or a calibration before comparing it with the full Gram volume. With that comparison completed, we can ask what isometric fiberwise duality does to this same geometry.

IV.11.5 Inverting the fibers

Does the dual metric exchange the base and fiber automatically? Buscher duality inverts the fiber block in fixed base coordinates. A separate Legendre change of base coordinates is what puts the answer into the same geometric form as the original metric. Keeping these two steps apart explains the inverse matrices and the factors of α'.

We remain on the constant patch of the preceding section, with $B = 0$, vanishing mixed base–fiber block and an initial constant physical dilaton Φ. All three angle translations are commuting Killing symmetries. Define the dimensionless fiber coefficient $E_F = G_F/\alpha' = H^{-1}$. Simultaneous dualization of these free angles yields

$$E'_F = E_F^{-1} = H, \qquad G'_F = \alpha'^2 G_F^{-1} = \alpha' H, \qquad G'_B = \alpha' H. \tag{IV.11.43}$$

For a single physical circle the same equation says $R'^2 = \alpha'^2/R^2$. Inserting just G_F^{-1} as a physical metric would have the wrong length units. Offdiagonal entries do not permit independent reciprocal operations on entries: the inverse is the full matrix inverse. The physical dual metric in the original base coordinates is

$$ds'^2 = \alpha' \left(dx^T H\, dx + d\widetilde{\theta}^T H\, d\widetilde{\theta} \right), \qquad \widetilde{\theta}_i \sim \widetilde{\theta}_i + 2\pi. \tag{IV.11.44}$$

The base has not yet changed. The dual angular coordinates can be identified with $2\pi a_i$ of the character torus in the preceding section, using the sourced physical dictionary.

The Gaussian measure gives the accompanying physical dilaton transformation

$$\Phi' = \Phi - \frac{1}{2}\log\det(G_F/\alpha') = \Phi + \frac{1}{2}\log\det H. \tag{IV.11.45}$$

It is constant because H is constant. As a consistency check on the toroidal measure, the fiber density is unchanged,

$$e^{-2\Phi'}\sqrt{\det G'_F} = \frac{e^{-2\Phi}}{\det H}\,\alpha'^{3/2}\sqrt{\det H} = e^{-2\Phi}\sqrt{\det G_F}. \tag{IV.11.46}$$

This check uses the physical dilaton of the sigma model. It does not identify that field with every scalar carrying the same letter in a geometric discussion. For variable coefficients the shift is generally variable and the simplifying statement here would no longer hold.

To recognize the block exchange, let $K(x) = x^T Hx/2$ be the strictly convex quadratic potential. Its Hessian is H. The Legendre coordinate and transform are

$$x' = \frac{\partial K}{\partial x} = Hx, \qquad K^*(x') = x'^T x - K(x) = \frac{1}{2}x'^T H^{-1}x', \qquad dx = H^{-1}dx'. \tag{IV.11.47}$$

The base block then transforms by pullback,

$$dx^T H dx = dx'^T H^{-1} dx', \qquad ds'^2 = \alpha'\left(dx'^T H^{-1}dx' + d\widetilde{\theta}^T H d\widetilde{\theta}\right). \tag{IV.11.48}$$

This is the original form with H replaced by H^{-1}. The Legendre map is a local coordinate change on the base, not an integral change of the angular lattice. It acts on an open patch where H is invertible. Figure IV.11.4 separates the physical inversion from this coordinate change.

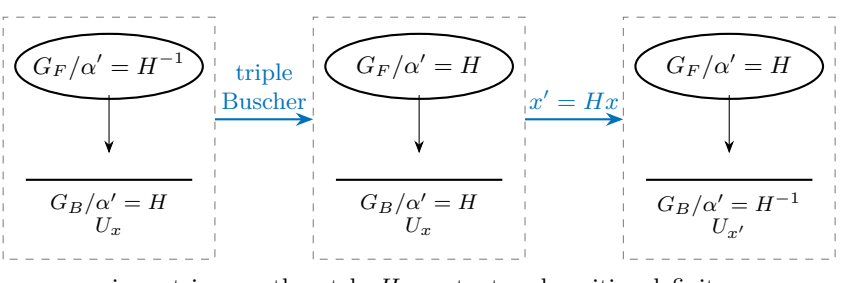


Figure IV.11.4: All matrices are dimensionless coefficients of ds^2/α'. Triple Buscher duality inverts the full fiber matrix while the original base coordinate x remains fixed. Pullback under $x' = Hx$ then rewrites the base with coefficient H^{-1}. Dashed boundaries indicate the edge of the chosen smooth patch; no singular fiber or global gluing is supplied by this diagram.

The geometric structures in the dual chart follow without a new ansatz. With the same book normalization they are

$$z' = x' + iH\widetilde{\theta}, \qquad J' = \alpha' \sum_i dx'_i \wedge d\widetilde{\theta}_i, \qquad \Omega'_{\mathrm{unit}} = \frac{\alpha'^{3/2}}{\sqrt{\det H}}\, dz'^1 \wedge dz'^2 \wedge dz'^3. \tag{IV.11.49}$$

They are closed in this constant model. The same positive dual angular orientation gives phase $-\pi/2$. This statement follows by replacing H with H^{-1} in the normalized-coframe computation, so it again compares the actual dual Gram volume with Ω'_{unit}.

For the matrix (IV.11.36) at $\alpha' = 6$, the complete dual fiber and Legendre-base blocks are

$$G'_F = \begin{pmatrix} 24 & 6 & 0 \\ 6 & 18 & 6 \\ 0 & 6 & 12 \end{pmatrix}, \qquad G'_{B,x'} = \begin{pmatrix} 5/3 & -2/3 & 1/3 \\ -2/3 & 8/3 & -4/3 \\ 1/3 & -4/3 & 11/3 \end{pmatrix}. \tag{IV.11.50}$$

The two products giving these blocks are

$$36(6H^{-1})^{-1} = 6H, \qquad (H^{-1})^T(6H)H^{-1} = 6H^{-1}. \tag{IV.11.51}$$

These products explain every component, including the zero $(1,3)$ entry of G'_F and the nonzero $(1,3)$ entry of the transformed base. They are not obtained by taking reciprocals of the individual fractions.

The coordinate map in this example is

$$x'_1 = 4x_1 + x_2, \qquad x'_2 = x_1 + 3x_2 + x_3, \qquad x'_3 = x_2 + 2x_3. \tag{IV.11.52}$$

For a base displacement $dx = (1,0,0)^T$, the original squared length is 24. Its image is $dx' = (4,1,0)^T$, and $G'_{B,x'}dx' = (6,0,0)^T$, again giving 24. This verifies the pullback on a displacement with nonzero image components. The fiber volume and coupling change are

$$\sqrt{\det G'_F} = \sqrt{6^3 \cdot 18} = 36\sqrt{3}, \qquad \Phi' - \Phi = \frac{1}{2}\log 18, \qquad \frac{e^{\Phi'}}{e^{\Phi}} = \sqrt{18}. \tag{IV.11.53}$$

The ratio of dual to original fiber volumes is 18, and the squared coupling ratio is also 18, consistent with (IV.11.46). The local coordinate periods and the dimensionful metric must both be retained to see this relation.

A simple degenerating family locates the algebraic obstruction. For $H_\varepsilon = \mathrm{diag}(\varepsilon, 2, 3)$ with $\varepsilon > 0$,

$$(G_F)_{11} = \frac{\alpha'}{\varepsilon}, \qquad (G'_F)_{11} = \alpha'\varepsilon, \qquad x'_1 = \varepsilon x_1, \qquad \Phi' - \Phi = \frac{1}{2}\log(6\varepsilon). \tag{IV.11.54}$$

At $\varepsilon = 0$, H_ε^{-1} and the invertible Legendre chart cease to exist. The original first fiber coefficient diverges while the dual one tends to zero. This family diagnoses failure of inversion; it is not a metric model of a singular Calabi–Yau fiber. In particular it gives no estimate of a disk correction or identification of the physical singular locus.

The original SYZ local calculation compares a tree-level brane-moduli metric with an isometric fiberwise dual metric. Our constant product realizes the relevant inverse blocks in a controlled example, with normalized special-Lagrangian fibers and flat-connection coordinates. An actual global construction must also determine how these patches glue and what happens where the smooth-fiber hypotheses fail. The pitfall is to replace the Killing-vector condition by the existence of a topological torus fibration. Chapter 10, *Fluxes and warping*, supplies further reasons to distinguish a formal geometric operation from a full background solution. Volume V, Chapters 3 and 4 will use mirror data to compute periods while preserving that distinction.

IV.11.6 From a gauge theory to a Laurent curve

How can a charge relation become the coefficient of a mirror polynomial? For a toric example we must first say which quantum field theory supplies the polynomial. The starting point is the Hori–Vafa result for a specified $U(1)$ gauged linear sigma model, with its periodic dual fields and exact twisted superpotential. The exponential terms in that result contain quantum information. The algebra that follows will use this result as a physical premise; it will not derive the quantum potential from a Newton polygon.

Use the source order of the four charged chiral fields, whose charges are $Q = (-1,-1,+1,+1)$. Dualizing their phases produces neutral twisted chiral variables Y_i with imaginary period $2\pi i$. These are different fields from the original charged chirals. With Σ the twisted chiral gauge field strength, the source result is

$$\widetilde{W} = \Sigma\left(\sum_{i=1}^{4} Q_i Y_i - t_{\mathrm{HV}}\right) + \mu\sum_{i=1}^{4} e^{-Y_i}, \qquad Y_i \sim Y_i + 2\pi i. \tag{IV.11.55}$$

The scale μ and the source complex FI parameter t_{HV} are kept with their source normalization. The linear coupling arises in phase dualization; the exponentials are the imported quantum contribution. The word twisted describes a supersymmetric F-term here and does not by itself establish a calculation in a topologically twisted worldsheet theory.

For the indicated nonzero-t geometric regime, eliminate Σ. Its equation imposes a constraint, and exponentiation turns it into a multiplicative one,

$$-Y_1 - Y_2 + Y_3 + Y_4 = t_{\mathrm{HV}}, \qquad X_i = e^{-Y_i} \neq 0, \qquad \frac{X_3X_4}{X_1X_2} = e^{-t_{\mathrm{HV}}}. \tag{IV.11.56}$$

Imaginary periods make each X_i single-valued and nonzero. If $\lambda = e^{t_{\mathrm{HV}}}$, solving for X_1 gives

$$X_1 = \lambda\frac{X_3X_4}{X_2}, \qquad \widetilde{W} = \mu\left(X_2 + X_3 + X_4 + \lambda\frac{X_3X_4}{X_2}\right). \tag{IV.11.57}$$

The ratios $x = X_3/X_2$ and $y = X_4/X_2$ are valid because all X_i are nonzero. They isolate a Laurent polynomial,

$$H_{\mathrm{curve}}(x,y) = \frac{\widetilde{W}}{\mu X_2} = 1 + x + y + \lambda xy, \qquad x,y \in \mathbb{C}^*, \qquad q_{\mathrm{book}} = e^{-t_{\mathrm{HV}}} = \lambda^{-1}. \tag{IV.11.58}$$

Here H_{curve} denotes a polynomial, whereas H in the local metric denoted a real matrix. The displayed zero locus is a complex curve in $(\mathbb{C}^*)^2$. Dividing a potential by μX_2 isolates this zero-curve algebra; it does not eliminate a dynamical field from the entire Landau–Ginzburg theory. In particular this division does not construct a mirror threefold or determine a full sigma-model metric.

The exact order of the four monomials records the original charge constraint. After division by X_2, their source-ordered exponents are

source field	X_1	X_2	X_3	X_4
monomial	xy	1	x	y
v_i	$(1,1)$	$(0,0)$	$(1,0)$	$(0,1)$
Q_i	-1	-1	$+1$	$+1$

. (IV.11.59)

The four points form a unit square in the fixed exponent lattice. Adding a height coordinate gives the integral matrix

$$A = \begin{pmatrix} 1 & 1 & 1 & 1 \\ 1 & 0 & 1 & 0 \\ 1 & 0 & 0 & 1 \end{pmatrix}, \qquad AQ^T = 0. \tag{IV.11.60}$$

The first row says $\sum_i Q_i = 0$; the other rows say $\sum_i Q_i v_i = 0$. One can recover the entire kernel directly. If $Ar = 0$, the last two equations give $r_3 = r_4 = -r_1$, and the first then gives $r_2 = r_1$. Thus

$$\ker_{\mathbb{Z}} A = \mathbb{Z}(1,1,-1,-1) = \mathbb{Z}Q. \tag{IV.11.61}$$

The two opposite sign choices generate the same lattice. A change of sign in only one entry would not. For instance changing Q_1 to $+1$ makes both the height sum and each coordinate sum equal to 2. The affine relation, rather than merely the shape of an unlabelled square, fixes the invariant.

For comparison with Chapter 4, put the fields in book toric order,

$$(Z_1, Z_2, Z_3, Z_4) = (X_2, X_3, X_4, X_1). \tag{IV.11.62}$$

The source charge row becomes

$$\begin{aligned} Q_{\mathrm{HV,reordered}} &= (-1,+1,+1,-1) = -Q_{\mathrm{book}}, \\ Q_{\mathrm{book}} &= (1,-1,-1,1), \qquad t_{\mathrm{ordered}} = -t_{\mathrm{HV}}. \end{aligned} \tag{IV.11.63}$$

Indeed multiplying the reordered constraint by -1 changes its FI right-hand side as well. Flipping the generator while leaving t unchanged would change the equation. The equality in (IV.11.63) concerns the source constraint normalization. It is not an identification of t_{HV} with the book's dimensionful Kähler integral on an arbitrary curve. The action-weight parameter q_{book} in (IV.11.58) retains the declared source translation.

At $\lambda = 5/2$, the normalized example is

$$H_{\mathrm{curve}} = 1 + x + y + \frac{5}{2}xy, \qquad (c_1, c_2, c_3, c_4) = \left(\frac{5}{2}, 1, 1, 1\right), \qquad q_{\mathrm{book}} = \frac{2}{5}. \tag{IV.11.64}$$

The coefficient order is $(xy, 1, x, y)$, inherited from (X_1, X_2, X_3, X_4), rather than the visual order of a polygon traversal. A scale and coordinate change give an equivalent coefficient description. For example take $H'_{\text{curve}} = 3H_{\text{curve}}(2x, -y)$; then

$$H'_{\text{curve}} = 3 + 6x - 3y - 15xy, \qquad \frac{c'_3 c'_4}{c'_1 c'_2} = \frac{6(-3)}{(-15)3} = \frac{2}{5}. \tag{IV.11.65}$$

The negative rational coefficients are legitimate complex torus-coordinate rescalings. They do not change the affine charge relation. The next section derives this invariance generally and asks when the zero curve itself becomes singular. Figure IV.11.5 keeps the charge labels and height relation visible.

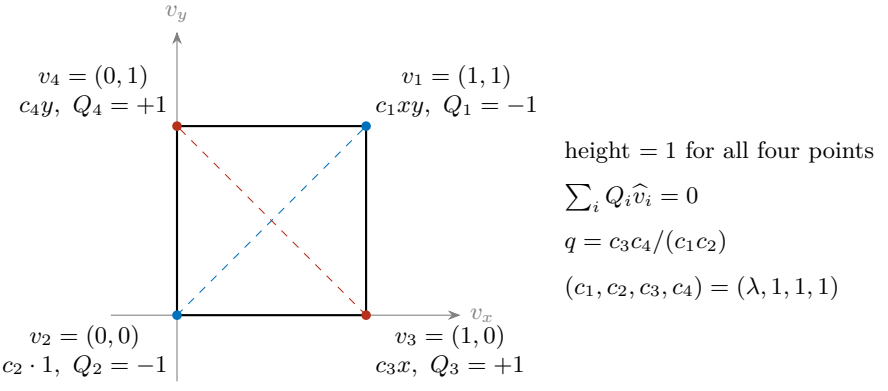


Figure IV.11.5: The four exponent vectors are labelled in source order, with all height coordinates equal to one. Opposite diagonals obey $\widehat{v}_1 + \widehat{v}_2 = \widehat{v}_3 + \widehat{v}_4$, where $\widehat{v}_i = (1, v_i)$. The source charges are $(-1, -1, +1, +1)$. The invariant uses all four coefficients and equals $1/\lambda$ for the normalized polynomial. This lattice relation supplies no five-brane dynamics.

The useful output for later toric constructions is a precisely ordered Laurent curve with an invariant coefficient ratio. Volume VII, Chapter 4 uses a Laurent curve and its Newton polygon in the NS5/D5 setting; that physical realization needs its own dictionary. Volume V, Chapters 3 and 4 will explain how to extract period information from appropriate mirror geometry. The pitfall here is to make that later physics a consequence of the elementary division in (IV.11.58). Our derivation establishes the curve algebra conditional on the imported quantum potential.

IV.11.7 Coefficients and singular points

Which part of the four coefficients is intrinsic, and how can a stationary point fail to be a curve singularity? Both questions can be answered within the Laurent chart. Keep all four coefficients nonzero and write the general polynomial in source order,

$$P(x, y) = c_1 xy + c_2 + c_3 x + c_4 y = a + bx + cy + dxy, \qquad (a, b, c, d) = (c_2, c_3, c_4, c_1). \tag{IV.11.66}$$

The two notations serve different purposes. The c_i preserve the charge order; a, b, c, d make differentiation transparent. Confusing those orders would invert or scramble the parameter extracted from the curve.

Let $C, s, t \in \mathbb{C}^*$ multiply the polynomial and rescale x, y. They act on the coefficients as

$$P'(x,y) = CP(sx,ty), \qquad (c_1', c_2', c_3', c_4') = (Cst\,c_1, Cc_2, Cs\,c_3, Ct\,c_4). \tag{IV.11.67}$$

Consequently the product determined by the charge relation is invariant,

$$q = \prod_{i=1}^{4} c_i^{Q_i} = \frac{c_3 c_4}{c_1 c_2}, \qquad q' = \frac{(Csc_3)(Ctc_4)}{(Cstc_1)(Cc_2)} = q. \tag{IV.11.68}$$

The cancellation of C is $\sum Q_i = 0$; cancellation of s, t is $\sum Q_i v_i = 0$. A common Laurent multiplication $x^u y^v$ translates every exponent by (u, v) and leaves those relations unchanged. It is invertible on $(\mathbb{C}^*)^2$, so it leaves the zero locus unchanged too. This is why the Newton polygon is meaningful up to a common lattice translation.

Conversely the invariant parametrizes the four-nonzero-coefficient square chart after these rescalings. Set $C = 1/a$, $s = a/b$ and $t = a/c$. Then

$$\frac{1}{a} P\left(\frac{a}{b}x, \frac{a}{c}y\right) = 1 + x + y + \frac{ad}{bc}xy, \qquad \lambda = \frac{ad}{bc} = q^{-1}. \tag{IV.11.69}$$

This requires $a, b, c \neq 0$. With $d \neq 0$ the square retains all four monomials and $q \neq 0$. It proves the completeness of the coefficient ratio within the specified rescaling freedom. It does not classify other Newton polygons or boundary charts with missing coefficients.

For the two coefficient examples, the first has $(a, b, c, d) = (1, 1, 1, 5/2)$ and $q = 2/5$. The second has $(6, 2, 3, 1)$ and $q = 1$. The latter normalizes by $C = 1/6$, $s = 3$, $t = 2$ to

$$\frac{1}{6} P(3x, 2y) = 1 + x + y + xy = (1 + x)(1 + y). \tag{IV.11.70}$$

The factorization suggests an intersection, but to identify a singularity in the torus we should check the gradient and zero value separately.

For a hypersurface $P = 0$ in $(\mathbb{C}^*)^2$, a singular point must have $P = 0$ and both first derivatives zero. Logarithmic derivatives $x\partial_x P$, $y\partial_y P$ give the same condition because $x, y \neq 0$. Ordinary differentiation gives

$$\partial_x P = b + dy, \qquad \partial_y P = c + dx, \qquad (x_*, y_*) = \left(-\frac{c}{d}, -\frac{b}{d}\right). \tag{IV.11.71}$$

With all four coefficients nonzero this point lies inside the torus. Substitution into the function, rather than just into its derivatives, gives

$$P(x_*, y_*) = a - \frac{bc}{d} = \frac{ad - bc}{d}, \qquad \Delta = ad - bc = c_1 c_2 (1 - q). \tag{IV.11.72}$$

Thus $\Delta = 0$, or $q = 1$, is the singular-curve condition in this chart. The gradient equation alone identifies a stationary point of a function on the ambient torus. It need not select any point of its zero curve.

The distinction is numerical in the $\lambda = 5/2$ example. Its stationary point and value are

$$(x_*, y_*) = \left(-\frac{2}{5}, -\frac{2}{5}\right), \qquad P(x_*, y_*) = 1 - \frac{2}{5} - \frac{2}{5} + \frac{5}{2}\frac{4}{25} = \frac{3}{5}, \qquad \Delta = \frac{3}{2}. \tag{IV.11.73}$$

Both derivatives vanish, but $P \neq 0$. The unique stationary point is off the zero level, so the zero curve has no singular point in this torus chart. In the second example the equations instead give

$$(x_*, y_*) = (-3, -2), \qquad P(x_*, y_*) = 6 - 6 - 6 + 6 = 0, \qquad \Delta = 6 - 2\cdot 3 = 0. \tag{IV.11.74}$$

Now it is a curve singularity. Every coefficient participates in this difference; merely observing a nonzero Hessian determinant would not answer whether the critical point is on the chosen level set.

The local form determines the type of the singularity. Translate to $u = x + c/d$, $v = y + b/d$. The linear terms cancel, and the polynomial becomes exactly

$$P = d\,uv + \frac{\Delta}{d}, \qquad \operatorname{Hess} P = \begin{pmatrix} 0 & d \\ d & 0 \end{pmatrix}, \qquad \det(\operatorname{Hess} P) = -d^2 \neq 0. \tag{IV.11.75}$$

For $\Delta = 0$ the branches $u = 0$ and $v = 0$ meet transversely. This is an ordinary node of the complex curve. In the second example no approximation is involved: $P = (x+3)(y+2)$. For $\Delta \neq 0$ the nearby zero curve is $uv = -\Delta/d^2$ and is smooth. The real slice in Figure IV.11.6 makes the crossing and its smoothing visible; the complex statement follows from the displayed local equation.

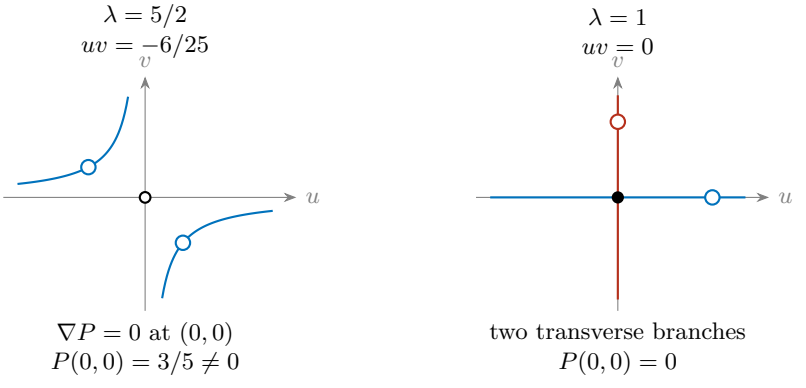


Figure IV.11.6: Real slices of the exact translated zero-curve equation. For the normalized $\lambda = 5/2$ example, $u = x + 2/5$, $v = y + 2/5$, and $uv = -6/25$; the origin is a stationary point of P but is off the zero curve. At $\lambda = 1$, $u = x + 1$, $v = y + 1$, and $uv = 0$ gives two transverse complex branches, whose real traces are the axes. Colored open circles exclude $x = 0$ or $y = 0$: the left chart requires $u, v \neq 2/5$, and the right requires $u, v \neq 1$. The black open origin lies off the left curve; the filled origin is the right node. This is an algebraic curve, not a SYZ base discriminant.

For the normalized polynomial the useful limiting statements can now be separated. At $\lambda = 1$ the algebraic curve has the node $(x, y) = (-1, -1)$. This is a limit of the curve family, not a license to extend every nonzero-t physical assumption used in eliminating the GLSM fields. At $\lambda = 0$, by contrast, the xy monomial disappears and the Newton polygon becomes a triangle. The original finite exponential $\lambda = e^{t_{\mathrm{HV}}}$ cannot vanish. Its limiting triangle is outside the four-nonzero-coefficient calculation. Finally $q = 0$ means $\lambda \to \infty$, not $\lambda \to 0$. Different coefficient charts are needed to analyze these boundaries without misleading normalizations.

The zero-curve discriminant is therefore fully calculable, but it is a discriminant of this algebraic family. Identifying it with the degeneration locus of a chosen special-Lagrangian fibration would require a separate geometric construction. Volume V, Chapters 3 and 4 use singularities together with periods and flat coordinates; the polynomial coefficients by themselves do not supply those identifications. The relevant pitfall is to confuse a stationary point, a singular zero curve and a physical singular fiber. Each has its own defining equations.

IV.11.8 What a global mirror would require

The smooth-fiber calculations reveal why the SYZ picture is attractive. A fiber position supplies three real parameters, and its flat unitary connection supplies three more. In the constant model the latter parameters form the dual torus and carry exactly the inverse metric expected from T-duality. The special-Lagrangian condition supplies the geometric compatibility of those fibers with the ambient complex and symplectic structures.

The original global SYZ argument begins with a stronger input than equality of one protected quantity. It assumes quantum mirror symmetry of the string theories. A pointlike brane has the original target as its moduli space; its proposed mirror is a brane wrapped on a special-Lagrangian three-cycle with a flat connection. Requiring these moduli spaces to describe the same physics motivates the fibration by three-tori. The dimension count uses deformation and flat-connection directions. It does not prove from $b_1 = 3$ that every individual three-cycle is topologically T^3, nor does it independently establish the initial quantum equivalence. The source presents the global picture as a proposal and computes a smooth local comparison within it.

There are three distinct geometric tasks left after our calculation. One must establish the existence of the appropriate fibers and family. One must glue local charts consistently with their integral lattices and monodromy. One must replace the smooth local description near degenerations with the required quantum-corrected one. A torus fiber as a topological object does not guarantee continuous Killing fields of the physical metric, so ordinary Buscher formulas cannot simply be applied to an arbitrary fibration. The constant matrix model made the isometry hypothesis exact; the general global problem does not inherit that simplification.

The original SYZ discussion identifies disk instantons as corrections to the brane-moduli geometry. Away from degenerating fibers at large radius, the source describes those corrections as exponentially suppressed. Near degenerations they can be important even when an overall radius is large. This is a qualitative physical mechanism in that

argument. We have not derived a disk count, a universal numerical error bound or a corrected global metric. In particular the failure of H_ε^{-1} at $\varepsilon = 0$ does not compute the missing disk terms.

The categorical question asks for different information again. In the original homological mirror proposal the symplectic manifold is closed with $c_1 = 0$; graded Lagrangian data and unitary local systems enter the proposed Fukaya construction. The differential and higher compositions count appropriate holomorphic disks with boundary conditions and holonomy factors. A list of objects or an isomorphism of vector spaces would miss those operations. The proposed comparison uses a derived Fukaya category, or a suitable enlargement, and a derived category of coherent sheaves on a dual complex algebraic space. The original statement also qualifies the expectation as a full triangulated subcategory embedding. We retain that qualification and those construction assumptions; we do not turn it into a universal equivalence theorem. Volume V, Chapter 6 develops the categorical tools at their stated scope.

These differences explain a common failed inference. Suppose two calculations produce the same protected ring. They have compared the multiplication of selected operators. They have not thereby identified all untwisted correlation functions, established existence of a torus fibration, or fixed every higher composition in a boundary category. Conversely our explicit free operator map has a broader free-theory scope, but its proof uses Gaussian fields and does not extend automatically to interacting targets.

The downstream route follows the object needed. For a toric Laurent curve and its lattice invariant, Volume VII, Chapter 4 can use the charge dictionary derived here while supplying its own brane interpretation. Volume V, Chapters 3 and 4 add periods, flat coordinates and enumerative extraction; the curve algebra alone does not prove those identifications. Volume V, Chapter 6 adds categorical boundary data. Later local mirror engineering and topological open-string constructions must preserve the same distinction between an explicit local calculation, an imported physical premise and a general proposal.

IV.11.9 Exercises

The first five problems have bounded numerical or algebraic submissions and a separately written explanation. Rational quantities in those submissions are exact strings, while integral charges and exponents are JSON numbers. The companion lists the full submission structure for each task. The written explanations, including all of Problem 6, require a reader's assessment; a numerical answer does not establish them.

1. **A free state and its mirror (III11-E1).** Take a rectangular supersymmetric two-torus with $\alpha' = 6$, radii $(4, 3)$, $n = (2, -1)$, $w = (-3, 2)$ and $B = 0$. Both angles have period 2π. Dualize the first circle by positive momentum–winding exchange. Submit both dual radii, both dual charge vectors, both chiral momenta and the imaginary parts of (τ', ρ') in the first-period chart. Show in writing why a second duality restores the full state, and distinguish a check of its weights from the operator argument in the text.

2. **A character as a physical position (III11-E2).** Take a smooth product T^3

with radii $(4,3,5)$, $\alpha' = 6$ and $A = \sum_i a_i d\theta_i$, where $a = (1/3, -2/5, 7/6)$. Use the positive dual angles $\widetilde{\theta}_i/(2\pi) = a_i$ modulo integers. Submit the three dual radii, all representative fractions in $[0,1)$ and all physical positions divided by 2π. Explain why a large gauge transformation changes the representative but not the dual point. State the flatness and topology assumptions; no spectrum identification is requested.

3. **The affine relation and its invariant (III11-E3).** Use the Hori–Vafa order $X_i = e^{-Y_i}$, $Q = (-1,-1,+1,+1)$ and $\sum_i Q_i Y_i = t_{\mathrm{HV}}$. Set $x = X_3/X_2$, $y = X_4/X_2$ and $e^{t_{\mathrm{HV}}} = 5/2$. Submit the charge row, the four Laurent exponent pairs in source order, four nonzero rational coefficients and $q = e^{-t_{\mathrm{HV}}}$. Any nonzero overall rational scale and nonzero rational rescaling of the torus coordinates is allowed. Explain why all four coefficients enter the invariant and why the resulting curve is not by itself the full mirror target.

4. **A critical point on the wrong level (III11-E4).** For $P = a + bx + cy + dxy$ on $(\mathbb{C}^*)^2$, derive the stationary point and evaluate the function there. Submit $(x_*, y_*, P(x_*, y_*), ad - bc)$ for $(a,b,c,d) = (1,1,1,5/2)$ and then $(6,2,3,1)$, in that order. Explain what changes if $d = 0$. Distinguish the algebraic zero-curve singularity from the discriminant of a chosen SYZ fibration.

5. **All metric components (III11-E5).** In the constant product (IV.11.27), take $\alpha' = 6$ and H as in (IV.11.36). Dualize all three isometric angles and then use $x' = Hx$. Submit all entries of the original base, original fiber, dual fiber and Legendre-base physical metric blocks as rational strings. In writing, derive the matrix inverse and explain why entrywise reciprocals fail, why α'^2 appears, and why invertibility and isometry are separate hypotheses.

6. **Which mirror statement? (III11-E6, written).** Compare the free-torus $(2,2)$ mirror automorphism, equality of one protected A/B ring, a derived/Fukaya categorical comparison with specified enhancements, and full quantum-string equivalence. Read the original SYZ discussion, physical PDF page 2 footnote 1 and pages 5–6. Identify the premise of its initial argument. Explain why smooth-fiber dualization is local and what fails without Killing vectors or at degenerations. State the missing existence, gluing and disk-correction information, and explain why a protected match cannot provide a general global SYZ proof.

IV.11.10 Take-home message

Take-home message

A mirror dictionary must name the objects it compares. The free torus map reflects one right-moving boson and fermion, transports the lattice cocycle and exchanges τ with ρ in the declared rectangular chart. A flat line system on an existing T^3 supplies a point of its character torus. In a constant positive-matrix model the normalized fiber phase is $-\pi/2$; triple isometric duality inverts the full physical fiber metric, and the Legendre base coordinate displays the exchanged blocks. Starting instead from the specified quantum GLSM potential gives the Laurent curve $1 + x + y + \lambda xy = 0$, whose invariant is $q = \lambda^{-1}$ and whose torus node occurs at $q = 1$. Global quantum and categorical statements require the additional premises and constructions appropriate to their objects.

Status and sources

§11.1. Mirror statements. The supersymmetry automorphism is defined in Hori and Vafa (2000), v3, physical PDF page 15, (2.30). A protected A/B comparison, an untwisted physical equivalence, the original categorical proposal and full quantum-string equivalence have distinct domains. The original SYZ quantum premise is explicit in Strominger et al. (1996), v2, physical PDF page 2 footnote 1; its initial argument is not proved here.

§11.2. Free operators and superspace. The operator calculation uses the free isometric physical-circle duality [WS]. The integral winding sum and current identification are in Hori and Vafa (2000), physical PDF pages 15–17, (2.31)–(2.44). The oscillator reflection is also explained in Johnson (2000), v3, physical PDF page 50, (127)–(129). Equations (IV.11.7)–(IV.11.9) spell out the Gaussian contractions, integral lattice pairing and cocycle pullback; the right fermion reflection supplies the supersymmetric map. Global measure, winding and spin/GSO premises are physical source inputs, not consequences of finite state comparisons. The physical radii, α' and positive charge exchange are defined above. The numerical lattice and signed level difference are bounded exact checks.

The independent superspace elimination uses Hori and Vafa (2000), physical PDF page 19, (2.52)–(2.57), rather than the component transformations (2.49)–(2.50). On physical PDF page 18, the literal printed (2.47), in the source's dimensionless radius r and noncompact scalar u, reads

$$d\tilde{s}^2 = du^2 + r^{-2}d\vartheta^2 = r^{-2}\big(r^4 du^2 + d\vartheta^2\big).$$

The first and last radial coefficients differ. The preceding source metric is $r^2(du^2 + d\varphi^2)$; angular duality leaves its spectator term $r^2 du^2$ unchanged. The last printed expression agrees with that calculation and with $\operatorname{Re}\Theta = r^2 u$ from superspace. The missing r^2 in the first expression is an explicitly derived source discrepancy, not a silently corrected quotation or a claim of a published erratum. Our physical-unit formula is (IV.11.14).

§11.3. Moduli and characters. The moduli and character calculations are restricted algebraic results [MATH]. The Kähler-period and physical circle units are defined above.

The comparison chart in Giveon et al. (1994), v1, physical PDF pages 30–31, (2.4.55)–(2.4.59), uses a second-period denominator and second-circle duality. The present first-period chart derives its own exchange directly. No arbitrary-B statement is inferred. For characters, $H_1(T^3, \mathbb{Z}) = \mathbb{Z}^3$, a fixed basis, flat unitary connections and the trivial line-bundle sector are stated hypotheses. The physical flat-connection/dual-position identification is a cited physical premise. Its original local source is Strominger et al. (1996), physical PDF page 4 (2.2) and pages 5–6 (2.10)–(2.13). The auxiliary sign and circumference comparison is Johnson (2000), physical PDF pages 62–63, (165) and (172), with positive potential. Its Insert 6 on physical PDF page 64 instead chooses negative potential; that angle has the opposite sign.

§§11.4–11.5. Constant local geometry. The constant-metric examples are conditional local geometric calculations [MATH], with the stated Hermitian metric and calibration normalizations. The normalized coframe, Gram determinant, explicit matrix inverse and Legendre pullback are derived here. The general closed-calibration minimization result is the cited theorem of Chapter 6, used only for an existing compact calibrated cycle with the stated metric and orientation. It is not an existence or spectrum theorem. The physical inversion uses the separate isometric free-duality premise. The smooth local comparison motivating it is Strominger et al. (1996), physical PDF pages 4–6, (2.1)–(2.13). The physical dilaton shift is calculated from the dimensionless fiber determinant; the source scalar called Φ in its geometric (2.14) is not imported as that dilaton. The ε family is an inversion boundary, not a constructed singular Calabi–Yau metric.

§11.6. Quantum potential and conditional algebra. The physical GLSM twisted superpotential is from Hori and Vafa (2000), physical PDF page 4 (1.2), and the conifold specialization on physical PDF page 56 (printed page 55). Its quantum exponential terms are a physical premise. The twisted form alone does not establish a twisted-worldsheet derivation. The constraint and Laurent algebra follow under the superpotential premise [MATH]. The comparison uses the declared toric ray order; reversing the charge generator reverses the FI constraint parameter. The chapter uses q_{book} as an action weight. No equality with an arbitrary physical curve period is imposed. The zero curve is not promoted to a full mirror target, nor to an equivalence of every GLSM observable.

§11.7. Invariant and node. The invariant and node calculations are exact algebra in the four-nonzero-coefficient torus chart [MATH]. All four coefficient factors, the height-one kernel, the singular-point value and the translated germ appear explicitly. The source polynomial is the same physical PDF page 56 of Hori and Vafa (2000). No identification of this curve discriminant with a chosen SYZ base discriminant is assumed. The $\lambda = 1$ node is a conditional algebraic limit; $\lambda = 0$ loses a monomial and lies outside the chart, and $q = 0$ corresponds to $\lambda \to \infty$.

§11.8. Global and categorical boundaries. Disk corrections and their qualitative large-radius/singular-fiber behavior are discussed in Strominger et al. (1996), physical PDF pages 5–6 after (2.10); the continuation proposal on physical PDF page 8 is not a global construction formula. Kontsevich (1994), v1, physical PDF pages 16–18 states the original closed $c_1 = 0$ setting, grading lift, unitary local systems and expected category construction. The full-triangulated-subcategory qualification on page 18 is retained. There is no universal homological mirror theorem asserted here.

Scope of the physical inputs. The cited mirror domains, global proposal, physical superpotential, correction mechanism, categorical proposal and local physical brane-coordinate identification remain physical inputs. The elementary calculations do not establish a stronger physical equivalence.

Exercises 1–5 ask for bounded calculations and Exercise 6 asks for written interpretation. Volume VII, Chapter 4 uses the Laurent and mirror-language calculations. Global SYZ constructions, general categorical equivalence, and the period and enumerative identifications require additional input.

References

Giveon, A., M. Porrati, and E. Rabinovici (1994). "Target space duality in string theory". In: *Phys. Rept.* 244. Source edition GPR_hep-th_9401139v1; physical PDF pages 27, 30, 31, pp. 77–202. DOI: 10.1016/0370-1573(94)90070-1. arXiv: hep-th/9401139.

Hori, K. and C. Vafa (Feb. 2000). *Mirror symmetry*. Source edition Hori_Vafa_hep-th_0002222v3; physical PDF pages 4, 15, 16, 17, 18, 19, 56. arXiv: hep-th/0002222.

Johnson, C. V. (July 2000). "D-brane primer". In: *Theoretical Advanced Study Institute in Elementary Particle Physics (TASI 99): Strings, Branes, and Gravity*. Source edition Johnson_hep-th_0007170v3; physical PDF pages 50, 62, 63, 64, pp. 129–350. DOI: 10.1142/9789812799630_0002. arXiv: hep-th/0007170.

Kontsevich, M. (Nov. 1994). *Homological Algebra of Mirror Symmetry*. Source edition alg-geom/9411018v1; physical PDF pages 16, 17, 18. arXiv: alg-geom/9411018.

Strominger, A., S.-T. Yau, and E. Zaslow (1996). "Mirror symmetry is T duality". In: *Nucl. Phys. B* 479. Source edition hep-th/9606040v2; physical PDF pages 2, 3, 4, 5, 6, 7, 8, pp. 243–259. DOI: 10.1016/0550-3213(96)00434-8. arXiv: hep-th/9606040.